In situ detection and characterisation of fluid mud and soft cohesive sediments by dynamic piezocone penetrometer testing

Dissertation zur Erlangung des akademischen
Doktorgrades in den Naturwissenschaften

Dr.rer.nat.

im Fachbereich Geowissenschaften
der Universität Bremen

Annedore Seifert

Bremen, Oktober 2010

Gutachter der Dissertation:

Prof. Dr. Achim Kopf

Prof. Dr. Tobias Mörz

Prüfer:

Prof. Dr. Heinrich Villinger

Prof. Dr. Burghard Flemming

Weitere Mitglieder des Prüfungsausschusses:

Dr. Christian Winter

Antje Lenhart

Tag des Promotionskolloquiums:

12.01.2011

TABLE OF CONTENTS

NARRATIVE OF THE PROJECT

In the beginning of my PhD thesis in summer 2005, intensive talks with the Federal Waterways Engineering and Research Institute (BAW) of Germany in Hamburg and with the Waterways and Shipping Administration of Emden (WSA Emden) led to the conclusion that there is a great demand on research of soft cohesive sediments in waterways, in particular fluid mud. Especially in the river Ems, high suspended sediment concentrations resulted in high dredging volumes to keep the waterways navigable. Authorities were looking for a reliable and efficient system to detect and characterise fluid mud in the waterways and harbours to reduce the rising dredging costs. Therefore, we considered a three-fold approach: 1) The idea was developed that a ship might be able to move fluid mud out of the waterway and/or to prevent consolidation due to turbulences and oxygen enrichment when the ship is passing through. If this hypothesis turns out to be correct, then a ship could be used to keep the waterways navigable instead of dredging the sediment. 2) Second, it was planned to study the interaction of ship movements with fluid mud by modelling different ship speeds and ship shapes in a flume in the laboratories of BAW. 3) In a third step it was planned to test the model results in the river Ems by using a ship equipped with instruments to detect fluid mud and its distribution during ship passage. However, problems occurred like filling the flume with fluid mud, to keep fluid mud in natural conditions in the flume, and to scale the sediment to the model ship size. Furthermore, it was difficult to get a ship equipped with sensors which would pass fluid mud layers since there was the possibility to get stuck in the riverbed. My first concept of the PhD research was not possible to realise anymore. Therefore I had to modify the whole research approach.

In 2006 my research was then focused on the development of a special *in situ* survey technique to detect both soft cohesive sediments and fluid mud. Additionally, laboratory tests of natural fluid mud and sediment cores were planned. At the same time, a dynamic cone penetrometer (CPTU) measuring *in situ* pore pressure and strength of sediments had been designed at MARUM. The lance was used in several studies to characterise consolidated marine sediments. However, it was not yet deployed to characterise soft cohesive sediments or even fluid mud suspensions, but showed potential to be a practicable and efficient way for testing these types of sediment.

In January and March 2006 I had the opportunity to participate into two research cruises in the Baltic Sea and tested soft gassy cohesive sediments with the new CPTU device. In the following months I analysed data from more than 50 deployments and categorised the pore pressure development. For additional ground thruthing, I determined the sediment properties of several sediment cores taken there. The CPTU proved to be a good and fast instrument to characterise soft cohesive sediments (Manuscript 3 of this thesis). In 2007 I had the opportunity to join two research cruises in the North Sea and carried out another appx. 50 CPTU tests into soft cohesive sediments. For a second approach of my research it was planned to compare the characterisation of mud layers in both Baltic Sea and North Sea. After several months of data analysis it transpired that these tests couldn't be used for further studies due to the influence of the stormy weather conditions during both cruises (heave obscuring the deceleration signals) and also

because of some technical problems of the lance (some transducers partly non-functional). Again, my research topic had to be modified because there was not another possibility to participate cruises into the North Sea to repeat the measurements.

During 2006 and 2007 I also followed the plan to test fluid mud layers *in situ*. However, the testing of fluid mud suspensions was even more difficult to realise. Initially I wanted to develop an electrical measuring chain which could be deployed for several tidal cycles in the water of the harbour of Emden to detect fluid mud by electrical conductivity changes. Nevertheless, numerous electrical measurements in the laboratory of fluid mud and clay suspensions with different salinities didn't attest the applicability of this method, but gave very small variations between the samples (and even the end members). Afterwards, I followed the second approach to deploy the dynamic CPTU. In cooperation with the WSA Emden and later as well with the Emden port authority it was possible to test the deployment of the CPTU from the ship. Unfortunately, in 2006 and 2007 the CPTU tests in the river Ems and in the harbour of Emden were not able to detect fluid mud. On one hand, there was sometimes no sufficient fluid mud concentration in the investigated areas and secondly, the chosen method of deployment of the CPTU and the way of data analysis was unsuccessful at that time. After having almost lost confidence that there is a chance to develop the new *in situ* testing method by CPTU during my research time and thinking of modifying the research topic, I figured out that new algorithm for fluid mud detection and CPTU data analysis and processing is required. Hence, in 2007/2008 I developed such an algorithm to analyse the obtained CPTU data for fluid mud detection. Before the algorithm for consolidated sediments had only been applied and turned out to be not applicable for fluid mud. And indeed, recalculation of CPTU data for fluid mud suspension and carrying out new tests in the beginning of 2008 proved that the lance was actually able to detect fluid mud as long as the standard cone is replaced by a custom-built plate with special pore pressure port. Laboratory tests of fluid mud properties completed my research until summer 2008. Anyhow, due to difficulties to get the possibility to join ship cruises for proper CPTU deployment, bad weather conditions on sea, technical problems, necessary PhD research topic modifications, and last but not least to develop a new *in situ* method took more time than expected. Three years of my contract with the University of Bremen terminated in summer 2008. In the second half of 2008 I took a family break and in spring 2009 I got a job in the industry. Hence, my PhD thesis will be published sometimes later after the actual research time.

ABSTRACT

Cohesive sediments or muds are common in marine and estuarine environments. During formation of mud deposits several mud states may appear, e.g. dilute suspension, fluid mud, and semi- to fully consolidated mud beds. Appearance and composition of cohesive sediments are highly variable. Shortcomings are apparent in current knowledge of the general relationships to predict the physical behaviour and transport mechanisms of the cohesive sediments in natural environments. Especially the influence of partially free gas resulting from degradation of organic material on the *in situ* sediment strength is not yet fully understood. Accumulation of gas bubbles may affect the stability of such sedimentary deposits largely. *In situ* techniques for measurements of physical properties are available, but often not suitable for soft cohesive sediments because of the use of heavy rigs which may disturb the sediment while testing. Also research is still needed to improve fluid mud detection with high accuracy. This thesis presents a novel approach to *in situ* characterise and classify soft consolidated mud as a function of fluid saturation and to detect fluid mud in its natural environment. Additionally this thesis outlines laboratory results about the relationship of the rheological behaviour of natural fluid mud to different parameters to provide substantial validation for numerical modelling studies. The findings will also help to understand the interaction between the newly applied *in situ* detection technique and the behaviour of fluid mud suspensions which has to be investigated further.

A dynamic piezocone penetrometer with pore pressure sensors (CPTU) was deployed in the marine environment of the western Baltic Sea and in the tidally influenced Ems estuary (Germany) to measure *in situ* strength and pore pressure of both consolidated mud and fluid mud suspension. CPTU measurements in the western Baltic Sea were complemented with sediment sampling by nine gravity cores served sedimentological characterisation and analysis of geotechnical properties as well as with high resolution echo-sounder profiles at selected locations.

The measurements in the marine consolidated mud of the western Baltic Sea show very variable changes in both pore pressure and sediment strength during CPTU deployments. Mainly initially sub-hydrostatic pore pressure values during penetration and a delayed response towards positive pressures thereafter occur. This signal is typically found in soft muds with high water content and undrained shear strength of 1.6.-6.4 kPa. Those pore pressure curves are further affected by enhanced consolidation and strength of individual horizons as well as by the presence of free gas. In contrast, a second type of pore pressure curve shows a well-defined peak in both pore pressure and cone resistance. The initial pore pressure increase during sediment penetration is followed by an exponential decay owing to dissipation. This signal is associated with normally consolidated mud, with indurated clay layers showing significantly higher undrained shear strength (up to 19 kPa).

The detection of fluid mud suspension by a dynamic CPTU highlights a novel approach to support surveying and management of areas with high suspended sediment concentrations (SSC). To enhance the resistance during penetration the originally conical device is modified with a disk configuration (33 x the area of the cone) for rapid fluid mud detection. The results show that suspended sediment concentrations ≥ 90 g/l can be identified by both disk resistance and pore pressure measurements, and furthermore the transition from fluid mud to consolidating mud once concentration exceed 150 g/l.

Fluid mud suspensions from the Ems estuary were not only tested *in situ* by CPTU measurements but also during laboratory experiments (e.g. sediment rheology, suspended sediment concentration (SSC), grain size distribution, organic content (TOC), and mineral composition). The focus lied on the potential influence of various parameters on their rheological behaviour. For comparison reason samples were taken from two different locations, from the river Ems and from the adjacent harbour of Emden. All fluid mud suspensions with suspended sediment concentration between 100 g/l and 200 g/l exhibit non-Newtonian shear thinning behaviour. Yield stress and viscosity at the yield point increase exponentially with an increase in SSC. Interestingly the river Ems suspensions reveal around 23 % higher shear stress than the suspensions from the harbour with the same SSC. Furthermore, the viscosity at the yield point of the river sample with SSC of 180 g/l, for example, is 3 times higher than the suspension of the harbour. It is concluded that grain size distribution and mineral composition are parameters which do not affect the rheological behaviour significantly, but that small variations of the samples from both locations may explain the subtle variations observed. In fact, variations in salinity, type of organic matter and floc strength are discussed to be the most influencing parameters on the rheological behaviour of the fluid mud suspensions.

The investigations presented in this thesis mainly show two major results:

(i.) Dynamic CPTU testing is a versatile approach for fast characterisation of marine and estuarine mud to be useful for both economical issues (navigation channel maintenance by dredging and rapid surveys for pipeline etc.) and geological scientific topics (sediment distribution and stability and its potential for remobilisation).

(ii.) Depending on the physical properties of fluid mud (Ems), gaseous organic mud (Baltic Sea), and clay-rich semi-consolidated and consolidated deposits (both areas), characteristic signals in sediment resistance and pore pressure allow a rapid identification and assessment of such deposits.

KURZFASSUNG

Kohäsive Sedimente, auch zum Teil als Schlick bezeichnet, sind weit verbereitet in marinen und ästuarinen Gebieten. Bei der Ablagerung dieser Sedimente können mehrere Zustandsformen auftreten z. B. verdünnte Suspension, Flüssigschlick (Fluid Mud) und Schlick mit unterschiedlichen Konsolidierungsgraden von teilweise bis ganz konsolidiert. Die Zustandsform und die Zusammensetzung der kohäsiven Sedimente sind in der natürlichen Umgebung hoch variabel. Aktuell besteht noch Forschungsbedarf über die natürlichen Zusammenhänge, um das physikalische Verhalten und die Transportmechanismen der kohäsiven Sedimente zu bestimmen. Insbesondere ist der Einfluss von teilweise freiem Gas im Sediment, das beim biologischen Abbau von organischem Material entsteht, auf die *in situ* Sedimentfestigkeit noch nicht vollständig verstanden. Eine Anreicherung von Gasblasen kann die Stabilität größerer Sedimentablagerungen stark beeinträchtigen. *In situ* Messgeräte zur Bestimmung der physikalischen Eigenschaften von Sedimenten werden bereits eingesetzt. Meistens sind aber diese Methoden nicht für weiche kohäsive Sedimente geeignet, da die schweren Messanlagen beim Testen störend wirken können. Weiterhin besteht Forschungsbedarf, Fluid Mud Suspensionen mit höherer Genauigkeit zu detektieren. Diese Doktorarbeit zeigt einen neuartigen Ansatz auf, um weichen konsolidierten Schlick als Funktion seiner Fluidsättigung *in situ* zu charakterisieren und zu klassifizieren, und um Fluid Mud in seiner natürlichen Umgebung zu detektieren. Zusätzlich zu den *in situ* Messverfahren werden Laborergebnisse vorgestellt, die die Zusammenhänge des rheologischen Verhaltens von natürlichem Fluid Mud zu verschiedenen Parametern beleuchten. Diese Ergebnisse können nicht nur wesentlich zur Validierung von numerischen Modellstudien beitragen, sondern auch zum Verständnis der Wechselwirkungen zwischen der neu angewendeten Detektionsmethode and dem Verhalten der Fluid Mud Suspension. Dazu besteht aber noch weiterer Untersuchungsbedarf.

Eine dynamische Piezocone Penetrometer Sonde (CPTU) mit eingebauten Porendruck Sensoren wurde in marinen Bereichen der westlichen Ostsee und im tidebeeinflussten Emsästuar eingesetzt, um *in situ* die Festigkeit und den Porendruck sowohl von konsolidiertem Schlick als auch von Fluid Mud Suspension zu messen. In der westlichen Ostsee wurden zusätzlich zu den CPTU Messungen neun Schwerelotkerne gewonnen, um die sedimentologischen und geotechnischen Eigenschaften des Schlicks im Labor zu bestimmen. An ausgesuchten Lokationen wurden auch ergänzend hochauflösende Echosounder Messungen durchgeführt.

Die CPTU Messungen im marinen konsolidierten Schlick der westlichen Ostsee zeigen stark variable Porendruck- und Sedimentfestigkeitsprofile. Am häufigsten tritt beim Eindringen der Sonde ins Sediment anfänglich ein sub-hydrostatischer Porendruck auf,

der danach verzögert zu positiven Drücken ansteigt. Dieses Porendrucksignal wurde typischerweise in weichem Schlick aufgezeichnet, der hohe Wassergehalte und undrainierte Scherfestigkeiten von 1,6 bis 6,4 kPa aufwies. Das Signal wird aber auch durch erhöhte Konsolidierungsgrade und Festigkeiten einzelner Sedimentlagen als auch durch das Vorhandensein von freiem Gas beeinflusst. Im Gegensatz dazu, weist ein zweiter Porendrucktyp Kurven mit gut definierten Spitzenwerten im Porendruck und Spitzenwiderstand auf. Dem anfänglichen Porendruckanstieg während der Eindringung der Sonde folgt ein exponentieller Druckabfall in der Dissipationsphase. Dieses Drucksignal tritt in normalkonsolidiertem Schlick mit eingeschalteten härteren Tonlagen auf, der signifikant höhere Scherfestigkeiten (bis zu 19 kPa) aufweist.

Die Detektion von Fluid Mud Suspensionen mit einer dynamischen CPTU Sonde ist ein neuartiger Ansatz, um Gebiete mit hohen Schwebstoffkonzentrationen zu untersuchen und zu managen. Dabei wurde die konische Spitze durch eine Scheibe (33 x der Fläche der Spitze) ersetzt, um somit den Widerstand während der Eindringung der Sonde zu vergrößern. Die Ergebnisse zeigen, dass durch Messungen des Scheibenwiderstandes und des Porendrucks Schwebstoffkonzentrationen $\geq$ 90 g/l nachgewiesen werden können. Zusätzlich ist es auch möglich, den Übergang von Fluid Mud zu konsolidiertem Schlick zu identifizieren, wenn die Konzentrationen 150 g/l übersteigen.

Die Fluid Mud Suspensionen wurden in dieser Studie nicht nur *in situ* mit der CPTU Sonde untersucht, sondern auch im Labor getestet (z. B. Sediment Rheologie, Schwebstoffkonzentration, Korngrößenverteilung, organischer Gehalt (TOC) und Mineralzusammensetzung). Der Schwerpunkt lag dabei auf der Untersuchung des potentiellen Einflusses verschiedener Parameter auf das rheologische Verhalten der Suspensionen. Dazu wurden für den Vergleich Proben von zwei unterschiedlichen Lokationen, aus dem Fluss Ems und aus dem Außenhafen von Emden, genommen. Alle Fluid Mud Suspensionen mit Schwebstoffkonzentrationen zwischen 100 und 200 g/l weisen ein nicht-Newtonsches scherverdünnendes Fließverhalten auf. Die Viskositäten bei der Fließgrenze und die Scherspannungen steigen exponentiell mit Zunahme der Schwebstoffkonzentration an. Interessanterweise zeigen die Proben aus der Ems eine um ca. 23 % höhere Scherfestigkeit auf als die Suspensionen aus dem Außenhafen mit gleichem Schwebstoffgehalt. Außerdem ist zum Beispiel bei der Probe aus der Ems mit einem Schwebstoffgehalt von 180 g/l die Viskosität bei der Fließgrenze dreimal so hoch wie die der Probe aus dem Außenhafen. Es wird zusammenfassend festgestellt, dass die Parameter Korngrößenverteilung und Mineralzusammensetzung keinen signifikanten Einfluss auf das rheologische Verhalten haben. Die vorhandenen kleineren Variationen der einzelnen Proben beider Lokationen können hier die geringen gemessenen Variationen erklären. Vielmehr wird diskutiert, dass die Variationen der Parameter Salinität, Art des organischen Materials und die Flockenfestigkeit den meisten Einfluss auf das rheologische Verhalten von Fluid Mud Suspensionen haben.

Die Untersuchungen dieser Doktorarbeit zeigen hauptsächlich zwei Ergebnisse:

(i.) Dynamische CPTU Messungen sind ein hervorragender Ansatz, um schnell marinen und ästuarinen Schlick zu charakterisieren. Dies ist sehr bedeutend für ökonomische Belange (Fahrrinnenunterhaltung durch Baggerarbeiten und schnelle Untersuchungen für Pipeline Verlegungen etc.) und für geologische wissenschaftliche Themen (Sedimentverteilung, Sediment-stabilität und Potential der Remobilisierung).

(ii.) In Abhängigkeit der physikalischen Eigenschaften von Fluid Mud (Ems), gashaltigem organischem Schlick (Ostsee) und tonreichen teilweise und ganz konsolidierten Ablagerungen (beide Gebiete) ist es möglich, durch charakteristische Signale des Sedimentwiderstandes und des Porendrucks diese Ablagerungen schnell zu identifizieren und zu bewerten.

1 INTRODUCTION

1.1 Motivation

Cohesive sediments, or mud as it generally referred to, are very common in estuarine and coastal areas around the world (e.g. Kirby 1988, Faas 1995, Friedrichs et al. 2000, Shi and Kirby 2003, Lefebvre et al. 2004, Uncles et al. 2006, Reed et al. 2009). The term mud commonly describes a complex mixture of fine-grained mineral sediment (clay and silt), small amounts of sand, water, and organic material of diverse nature (e.g. Winterwerp and van Kesteren 2004, McAnally et al. 2007a).

An understanding of the character, generation, and transport of mud has a significant economical and ecological importance. Often mud accumulates in navigation channels or harbour basins and could impede navigability of ships (e.g. Delefortrie et al. 2005, Wurpts and Torn, 2005). However, owing to the globalisation worldwide maritime trade utilising larger vessels is increasing, and harbours and waterways have to be deepened to accommodate the new market requirements and to safeguard navigability. As a consequence, the cost of routine infrastructure maintenance (e.g. dredging) is rising rapidly. Many other engineering applications, such as reclamation of intertidal flats, or constructions of cables, pipelines, and exploration platforms in marine environments require a comprehensive appraisal of the character and behaviour of mud (e.g. Lee and Ng 1999, Black et al. 2002, Arulrajah et al. 2005, Randolph et al. 2005, Schlue 2008). From an ecological point of view mud is of great interest as it contributes to eutrophication and also carries pollutants (e.g. McAnally et al. 2007a, Zaldívar et al. 2008). Nowadays, cohesive sediments are often contaminated, as many pollutants, in particular heavy metals adhere easily to the sediment particles, because of their high specific area and chemical constitution (e.g. Velde 1995). Therefore, prediction and management of mud require research on important parameters to characterise mud (grain size distribution, strength, organic content, mineral content, etc.) as well as on parameters controlling its mechanical behaviour (settling velocity, consolidation, rheological behaviour of fluid mud, etc.). However, during sampling, transport and laboratory tests the mud properties could be affected. For this reason recent research is

concentrating on *in situ* measurements of mud characteristic and distribution (e.g. Fontein et al. 2006, McAnally et al. 2007b). This is especially a challenge in areas where the mud is enriched with free gas which strongly influences the mud properties (e.g. Sills et al. 1991, Brandes 1999).

1.2 Thesis outline

This thesis incorporates three manuscripts which are ordered by the sediment type investigated and not chronologically. Each one is presented in a separate chapter and stands alone as separate piece of work with its own introduction, methods, results, discussion and conclusions.

After a short introduction to the general context, Chapter 1 closes with an outline of the thesis.

Chapter 2 outlines the scientific rationale of this thesis. It includes a summary of the processes forming a consolidated mud bed and a detailed focus on the investigated physical states and properties of mud.

Chapter 3 presents an overview of the research areas.

Chapter 4 provides a short introduction to cone penetrometer testing in general and a description of the research progress to detect soft and fluid mud by dynamic piezocone penetrometer measurements.

Manuscript 1 and Manuscript 2 focus on the properties of fluid mud in estuarine environments and harbours. Manuscript 1 concentrates on the rheological behaviour of fluid mud and the influence of various parameters (“Rheological characteristic of natural fluid mud and the influence of different parameters“. In review, *Applied Rheology*). While Manuscript 1 focuses on laboratory investigations of fluid mud, Manuscript 2 is providing *in situ* detection and characterisation of fluid mud and the underlying sediment by dynamic piezocone penetrometer measurements (“A modified dynamic CPTU penetrometer for fluid mud detection“).The latter paper is currently in review with *Journal of Geotechnical and Geoenvironmental Engineering*, American Society of Civil Engineering (ASCE). Since the original manuscript (Manuscript 2a) to this journal was found too long, the revised version under review was condensed to half

the length to meet the format of a Technical Note (Manuscript 2b). Both versions of the manuscript are included to ensure that none of the work and data was put in goes missing.

Manuscript 3 presents *in situ* characterisation of soft cohesive sediments in marine environments. In particular, it focuses on the pore pressure and strength measurements of gaseous mud and was presented at EGU Vienna 2007, as well as a peer-reviewed paper ("In situ pore-pressure evolution during dynamic CPT measurements in soft sediments of the western Baltic Sea". *Geo-Marine Letters* (2008), 28(4), 213-227).

Finally, the conclusions of the thesis are drawn in Chapter 8 and an outlook for future scientific work will be provided.

The appendix comprises an overview of all cone penetrometer tests during this research and lists additional publications (abstract of the international conference EGU and cruise reports) as well as a summary of all determined sediment data of cores taken in Baltic Sea and samples from the river Ems and the harbour of Emden.

2 FORMATION OF MUD DEPOSITS

This chapter focuses on a brief description of the processes governing the formation of mud deposits and gives definitions of different mud states. Besides, a detailed introduction of the mud states which were investigated during research of this thesis is presented.

2.1 General processes and mud states

The vertical dynamics of mud is governed by a complex of physical, chemical and biological processes. To predict the movement of mud a combination of the nature of the hydrodynamic of the water and the influence of the water to the movement of mud has to be investigated. However, commonly accepted key processes are flocculation, settling and deposition, consolidation, and erosion and entrainment. Figure 1 shows a schematic picture of the processes forming a consolidated mud and it indicates the different mud states. In natural conditions, different processes are interacting and they are highly variable in time and space. Therefore, any state or process may be bypassed, for example, fluid mud may be eroded without passing through consolidation. Particularly in estuaries, processes are strongly cyclic as deposition, partial consolidation and resuspension of mud occurs repeatedly with the tides (Uncles 2002).

Cohesive sediment particles tend to agglomerate to flocs while settling due to collisions between sediment grains which are encouraged by differences in electrochemical forces (cohesion), settling velocity, turbulence, and Brownian motion (e.g. van Leussen 1988). The flocs fall through the water column towards a bed as a result of gravitational force acting on the particles, opposed by turbulent mixing processes. During that stage suspended particles might undergo aggregation processes as well as break-up of the flocs. At sufficiently high concentrations or sufficiently low turbulence levels, for example during slack tide in an estuary, the concentration towards the bed further increases. Local regions of strong gradients in suspended sediment concentration (lutoclines) can exist, which has been observed in various estuaries (e.g. Lesourd et al. 2003, Dyer et al. 2004, Guan et al. 2005). The concentration of suspended sediment due

to settling may soon have increased to a level that particles hinder each other. Because of hindered settling effects the effective settling velocity is reduced (Dankers and Winterwerp 2007). However, suspended particles may settle through the layer of high sediment concentration, deposit on to the soft mud layer of flocculated sediment and eventually become part of the bed due to consolidation (McAnally and Mehta 2002). Because of stresses caused by turbulent flow or by waves sediment from surface can be eroded and the particles may begin the process anew.

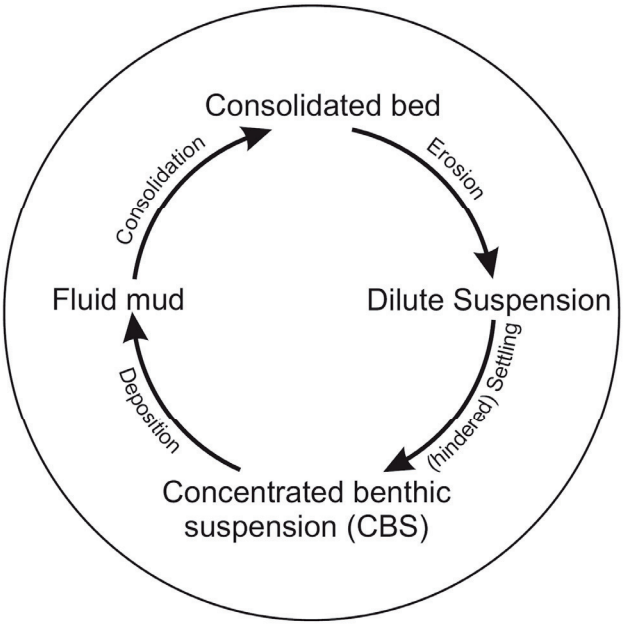

Fig. 1 Model showing states of mud occurrences and linking processes (mud states after Berlamont and Toorman 2000).

Various classifications of mud states related to the processes can be found in the literature (e.g. Kirby 1988; Winterwerp 1999; Bruens 2003). However, a comprehensive summary of definitions is given in Whitehouse et al. (2000). In general, cohesive sediments can be considered to exist in four states whereby not all classes have to occur at the same time (Fig. 1). The EU research project COSINUS suggests the following categories based on local concentrations, its vertical gradient, and flow speed (Berlamont and Toorman 2000):

1. Dilute suspension – Newtonian flow behaviour; fully turbulent; typical dry mass concentration less than 1 g/l

2. Concentrated benthic suspension (CBS) – still Newtonian flow behaviour; significant amount of stratification, but sediment still kept in suspension by turbulence; typical dry mass concentrations of less than 10 g/l
3. Fluid mud – non-Newtonian flow behaviour often with a high viscosity; mud flocs become space filling; flow is generally laminar
4. Consolidated bed – formed from settling from suspension or from consolidation of fluid mud.

In addition to the physical processes the formation of mud is influenced by biological processes. Generally, two opposite major aspects of the biological influence can be distinguished: i) sediment stabilisation, and ii) sediment destabilisation (e.g. Widdows and Brinsley 2002). Bacteria and microphytobenthos tend to stabilise sediments as they secrete sticky extracellular polymeric substances (EPS; Wotton 2004). The flexible EPS coat connects particles of the sediment and is known to enhance cohesion and adhesion of the sediments (Black et al. 2002). Thus, the erosion threshold could be increased (Tolhurst et al. 2002). On the other hand, bioturbation of benthic fauna could increase sediment erodibility and resuspension rate due to increased porosity and permeability (Black et al. 2002). However, interdisciplinary research between physical and biological processes related to mud formations is still rare and the complex influence of biotic factors to sediment dynamic is poorly understood.

Recent research shows that a major shortcoming in knowledge on the cohesive sediment behaviour lies in a lack of understanding and *in situ* measuring concentrated near-bed suspensions (Berlamont and Toorman 2000; McAnally et al. 2007b). *In situ* measurements are required as the concentrated suspensions and the soft consolidated bed are very easily disturbed. Sampling, transport and laboratory measurements may affect the physical properties. In this line of thoughts, this thesis focuses on the *in situ* characterisation of the last two states of mud – fluid mud and soft consolidated mud – to obtain reliable measured sediment properties.

2.2 Fluid mud

Fluid mud (FM) properties, particularly its rheological ones, are important for the prediction of fluid mud flow (e.g. whether mud deposited on a slope can flow under gravity), for the estimation of sensitivity to erodibility and damping of turbulence. The latter is essential for storm surge estimations, turbidity generation and design of navigation channels. When waves travel over fluid mud layers the wave energy is easily dissipated because of high FM viscosity (e.g. Jain and Mehta 2009). Furthermore, fluid mud may reduce bottom shear stress, compared to sand and/or consolidated mud beds, and larger tidal amplitudes may occur (Gabioux et al. 2005). Nowadays, hydro-sedimentary models implement the fluid mud–wave interactions for prediction of FM distribution, transport and wave propagation (amongst others Toorman et al. 2002; Winterwerp et al. 2007; Soltanpour and Haghshenas 2009). Nevertheless, modelling requires an accurate quantitative description of fluid mud properties especially its flow behaviour.

Fluid mud does not only have a large influence on to the physical properties of estuarine and coastal environments, but also on the biological and ecological system. Rapid oxygen decrease to almost zero in the transition from water to fluid mud was observed in estuaries (Abril et al. 2000, Schöl et al. 2006). Hence, anoxic conditions in fluid mud layers could contribute to eutrophication. However, the affect of depleted oxygen on the physical properties of fluid mud and the relation of the occurrence of fluid mud and the consequences to the biology and ecology of the estuaries are poorly understood.

Fluid mud can be formed by settling from a mud suspension, or by fluidisation and liquefaction, for instance induced by waves, of a consolidating mud. The suspension becomes a fluid mud when the concentration is high enough and the time for accumulation sufficiently long for the particles to form a space-filling network structure. Suspended sediment concentrations of FM naturally vary between 10 and several 100 g/l depending on mud sources and composition (Winterwerp and van Kesteren 2004). Once fluid mud is formed further compaction occurs due to self-weight consolidation if the suspension is not mixed into the overlying water column by entrainment. The difference between fluid mud and consolidating mud is that the latter is characterised by the occurrence of measurable effective stress whereas in fluid mud

the particles are still fluid-supported with zero effective stress (Sills and Elder 1986; Mehta 1991).

In general, rheological studies have been performed on artificial cohesive sediment suspensions (as reviewed by Coussot 1997), although some rheological characterisation of natural mud has been done as well (e.g. O'Brien and Julian 1988; Aijaz and Jenkins 1994; van Kessel and Blom 1998; Faas and Wartel 2006). During formation of fluid mud the rheological properties are changing from Newtonian to non-Newtonian, i.e. non-linear response to the shear rate (Fig. 2).

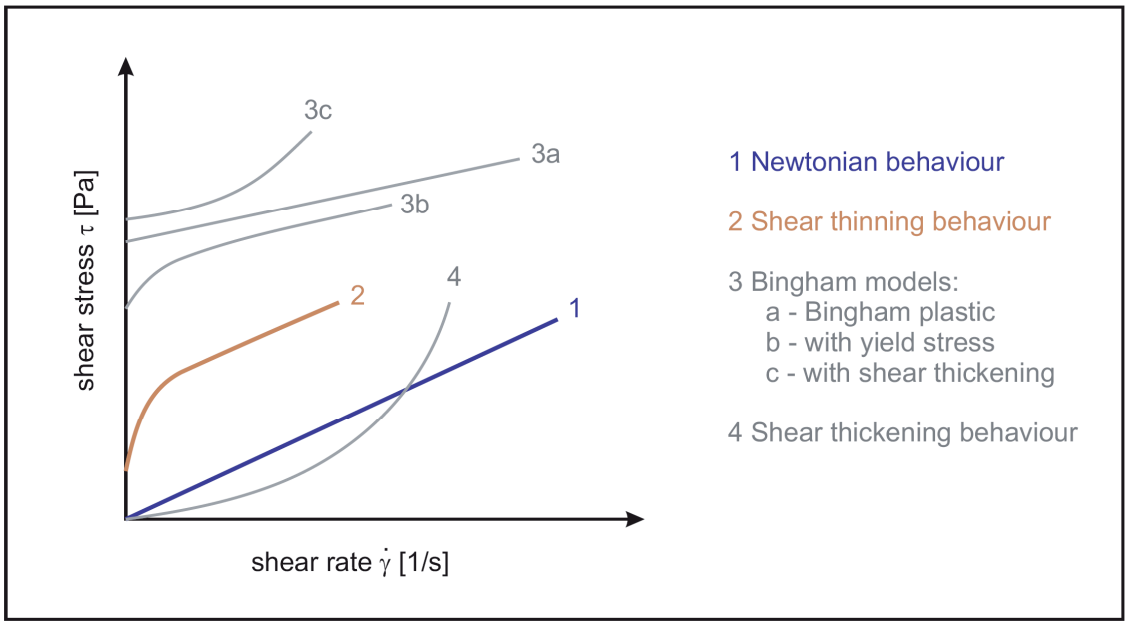

Fig. 2 Rheological models (after Whitehouse et al. 2000 and references therein)

The flow properties are strongly influenced by the characteristic of the mud (sediment concentration, salinity, mineralogical composition, organic matter and pH) and by the hydrodynamic conditions (Berlamont et al. 1993). Furthermore, the stress response of fluid mud suspension depends on its stress history known as thixotropy. Thus, for a given density different rheological properties may occur. However, the viscosity of fluid mud is typically several orders of magnitude larger than that of clear water (Whitehouse et al. 2000). In general, fluid mud is characterised by a yield stress and a flow behaviour which can be described by the Herschel-Bulkley-Model a generalisation of the Bingham Model exhibiting shear thinning behaviour with decreasing viscosity by increasing

applied stress (Fig. 2; Coussot 1997; Winterwerp and van Kesteren 2004). Besides, there are more complex models of the stress-shear relationships developed by Toorman (1997) and van Kessel and Blom (1998) incorporating thixotropy and structural changes within particle aggregates due to shearing. However, because of the influence of many parameters, the flow properties of natural fluid mud are difficult to generalise. Nowadays, there is still a lack of reliable data for natural fluid mud, particularly with regard to the direct influence of sediment concentration, salinity, organic content, floc size, and mineral composition. Therefore, research of this thesis is concentrating on the influence of various parameters on the rheological behaviour of natural fluid mud and will be discussed more in Manuscript 1.

Another important aspect of fluid mud is its role in hampering navigability of waterways as fluid mud may affect the manoeuvrability of vessels. Authorities maintain waterways safely navigable by dredging large amounts of mud which involve a lot of costs. If the density and viscosity of FM is sufficiently low, it is navigable. However, the transition between navigable and non-navigable fluid mud conditions is difficult to define. Measurement of density is the most common criteria of navigable depth (McAnally et al. 2007b). Due to the thixotropic behaviour of FM this method does not necessarily result in efficient dredging. In fact, the rheological behaviour of fluid mud is a more direct parameter for assessment of the nautical depth although it is still complex to measure (Teeter 1992, Greiser et al. 2002). Since fluid mud is easily disturbed, sampling may be a problem. In addition, other factors such as different mud provenance and laboratory equipment making it difficult to generalise the fluid mud properties (Ngyuen et al. 2006). Consequently, *in situ* measurements are required not only to determine navigable depth in waterways but also to better define processes between FM and overlying water or/and underlying sediment and to provide information for improving models. Different *in situ* techniques such as acoustic depth sounder or density probes have been developed although some are difficult to deploy or less reliable when applied very close to bed. Anyhow, recently McAnally et al. (2007b) gave a comprehensive summary of the variability of instruments and concluded that research is still needed to provide a rapid and accurate detection and characterisation of fluid mud. In this regard, a new *in situ* technique to detect fluid mud as well as the depth and

strength of the underlying sediments by mainly dynamic pressure and strength measurements is introduced in Manuscript 2 of this thesis.

2.3 Mud of different consolidation states

The transition from a loosely packed layer of fluid mud to a compacted mud occurs due to further self-weight consolidation. Pore water is driven out of the flocs and the space between the flocs caused by the submerged weight of subsequently depositing particles which lead to an increase of density and a decrease in void ratio and permeability through time. The fluid-supported suspension is changing to a particle interacting framework where the skeleton of the sediment network has the capacity to carry part of its own weight. Thus, during consolidation the load is gradually transferred from the fluid phase of the soil to the developing soil frame and therewith the pore water pressure become subsequently less than the total vertical stress leading to an increase in effective stress. The development of effective stresses (difference between total stress and pore water stress) during consolidation was first proposed by Terzaghi and Peck (1948). Sills and Elder (1986) and Sills (1998) used the existence of effective stresses to define the transition from suspension to a soft consolidating mud (Fig. 3).

From settling column experiments, Sills and Elder (1986) conclude that the transition point depend on various factors such as sedimentation rate, initial concentration and time. Therefore, it can be identified by a concentration range (for example: 80 g/l and 220 g/l for Combwich mud; Sills and Elder 1986) rather than by a unique density or concentration. However, consolidation processes lead to an increase in strength of the mud bed and in the resistance of the bed to erosion. For detailed description and modelling of the consolidation processes the reader is referred amongst others to Toorman (1996), Winterwerp (1999), Merckelbach (2000) and Merckelbach and Kranenburg (2004).

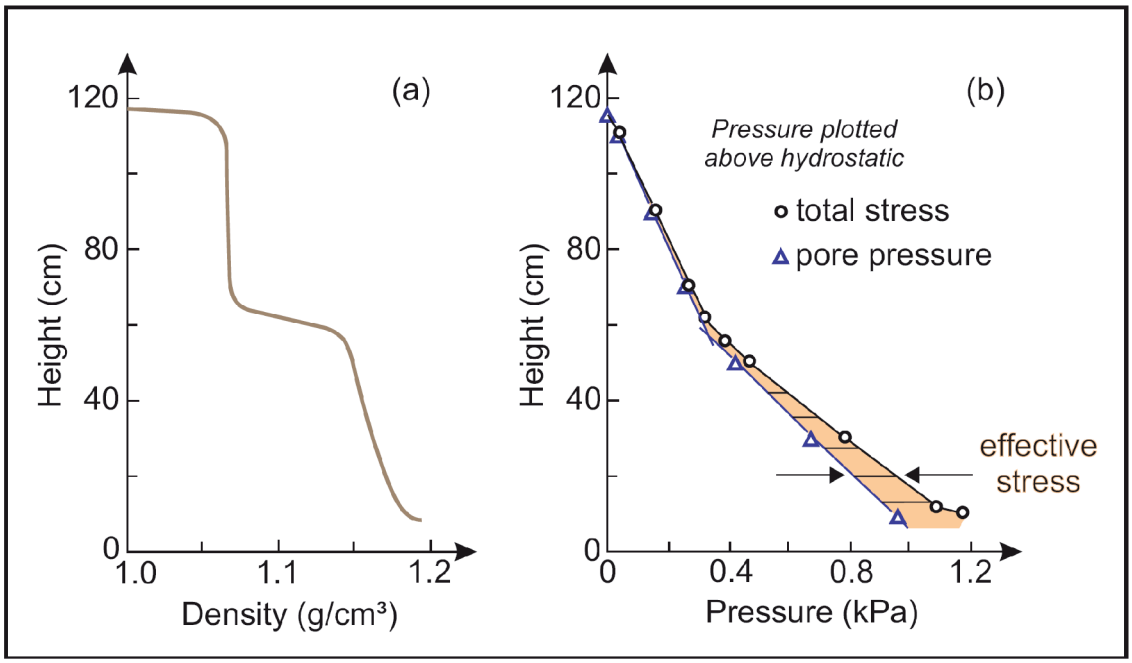

Fig. 3 Development of effective stress during settling of an estuarine silty clay in tap water, a) density profile during settling, b) corresponding total stress and pore pressure profiles (after Sills and Elder 1986).

For engineering purposes, for example installations of shallow and deep foundations or slope stability, deformation and strength of sediments are essential parameters to determine the interaction of the structures with the sediment. The mechanical behaviour of sediments is a result of the characteristics of the skeleton and the medium occupying the pore volume. Commonly, this medium will be water in a marine environment. Sediment with pore volume fully occupied by water is defined as saturated sediment. However, due to degradation of organic material and other microbial activity, gas will be produced and may either occur freely as bubbles or can be dissolved in the pore water. These sediments are defined as partially saturated sediments. Free gas in shallow marine sediments is globally distributed (Fleischer et al. 2001) and has a profound impact on the strength and stability of the sediment. For example, the sediment strength could remain low at great depth because free gas is retarding the self-weight consolidation and causes under-consolidated conditions (Wichman et al. 2000). Disturbances by natural events or human activities could cause instability of the sediments resulting in submarine landslides or foundation collapse. Moreover, gas bubbles could grow in the sediment generating extensional cracks and hence, favouring

sediment instability. It demonstrates that soft muddy sediments, in particular when containing free gas, are easily disturbed. For this reason, the normal recovery of sediment samples from seafloor, for example by coring, could result in sample disturbances due to degassing and may affect the measured physical sediment properties. Besides, acoustic profiling is often used for sediment investigation. But the presence of free gas in sediments often alters the acoustic sediment properties causing turbidity zones in the measured acoustic data (e.g. Slowey et al. 1996, Anderson et al. 1998). Therefore, characterisation of these sediments requires *in situ* instruments in order to obtain meaningful, trustworthy measurements. Manuscript 3 introduces new *in situ* strength and pore pressure measurements to characterise soft cohesive sediments and discusses the possible influence of free gas.

3 RESEARCH AREAS

Fluid mud and soft mud characteristics were investigated in the Ems estuary and in the marine environments of the Baltic Sea when carrying out the research of this thesis. The material studied is believed to be representative since individual surveys were months to a few years apart and carried out at different times of the year. In order to set the stage for the Manuscripts 1 to 3, either study areas are described in this chapter.

3.1 The river Ems

The macrotidal Ems estuary is located at the border between Germany and the Netherlands and discharges into the North Sea. It is an important navigation channel for sea-going vessels and river ships, and has to provide significant navigable depth since the Meyer shipyard upstream (town of Papenburg) launches its cruise ships on it regularly. Figure 4 shows the locations of the sampling points of the investigated fluid mud (see also Manuscript 1 and 2).

Natural and anthropogenic changes over the past centuries have strongly influenced the hydrodynamic and morphodynamic system of the tidal Ems (Talke and de Swart 2006). Natural effects include, for example, variation of the discharge, sea level rise, changes of amplitude and frequency of storm surge while anthropogenic changes are such as deepening and streamlining of the navigation channel. Jensen et al. (2003) determined an increase of the mean tidal range in the river Ems whereby the mean low water is decreasing and the mean high water increasing because of both sea level rise and deepening of the navigation channel. Although, the anthropogenic changes of the river are concluded to be the main reasons for the decrease of the mean low water. This observation is suggested to arise with a decrease of the hydraulic roughness of the entire estuary due to deepening of the navigation channel. Overall, Jensen et al. (2003) have calculated an increase of the tidal range by about 1.5 m since 1960 in Papenburg, located around 41 km upstream from Emden (Fig. 4). As a consequence of the changed tidal dynamic, the tidal velocities are increased and the flood phase is shortened (Jürges

and Winkel 2003). Thus, the hydrodynamics changed to an asymmetric, flood dominated tidal system.

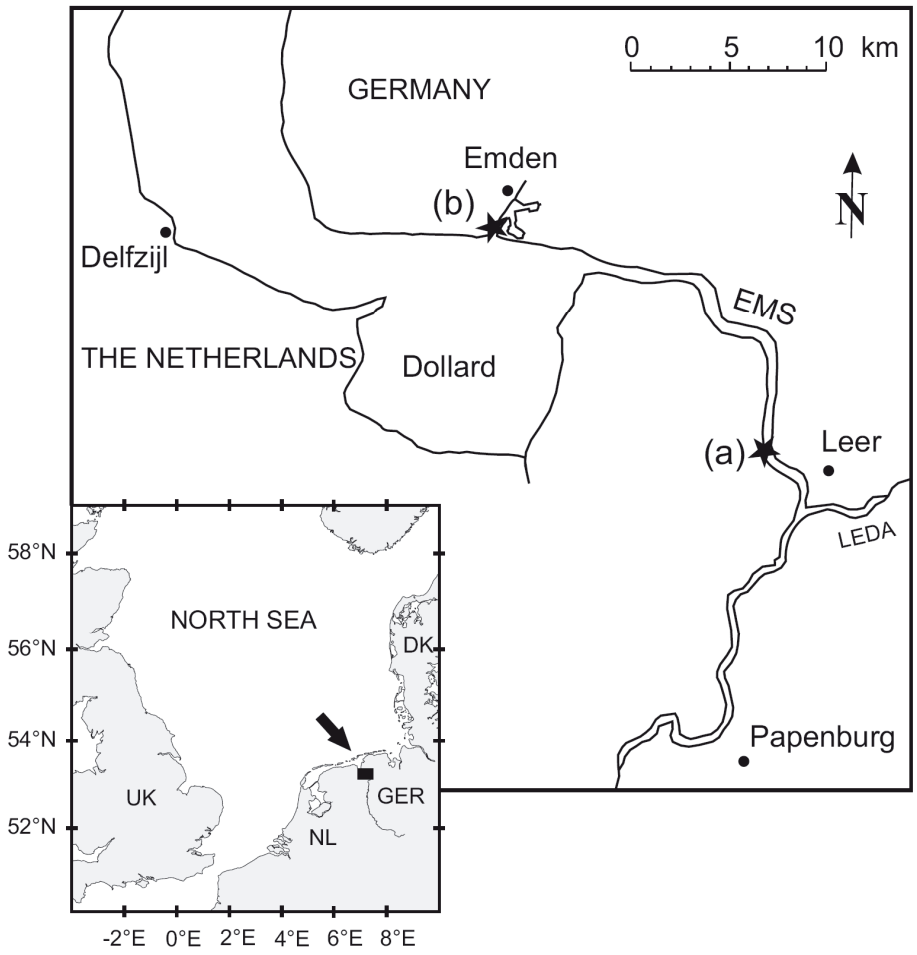

Fig. 4 *Map of the sampling area in the Ems estuary: (a) river km 18 and (b) tide affected outer harbour of Emden. Note the town of Papenburg in the SE of the map. Inset shows overall map of the central North Sea and neighbouring countries.*

The hydrodynamic changes have also altered the morphodynamic system of the Ems estuary. Sediment concentrations in the surface water of the turbidity maximum zone have increased dramatically from about 100 mg/l in 1954 to about 300-400 mg/l in the 1970's and 1980's (de Jonge 1983) up to nowadays of almost 5 g/l during the summer months (Talke and de Swart 2006). Furthermore, the turbidity maximum zone (TMZ) has moved upstream (Wurpts and Torn 2005). Various mechanisms in time and space are responsible for the formation and distribution of the TMZ in estuaries such as

physical, chemical and biological processes, seasonal and tidal variability as well as morphological conditions (e.g. Uncles 2002). However, Spingat and Oumeraci (2000) and Jürges and Winkel (2003) suggest that the extension of the TMZ in the river Ems towards the freshwater zone (Papenburg) during low freshwater inflow is related to the tidal asymmetry which in turn is influenced by anthropogenic changes as described above. Overall, the variable location of the TMZ in the Ems estuary comprises a range of over 30 km (Spingat and Oumeraci 2000).

An increase in turbidity in turn could cause an increase of accumulating sediments on to the bed. In the Ems estuary, particularly near-bed fluid mud layers are formed reaching thicknesses of up to 2 m (Talke and de Swart 2006). Therefore, practical consequences arise such as channel navigability and dredging requirements. In 2004, for example, a high amount of about 8 Mio m³ sediments had to be dredged out of the Ems fairway and estuary to ensure navigability, which cost around 10-15 Mio EUR (Krebs 2006). On the other hand, high concentrations of fluid mud and soft muds could reduce the hydraulic roughness of the estuary and, thus, alter the tidal velocity and propagation (Jürges and Winkel 2003, Gabioux et al. 2005). Additionally, high turbidity also affects the biological system of the Ems estuary as oxygen concentration is decreased by the turbidity and the formation of fluid mud layers in the near–bed zone during slack tides lead to anoxic conditions (Schöl et al. 2006).

3.2 Baltic Sea

The Baltic Sea is the largest brackish water in the world located in Northern Europe and is intensively influenced by human impacts such as shipping, fishing, mining of resources, wind parks, pipelines as well as damping of dredged material. Therefore, characterisation of sediments and processes of sediment dynamic in coastal areas and shallow seas are of increasing interest. The study areas of soft mud deposits discussed in Manuscript 3 are situated in the south-western Baltic Sea, namely Gelting Bay, Eckernförde Bay and Mecklenburg Bay (Fig. 5).

In general, the relatively shallow (average depth 52 m; max. 459 m) and semi-enclosed Baltic Sea is divided in sub-basins formed by Pleistocene glacial erosion processes (Duphorn et al. 1995). A limited water exchange to the North Sea and with it to the

oceans exists in the western part through the narrow Danish straits (Fig. 5). The hydrodynamic and sedimentary processes are heavily influenced by this characteristic. While a surface layer of brackish water discharges in the North Sea, the more saline oxygen-enriched water from the North Sea is moving in the opposite direction due to differences in salinity. However, the water exchange of North and Baltic Sea is also driven by atmospheric-climatic conditions, which will induce differences in the water levels between the Danish straits and the rest of the Baltic Sea (Duphorn et al. 1995). Therefore, from west to east salinity and oxygen supply is decreasing in the basins.

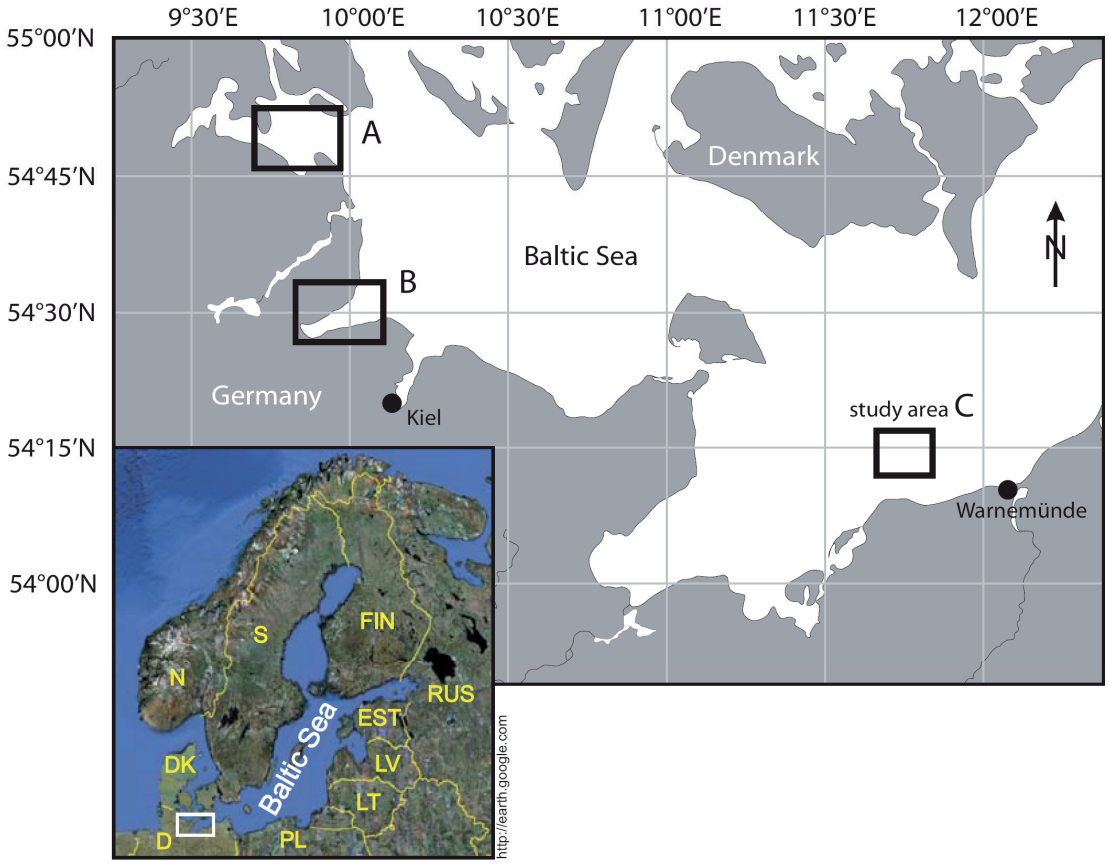

Fig. 5 Map of the south-western Baltic Sea with locations of the study areas Gelting Bay (A), Eckernförde Bay (B) and Mecklenburg Bay (C). *Inset shows overview map of the Baltic Sea and countries surrounding it.*

Furthermore, the inflow of the more saline water from the North Sea builds up a seasonal variable vertical stratification in the water column (halocline). Stagnation of

water inflow from the North Sea could lead to oxygen depletion in the bottom water of the sub-basins (e.g. Duphorn et al. 1995, Orsi et al. 1996). In addition, high supply of organic matter could cause anoxic conditions due to degradation processes. Anoxic conditions implicate not only a reduction in benthic activity but also the occurrence of free gas mainly methane which will be formed during processes of anaerobic decomposition of organic matter (e.g. Crill and Martens 1983, Wilson 2007). The study areas of the south-western Baltic Sea are known for the occurrence of free gas in the shallow sub-surface which is controlled by the amount of organic matter as well as by temperature and pressure variations (Wilkens and Richardson 1998, Heyer and Berger 2000, Wever et al. 2006).

Morphology and nature of sediments in the Baltic Sea are highly variable in space and time and reflect the influence of the complex postglacial development and of multiple transgression and regressions during the evolution of the Baltic Sea (Duphorn et al. 1995). However, recent sedimentation can be generally distinguished by two sedimentation regimes: the basins and the coastal fringes (Duphorn et al. 1995, Lemke 1998, Bobertz 2000). In the shallow coastal areas mainly sandy sediments are dominating, whereas fine-grained mud is found in the deeper basins. Various mixtures of these sediments could occur depend on the interrelation of morphology, waves and currents. Additionally, coarse clastic residual sediments are found in high energetic areas where the fine-grained sediment was eroded and removed by waves and currents.

The accumulation of mud in the basins of the Baltic Sea started at around 8.000 years BP during the stage known as Littorina transgression where a permanent link to the ocean was established and hence, induced currents could supply mud to the deeper basins (Duphorn et al. 1995). The lower boundary of the mud layer can be clearly differentiated in seismic profiles and core data thus, enabling the calculation of accumulation rates. The accumulation of mud may be strongly variable in the sub-basins, but an average rate of 1 – 1.5 mm per year could be determined by Duphorn et al. 1995. However, local areas exhibit higher sedimentation rates as known for example from Eckernförde Bay, one of the study area in this thesis, revealing a mean accumulation rate of 3.9 mm per year (Nittrouer et al. 1998) and even locally rating up to 10 mm per year (Bentley et al. 1996). The mud deposits of the study areas reach thicknesses of 7 m in Mecklenburg Bay (water depth up to 26 m; Niedermeyer 1987)

and even 8 m in Eckernförde Bay (water depth up to 30 m; Orsi et al. 1996). The main source for the surface sediments is glacial till eroded from the coast and shallow water areas (Gingele and Leipe 1997 and references therein). Moreover, strong currents generated during storm events could deposit sequences of distinct sediment layers with slightly coarser grain size than adjacent sediments in the central basin which will be interbedded in the soft mud (Milkert 1994).

4 CONE PENETROMETER TESTING (CPT)

4.1 Introduction to cone penetrometer testing

Cone penetration tests (CPT) are widely used to determine physical and mechanical properties of sediment layers in onshore and offshore settings. Since the 1930s the method became the most versatile among the vast number of *in situ* tools for soil exploration. A 60° cone, with a 10 or 15 cm² base area, on the end of rods is moved into the sediment (Fig. 6). In the meantime the resistance to penetration of the cone and sleeve will be continuously measured usually by strain gauge load cells. Moreover, piezocone penetrometers (CPTU) simultaneously measure even the pore pressure typically on the cone (u_1), behind the cone (u_2) and / or behind the friction sleeve (u_3) as shown in Fig. 6. With the parameters derived the user is able not only to identify the sediment stratigraphy, but also to classify the sediment and even derive secondary parameters such as undrained shear strength and permeability. For further information of cone penetration tests and their interpretation the reader is referred to Lunne et al. (1997).

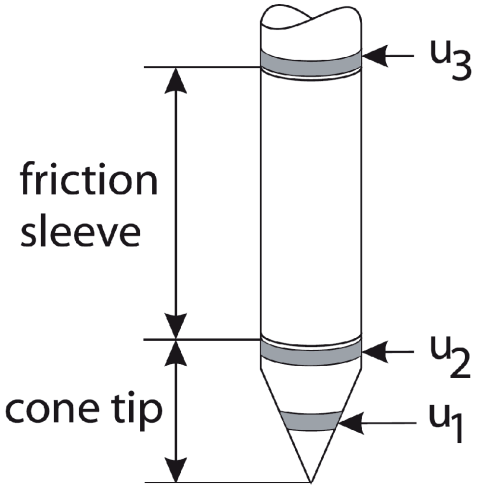

Fig. 6 Schematic sketch of a standard CPTU cone and the typical locations of the piezo-elements.

Standard tests are carried out by pushing the lance into the sediment at a constant rate of 2 cm/s. Heavy hydraulic platforms are needed for efficient pushing. Especially in

offshore settings heavy seabed rigs of the CPTU equipment are difficult to operate and could disturb the sediments being investigated. Therefore, dynamic penetrometers have been developed, which will be lowered at rates higher than 2 cm/s up to free fall through the water column and when it penetrates the sediment the instrument decelerates until certain depth (e.g. Elsworth and Lee 2005; Osler et al. 2006; Stoll et al. 2007; Stegmann 2007). The enhanced impact velocity affects both the initial peak of cone resistance as well as the pore pressure measurement. The former can be accounted for by introducing stress-strain factors for different materials (e.g. Dayal and Allen 1975; Roy et al. 1982), while the latter requires time for the pore pressure value to equilibrate to its ambient value. Stoll and Sun (2005) and Stoll et al. (2007) compared results of quasi-static and dynamic penetrometers, and concluded that the latter accentuates excursions in the data profile. However, dynamic CPTU devices become more and more an effective alternative to the standard tests.

Nevertheless, there is still a lack of knowledge in interpretation of dynamic CPT/CPTU data and especially investigation of soft sediments where standard CPTU operations with heavy rigs are not practicable. Innovative dynamic CPTU pore pressure measurements of soft mud containing partially free gas will be discussed in Manuscript 3. Also, as mentioned in the chapters above, new *in situ* methods for fluid mud detection are in great demand. Therefore, as a new approach this thesis is concentrating on the development of a method to detect fluid mud by a dynamic CPTU (Manuscript 2), designed at MARUM (Center for Marine Environmental Sciences), University of Bremen (Fig. 7).

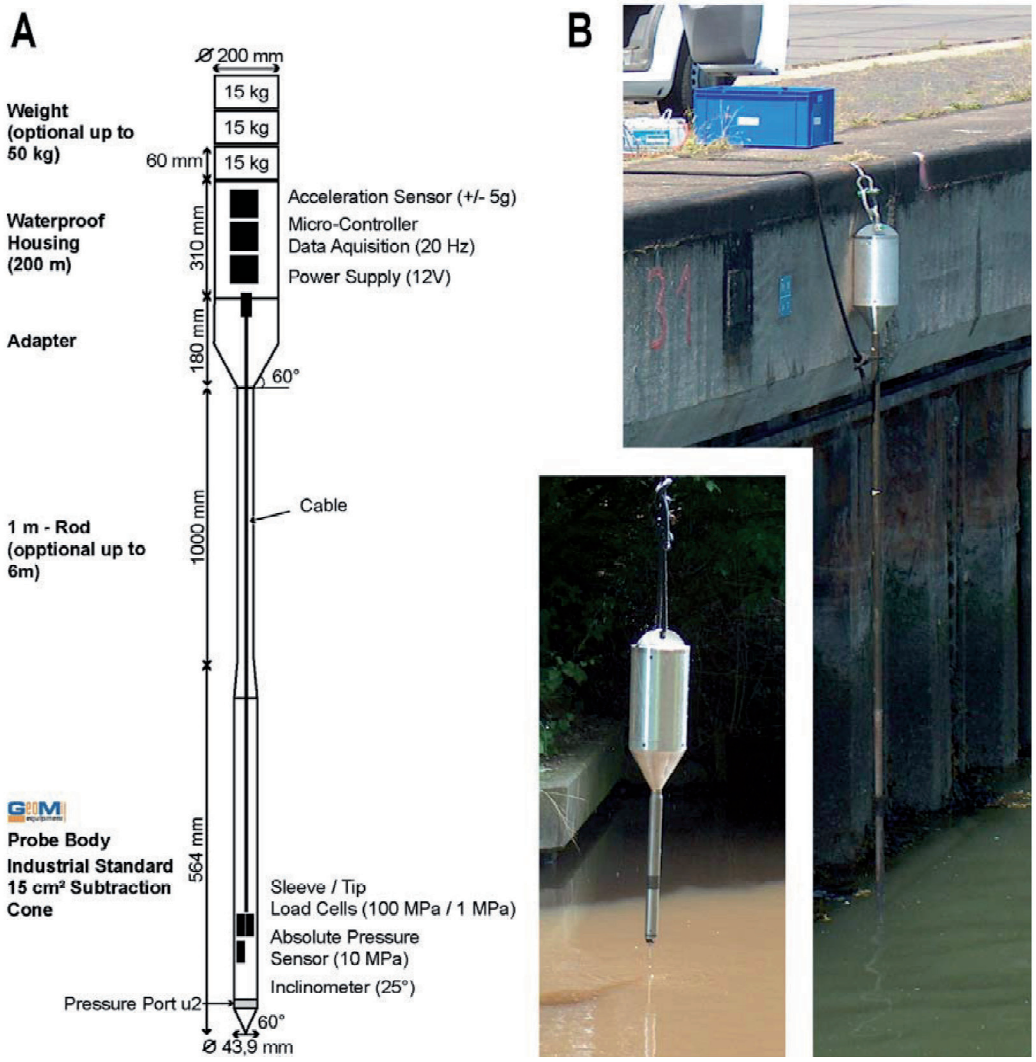

Fig. 7 A) schematic diagram of the dynamic CPTU designed at MARUM (Center for Marine Environmental Sciences), B) Photos of the CPTU with different configuration (5-m long and short version without extension rods); after Stegmann 2007.

4.2 Research progress to detect soft and fluid mud by dynamic CPTU

In 2005 a dynamic piezocone penetrometer (CPTU) measuring *in situ* pore pressure and strength of sediments was designed at MARUM (for details see Stegmann et al. 2006, Fig. 7). The modular lance was used in several studies to characterise marine sediments (the reader is referred to Stegmann 2007). However, it was not yet deployed to characterise soft cohesive sediments or even fluid mud suspensions, but showed the potential to be a practicable and efficient way for testing these types of sediment.

During two research cruises in January and March 2006 in the Baltic Sea the CPTU proved to be a versatile and fast instrument to characterise soft cohesive sediments. The results are discussed in Manuscript 3.

Intensive talks with the Federal Waterways Engineering and Research Institute (BAW) of Germany in Hamburg and with the Waterways and Shipping Administration of Emden (WSA Emden) at the beginning of this thesis led to the conclusion that there is a great demand on research of soft cohesive sediments in waterways, in particular fluid mud. Authorities were looking for a reliable and efficient system to detect and characterise FM in the waterways and harbours to reduce the rising dredging costs. At that time standard acoustic depth sounders were used to detect the nautical depth in the Ems estuary, which was very unsatisfactory as the signals only showed density gradients and not a specific density. Furthermore, the interpretation of the acoustic signals strongly depended on the interpreter and it was not possible to define specific physical properties of the mud such as different densities and viscosities (Liebetruth 2004). Consequently, research should concentrate on the physical properties, in particular the rheological behaviour of fluid mud. Moreover, special *in situ* survey technique to define navigable depth by non-acoustical criteria should be developed. In this context, the research of this thesis was not only concentrated on *in situ* characterisation of soft cohesive sediments, but also on *in situ* FM detection.

In situ detection of fluid mud suspension using a CPTU-device is a great challenge as it was never tested before. Nevertheless, research in modification of the lance and of the mode of deployment as well as a development of new data analyses led finally to a success. The research progress will be explained in the following (see also flow chart, Fig. 9):

In the beginning of this thesis several CPTU measurements in fluid mud suspensions were carried out. Unfortunately, at these times the suspended sediment concentration near the bed of the river Ems was beyond the instrument‘s resolution. Simultaneously we designed a disk (25 cm across), which was temporarily replacing the cone in the frontal part to enhance the sensitivity of the instrument to fluid mud (Fig. 8).

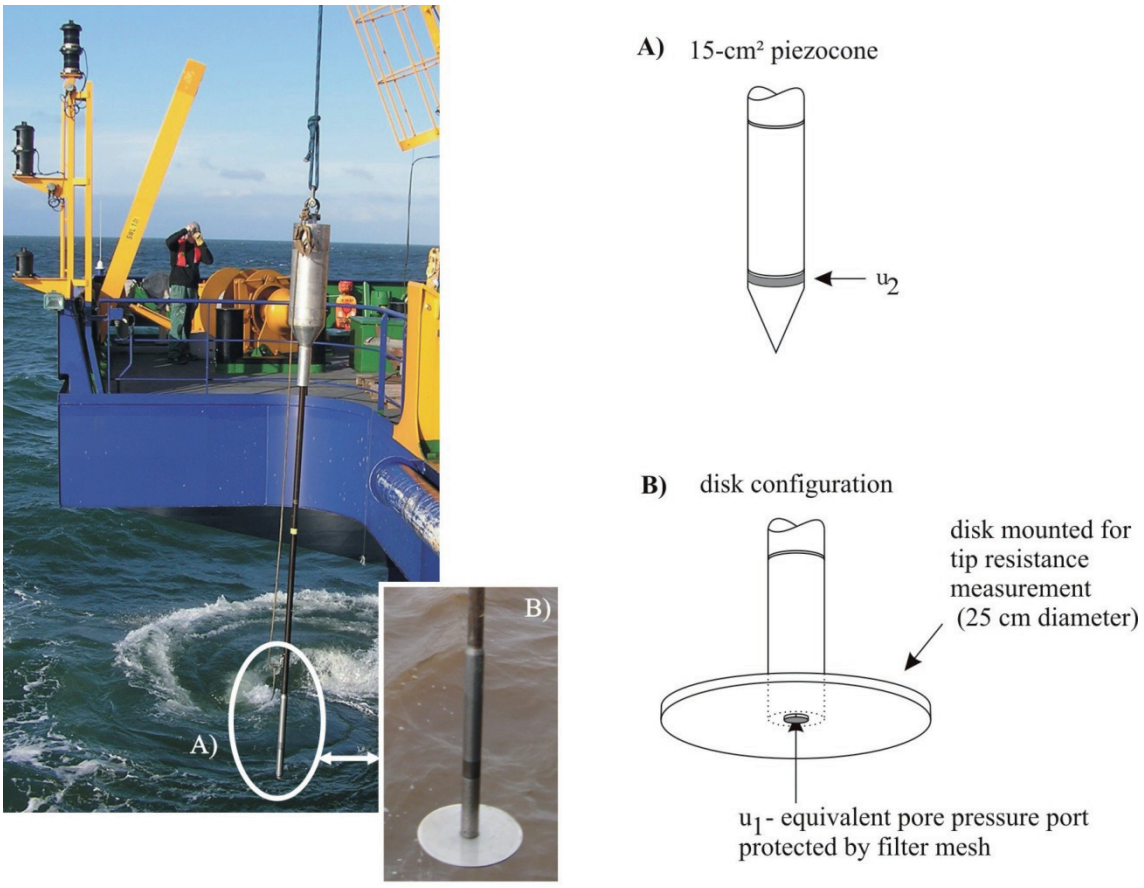

Fig. 8 Configuration of dynamic CPTU deployment: A) 15-cm² piezocone deployed for soft consolidated mud and fluid mud, B) disk configuration deployed for fluid mud detection.

The configurations of the CPTU probe both cone and disk were tested in the harbour of Emden (adjacent to the river Ems; Figs. 4, 8). The dynamic CPTU was veered continuously by a winch through the water column, impacted the bottom, and penetrated the sediment. The raw data was standardised further processed as it was done for the data of the consolidated sediments e.g. Baltic Sea. Unfortunately, no fluid mud could be detected by the CPTU although the ship echo sounder showed a thick fluid layer. At that time it was believed that maybe the method of veering from continuously to stepwise lowering of the lance has to be changed for possible detection (see flow chart in Fig. 9 and Table in Appendix A1).

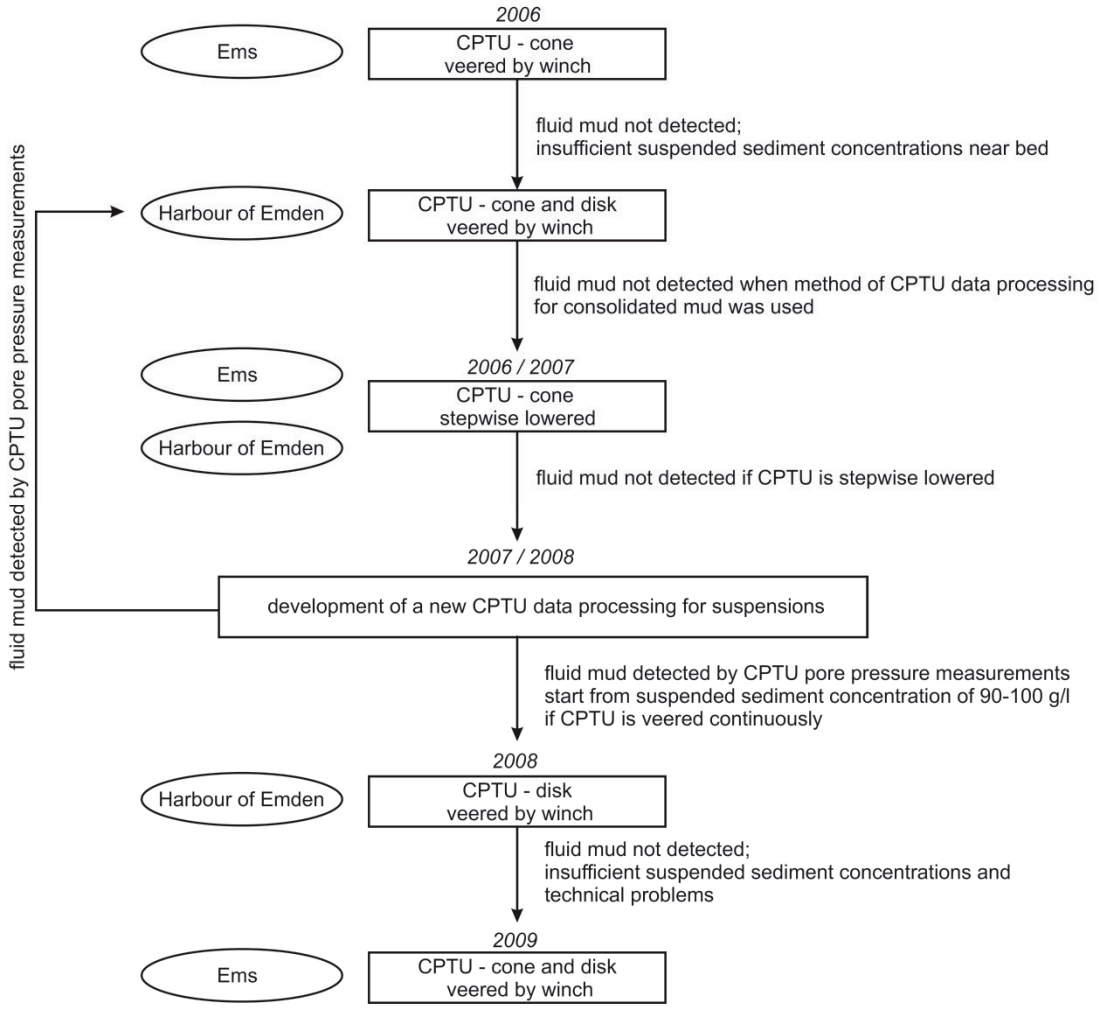

Fig. 9 Flow chart of the research progress to detect *in situ* fluid mud by CPTU measurements in the river Ems and in the harbour of Emden *(see also Table in Appendix A1)*.

The method of stepwise lowering was chosen because fluid mud consists of a network of flocs (see Chapter 2). The particles are fluid-supported thus the pore pressure could be higher than the hydrostatic pressure. It was conceivable that there is a possibility to detect the elevated pore pressure by the CPTU-device. Therefore, the lance was veered in 20 to 30 cm steps while at each depth the lance was left for around 5 minutes to measure the ambient pressure. However, several deployments in 2006 and 2007 showed that it was not possible to detect fluid mud by this method. The pore pressure was maybe too low for the detection by the CPTU.

During the course of this research it was further found that the CPTU data analysing might have to be modified for fluid mud deployment data. Usually the sediment

penetration depth of the dynamic CPTU-instrument is determined via twofold integration of the acceleration data, which is measured by sensors mounted in the lance. However, in fluid mud suspensions the acceleration sensors will not detect changes as the resistance of the suspensions is still too low to measurably decelerate the lance. Hence, the deployment of the CPTU in suspension required new data processing. In 2007/2008 a new way of determining the penetration depth by pressure changes was developed. The approach of detecting the impact using excess pore pressure curves (difference between absolute pore pressure and hydrostatic pressure) was followed, which occur when the properties of the FM suspension has changed compared to water. That point could be used as the beginning of the impact of the CPTU in fluid mud and sediment underlying it. The already obtained CPTU data in 2006 had to be recalculated and results attested that indeed fluid mud was detected by the CPTU-device. Also it was found out that veering of the lance with constant velocity was the proper method.

It could be concluded that fluid mud is detectable by dynamic CPTU-devices if the lance is veered continuously and if the concentration of the fluid mud is sufficiently high to develop an excess pore pressure signal during the impact of the lance. In Manuscript 2 further discussion on fluid mud detection by CPTU is presented.

REFERENCES

Abril, G., Riou, S. A., Etcheber, H., Frankignoulle, M., de Wit, R., and Middelburg, J. J. (2000). "Transient, Tidal Time-scale, Nitrogen Transformations in an Estuarine Turbidity Maximum-Fluid Mud System (The Gironde, South-west France)." *Estuarine, Coastal and Shelf Science*, 50(5), 703-715.

Aijaz, S., and Jenkins, S. (1994). "On the electrokinetics of shear stress behaviour in fluid-mud suspensions." *Journal of Geophysical Research*, 99(C6), 12,697-12,706.

Anderson, A. L., Abegg, F., Hawkins, J. A., Duncan, M. E., and Lyons, A. P. (1998). "Bubble populations and acoustic interaction with the gassy floor of Eckernförde Bay." *Continental Shelf Research*, 18(14-15), 1807-1838.

Arulrajah, A., Nikraz, H., and Bo, M. W. (2005). "In-situ testing of Singapore marine clay at Changi." *Geotechnical and Geological Engineering,* 23, 111-130.

Bentley, S. J., Nittrouer, C. A., and Sommerfield, C. K. (1996). "Development of sedimentary strata in Eckernförde Bay, southwestern Baltic Sea." *Geo-Marine Letters*, 16(3), 148-154.

Berlamont, J., and Toorman, E. (editors) (2000). "COSINUS Final Scientific Report." Hydraulics Laboratory, K.U. Leuven.

Berlamont, J., Ockenden, M., Toorman, E., and Winterwerp, J. (1993). "The characterisation of cohesive sediment properties." *Coastal Engineering*, 21(1-3), 105-128.

Black, K. S., Tolhurst, T. J., Paterson, D. M., and Hagerthey, S. E. (2002). "Working with Natural Cohesive Sediments." *Journal of Hydraulic Engineering*, 128(2), 2-8.

Bobertz, B. (2000). "Regionalisierung der sedimentären Fazies der südwestlichen Ostsee," Ph.D. Thesis, Ernst-Moritz-Arndt-Universität Greifswald, Greifswald.

Brandes, H. G. (1999). "Predicted and Measured Geotechnical Properties of Gas-Charged Sediments." *International Journal of Offshore and Polar Engineering,* 9(3), 219-225.

Bruens, A. (2003). "Entraining mud suspensions," Ph.D. Thesis, Delft University of Technology, Delft.

Coussot, P. (1997). *Mudflow Rheology and Dynamics*, A.A. Balkema, Rotterdam.

Crill, P. M., and Martens, C. S. (1983). "Spatial and temporal fluctuations of methane production in anoxic coastal marine sediments." *Limnology and Oceanography*, 28(6), 1117-1130.

Dayal, U., and Allen, J. H. (1975). "The Effect of Penetration Rate on the Strength of Remolded Clay and Sand Samples." *Canadian Geotechnical Journal*, 12, 336-348.

de Jonge, V. N. (1983). "Relations between annual dredging activities, suspended matter concentrations, and the development of the tidal regime in the Ems Estuary." *Canadian Journal of Fisheries and Aquatic Sciences*, 40(1), 289-300.

Dankers, P. J. T., and Winterwerp, J. C. (2007). "Hindered settling of mud flocs: Theory and validation." *Continental Shelf Research*, 27(14), 1893-1907.

Delefortrie, G., Vantorre, M., and Eloot, K. (2005). "Modelling navigation in muddy areas through captive model tests." *Journal of Marine Science and Technology,* 10(4), 188-202.

Duphorn, K., Kliewe, H., Niedermeyer, R.-O., Janke, W., and Werner, F. (eds.) (1995). *Die deutsche Ostseeküste*, Gebrüder Borntraeger, Berlin, Sammlung geologischer Führer 88.

Dyer, K. R., Christie, M. C., and Manning, A. J. (2004). "The effects of suspended sediment on turbulence within an estuarine turbidity maximum." *Estuarine, Coastal and Shelf Science*, 59(2), 237-248.

Elsworth, D., and Lee, D. S. (2005). "Identation of a free-falling lance penetrometer into a poroelastic seabed." *Int. J. Numer. Anal. Meth. Geomech.*, 29, 141-162.

Faas, R. W. (1995). "Mudbanks of the Southwest Coast of India III: Role of Non-Newtonian Flow Properties in the Generation and Maintenance of Mudbanks." *Journal of Coastal Research,* 11(3), 911-917.

Faas, R., and Wartel, S. (2006). "Rheological properties of sediment suspensions from Eckernförde and Kieler Förde Bays, western Baltic Sea." *International Journal of Sediment Research*, 21(1), 24-41.

Fleischer, P., Orsi, T. H., Richardson, M. D., and Anderson, A. L. (2001). "Distribution of free gas in marine sediments: a global overview." *Geo-Marine Letters*, 21(2), 103-122.

Fontein, W., Werner, C., and van der Wal, J. "Assessing nautical depth efficiently in terms of rheological characteristics." *Proceedings of the 15th International Congress of the International Federation of Hydrographic Societies: Evolution in hydrography, 6th-9th November 2006, Provincial House Antwerp, Belgium*, 149-152.

Friedrichs, C. T., Wright, L. D., Hepworth, D. A., and Kim, S. C. (2000). "Bottom-boundary-layer processes associated with fine sediment accumulation in coastal seas and bays." *Continental Shelf Research,* 20(7), 807-841.

Gabioux, M., Vinzon, S. B., and Paiva, A. M. (2005). "Tidal propagation over fluid mud layers on the Amazon shelf." *Continental Shelf Research*, 25, 113-125.

Gingele, F. X., and Leipe, T. (1997). "Clay mineral assemblages in the western Baltic Sea: recent distribution and relation to sedimentary units." *Marine Geology*, 140, 97-115.

Greiser, N., Gamnitzer, R., and Rupp, J. (2002). "Pseudoplasticity of Cohesive Sediments: Causes and Innovative Techniques for Pre-Dredging Surveys." *Proceedings of CEDA (Central Dredging Association) Dredging Days 2002: Dredging without boundaries.* Casablanca, Morocco.

Guan, W. B., Kot, S. C., and Wolanski, E. (2005). "3-D fluid-mud dynamics in the Jiaojiang Estuary, China." *Estuarine, Coastal and Shelf Science*, 65, 747-762.

Heyer, J., and Berger, U. (2000). "Methane Emission from the Coastal Area in the Southern Baltic Sea." *Estuarine, Coastal and Shelf Science*, 51(1), 13-30.

Jain, M., and Mehta, A. J. (2009). "Role of basic rheological models in determination of wave attenuation over muddy seabeds." *Continental Shelf Research*, 29(3), 642-651.

Jensen, J., Mudersbach, C., and Blasi, C. (2003). "Hydrological changes in tidal estuaries due to natural and anthropogenic effects." *Proceedings of the 6. International MEDCOAST 2003 Conference*, Ravenna, Italy.

Jürges, J., and Winkel, N. (2003). "Ein Beitrag zur Tidedynamik der Unterems." *Mitteilungsblatt der Bundesanstalt für Wasserbau (BAW)*, 29-31.

Kirby, R. (1988). "High Conentration Suspension (Fluid Mud) Layers in Estuaries." *Physical Processes in Estuaries*, J. Dronkers and W. van Leussen, eds., Springer-Verlag, Berlin,Heidelberg, 463-487.

Krebs, M. (2006). "Gewässerkundliche Aspekte zur Optimierung der Unterhaltungsbaggerungen im Emsästuar." *BAW/BfG - Kolloquium: Erfahrungsaustausch zur Untersuchung und Einschätzung von Transportprozessen in Ästuaren und Wattgebieten und zum Sedimentmanagement in Tidegewässern 8./9.11.2006*, Hamburg.

Krone, R. B. (1986). "The significance of aggregate properties to transport processes." *Proceedings of a Workshop on Estuarine Cohesive Sediment Dynamics, November 12-14, 1984, Tampa, Florida*, A. J. Mehta, ed., Springer-Verlag, Berlin, 66-84.

Lee, K.-M., and Ng, P. C. C. (1999). "A geotechnical investigation of marine deposits in a nearshore seabed for land reclamation." *Canadian Geotechnical Journal*, 36, 981-1000.

Lefebvre, J. P., Dolique, F., and Gratiot, N. (2004). "Geomorphic evolution of a coastal mudflat under oceanic influences: an example from the dynamic shoreline of French Guiana." *Marine Geology,* 208, 191-205.

Lemke, W. (1998). "Sedimentation und paläogeographische Entwicklung im westlichen Ostseeraum (Mecklenburger Bucht bis Arkonabecken) vom Ende der Weichelvereisung bis zur Litorinatransgression." Postdoctoral Thesis. Institut für Ostseeforschung Warnemünde, Warnemünde.

Lesourd, S., Lesueur, P., Brun-Cottan, J. C., Garnaud, S., and Poupinet, N. (2003). "Seasonal variations in the characteristics of superficial sediments in a macrotidal estuary (the Seine inlet, France)." *Estuarine, Coastal and Shelf Science*, 58(1), 3-16.

Liebetruth, F. (2004). "Ermittlung der Nautischen Sohle Ems km 47,3 bis km 48,1 - Stellungnahme zu den geotechnischen, rheologischen und Echolot - Vergleichsuntersuchungen vom 08. bis 10. September 2003." *BAW 0250110107*, unpublished.

Lunne, T., Robertson, P. K., and Powell, J. J. M. (1997). *Cone Penetration Testing in Geotechnical Practice*, E & FN Spon, London and New York.

McAnally, W. H., and Mehta, A. J. (2002). "Significance of Aggregation of Fine Sediment Particles in Their Deposition." *Estuarine, Coastal and Shelf Science*, 54(4), 643-653.

McAnally, W. H., Friedrichs, C., Hamilton, D., Hayter, E., Shrestha, P., Rodriguez, H., Sheremet, A., and Teeter, A. M. (2007a). "Management of Fluid Mud in Estuaries, Bays, and Lakes. I: Present State of Understanding on Character and Behavior." *Journal of Hydraulic Engineering*, 133(1), 9-22

McAnally, W. H., Teeter, A. M., Schoellhamer, D. H., Friedrichs, C., Hamilton, D., Hayter, E., Shrestha, P., Rodriguez, H., Sheremet, A., and Kirby, R. (2007b). "Management of Fluid Mud in Estuaries, Bays, and Lakes. II: Measurements, Modeling, and Management." *Journal of Hydraulic Engineering*, 133(1), 23-28.

Mehta, A. J. (1991). "Understanding Fluid Mud in a Dynamic Environment." *Geo-Marine Letter*, 11(3-4), 113-118.

Merckelbach, L. M. (2000). "Consolidation and strength evolution of soft mud layers," Ph.D. Thesis, Technical University of Delft, Delft.

Merckelbach, L. M., and Kranenburg, C. (2004). "Determining effective stress and permeability equations for soft mud from simple laboratory experiments." *Géotechnique*, 54(9), 581-591.

Milkert, D. (1994): "Auswirkungen von Stürmen auf die Schlicksedimente der westlichen Ostsee. (Influences of storms on muddy sediments in the western Baltic Sea)." *Berichte/Reports Geologisches Paläontologisches Institut, no 66*, Universität Kiel, Kiel.

Møller, P. C. F., Mewis, J., and Bonn, D. (2006). "Yield stress and thixotropy: on the difficulty of measuring yield stresses in practice." *Soft Matter*, 2, 274-283.

Niedermeyer, R.-O. (1987). "Beiträge zur komplexen Untersuchung von rezenten Sedimentationsprozessen in Schlickgebieten der westlichen und mittleren Ostsee," Ph.D. Thesis, Ernst-Moritz-Arndt-Universität Greifswald, Greifswald.

Nittrouer, C. A., Lopez, G. R., Donelson Wright, L., Bentley, S. J., D'Andrea, A. F., Friedrichs, C. T., Craig, N. I., and Sommerfield, C. K. (1998). "Oceanographic processes and the preservation of sedimentary structure in Eckernförde Bay, Baltic Sea." *Continental Shelf Research*, 18(14-15), 1689-1714.

Nguyen, Q. D., Akryd, T., de Kee, D. C., and Zhu, L. (2006). "Yield stress measurements in suspensions: an inter-laboratory study." *Korea-Australia Rheology Journal*, 18(1), 15-24.

O'Brien, J. S., and Julien, P. Y. (1988). "Laboratory Analysis of Mudflow Properties." *Journal of Hydraulic Engineering*, 114(8), 877-887.

Orsi, T. H., Werner, F., Milkert, D., Anderson, A. L., and Bryant, W. R. (1996). "Environmental overview of Eckernförde Bay, northern Germany." *Geo-Marine Letters*, 16(3), 140-147.

Osler, J., Furlong, A., Christian, H., and Lamplugh, M. (2006). "The integration of the Free Fall Cone Penetrometer (FFCPT) with the Moving Profiler (MVP) for the rapid assessment of seabed characteristics." *Canadian Hydrographic Conference 2006*, Halifax.

Randolph, M. F., Cassidy, M., Gourvenec, S., and Erbrich, C. (2005). "Challenges of Offshore Geotechnical Engineering." *16th International conference on soil mechanics and geotechnical engineering,* Osaka, Japan, 1-54.

Reed, A. H., Faas, R. W., Allison, M. A., Calliari, L. J., Holland, K. T., O'Reilly, S. E., Vaughan, W. C., and Alves, A. (2009). "Characterization of a mud deposit offshore of the Patos Lagoon, southern Brazil." *Continental Shelf Research*, 29(3), 597-608.

Roy, M., Tremblay, M., Tavenas, F., and La Rochelle, P. (1982). "Development of pore pressures in quasi-static penetration tests in sensitive clay." *Canadian Geotechnical Journal*, 19, 124-138.

Schlue, B. (2008). "Beneficial on-site reuse of dredged harbor mud: A geotechnical challenge in alternative sediment management," Ph.D., University of Bremen, Bremen.

Schöl, A., Günster, C., Krings, W., Kirchesch, V., and Rätz, W. (2006). "Zusammenhänge zwischen Sauerstoffhaushalt und Schwebstoffverteilung in der Unterems, Naturmessungen und Laboruntersuchungen." *BAW/BfG - Kolloquium: Erfahrungsaustausch zur Untersuchung und Einschätzung von Transportprozessen in Ästuaren und Wattgebieten und zum Sedimentmanagement in Tidegewässern 8./9.11.2006*, Hamburg.

Shi, Z., and Kirby, R. (2003). "Observations of Fine Suspended Sediment Processes in the Turbidity Maximum at the Northern Passage of the Changjiang Estuary, China." *Journal of Coastal Research*, 19(3), 529-540.

Sills, G. (1998). "Development of structure in sedimenting soils." *Philosophical Transactions of the Royal Society A: Mathematical, Physical and Engineering Sciences*, 356(1747), 2515-2534.

Sills, G., and Elder, D. M. (1986). "The transition from sediment suspension to settling bed." *Proceedings of a Workshop on Estuarine Cohesive Sediment Dynamics*, *November 12-14, 1984*, Tampa, Florida, A. J. Mehta, ed., Springer-Verlag, Berlin, 192-205.

Sills, G. C., Wheeler, S. J., Thomas, S. D., and Gardner, T. N. (1991). "Behaviour of offshore soils containing gas bubbles." *Géotechnique*, 41(2), 227-241.

Slowey, N. C., Bryant, W. R., and Lambert, D. N. (1996). "Comparison of high-resolution seismic profiles and the geoacoustic properties of Eckernförde Bay sediments." *Geo-Marine Letters*, 16(3), 240-248.

Stegmann, S. (2007). "Design of a free-fall penetrometer for geotechnical characterisation of saturated sediments and its geological application," Ph.D. Thesis, University of Bremen, Bremen.

Stegmann, S., Villinger, H., and Kopf, A. (2006). "Design of a Modular, Marine Free-Fall Cone Penetrometer." *Sea Technology*, 47(2), 27-33.

Stoll, R. D., and Sun, Y.-F. (2005). "Using Penetrometer to Measure Sea Bed Properties." *Coastal Geosciences: Annual Reports: FY05*, Office of Naval Research, Science & Technology, Ocean Battlespace Sensing (32).

Stoll, R. D., Sun, Y.-F., and Bitte, I. (2007). "Seafloor Properties From Penetrometers Tests." *IEEE Journal of Oceanic Engineering*, 32(1), 57-63.

Soltanpour, M., and Haghshenas, S. A. (2009). "Fluidization and representative wave transformation on muddy beds." *Continental Shelf Research*, 29(3 (On the dynamics of mud deposits in coastal areas)), 666-675.

Talke, S. A., and de Swart, H. E. (2006). "Hydrodynamics and Morphology in the Ems/Dollard Estuary: Review of Models, Measurements, Scientific Literature, and the Effects of Changing Conditions." *IMAU Report #R06-01*, Institute for Marine and Atmospheric Research Utrecht (IMAU), University of Utrecht.

Teeter, A. M. (1992). "Evaluation of new fluid mud survey system at field sites." *Dredging Research Technical Notes DRP-2-04*, US Army Engineer Waterways Experiment Station, Vicksburg, MS.

Terzaghi, K., and Peck, R. B. (1948). *Soil Mechanics in Engineering Practice*, John Wiley and Sons, New York.

Tolhurst, T. J., Gust, G., and Paterson, D. M. (2002). "The influence of an extracellular polymeric substance (EPS) on cohesive sediment stability." *Fine Sediment Dynamics in the Marine Environment*, J. C. Winterwerp and C. Kranenburg, eds., Elsevier Science B.V., 409-425.

Toorman, E. A. (1996). "Sedimentation and self-weight consolidation: general unifying theory." *Géotechnique*, 46(1), 103-113.

Toorman, E. A. (1997). "Modelling the thixotropic behaviour of dense cohesive sediment suspensions." *Rheologica Acta*, 36(1), 56-65.

Toorman, E., Bruens, A., Kranenburg, C., and Winterwerp, J. C. (2002). "Interaction of suspended cohesive sediment and turbulence." Fine Sediment Dynamics in the Marine Environment, J. C. Winterwerp and C. Kranenburg, eds., Elsevier Science B.V., 7-23.

Uncles, R. J. (2002). "Estuarine Physical Processes Research: Some Recent Studies and Progress." *Estuarine, Coastal and Shelf Science*, 55(6), 829-856.

Uncles, R. J., Stephens, J. A., and Law, D. J. (2006). "Turbidity maximum in the macrotidal, highly turbid Humber Estuary, UK: Flocs, fluid mud, stationary suspensions and tidal bores." *Estuarine, Coastal and Shelf Science,* 67, 30-52.

van Kessel, T., and Blom, C. (1998). "Rheology of cohesive sediments: comparison between a natural and an artificial mud." *Journal of Hydraulic Research*, 36(4), 591-602.

van Leussen, W. (1988). "Aggregation of Particles, Settling Velocity of Mud Flocs: A review." *Physical Processes in Estuaries*, J. Dronkers and W. van Leussen, eds., Springer-Verlag, Berlin,Heidelberg, 348-403.

Velde, B. (ed.) (1995). *Origin and Mineralogy of Clays - Clays and the Environment*, Springer-Verlag, Berlin Heidelberg.

Wever, T. F., Lühder, R., Voß, H., and Knispel, U. (2006). "Potential environmental control of free shallow gas in the seafloor of Eckernförde Bay, Germany." *Marine Geology*, 225, 1-4.

Whitehouse, R., Soulsby, R., Roberts, W., and Mitchener, H. (2000). *Dynamics of esturine muds - A manual for practical applications*, HR Wallingford Limited and Thomas Telford Limited.

Wichman, B. G. H. M., Sills, G. C., and Gonzalez, R. (2000). "Experimental validation of a finite strain theory for gassy mud." *Canadian Geotechnical Journal*, 37, 1227-1240.

Widdows, J., and Brinsley, M. (2002). "Impact of biotic and abiotic processes on sediment dynamics and the consequences to the structure and functioning of the intertidal zone." *Journal of Sea Research*, 48(2), 143-156.

Wilkens, R. H., and Richardson, M. D. (1998). "The influence of gas bubbles on sediment acoustic properties: in situ, laboratory, and theoretical results from Eckernförde Bay, Baltic Sea." *Continental Shelf Research*, 18, 1859-1892.

Wilson, S. T. (2007). "The production of biogenic gases in the marine environment," Ph.D. Thesis, UHI Millennium Institute, Oban, UK.

Winterwerp, H. (1999). "On the dynamics of high-concentrated mud suspensions." *Report No.99.3*, TU Delft, Faculty of Civil Engineering and Geosciences, Delft.

Winterwerp, J. C., and van Kesteren, W. (2004). *Introduction to the physics of cohesive sediment in the marine environment*, Elsevier B.V., Amsterdam.

Winterwerp, J. C., de Graaff, R. F., Groeneweg, J., and Luijendijk, A. P. (2007). "Modelling of wave damping at Guyana mud coast." *Coastal Engineering*, 54, 249-261.

Wotton, R. S. (2004). "The ubiquity and many roles of exopolymers (EPS) in aquatic systems." *Scientia Marina*, 68(S1), 13-21.

Wurpts, R., and Torn, P. (2005). "15 Years Experience with Fluid Mud: Definition of the Nautical Bottom with Rheological Parameters." *Terra et Aqua*, 99, 22-32.

Zaldívar, J. M., Cardoso, A. C., Viaroli, P., Newton, A., de Wit, R., Ibañez, C., Reizopoulou, S., Somma, F., Razinkovas, A., Basset, A., Holmer, M., and Murray, C. N. (2008). "Eutrophication in Transitional waters: An overview." *Transitional Waters Monographs 2008*, 2, 1-78.

MANUSCRIPT 1

Rheological characteristic of natural fluid mud and the influence of different parameter

Annedore Seifert, Achim Kopf

MARUM - Center for Marine Environmental Sciences, University of Bremen, P.O. Box 330440, 28334 Bremen, Germany

In review, *Applied Rheology*

Abstract

The rheological behaviour of fluid mud suspensions from the German river Ems and its adjacent harbour of Emden is examined regarding the potential influence of various parameters on their rheology. Therefore, physical properties of fluid mud suspensions with suspended sediment concentrations (SSC) between 100 g/l and 200 g/l are determined. All fluid mud suspensions tested exhibit non-Newtonian shear thinning behaviour whereby the shear stress is increasing with rising SSC for a particular shear rate. Comparing the samples from both locations, the suspensions of the river Ems reveal around 23 % higher shear stress than the suspensions from the harbour of Emden with the same SSC. For example, the yield stress of the river sample with SSC of 180 g/l is 1.7 times higher than the suspension of the harbour while the viscosity at the yield point is 3 times higher. Because of small variations in grain size distribution, with ~77 % silt as the main fraction, and in mineral composition of the samples from both locations, these parameters are concluded to be insignificant determinants of the different rheological behaviour. Similarly, oxygen content is found to be close to zero in all fluid mud samples. Instead, variations in salinity, type of organic matter, and floc strength are determined to significantly influence the rheological behaviour of the fluid mud suspensions.

Keywords: Fluid mud; Rheology; Shear thinning; Yield stress; Ems; Harbour of Emden

Introduction

Fluid mud suspensions have been observed in many estuarine and nearshore continental shelf environments [1, 2, 3, 4, 5, 6]. The study of character and transport of fluid mud is of great interest from both economical and ecological points of view as it may hinder navigability of ships and also contribute to eutrophication and to contaminant transport [7]. Managements of coastal areas are supported by hydro-sedimentary models to predict distribution and transport of fluid mud as well as its influence on damping of wave energy in these areas [8, 9, 10, 11, 12, 13, 14, 15]. However, modelling requires accurate quantitative description of fluid mud parameters such as density, particle size, and rheological parameters.

Fluid mud is a highly concentrated suspension of fine-grained sediment rich in clay minerals and organic matter. Suspended sediment concentrations (SSC) naturally vary between several 10 and 100 g/l depending on mud sources and composition [7, 16, 17]. Fluid mud can be distinguished not only by the sediment concentration but also by its rheological characteristic. In contrast to water with Newtonian flow behaviour fluid mud exhibits a yield stress and non-Newtonian flow behavior [e.g. 8, 17, 18, 19]. Its viscosity is typically several orders of magnitude larger than that of clear water [16]. Investigations have shown, that the flow curve can be described by the Herschel-Bulkley-Model, a generalisation of the Bingham Model, exhibiting shear thinning behaviour with decreasing viscosity by increasing applied stress [17, 19, 20]. Furthermore, the rheology of fluid mud depends strongly on its SSC exhibiting increasing shear stress with increase in concentration for a particular shear rate [e.g. 7].

Rheology of natural mud is difficult to determine and varies with the instrumentation used. It cannot easily be generalised due to many factors such as different mud sources, sampling technique, laboratory equipment etc. [7, 21, 22]. Rheological lab studies have often been performed on artificial cohesive sediment suspensions (as reviewed by Coussot [19]), although some rheological characterisation of mud samples from natural sites has been done by Aubry et al. [20], O'Brien and Julien [23], Aijaz and Jenkins [24], van Kessel and Blom [25], Wurpts and Torn [26], and Faas and Wartel [27]. Aijaz and Jenkins [24] proposed a relation between shear stress and salinity of natural fluid mud suspension. They observed a logarithmic increase of shear stress with increasing

salinity due to elektrokinetic properties. Due to natural variability in fluid mud constituents, there is still a lack in precise physical determination of the rheological behaviour of natural fluid mud, particularly with regard to the direct influence of SSC, salinity, organic content, floc size, and mineral composition.

In this study the rheological behaviour and physical properties of natural fluid mud from the German river Ems and its adjacent harbour of Emden are investigated (Fig. 1). A large amount of fluid mud is accumulating in both provinces, which may reach up to 2-4 m thickness at slack water [5, 26, 28]. Suspended particles from the river will be transported into the tide affected harbour of Emden, accumulating due to less currents energy and forming thick fluid mud layers in there [29, 30]. Greiser et al. [28] and Wurpts and Torn [26] studied the rheological behaviour of the fluid mud in the harbour of Emden, but so far there is no similar study for the river Ems. However, a comparison of the fluid mud character of both locations may be vital to provide a better understanding of the parameters that influences rheological behaviour of natural mud suspensions.

Materials and Methods

Materials

Fluid mud samples were collected between June 2006 and April 2008 in the German river Ems at river km 18 which is known to be in the area of the upstream boundary of the turbidity maximum zone (Fig. 1; [31]). Also, samples were taken in the tidally affected outer harbour of Emden, which is situated ~ 22 river km downstream of the tested location in the river Ems. During slack water, sampling of the fluid mud was achieved by 2 m-long Rumohr-type gravity cores [32]. Coring was carried out in the river Ems (1) and harbour of Emden (2) on various occasions. For sub-sampling of the mud suspensions, pre-drilled holes in the core liner (20 cm distances) were opened incrementally from top to bottom after core recovery.

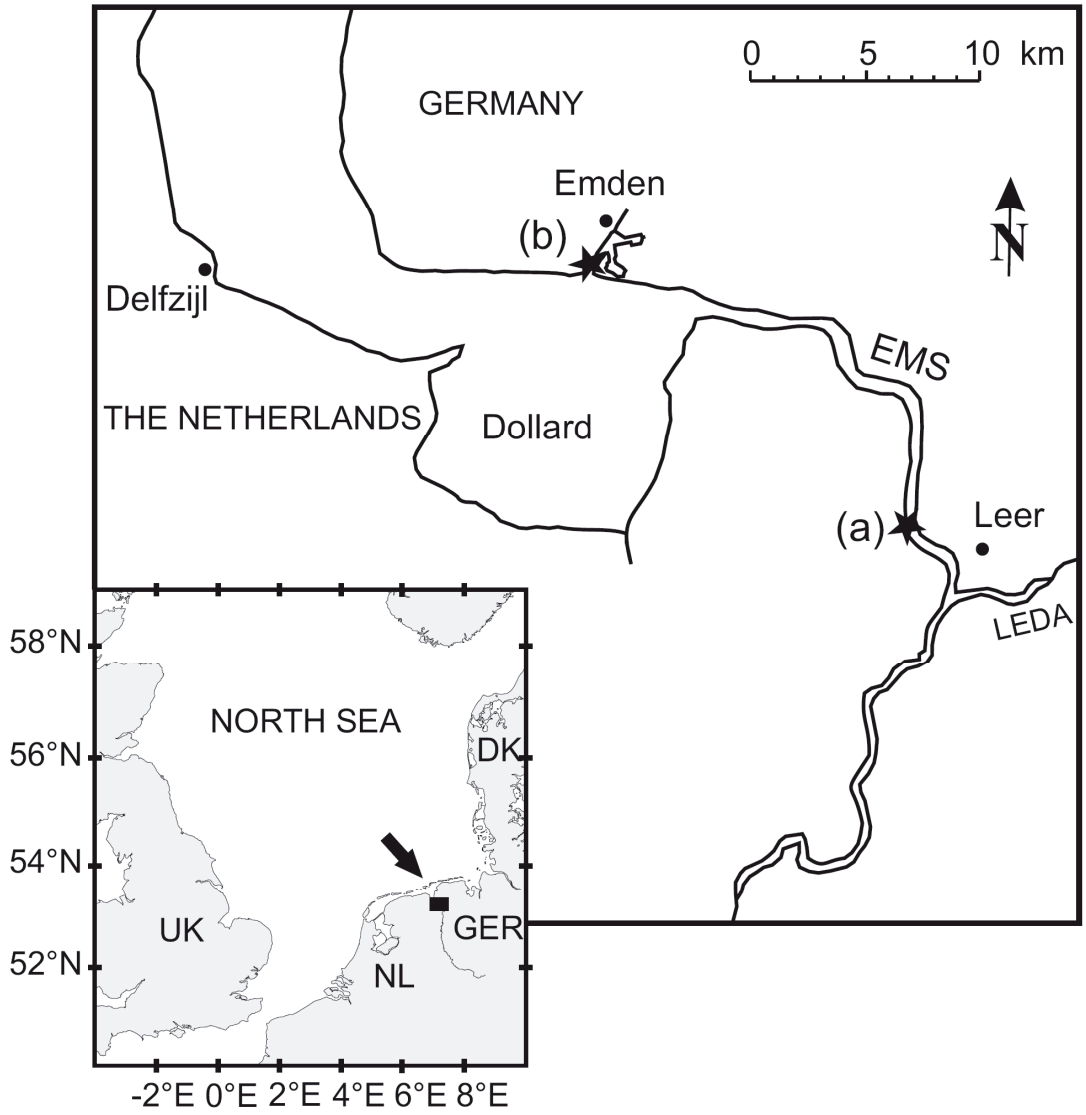

Fig. 1 Map of the river Ems with locations of the sampling points: **(a)** river km 18 and **(b)** tide affected outer harbour of Emden.

In this study, we present selected fluid mud samples from each core with a suspended sediment concentration (SSC) between 100 and 200 g/l as the top samples in the cores of the harbour of Emden started with SSC around 100 g/l and 200 g/l showed to be the upper limit of the rheological measurements due to instrument related difficulties (see Experimental methods).

Experimental methods

Sediment properties

Immediately after sampling, while on board the ship, salinity and dissolved oxygen of the fluid mud samples were simultaneously measured by a multi-parameter instrument (WTW Multi 350i). In the laboratory, suspended sediment concentration and grain size distribution were determined for all samples. The former was done by weighing dry mass per unit sample volume, the latter by means of a Beckman Coulter Laser Particle Sizer. Before measuring the grain size, organic matter was removed by oxidation with a 35 % H_2O_2 solution and Sodiumpyrophosphate was added to the samples to prevent formation of aggregates during analysis. Total organic carbon (TOC) of the suspended sediment was quantified using a LECO CS 200 analyser. Prior to analysing, the inorganic carbon was removed by addition of HCl. Furthermore, dried and pulverised fluid mud samples were used for the semiquantitative evaluation of bulk mineralogy by means of X-ray diffractometer (XRD) (for details, see [33]).

Sediment rheology

Rheological measurements were performed at constant temperature of 20°C using a Bohlin CS 10 rheometer with concentric cylinder system and double gap geometry. All rheological measurements were repeated at least two times to ensure good reproducibility of the data whereas the cylinder was always reloaded with a new mud sample to prevent thixotropic effects. For SSC over 200 g/l, the mud was to stiff too ensure homogenous load, and hence restricted the rheological measurements to that limit. Two types of stress-controlled rheological tests have been performed: i) steady state tests to determine equilibrium flow curves and ii) transient tests at very low shear rates (10^{-4} to 10^{0} 1/s) to directly measure the yield stress (τ_y) [34]. In stress controlled experiments, shear stress (τ) is applied to the suspension and the shear rate ($\dot{\gamma}$) is measured. The viscosity (η; also apparent viscosity) will be calculated as a ratio of shear stress to shear rate: $\eta = \tau / \dot{\gamma}$. To determine the yield stress of the fluid mud suspensions, the shear stress was increased linearly from zero to a level well above the yield stress, thereby recording the resulting shear rate and calculating the viscosity. Fig.

2 shows one yield stress test from river sample E6. Initially, the viscosity of the suspension increases with increasing stress, indicating elastic deformation of a solid-like behaviour. When the stress reaches a certain critical value, which is defined as the yield stress (τ_y), the suspension starts to flow with decreasing viscosity exhibiting liquid-like behaviour (Fig. 2). At that point, the initial state of the material is non-recoverable. Hence, the yield stress is determined as the stress limit between non-flow and flow conditions, at that point where the suspension reaches its maximum viscosity (η_y).

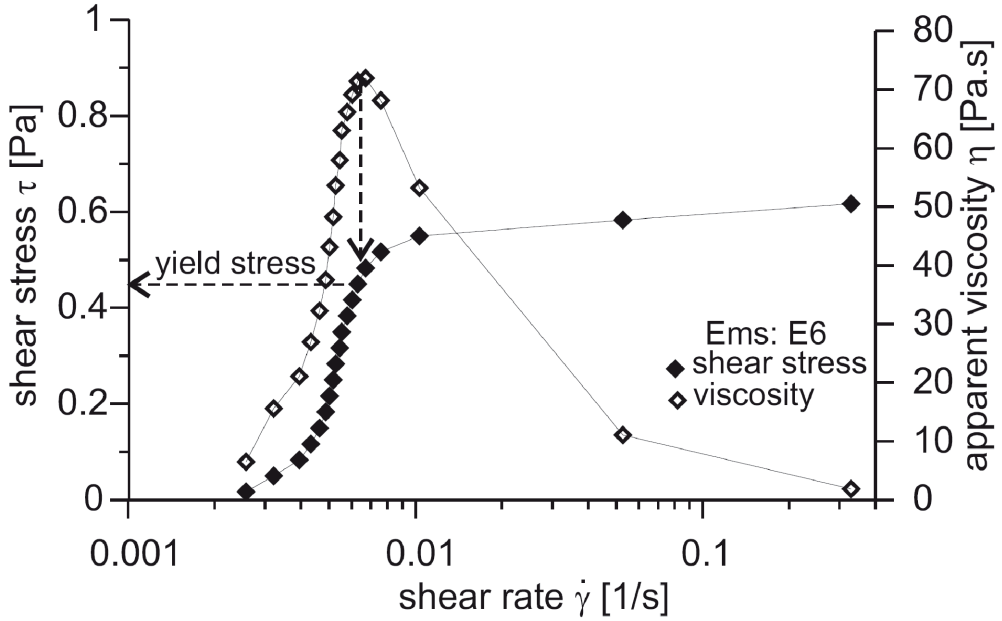

Fig. 2 Yield stress determination by low-shear rate tests, exemplified for the river fluid mud suspension E6. With increasing shear stress the viscosity is increasing until a critical shear stress at which the fluid starts to flow.

Results

A wide range of laboratory analysis of the sedimentological and rheological properties of fluid mud samples from river Ems and harbour of Emden were conducted in this study. A summary of the results is given in Tabs. 1 and 2.

Sediment characteristics

The SSC of the samples investigated in this study varied from 113 to 200 g/l (Tab. 1 and Fig. 3). When comparing the samples from both locations (Fig. 3), it is obvious that

the sample E6 from the river has almost the same SSC as the sample a1 from the harbour and likewise for samples E7 and a3. Grain size distributions of the suspended sediment of all samples are similar, being dominated by silt (approx. 77 %), and lesser amounts of clay (approx. 21 %) and sand (approx. 2 %). However, only small variations in grain size distribution are determined when comparing the samples with the same SSC.

Table 1 Summary of the sediment properties of the fluid mud suspensions from the river Ems and the harbour of Emden.

Lokation and sample no.		Date	SSC	Yield stress (τ_y)	Viscosity at yield point (η_y)	Salinity	Oxygen content	Organic content	Grain size distribution [Vol %]		
			[g/l]	[Pa]	[Pa.s]		[mg/l]	TOC %	Clay (<2µm)	Silt	Sand
River Ems	E6	14.06.07	113	0.5	72	1.1	1.82	3.8	18.0	78.0	4.1
	E7	14.06.07	182	3.4	4250	1.0	0.06	3.8	17.8	77.4	4.9
Harbour of	a1	19.06.07	117	0.5	74	13.5	0.10	3.6	21.7	75.3	3.0
Emden	a2	19.06.07	144	0.8	294	13.7	0.08	3.6	22.7	75.5	1.8
	a3	19.06.07	182	2.1	1405	12.8	0.06	3.5	21.5	76.5	2.0
	a4	19.06.07	200	3.7	4579	11.8	0.06	3.6	23.4	74.6	2.0
	a1-1	01.04.08	127	0.6	122	5.8	0.50	4.1	21.9	77.5	0.6
	a1-2	01.04.08	136	0.7	175	5.2	0.55	4.2	19.9	77.8	2.4
	a1-3	01.04.08	161	1.6	670	7.3	0.36	4.2	19.8	77.9	2.3
	a1-4	01.04.08	192	3.8	5142	8.8	0.04	4.5	21.0	78.3	0.7

Fluid mud from the river (samples E6/E7) exhibit approximately 2 % more silt and 2 % more sand than the harbour samples (a1/a3), but around 4 % less clay (Tab. 1). The total organic content (TOC) of all samples is high with values ranging between 3.5 to 4.5 %. Furthermore, all fluid mud suspensions show very low oxygen content close to zero except for sample E6 being 1.8 mg/l (Tab. 1). When considering all samples recovered by the cores in either location, an abrupt drop in oxygen content from several mg/l to almost zero could be observed when the SSC reaches about 100 g/l. For example, samples of the river with SSC of ~55 g/l still consists approx. 3.5 mg/l dissolved oxygen while surface water samples from the harbour with only 0.3 g/l SSC exhibit an oxygen content of 8.5 mg/l. Hence, the formation of fluid mud seems to coincide with very low dissolved oxygen content at these locations.

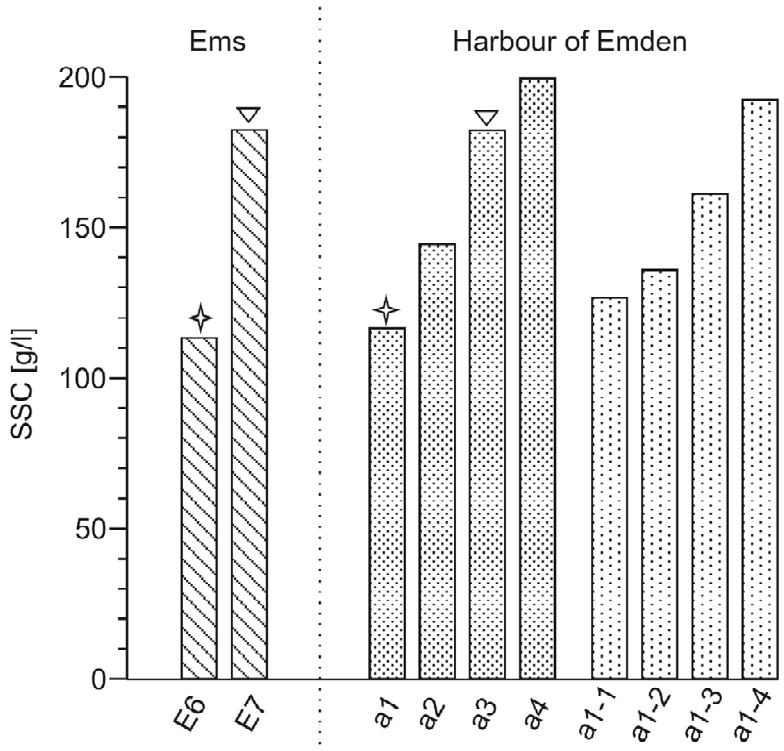

Fig. 3 SSC of fluid mud suspensions from the river Ems and the harbour of Emden. The symbols on the bars mark samples from the river and the harbour of the same concentration (E6/a1 and E7/a3). See also Tab. 1.

The salinity of the fluid mud suspensions is very different because the harbour is located closer to the North Sea than to the river location (Fig. 1). While the river samples show salinity values of only about 1, the harbour suspensions exhibit higher salinities of around 7 for samples a1-1 to a1-4 and up to a salinity of 13 for the samples a1 to a4 (Tab. 1). The determined mineral composition is summarised in Tab. 2. For all samples, clay minerals and micas are the main components of the fluid mud samples (37 – 54 %), followed by quartz (15 – 35 %), feldspars (8 – 18 %), and calcite (4 – 12 %). Similar to results from grain size distributions only small variations in mineral content were detected between the river samples (E6/E7) and harbour samples (a1/3; Tab. 2).

Rheology

All tested fluid mud suspensions exhibit non-Newtonian flow behaviour and yield stresses as demonstrated in a shear stress/shear rate diagram [Fig. 4a (see also Tab. 1)]. The flow curves can be described by the Herschel-Bulkley-Model with pronounced shear thinning in all samples (Fig. 4). The decrease in apparent viscosity with increasing

shear rate occurs after the yield stress is exceeded and the fluid mud starts to flow (Fig. 4b). However, the flow curves of all fluid mud samples in Fig. 4a confirm the strong dependence of the shear stress on SSC: with increasing SSC the shear stress is also increasing for a particular shear rate. But remarkable is the higher shear stress of about 21 % and 25 % of the samples from the river (E6 and E7) compared to the samples from the harbour (a1 and a3) with almost the same SSC (Figs. 3 and 4a).

Table 2 Mineral composition of the fluid mud from the river Ems and the harbour of Emden.

Location and sample no.		Mineral content [%] Clay minerals and micas	Quartz	Feldspars	Calcite
River Ems	E6	54	21	18	4
	E7	49	25	18	8
Harbour of	a1	52	15	12	7
Emden	a2	37	27	15	12
	a3	49	32	8	10
	a4	48	35	8	9
	a1-1	48	26	17	8
	a1-2	39	30	17	10
	a1-3	50	26	17	6
	a1-4	44	32	14	9

Besides, the examined yield stresses and viscosities at the yield point are generally increasing exponentially with increasing SSC, ranging from 0.45 to 3.78 Pa and from 72 to 5142 Pa s, respectively (Tab. 1, Fig. 5). Comparing Figs. 5a and b, it is obvious that the increase of viscosity with SSC is greater than the increase of yield stress. For example, the increase of viscosity from sample a1 to a3 is around 5-times greater than the increase in yield stress and 10-times greater from E6 to E7. A difference between the samples from the river and the harbour with the same SSC, like in the flow behaviour as mentioned above, is only occurring in samples with higher SSC (a3 and E7, respectively) probably due to the exponential relationship between yield stress/viscosity and SSC. However, yield stress of the river sample E7 is approximately 1.7-times higher than that of the sample from harbour a3, whereas viscosity at the yield point is 3-times higher (Fig. 5).

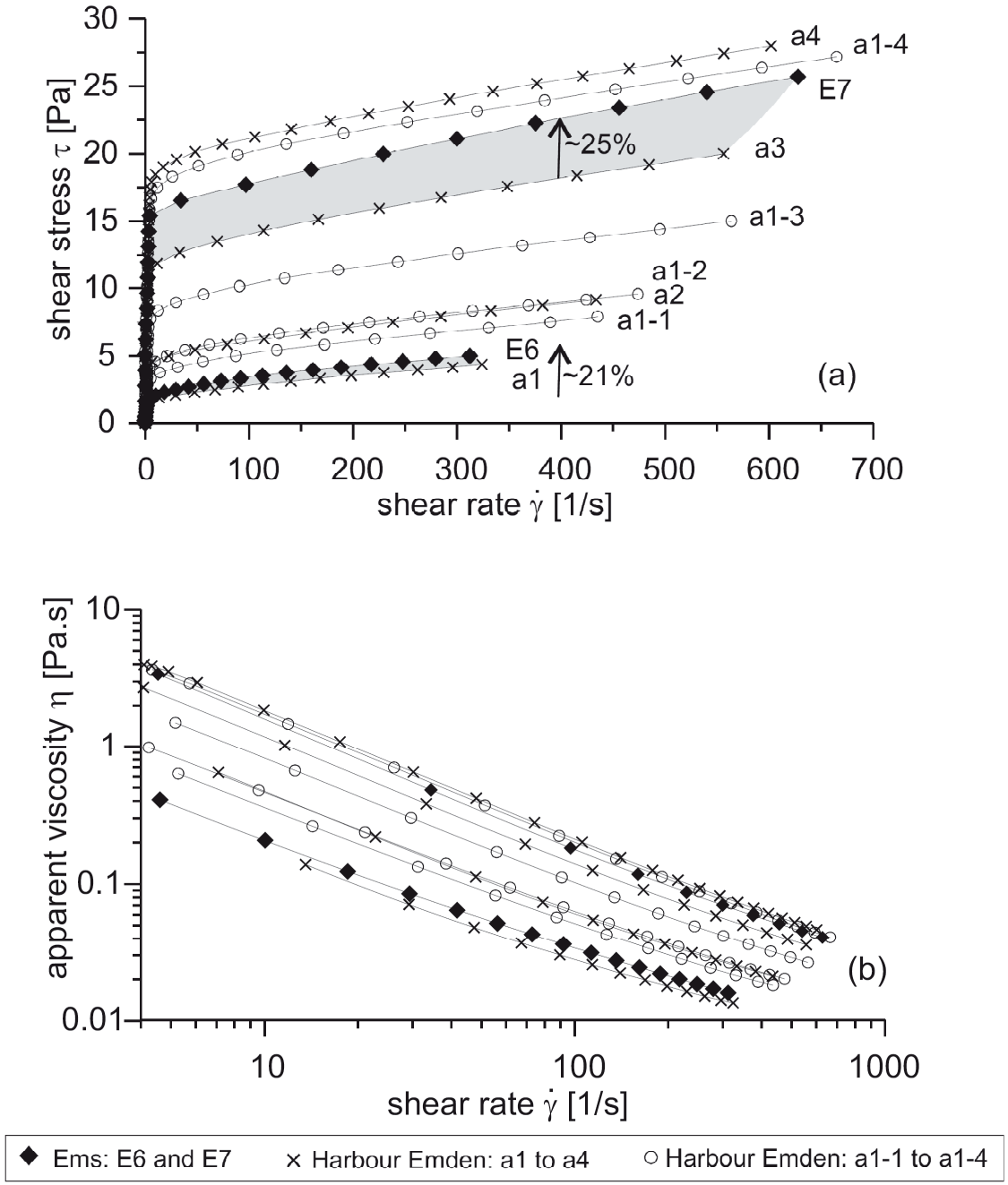

Fig. 4 (a) Shear stress/shear rate flow curves of the fluid mud suspensions from the river Ems and the harbour of Emden. With increase in SSC the shear stress is increasing for a particular shear rate (cf. Tab. 1). Shaded zones illustrate the higher shear stress of the samples of river Ems compared to the samples of the harbour of Emden with the same SSC (E6/a1 ~21% and E7/a3 ~25 %). **(b)** Apparent viscosity/shear rate diagram of the fluid mud suspensions. Response of all fluid mud samples is shear thinning through the range of SSC. The decrease in apparent viscosity with increasing shear rate appears after the yield stress is exceeded (cf. Fig. 2). Note different scales.

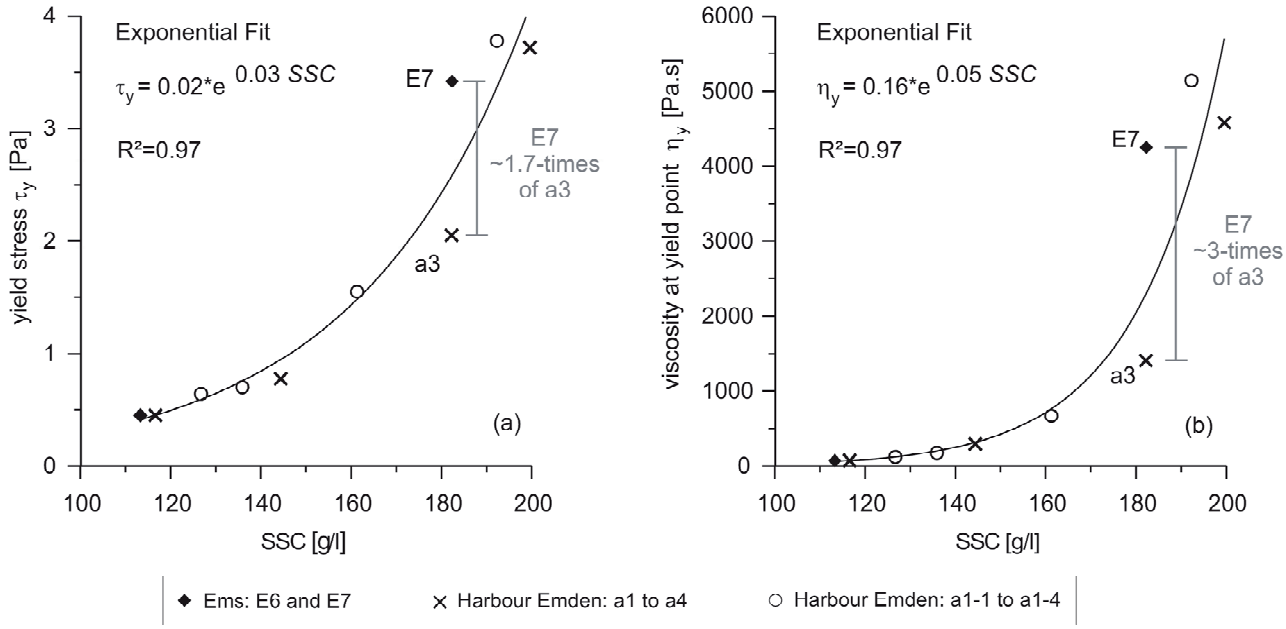

Fig. 5 Yield stress (a) and viscosity at the yield point (b) in dependence of SSC of the samples from the river Ems and the harbour of Emden. They can be satisfactorily fitted by an exponential function.

Discussion

Rheological properties of fluid mud are difficult to characterise unambiguously as they depend on hydrodynamic conditions and characteristics of the mud [7]. Nevertheless, all fluid mud suspensions from the river Ems and the harbour of Emden that were tested in this study exhibit non-Newtonian shear thinning flow behaviour and a yield stress similar to those of muds at higher sediment concentrations (Fig. 4; [16, 17]). Increasing shear stress applied to a mud suspension leads to a break-up of the flocculated aggregates, and hence, apparent viscosity decreases and shear thinning flow occurs (Fig. 4b; [19, 27, 35]. Rheological tests of fluid mud from the harbour of Emden by Greiser et al. [28] and Wurpts and Torn [26] agree with our results.

As the viscosity of the fluid mud is strongly rate-dependent, the yield stress may be a unique value for a given material. However, determination of the yield stress of mud suspensions strongly depends on the methods being used, i) indirect: extrapolated from the flow curve, or ii) direct: controlled stress rheometer tests [21]. However, our direct yield stress tests show a strong exponential dependence of the yield stress from SSC (Fig. 5). Such exponential increase of the yield stress and the viscosity at the yield point

with increasing SSC on mud suspensions was also observed by other researchers, e.g. by O'Brien and Julien [23] on natural mudflow deposits in Colorado, or by Aubry et al. [20] on estuarine mudflats of the French river La Penzé. McAnally et al. [7] summarised the relationship of SSC and yield stress for various fluid muds, compared to which our samples lie in between Gulfport Harbour and Calcasieu Channel samples (Fig. 6).

The rheological behaviour of mud suspensions depends on many factors such as SSC, organic content, salinity, grain size distribution and mineralogy [e.g. 16]. We have obtained increasing shear stress with increasing SSC for a particular shear rate and an exponential relationship between yield stress and SSC, as mentioned above (Figs. 4a and 5). However, fluid mud samples of the river Ems (samples E6 and E7) show a 21 – 25 % higher shear stress than samples from the harbour, which have the same SSC (Fig. 4a). It is conceivable that parameters other than SSC additionally affect the rheological behaviour of the samples, as discussed in the following.

Fluid mud in the river Ems and harbour of Emden consists of high organic content (3.5-4.5 % TOC, Tab. 1). Gresikowski et al. [29] investigated the composition and structure of the suspended particles in the river Ems and discovered that mineral grains of the particles are covered and connected densely by particulate organic matter and extracellular polymeric substances (EPS) forming large aggregates. EPS, derived from bacteria and microphytobenthos, form a hydrated sticky gel [36], which is known to enhance cohesion and the elasticity of the sediment [37, 38, 39]. Hence, organic matter is probably stabilising the sediment. Among others, Tolhurst et al. [39] determined that natural mud from the Eden estuary in Scotland with EPS was 4.5 times more resistant against erosion as sediment where organic matter had been removed. Besides, Faas and Wartel [27] detected an 80 % loss of yield stress in mud suspensions from Eckernförde Bay (Baltic Sea) after removal of organic matter. In contrast, Wurpts and Torn [26] state that high organic content in fluid mud of the harbour of Emden leads to a lower yield stress and lower viscosity due to lower friction between the particles coated by EPS. For example, these authors measured a yield stress of 1 kPa of an anorganic sample while the organic harbour mud of the same concentration only revealed a yield stress of 30 Pa. Organic content could be an influencing factor to the strength of suspensions, but samples from the river Ems (E6/E7) and the harbour of Emden (a1/a3)

have almost the same organic content (3.5 – 3.8 % TOC; Tab. 1). On the other hand, it cannot be ruled out that the harbour samples contain higher EPS/TOC ratios than those of the river samples. Thus, the slime is reducing the viscosity and, according to Wurpts and Torn [26], also the yield stress. Therefore, other parameters may be responsible for the higher shear strength of the river mud suspensions.

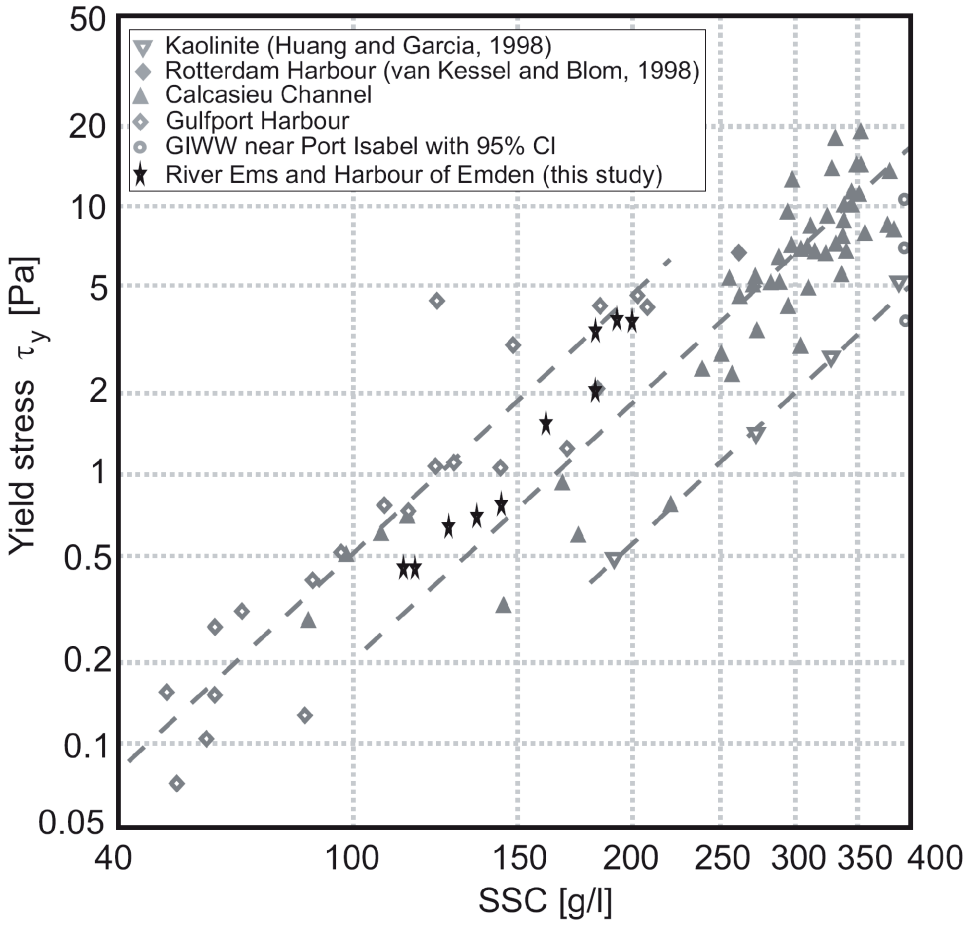

Fig. 6 Yield stress in dependence of SSC for various fluid muds. The samples of the river Ems and the harbour of Emden behave similar as fluid muds from Gulfport Harbour and Calcasieu Channel (modified after [7]).

It is known that salinity influences electrochemical bondings between particles, and hence increases the strength of suspensions [40]. Aijaz and Jenkins [24] have tested natural mud suspensions for different salinity and generally observed a logarithmic increase of shear stress with increasing salinity. They also found that rising salinity from 3 to 30 will result in a 15 – 20 % increase in shear stress, while at a salinity range from 0 to 3 the shear stress increases more rapidly. Given the different locations of the

tested samples in the Ems river and Emden harbour, there is a profound difference in salinity at any given time in the tidal cycle (Ems: 1 and harbour: 7 and 13; Fig. 1 and Tab. 1). For a direct and valid comparison of the mud at these two locations, it is vital that all samples have the same salinity. Following Aijaz and Jenkins [24], the increasing salinity from 1 to 13 of the river samples (samples E6/E7) causes an even higher shear stress (around 40 % or higher) than that of the harbour samples of the same SSC (samples a1/a3). Hence, salinity is strongly influencing the shear stress of fluid mud suspensions.

Grain size distribution also influences the shear stress of suspensions. Coussot and Piau [41] stated that the higher the ratio of clay volume to total solid volume, the greater the yield stress. However, the river samples (E6/E7) have approximatly 4 % less clay fraction than the harbour samples (a1/a3; Tab. 1), and material of both locations shows the same amount of clay minerals and micas (Tab. 2). Therefore, the clay content may not be the controlling factor for higher shear stress of the river samples. On the other hand, added sand in suspensions can increase the apparent viscosity and yield stress due to increasing maximum packing concentration as the grain size distribution widens [19]. Because the river samples have around 2 % more sand than the harbour samples, this may influence their shear stress. However, this subtle increase in sand may not be significant and considering that there is also not a big difference in mineralogical composition of the samples, it can be concluded that the influence of grain size distribution and mineral composition on shear stress of the tested suspensions is negligible in our study.

Along a similar avenue of reasoning, individual particles may not be the only factor to be considered. Particles are oftentimes aggregated into flocs in mud suspensions, and Eisma [42] observed flocs of up to 4 mm in diameter in the Ems estuary. Therefore, floc rather than grain size should be considered for rheology. Because the shear stress is transferred by flocs, the floc strength is an important factor for the rheological behaviour of suspensions [43]. Flocs aggregated in turbulent environments are stronger and denser because of collision than those formed by differential settling velocity [44]. This aspect may explain the higher shear stress of the river samples where the current is a lot stronger than in the harbour basin.

Conclusions

The purpose of this study was to verify the parameters that influence rheological behaviour of fluid mud suspensions by comparing samples collected from the river Ems and the harbour of Emden. In general, all samples exhibit non-Newtonian shear thinning behaviour and all samples have a true initial yield stress. Yield stress and viscosity are increasing exponentially with an increase in SSC. Although the particles in the harbour of Emden originate from the river Ems, the river samples exhibit around 23 $\pm$2 % higher shear stress and for SSC of 180 g/l, for example, a 70 % higher yield stress than samples of the harbour with the same SSC. Insignificant variations in mineral composition and grain size distribution of the samples from both locations lead us to the conclusion that these parameters have a negligible effect on rheological behaviour. In fact, parameters such as salinity, type of organic matter, and floc strength may provide the major controls on the shear stress of the fluid mud suspensions of the river Ems and the harbour of Emden.

Acknowledgement We thank the captain and crew of the vessel *Delphin* and the Emden port authorities for their support during our study. We also thank the captain and crew of the vessel *Senckenberg* and K. Schrottke for their support and cooperation. The institute IUV of the University of Bremen, in particular U. Kück, is acknowledged for kindly provide the rheometer and for discussions on test procedures. For kindly providing the WTW instrument (Multi 330i) T. Mörz is thanked. B. Kockisch, C. Vogt, and J. Stuut are thanked for the support with laboratory measurements and data analysis. Funding was granted by DFG-Research Center / Excellence Cluster „The Ocean in the Earth System“.

References

[1] Kineke GC, Sternberg RW, Trowbridge JH, Geyer WR: Fluid mud processes on the Amazon continental shelf, Continental Shelf Research 16 (1996) 667-696.

[2] Abril G, Riou SA, Etcheber H, Frankignoulle M, deWit R, Middelburg JJ: Transient, tidal time-scale, nitrogen transformations in an estuarine turbidity maximum--fluid mud system (the Gironde, south-west France), Estuarine, Coastal and Shelf Science 50 (2000) 703-715.

[3] Lesourd S, Lesueur P, Brun-Cottan JC, Garnaud S, Poupinet N: Seasonal variations in the characteristics of superficial sediments in a macrotidal estuary (the Seine inlet, France), Estuarine, Coastal and Shelf Science 58 (2003) 3-16.

[4] Uncles RJ, Stephens JA, Law DJ: Turbidity maximum in the macrotidal, highly turbid Humber estuary, UK: Flocs, fluid mud, stationary suspensions and tidal bores, Estuarine, Coastal and Shelf Science 67 (2006) 30-52.

[5] Talke SA and de Swart HE: Hydrodynamics and morphology in the Ems/Dollard estuary: Review of models, measurements, scientific literature, and the effects of changing conditions, Institute for Marine and Atmospheric Research Utrecht (IMAU), University of Utrecht (2006).

[6] Schrottke K, Becker M, Bartholomä A, Flemming BW, Hebbeln D: Fluid mud dynamics in the Weser estuary turbidity zone tracked by high-resolution side-scan sonar and parametric sub-bottom profiler, Geo-Marine Letters 26 (2006) 185-198.

[7] McAnally WH, Friedrichs C, Hamilton D, Hayter E, Shrestha P, Rodriguez H, Sheremet A, Teeter AM: Management of fluid mud in estuaries, bays, and lakes. I: Present state of understanding on character and behavior, Journal of Hydraulic Engineering 133 (2007) 9-22.

[8] Winterwerp H: On the dynamics of high-concentrated mud suspensions, TU Delft, Faculty of Civil Engineering and Geosciences (1999).

[9] Dearnaley MP, Roberts W, Jones SE, Leurer KC, Lintern DG, Merckelbach LM, Sills G, Toorman E, Winterwerp JC: Measurement and modelling of the properties of cohesive sediment deposits in fine sediment dynamics in the marine environment, JC Winterwerp and C Kranenburg, Elsevier Science B.V., (2002) 57-73.

[10] Delefortrie G, Vantorre M, Eloot K: Modelling navigation in muddy areas through captive model tests, Journal of Marine Science and Technology 10 (2005) 188-202.

[11] Gabioux M, Vinzon SB, Paiva AM: Tidal propagation over fluid mud layers on the Amazon shelf, Continental Shelf Research 25 (2005) 113-125.

[12] Guan WB, Kot SC, Wolanski E: 3-d fluid-mud dynamics in the Jiaojiang estuary, china, Estuarine, Coastal and Shelf Science 65 (2005) 747-762.

[13] Kaihatu JM, Sheremet A, Holland KT: A model for the propagation of nonlinear surface waves over viscous muds, Coastal Engineering 54 (2007) 752-764.

[14] Jain M and Mehta AJ: Role of basic rheological models in determination of wave attenuation over muddy seabeds, Continental Shelf Research 29 (2009) 642-651.

[15] Soltanpour M and Haghshenas SA: Fluidization and representative wave transformation on muddy beds, Continental Shelf Research 29 (2009) 666-675.

[16] Whitehouse R, Soulsby R, Roberts W, Mitchener H: Dynamics of esturine muds - a manual for practical applications, HR Wallingford Limited and Thomas Telford Limited, (2000).

[17] Winterwerp JC and van Kesteren W: Introduction to the physics of cohesive sediment in the marine environment, Elsevier B.V., Amsterdam (2004).

[18] Berlamont J, Ockenden M, Toorman E, Winterwerp, J: The characterisation of cohesive sediment properties, Coastal Engineering 21 (1993) 105-128.

[19] Coussot P: Mudflow rheology and dynamics, A.A. Balkema, Rotterdam (1997).

[20] Aubry T, Razafinimaro T, Jacinto RS, Bassoulet P: Rheological properties of a natural estuarine mud, Applied Rheology 13 (2003) 142-149.

[21] Nguyen QD, Akryd T, deKee DC, Zhu L: Yield stress measurements in suspensions: An inter-laboratory study, Korea-Australia Rheology Journal 18 (2006) 15-24.

[22] Møller PCF, Mewis J, Bonn D: Yield stress and thixotropy: On the difficulty of measuring yield stresses in practice, Soft Matter 2 (2006) 274-283.

[23] O'Brien JS and Julien PY: Laboratory analysis of mudflow properties, Journal of Hydraulic Engineering 114 (1988) 877-887.

[24] Aijaz S and Jenkins S: On the electrokinetics of shear stress behaviour in fluid-mud suspensions, Journal of Geophysical Research 99 (1994) 12,697-612,706.

[25] van Kessel T and Blom C: Rheology of cohesive sediments: Comparison between a natural and an artificial mud, Journal of Hydraulic Research 36 (1998) 591-602.

[26] Wurpts R and Torn P: 15 years experience with fluid mud: Definition of the nautical bottom with rheological parameters, Terra et Aqua 99 (2005) 22-32.

[27] Faas R and Wartel S: Rheological properties of sediment suspensions from Eckernförde and Kieler Förde bays, western Baltic Sea, International Journal of Sediment Research 21 (2006) 24-41.

[28] Greiser N, Gamnitzer R, Rupp J: Pseudoplasticity of cohesive sediments: Causes and innovative techniques for pre-dredging surveys in Proceedings of CEDA (Central Dredging Association) Dredging Days 2002: Dredging without boundaries CEDA Dredging Days 2002, October 2002, Casablanca, Morocco (2002).

[29] Gresikowski S, Harms H, Greiser N, Gamnitzer R, Wurpts R: Fluid mud im Emder Außenhafen - seine Herkunft und das Transportverhalten, HANSA 133 (1996) 73-76.

[30] Nasner H: Maintenance work in harbours with fluid-mud in Third Chinese-German Joint Symposium on Coastal and Ocean Engineering, National Cheng Kung University, Tainan (Taiwan), November 8-16, (2006), 1-14.

[31] Spingat F and Oumeraci H: Schwebstoffdynamik in der Trübungszone des Ems - Ästuars - Anwendung eines Analysenkonzeptes für hoch aufgelöste und dauerhaft betriebene Gewässergütemessungen, Die Küste 62 (2000) 159-219.

[32] Meischner D and Rumohr J: A light-weight, high-momentum gravity corer for subaqueous sediments, Senckenbergiana maritima 6 (1974) 105-117.

[33] Vogt C, Lauterjung J, Fischer RX: Investigation of the clay fraction (<2 μm) of the clay minerals society reference clays, Clays and Clay Minerals 50 (2002) 388-400.

[34] Bohlin Instruments GmbH: Benutzerhandbuch für Bohlin rheometer, (2001).

[35] Dyer KR: Sediment processes in estuaries: Future research requirements, Journal of Geophysical Research 94 (1989) 14,327-314,339.

[36] Wotton RS: The ubiquity and many roles of exopolymers (EPS) in aquatic systems, Scientia Marina 68 (2004) 13-21.

[37] Ransom B, Bennett RH, Baerwald R, Shea K: TEM study of in situ organic matter on continental margins: Occurrence and the "monolayer" hypothesis, Marine Geology 138 (1997) 1-9.

[38] Black KS, Tolhurst TJ, Paterson DM, Hagerthey SE: Working with natural cohesive sediments, Journal of Hydraulic Engineering 128 (2002) 2-8.

[39] Tolhurst TJ, Gust G, Paterson DM: The influence of an extracellular polymeric substance (EPS) on cohesive sediment stability in fine sediment dynamics in the marine environment, JC Winterwerp and C Kranenburg, Elsevier Science B.V., (2002) 409-425.

[40] van Olphen H: An introduction to clay colloid chemistry: For clay technologists, geologists, and soil scientists, Jon Wiley & Sons, Inc., New York, London (1963).

[41] Coussot P and Piau JM: On the behavior of fine mud suspensions, Rheologica Acta 33 (1994) 175-184.

[42] Eisma D: Particle size of suspended matter in estuaries, Geo-Marine Letters 11 (1991) 147-153.

[43] Kranenburg C: Effects of floc strength on viscosity and deposition of cohesive sediment suspensions, Continental Shelf Research 19 (1999) 1665-1680.

[44] Krone RB: The significance of aggregate properties to transport processes in Proceedings of a workshop on estuarine cohesive sediment dynamics, AJ Mehta, Springer-Verlag, Berlin, Tampa, Florida, November 12-14, 1984 (1986) 66-84.

MANUSCRIPT 2A (ORIGINAL MANUSCRIPT)

A modified dynamic CPTU penetrometer for fluid mud detection

Annedore Seifert, Achim Kopf

MARUM - Center for Marine Environmental Sciences, University of Bremen, P.O. Box 330440, 28334 Bremen, Germany

Original Manuscript

Abstract

Rising maintenance costs in areas of high suspended sediment concentrations to guarantee save ship passage in harbors and motorways demand new efficient and accurate methods to define navigable depths. One particularly complex phenomenon is the episodic, tidally driven variation of this depth level as a result of fluid mud settlement. We present results from dynamic cone penetration testing with pore pressure measurement (CPTU) as a non-acoustical, direct device to support surveying and management of these areas. The new technique is modular and utilizes a disk configuration for fluid mud detection. Both disk resistance and pore pressure measurements accurately identify suspended matter concentrations ≥ 90 g/l, and the transition from fluid mud to consolidating mud once concentrations exceed 150 g/l. Hence, the procedure attests the potential for rapid, reliable assessment of a fluid mud layer and concurrent characterization of the underlying consolidated sediment by monitoring the pore pressure and strength changes during penetration.

Keywords: Fluid mud; Cohesive soils; Cone penetration testing

Introduction

Owing to globalization worldwide maritime trade utilizing larger vessels is increasing, and harbors and waterways have to be deepened to accommodate for the new market requirements and ensure navigability. Regulation and dredging of rivers and harbors are conducted, which in turn influence the morphology, hydrodynamics and amounts of suspended matter. In regions affected by tidal variations, thick layers of fluid mud, a

highly concentrated suspension of clay minerals and organic matter, settle in harbors and estuaries (e.g. Kineke et al. 1996; Lesourd et al. 2003; Guan et al. 2005; Uncles et al. 2006; Talke and de Swart 2006). Suspended sediment concentrations (SSC) of these layers naturally varies between several 10 and 100 g/l depending on mud sources and composition (Whitehouse et al. 2000; Winterwerp and van Kesteren 2004; McAnally et al. 2007a). Fluid mud exhibits a non-Newtonian flow behavior in contrast to Newtonian behavior of water (e.g. Coussot 1997; Winterwerp and van Kesteren 2004), and hence may hamper navigability of ships. Its viscosity is typically 1-4 orders of magnitude larger than that of clear water (Whitehouse et al. 2000), and its yield stress correlates positively with increasing SSC at a given shear rate (e.g. McAnally et al. 2007a).

The demand to develop routine methods for fluid mud identification and subsequent maintenance work (e.g. dredging) is rising rapidly. Among the methods utilized, acoustic echo sounders are most common to determine navigable depth in ports and channels, but their results are ambiguous since changes in p-wave velocity are a crude measure for density or viscosity of the fluid mud layer (Buchanan 2005). Alternatively, a number of probes equipped with optical backscatter, electric resistivity, nuclear transmission, ultra-sonic sensors or tuning fork systems were especially developed to detect suspended matter, density and/or fluid mud thickness (e.g. Greiser et al. 2002; Fontein et al. 2006). Van Kessel and Fontijn (2000) introduced a constantly pushed miniature sounding instrument to measure bed strength and pore pressure in soft, saturated cohesive sediments, however, the procedure is so far restricted to the laboratory. *In situ* constant-rate cone penetration tests (CPT) are not feasible, because the heavy rigs cause artifacts and soft mud and suspensions are below the resolution of standard CPT devices. Nowadays, rheological properties are preferred as criteria for the assessment of the nautical depth over density, because mud of a given density may differ in viscosity due to thixotropic behavior (McAnally et al. 2007b), however, laboratory rheometer testing is labour-intensive and an indirect approach to the problem.

In this pilot study we make use of a new CPTU instrument with a modified, enlarged tip and a dynamic mode of penetration (see Stegmann et al. 2006) to enhance the sensitivity for fluid mud detection (Fig. 1B). The main objective was to monitor variations in dynamic mechanical response (pore pressure and tip resistance) in the harbor of Emden,

river Ems, Germany, which is known for tidally-driven, m-thick fluid mud deposition (Wurpts and Torn 2005).

Methods and Materials

A dynamic CPTU instrument was deployed in the tidally-affected outer harbor of Emden, Germany. Pore pressure response and sediment resistance during penetration were measured in the fluid mud layer and underlying consolidated beds. The CPTU probe was run in two configurations (Fig. 1). A standard 15 cm^2 CPTU cone with the pore pressure monitored in u_2 position was used when deep penetration was desired. For the detection of the suspended matter, we replaced the cone with a disk (25 cm across, ~490 cm^2) where a central boring accesses a pore pressure port (similar to the u_1 position in a standard CPTU cone; Lunne et al. 1997). The disk serves to enhance the sensitivity of the strain gauge measuring tip resistance when profiling weaker, more viscous media. The filter ring and the borings towards the pressure transducer are carefully saturated with seawater on deck prior to deployment. Once the CPTU instrument is lowered into the water column, a 5 min. halt at 1 m water depth is additionally taken to allow trapped gas bubbles to escape and fully saturate the tubing. After each deployment, the filter is replaced to ensure that clay and other fines do not hamper its permeability.

During a typical deployment, the instrument is lowered through the water column on a winch-cable, impacts the bottom, and dynamically penetrates the sediment. During profiling, tip resistance (q_t), sleeve friction (f_s), temperature, tilt, pore pressure and deceleration are recorded. The latter enables us to calculate the velocity during profiling (1^{st} integration) and total penetration depth of the instrument (2^{nd} integration). During all tests the instrument passed the water column at 0.68±0.08 m/s winch speed and then show non-linear deceleration as a function of the profiled material until all momentum is lost and the instrument comes to a complete halt.

Of the total 47 deployments, 11 were conducted with the cone while 36 were carried out in disk configuration (Fig. 1). For each CPTU record, the excess pore pressure was

determined as the difference between the measured absolute pressure and the hydrostatic pressure at a given depth during profiling.

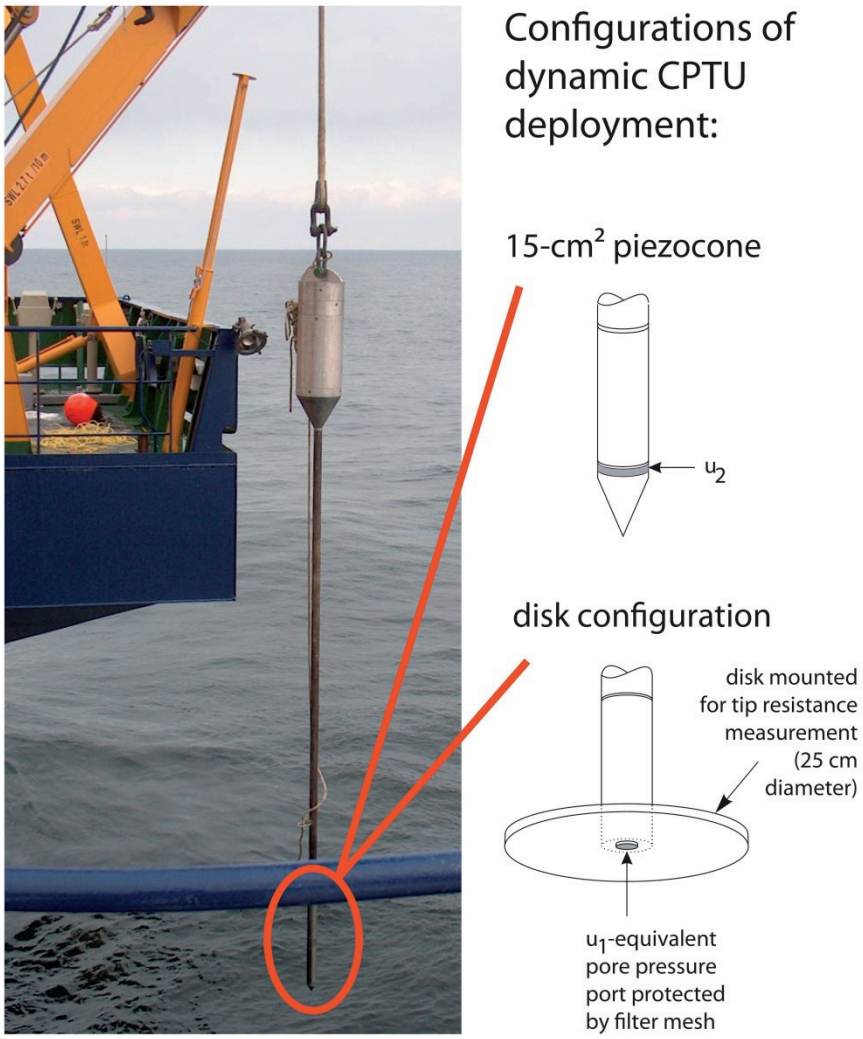

Fig. 1: The dynamic CPTU instrument comprises a modular design (Stegmann et al. 2006) and for this study was used with a total length of 3m and two different tips. Left-hand side shows photograph of the device; right-hand side illustrates cone configuration (top) and disk configuration (bottom). See text.

To ground-truth the CPTU results, water and sediment samples were collected regularly. In this short note, we can show only a limited data set around slack tide, i.e. when current velocities are sufficiently low for fluid mud deposition. In parallel to the CPTU deployments, we sampled water in 1 m depth interval at high water slack tide (00:50 p.m.; water samples W1250) and also one hour later (02:00 p.m.; water samples W1400) during the onset of ebb current until the suspension was to stiff for being

pumped. For reference, we took an overlapping 2 m- long gravity core with a Perspex core liner (Meischner and Rumohr 1974) at high-water slack tide and sub-sampled the suspension and underlying fluid mud layer through pre-drilled, taped-shut holes in the core liner (20 cm distance). The firm mud of the nautical sole remained as whole core in the liner. In the laboratory all samples were analyzed for SSC by weighing dry mass per unit sample volume.

Results

We first compare CPTU deployments with disk and cone configuration at slack tide and relate it to the sediment and overlying fluid mud and suspended matter (Fig. 2). SSC is well below 10 g/l in the suspended harbor water, steps to ~110 g/l in the fluid mud layer, and then steadily increases to >400 g/l in the nautical sole. This increase with depth is mirrored by a subtle increase in disk resistance in the fluid mud (~6 kPa), and a very steep rise to values >16 kPa (Fig. 2A).

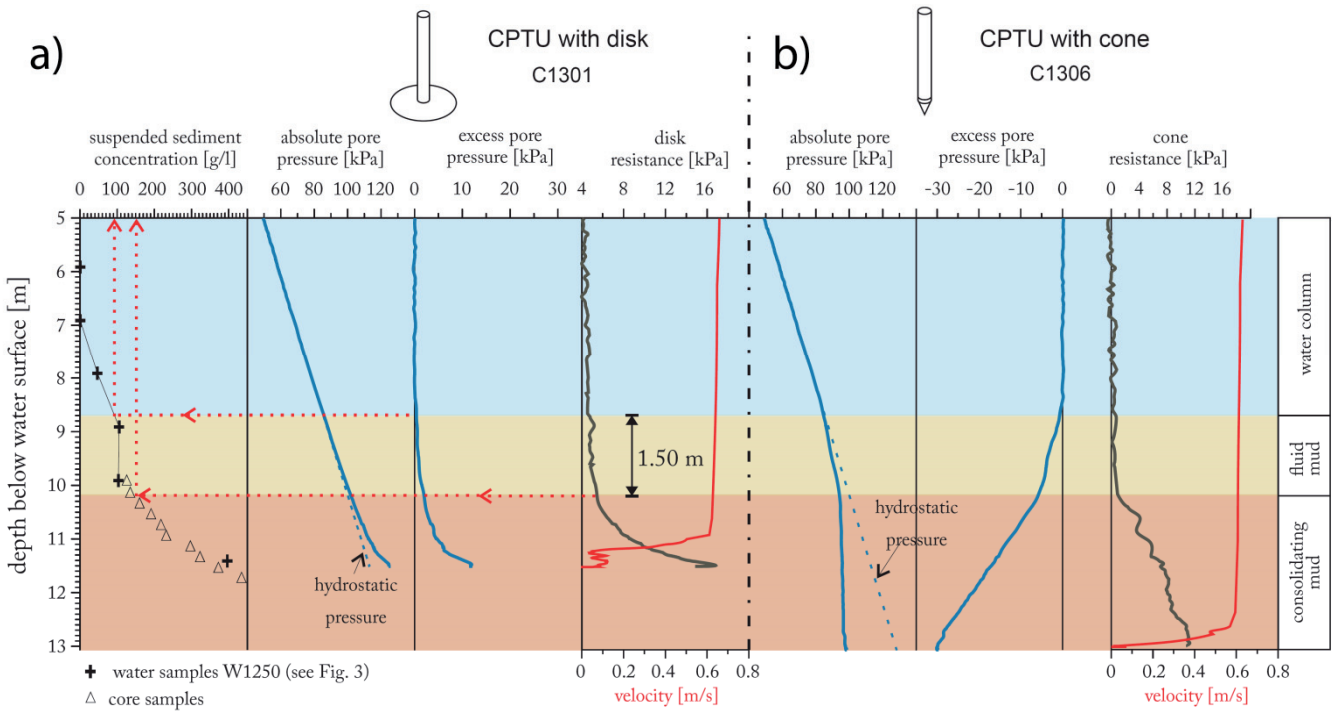

Fig. 2: Typical data profiles recorded with the dynamic CPTU instrument (disk and cone configuration) to detect fluid mud and underlying consolidated sediment compared to the corresponding SSC profiles. a) CPTU disk configuration with disk resistance profile. b) CPTU cone configuration with qc profile. Velocity from integrating deceleration is shown as red graphs.

Accordingly, the fluid mud layer at that time was ~150 cm thick. In contrast, the cone configuration fails to detect the fluid mud layer because the probe lacks sensitivity. However, q_c increases in the mud of the nautical sole (up to ~10 kPa) and terminal sub-bottom depth increases by appx. 150 cm; Fig. 2B). Interestingly, excess pore pressure is most indicative of fluid mud, although disk configuration shows an increase whereas the cone measures subhydrostatic values. These overall trends are enhanced in the underlying mud, i.e. a rise to +15 kPa (disk) and –30 kPa (cone) were measured once the instrument fully penetrated (Fig. 2). Those excursions will be discussed within the context of all our data and aspects related to full flow penetration and rate-dependency owing to dynamic profiling.

Figure 3 provides a broader overview of CPTU deployments bracketed by SSC data from water sampling at Emden harbor. During and at least 90 mins after slack tide, elevated suspended sediment concentrations (SSC above 10 g/l) were generally found below 7 m water depth, occupying around 30 % of the whole water column. Sharp concentration gradients at 7 - 9 m and, ~70 mins. later at 6 - 8 m depth during ebb current (water samples W1250 and W1400 in Fig. 3) attest a 150-cm-layer fluid mud of ~100 g/l. A second steeper concentration and density gradient from 100 to 400 g/l (~1.1 to 1.24 g/cm^3) was observed below and is interpreted as mud of the nautical sole (Figs. 2, 3).

When comparing the wealth of disk measurements, we usually observe very similar exponential increases in the mud layer, ending around 13±2 kPa (see sub-set in Fig. 3). This value is higher than that using the cone, which is in agreement with experiments with cone and plate by e.g., Chung et al. (2006). For tip resistance, a factor of ~33 lies between the cone and disk areas, and with cone configuration tip resistance in fluid mud is well below the detection limit of the CPTU (15 cm^2). With the disk, however, the layer provides measurable resistance, which when normalized ranges 0.5-1.5 kPa above the suspension of Emden harbor water above; Fig. 2). The pore pressure response during the disk penetration tests show coherent values near hydrostatic in the water column, followed by a subtle increase to in the fluid mud, and a strong rise to generally >10 kPa in the consolidating mud underneath (Fig. 3). Effects of internal waves in the fluid mud body or wave activity from wind or currents are ≤10-15 cm at Emden harbor

and here considered negligible compared to 2-3 kPa excess pore pressure obtained with the disk.

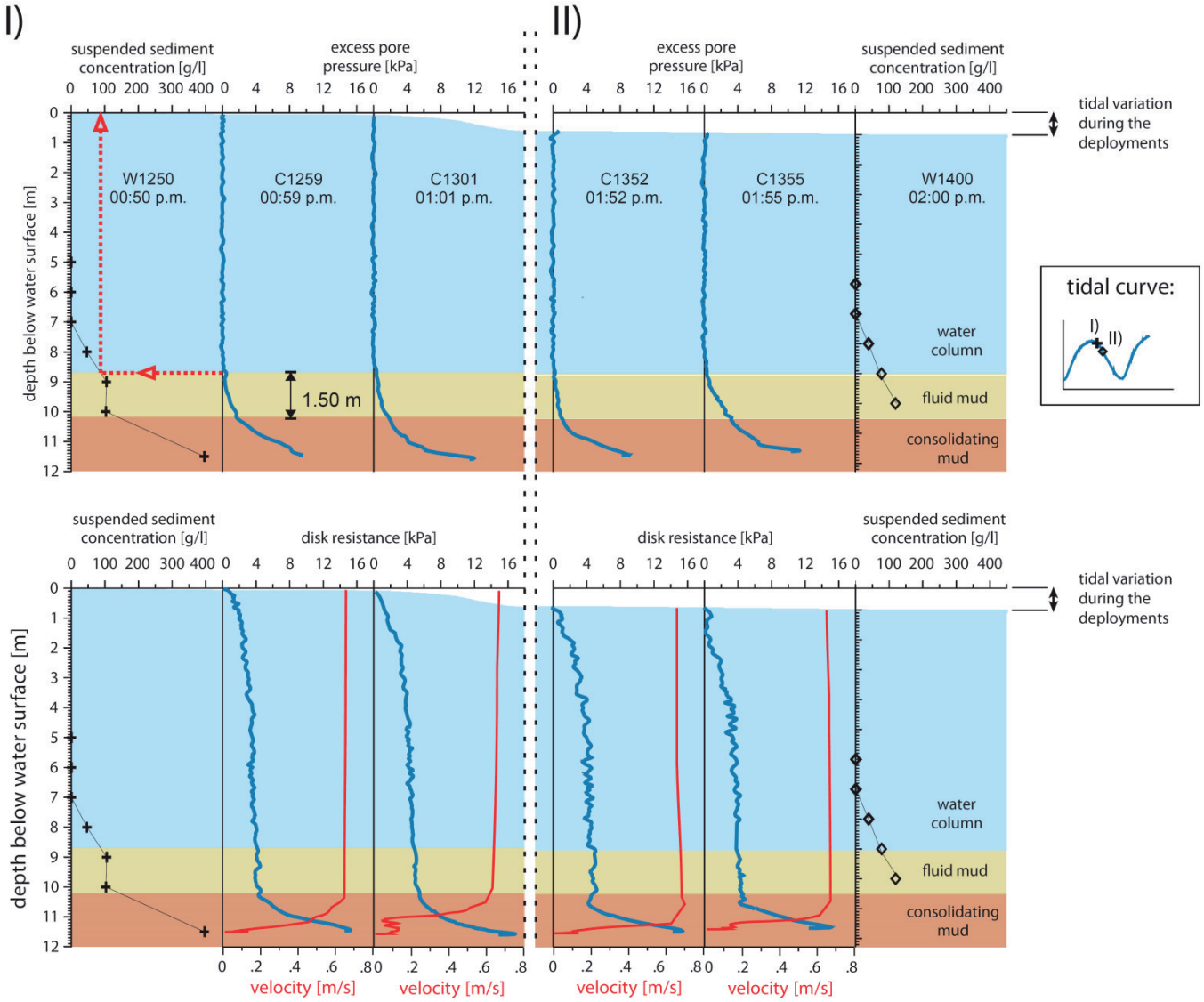

Fig. 3: Comparison of pore pressure (upper row) and disk resistance profiles (lower row) of CPTU disk configuration during slack water (I) and appx. one hour later (II) and corresponding SSC profiles. Velocity from integrating deceleration shown as red graphs overly disk resistance profiles.

Discussion

CPTU devices are commonly used for *in situ* characterization of onshore and offshore sediments by measuring changes in pore pressure and strength during penetration (e.g. Robertson 1990; Baltzer et al. 1994; Lunne et al. 1997; Finke et al. 2001). However, in order to detect fluid mud at the transition from fluid with suspended matter to solid

mud, we here report the first use of a dynamic CPTU probe. This instrument has previously proven versatile in geotechnically characterizing a variety of geological settings (Stegmann, 2007; Stegmann et al. 2007; Kopf et al. 2009). Measurements of sediments at different *in situ* stress states attested that (i) compaction history and/or fluid content cause characteristic pore pressure excursions in the data profile collected (Stegmann et al. 2007; van Baars and van de Graaf 2007; Seifert et al. 2008), and that (ii) dynamic deployments serve to accentuate sediment properties compared to pushed, quasi-static (20 mm/s) cone penetration tests (Stoll et al. 2007; Stegmann 2007). These two points, namely the pore pressure response and rate-effects and their repercussions, represent the crucial aspects of the discussion of our results.

A near-linear excess pore pressure development in a 150-cm-layer of fluid mud was detected by the CPTU probe with both disk and cone configurations in the harbor of Emden (Figs. 2 and 3). Our observations, both from the *in situ* CPTU measurements and ParCa (particle camera; Ratmeyer and Wefer, 1996) observations, suggest that within Emden harbor properties change from a non-structural, fluid-supported suspension above this layer to a structured, framework-supported fluid mud with ~90-100 g/l SSC. It is known that the occurrence of fluid mud can attenuate waves due to viscous dissipation of wave energy in this layer (e.g. de Wit and Kranenburg 1997; Kaihatu et al. 2007; Winterwerp et al. 2007; Jain and Mehta 2009), with part of this energy being reduced by increasing pore pressures (Nairn and Willis 2002). When the CPTU probe hits the fluid mud layer, stress is applied to the fragile network of aggregates, potentially causing an excess pore pressure excursion since the fluid cannot easily dissipate through the dense structural network. This elevated pore pressure is otherwise aiding resuspension of the fluid mud layer (which supports very low effective stresses) once ebb currents pick up and transport it seaward.

Depending on stress state and tip configuration during the deployment, the pore pressure excursion either deflects towards sub- or suprahydrostatic values. From our data, positive excess pore pressures were recorded with the disk, while sub-hydrostatic pressures were found for the cone configuration (Fig. 2). Different signatures can be measured not only because of differences in sediment properties (which we assume constant in the fluid mud layer during the measurements for this study), but also due to different position of the filter element and pressure port. It was located directly at the tip

(u_1 – similar to our disk configuration) or behind the cone (u_2) (e.g. Lunne et al. 1997; Song and Voyiadjis 2005, Fig. 1). The pressure resulting from the displacement generated by the disk when driving of the probe through the mud in the harbor of Emden is interpreted to be predominantly normal stress-induced and, therefore, positive in magnitude (Burns and Mayne 2002; Figs. 2A and 3). The test is envisaged partly drained, because material underneath the disk is compacted during deployment. In contrast, the cone penetration is more rapid and thus undrained (see velocity profile in Fig. 2B). Here, the filter location on the shaft where the sediment experiences mainly shear stress (e.g. Burns and Mayne 1998; Kim and Tumay 2004) and measured excess pore pressures during penetration exhibit a constant linear decrease during CPTU profiling. One explanation offered by Mahajan and Budhu (2006) are viscous effects on penetrating shafts in clays, which depend on the size of the disturbed zone around the shaft, the shear viscosity, and the velocity profile within this zone. Viscous drag increases if the perturbed zone around the shaft is less than four times the shaft radius, which is given in fluid mud and at least likely in the stiffer mud underneath. From our experience based on over a thousand impacts of the CPTU instruments in marine and lacustrine sediments, we additionally postulate that the drag force developed during the passage of cohesive, clay-rich sediments induces suction at the filter and underlying borings of the pore pressure port. This net displacement of material away from the pore pressure transducer may explain negative values, which decrease linearly while the drag force increases with sediment strength and hence penetration depth (Fig. 2B). Sub-hydrostatic excess pore pressures in very soft muds in the Baltic Sea during the impact of a CPTU instrument were described as ‘skin effect’ (Seifert et al. 2008). There, the highly compressible mud revealed a non-Newtonian flow behavior (Silva and Brandes 1998) and similarly a thin layer of fluid mud (Faas and Wartel 2006), so the response to dynamic CPTU penetration represents a valid comparison to Emden harbor mud. Christian et al. (unpublished; see data example at http://www.brooke-ocean.com/ffcpt-01.html) equally show negative pore pressure excursions in very soft clay. Other negative pore pressure signals during such CPTU tests were reported from fresh, unconsolidated mud volcano fluids, where the drag force was related to methane flux through the mud (Kopf et al. 2009). Similarly, standard CPTU tests in high organic soft cohesive sediments by van Baars and van de Graaf (2007; theirs Figs. 7 and 8) yielded

sub-hydrostatic pore pressure signals and dilational sediment response upon penetration. Although we acknowledge that the viscous effects postulated by Mahajan and Budhu (2006) are not unambiguously accepted, findings in our study and earlier work imply dilation to occur in very soft, clay mineral-rich deposits in the shallow sub-seafloor. The detailed mechanisms governing dilation may be subject to numerical approaches in future studies.

It is widely accepted that rate effects prevail in advancing penetrometers, and that a positive correlation exists between tip resistance and penetration rate as long as undrained conditions exist (e.g. Bemben and Myers 1974; Roy et al. 1982; Chung et al. 2006). This response flips in partially or fully drained conditions once the rate is sufficiently slow for the consolidation to occur, so that tip resistance increases. The transition point from undrained to partially drained can be determined by twitch tests at variable rate (Randolph and House 2001).

Despite the fact that there is still limited understanding of the parameters governing viscous effects, the way the disk configuration in this study is used (i.e. a negligible deviation from vertical during penetration) would suggest that at least the pore pressure signal is independent of full flow dynamics because of the position of the boring and overall geometry (Fig. 1). To the authors' knowledge, there is unfortunately no method to date that allows correction of the pore pressure response in CPTU data for rate effects.

In general, dynamic deployments serve to accentuate sediment properties compared to pushed, quasi-static (20 mm/s) cone penetration tests (Stoll et al. 2007; Stegmann 2007). This effect may be masked by the strength increase due to viscous effects during rapid penetration (e.g. Kulhawy and Mayne, 1990). For regular CPTU tests in sediments and soils, a rate-dependent correction with different strain rate factors is required to relate absolute values to standard deployments (see Dayal and Allen, 1975). The strain rate factor is $F_{ac} = 1 + K \log (v/v_{ind})$, where K is a sediment-specific factor, v is the rate of the dynamic penetrometer while v_{ind} is the industry standard, i.e. quasi-static rate of 20 mm/s (Lunne et al., 1997). For this study only the lowermost portion of each deployment has velocities close to 20 mm/s and while all other data show elevated values and would require a rate-dependent correction. However, two reasons stop us

from this exercise: (i) For suspensions and fluid mud, no K values are provided by Dayal and Allen (1975); and (ii) a calculation is meaningless since fluid mud detection cannot be done with regular pushed CPTU devices for their low sensitivity. Also, tests with very slow winch speeds (10 cm/s) did not allow us to detect the fluid mud and only dynamic deployment where the instrument tip "hits" the thick suspension causes stresses sufficiently high for the strain gauges of the CPTU to deform.

One final aspect to be regarded is the contention that disk (or plate) geometries are commonly viewed as full flow penetrometers. "Full-flow" penetrometers provide a measure of the pressure differential necessary to induce soil flow around a symmetric geometric probe, which in principal resembles a viscosity measurement as they induce plastic flow of the material around the probe (Yafrate and DeJong 2007). Provided that the disk deployments monitored pore pressure in the centre of a fairly large disk (i.e., in u_1 position rather than u_2 behind geometric probe), and given further that tilt is <5° and the disk hits seafloor-parallel, we assume the excess pore pressure values meaningful. Nevertheless, it should be noted that the deployments merely serve to accurately detect the fluid mud layer at a given depth, whereas absolute pressure data are not to be taken further at this stage.

In conclusion, *in situ* measurements of disk resistance or pore pressure of the CPTU instrument seems to be a time-efficient and accurate qualitative method to identify fluid mud. Additional deployments over entire tidal cycles during different times in the year, ideally in different regions of fluid mud, are required (i) to fully assess the viability of this method, (ii) to tune the CPTU instrument with regard to density and/or viscosity criteria to monitor navigable depth, and (iii) to come to reliable quantitative results concerning the pore pressure and tip resistance stripped of viscous rate effects.

Acknowledgements We thank the captain and crew of the vessel *Delphin* and Uwe Boekhoff (Emden port authorities) for their support during our study. We also thank the captain and crew of the vessel *Friesland* and Martin Krebs (Waterways and Shipping Board *WSA* Emden) for their cooperation. The Waterways and Shipping Directorate Aurich is acknowledged for kindly providing the water level data. M. Lange, H. Hanff and N. Stark are acknowledged for assistance throughout the campaign. Funding was granted by DFG (via MARUM Research Centre).

References

Baltzer, A., Cochonat, P., and Piper, D. J. W. (1994). "In situ geotechnical characterization of sediments on the Nova Scotian Slope, eastern Canadian continental margin." *Marine Geology*, 120, 291-308.

Bemben, S. M., and Myers, H. J. (1974). "The influence of rate of pen- etration on static cone resistance in Connecticut River Valley varved clay." *Proc., European Symp. on Penetration Testing*, ESOPT, National Swedish Building Research, Stockholm, 2.2, 33–34.

Buchanan, L. (2005). "Surveying in Fluid Mud - The effects on bathymetry of suspended sediment in the water column." *Hydro International*, 9(6), 26-29.

Burns, S. E., and Mayne, P. W. (1998). "Monotonic and dilatory pore-pressure decay during piezocone tests in clay." *Canadian Geotechnical Journal*, 35(6), 1063-1073.

Burns, S. E., and Mayne, P. W. (2002). "Analytical cavity expansion-critical state model for piezocone dissipation in fine-grained soils." *Soils and Foundations - Japanese Geotechnical Society*, 42(2), 131-137.

Chung, S.F., Ramdolph, M.F., and Schneider, J.A. (2006). "Effect of Penetration Rate on Penetrometer Resistance in Clay." Jounal of Geotechnical and Geoenvironmental Engineering, 132(9):1188-1196

Coussot, P. (1997). *Mudflow Rheology and Dynamics*, A.A. Balkema, Rotterdam.

Dayal, U., and Allen, J.H. (1975). "The effect of Penetration Rate on the Strength of Remolded Clay and Sand Samples." *Canadian Geotechnical Journal,* 12, 336-348.

de Wit, P. J., and Kranenburg, C. (1997). "The Wave-induced Liquefaction of Cohesive Sediment Beds." *Estuarine, Coastal and Shelf Science*, 45(2), 261-271.

Faas, R., and Wartel, S. (2006). "Rheological properties of sediment suspensions from Eckernförde and Kieler Förde Bays, western Baltic Sea." *International Journal of Sediment Research*, 21(1), 24-41.

Finke, K. A., Mayne, P. W., and Klopp, R. A. (2001). "Piezocone penetration testing in Atlantic Piedmont residuum." *Journal of Geotechnical and Geoenvironmental Engineering*, 127(1), 48-54.

Fontein, W., Werner, C., and van der Wal, J. (2006). "Assessing nautical depth efficiently in terms of rheological characteristics." *Proc., 15th International Congress of the International Federation of Hydrographic Societies, Evolution in hydrography,* Antwerp, Belgium, 149-152.

Greiser, N., Gamnitzer, R., and Rupp, J. (2002). "Pseudoplasticity of Cohesive Sediments: Causes and Innovative Techniques for Pre-Dredging Surveys." *Proc., CEDA Dredging Days 2002: Dredging without boundaries,* Casablanca, Morocco*,* 1-7.

Guan, W. B., Kot, S. C., and Wolanski, E. (2005). "3-D fluid-mud dynamics in the Jiaojiang Estuary, China." *Estuarine, Coastal and Shelf Science*, 65, 747-762.

Jain, M., and Mehta, A. J. (2009). "Role of basic rheological models in determination of wave attenuation over muddy seabeds." *Continental Shelf Research*, 29(3), 642-651.

Kaihatu, J. M., Sheremet, A., and Holland, K. T. (2007). "A model for the propagation of nonlinear surface waves over viscous muds." *Coastal Engineering*, 54, 752-764.

Kim, D.-K., and Tumay, M. T. (2004). "Miniature Piezocone Test Results in Cohesive Soils." *Electronic Journal of Geotechnical Engineering (EJGE)*, 9D, 1-21.

Kineke, G. C., Sternberg, R. W., Trowbridge, J. H., and Geyer, W. R. (1996). "Fluid mud processes on the Amazon continental shelf." *Continental Shelf Research*, 16(5/6), 667-696.

Kopf, A., Stegmann, S., Delisle, G., Panahi, B., Aliyev, C. S., and Guliyev, I. (2009). "In situ cone penetration tests at the active Dashgil mud volcano, Azerbaijan: Evidence for excess fluid pressure, updoming, and possible future violent eruption." *Marine and Petroleum Geology*, 26(9): 1716-1723.

Kulhawy, F.H., and Mayne, P.W. (1990). “Manual on estimating soild properties for foundation design.” *Final report of EPRI Research Project 1493-6*, Cornell Univ., New York, 308pp.

Lesourd, S., Lesueur, P., Brun-Cottan, J. C., Garnaud, S., and Poupinet, N. (2003). "Seasonal variations in the characteristics of superficial sediments in a macrotidal estuary (the Seine inlet, France)." *Estuarine, Coastal and Shelf Science*, 58(1), 3-16.

Lunne, T., Robertson, P. K., and Powell, J. J. M. (1997). *Cone Penetration Testing in Geotechnical Practice*, E. & F.N. Spon, London and New York.

Mahajan, S., and Budhu, M. (2006). "Viscous effects on penetrating shafts in clays." *Acta Geotechnica*, 1(3), 157-165.

McAnally, W. H., Friedrichs, C., Hamilton, D., Hayter, E., Shrestha, P., Rodriguez, H., Sheremet, A., and Teeter, A. M. (2007a). "Management of Fluid Mud in Estuaries, Bays, and Lakes. I: Present State of Understanding on Character and Behavior." *Journal of Hydraulic Engineering*, 133(1), 9-22.

McAnally, W. H., Teeter, A. M., Schoellhamer, D. H., Friedrichs, C., Hamilton, D., Hayter, E., Shrestha, P., Rodriguez, H., Sheremet, A., and Kirby, R. (2007b). "Management of Fluid Mud in Estuaries, Bays, and Lakes. II: Measurements, Modeling, and Management." *Journal of Hydraulic Engineering*, 133(1), 23-28.

Meischner, D., and Rumohr, J. (1974). "A light-weight, high-momentum gravity corer for subaqueous sediments." *Senckenbergiana maritima,* 6(1),105–117.

Nairn, R. B., and Willis, D. H. (2002). "Erosion, Transport, and Deposition of Cohesive Sediments." *Coastal Engineering Manual, Part III, Coastal Sediment Processes, Chapter III-5, Engineer Manual 1110-2-1100*, D. King, ed., U.S. Army Corps of Engineers, Washington, DC.

Randolph, M. F., and House, A. R. (2001). “The complementary roles of physical and computational modelling.” *Int. J. of Physical Modelling in Geotechnics*, 1(1), 1–8.

Ratmeyer, V., and Wefer, G. (1996). “A high resolution camera system (ParCa) for imaging particles in the ocean: System design and results from profiles and a three-month deployment”. *Journal of Marine Research*, 54: 589-603.

Robertson, P. K. (1990). "Soil classification using the cone penetration test." *Canadian Geotechnical Journal*, 27: 151-158.

Roy, M., Tremblay, M., Tavenas, F., and La Rochelle, P. (1982). “Development of pore pressures in quasi-static penetration tests in sensitive clay.” *Canadian Geotechnical Journal*, 19(2), 124–138.

Seifert, A., Stegmann, S., Mörz, T., Lange, M., Wever, T. and Kopf, A. (2008). "In situ pore-pressure evolution during dynamic CPT measurements in soft sediments of the western Baltic Sea." *Geo-Marine Letters*, 28(4), 213-227.

Silva, A. J., and Brandes, H. G. (1998). "Geotechnical properties and behavior of high-porosity, organic-rich sediments in Eckernförde Bay, Germany." *Continental Shelf Research*, 18, 1917-1938.

Song, C. R., and Voyiadjis, G. Z. (2005). "Pore pressure response of saturated soils around a penetrating object." *Computers and Geotechnics*, 32(1), 37-46.

Stegmann, S., Villinger, H., and Kopf, A. (2006). "Design of a Modular, Marine Free-Fall Cone Penetrometer." *Sea Technology*, 47(2), 27-33.

Stegmann, S. (2007). "Design of a free-fall penetrometer for geotechnical characterisation of saturated sediments and its geological application." PhD thesis, University of Bremen, Bremen, Germany

Stegmann, S., Strasser, M., Anselmetti, F., and Kopf, A. (2007). "Geotechnical in situ characterisation of subaquatic slopes: The role of pore pressure transients versus frictional strength in landslide initiation." *Geophysical Research Letter*, 34, L07607.

Stoll, R.D., Sun, Y.-F., and Bitte, I. (2007). "Seafloor Properties From Penetrometers Tests." *IEEE Journal of Oceanic Engineering*, 32(1), 57-63.

Talke, S. A., and de Swart, H. E. (2006). "Hydrodynamics and Morphology in the Ems/Dollard Estuary: Review of Models, Measurements, Scientific Literature, and the Effects of Changing Conditions." Institute for Marine and Atmospheric Research Utrecht (IMAU), IMAU Report #R06-01, University of Utrecht, Utrecht, The Netherlands.

Uncles, R. J., Stephens, J. A., and Law, D. J. (2006). "Turbidity maximum in the macrotidal, highly turbid Humber Estuary, UK: Flocs, fluid mud, stationary suspensions and tidal bores." *Estuarine, Coastal and Shelf Science*, 67, 30-52.

van Baars, S., and van de Graaf, H. C. (2007). "Determination of Organic Soil Permeability Using The Piezocone Dissipation Test." *Environmental and Engineering Geoscience*, XIII(13), 197-203.

van Kessel, T., and Fontijn, H. L. (2000). "Miniature sounding tests on soft saturated cohesive soils." *Géotechnique*, 50(5), 537-546.

Whitehouse, R., Soulsby, R., Roberts, W., and Mitchener, H. (2000). *Dynamics of estuarine muds - A manual for practical applications*, HR Wallingford Limited and Thomas Telford Limited, London.

Winterwerp, J. C., and van Kesteren, W. (2004). *Introduction to the physics of cohesive sediment in the marine environment*, Elsevier B.V., Amsterdam.

Winterwerp, J. C., de Graaff, R. F., Groeneweg, J., and Luijendijk, A. P. (2007). "Modelling of wave damping at Guyana mud coast." *Coastal Engineering*, 54, 249-261.

Wurpts, R., and Torn, P. (2005). "15 Years Experience with Fluid Mud: Definition of the Nautical Bottom with Rheological Parameters." *Terra et Aqua*, 99, 22-32.

Yafrate, Y.N., and DeJong, J.T. (2007). “Influence of Penetration Rate on Measured Resistance with Full Flow Penetrometers in Soft Clay.” *ASCE Conference Proceedings, Soft Soils: Field testing and modeling,* 1-10. (doi 10.1061/40917(236)9)

MANUSCRIPT 2B (TECHNICAL NOTE)

A modified dynamic CPTU penetrometer for fluid mud detection

Annedore Seifert, Achim Kopf

MARUM - Center for Marine Environmental Sciences, University of Bremen, P.O. Box 330440, 28334 Bremen, Germany

Technical Note, in review

Journal of Geotechnical and Geoenvironmental Engineering (ASCE)

Abstract

Rising maintenance costs in areas of high suspended sediment concentrations to guarantee save ship passage in harbors and motorways demand new efficient and accurate methods to define navigable depths. One particularly complex phenomenon is the episodic, tidally driven variation of this depth level as a result of fluid mud settlement. We present results from dynamic cone penetration testing with pore pressure measurement (CPTU) as a non-acoustical, direct device to support surveying and management of these areas. The new technique is modular and utilizes a disk configuration for fluid mud detection. Both disk resistance and pore pressure measurements accurately identify suspended matter concentrations ≥ 90 g/l, and the transition from fluid mud to consolidating mud once concentrations exceed 150 g/l. Hence, the procedure attests the potential for rapid, reliable assessment of a fluid mud layer and concurrent characterization of the underlying consolidated sediment by monitoring the pore pressure and strength changes during penetration.

Keywords: Fluid mud; Cohesive soils; Cone penetration testing

Introduction

Worldwide maritime trade utilizing larger vessels is increasing, and harbors and waterways have to be deepened to accommodate for these requirements and ensure navigability. Regulation and dredging of rivers and harbors are conducted, which in turn influence the morphology, hydrodynamics and amounts of suspended matter. In regions

affected by tidal variations, thick layers of fluid mud (hereafter FM), a highly concentrated suspension of clay minerals and organic matter, settle in harbors and estuaries (e.g. Kineke et al. 1996; Guan et al. 2005). Suspended sediment concentrations (SSC) of these layers naturally vary between several 10 and 100 g/l depending on mud sources and composition (McAnally et al. 2007a). Fluid mud exhibits a non-Newtonian flow behavior in contrast to Newtonian behavior of water (e.g. Coussot 1997; Winterwerp and van Kesteren 2004), a viscosity typically 1-4 orders of magnitude larger than that of clear water, and a yield stress that correlates positively with increasing SSC at a given shear rate (e.g. McAnally et al. 2007a).

The demand to develop routine methods for FM identification *in situ* is rising rapidly. Nowadays, rheological properties are preferred as criteria for the assessment of the nautical depth over density, because mud of a given density may differ in viscosity due to thixotropic behavior (McAnally et al. 2007b), however, their reliable measurement is confined to the laboratory. Among the *in situ* methods utilized, acoustic echo sounders are most common to determine navigable depth in ports and channels, but their results are ambiguous since changes in p-wave velocity are a crude measure for density or viscosity of the FM layer (Buchanan 2005). Alternatively, a number of probes equipped with optical backscatter, electric resistivity, nuclear transmission, ultra-sonic sensors or tuning fork systems were especially developed to detect suspended matter, density and/or fluid mud thickness (e.g. Greiser et al. 2002). *In situ* constant-rate CPTU deployments are not feasible, because the heavy rigs cause artifacts and the resistance soft mud and suspensions is below the resolution of standard CPTU devices. As a consequence, the main objective of this study in Emden harbor (Germany) was to identify variations in dynamic mechanical response (pore pressure and tip resistance) by a dynamic, lightweight CPTU-Probe (Stegmann et al. 2007).

Methods and Materials

A dynamic CPTU-instrument was deployed in the tidally-affected outer harbor of Emden, Germany, where m-thick fluid mud deposition was reported earlier (Wurpts and Torn 2005). Pore pressure response and sediment resistance during penetration were

measured in the fluid mud layer and underlying consolidated beds. The CPTU probe was run in two configurations (Fig. 1). A 15 cm^2 CPT-cone with u_2 pore pressure port was used when deep penetration was desired. For the detection of the FM, we replaced the cone with a disk (25 cm across, ~490 cm^2) where a central boring accesses a pore pressure port (similar to the u_1 position in a standard CPTU cone; Lunne et al. 1997). The disk serves to enhance the sensitivity of the strain gauge measuring tip resistance when profiling weaker, more viscous media. The filter ring and the borings towards the pressure transducer are carefully saturated with seawater on deck prior to deployment, gets additionally saturated during a 5 min. halt at 5 m water depth to allow trapped gas bubbles to escape, and is replaced after each deployment since clay and other fines may hamper its permeability.

During a typical deployment, the instrument is lowered through the water column on a winch-cable, impacts the bottom, and dynamically penetrates the sediment. During profiling, tip resistance (q_t), sleeve friction (f_s), temperature, tilt, pore pressure and deceleration are recorded. The latter enables us to calculate the velocity during profiling (1st integration) and total penetration depth of the instrument (2nd integration). During all tests the instrument passed the water column at 0.68±0.08 m/s winch speed and then show non-linear deceleration as a function of the profiled material until all momentum is lost and the instrument comes to a complete halt.

To ground-truth the CPTU results, water and sediment samples were collected around slack tide when current velocities are sufficiently low for fluid mud deposition. We sampled the water column in 1 m depth-intervals into the FM layer using a pump, and additionally took an overlapping 2 m- long gravity core into the FM and nautical sole, which got sub-sampled in 0.2 m depth-intervals. In the laboratory all samples were analyzed for SSC by weighing dry mass per unit sample volume.

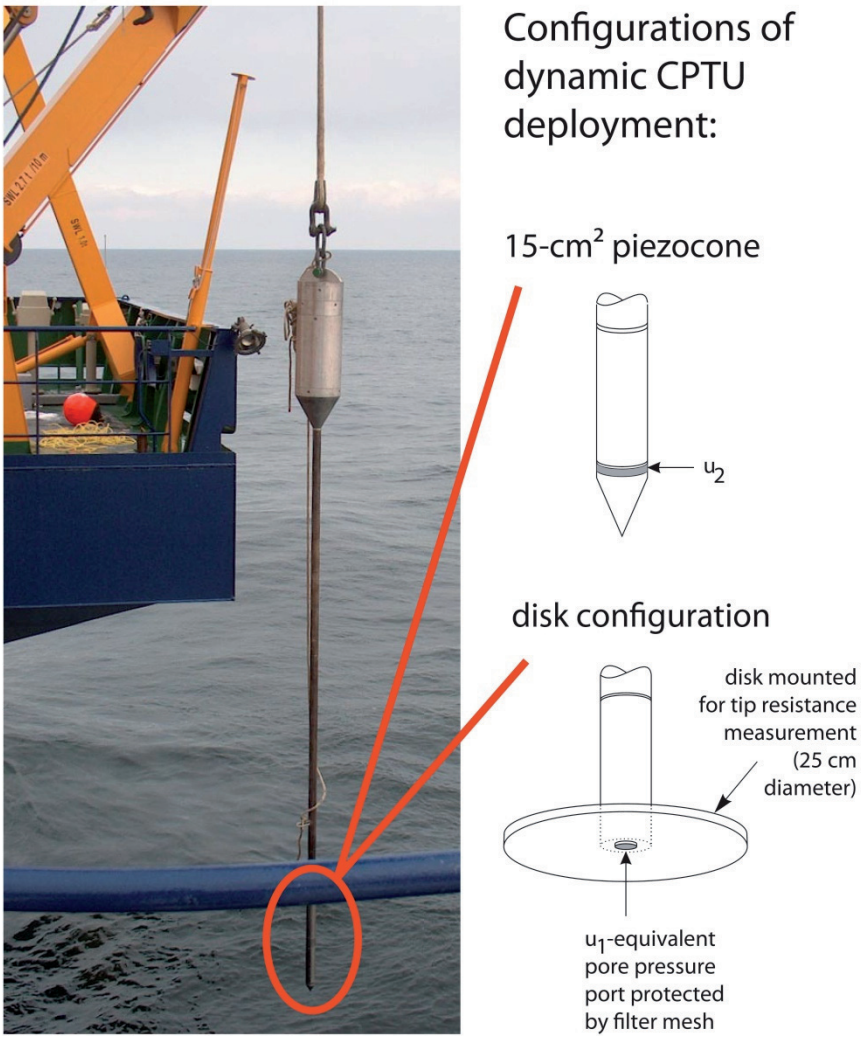

Fig. 1: The dynamic CPTU-instrument comprises a modular design and for this study was used with a total length of 3m and two different tips. Left-hand side shows photograph of the device; right-hand side illustrates cone (top) and disk configurations (bottom).

Results

We here compare a few of the total of 47 CPTU deployments with disk (11) and cone (36) configuration at slack tide and relate them to the sediment and overlying FM and suspended matter (Fig. 2). SSC is well below 10 g/l in the suspended harbor water, steps to ~110 g/l in the FM layer, and then steadily increases to up to 400 g/l (~1.1 to 1.24 g/cm^3) in the nautical sole. This is mirrored by a subtle increase in disk resistance in the

~150 cm-thick fluid mud layer (~6 kPa), and a very steep rise to values >16 kPa below (Fig. 2A). In contrast, the cone configuration fails to detect the fluid mud layer because the probe lacks sensitivity. However, q_c increases in the mud of the nautical sole (up to ~10 kPa) and terminal sub-bottom depth increases by ~150 cm (Fig. 2B). Interestingly, excess pore pressure is most indicative of fluid mud, although disk configuration shows an increase whereas the cone measures subhydrostatic values. These overall trends are enhanced in the underlying mud, i.e. a rise to +15 kPa (disk) and –30 kPa (cone) were measured once the instrument fully penetrated (Fig. 2). For the fluid mud, the most important finding is that disk CPTU deployments record up to 16 kPa, which when normalized for the enhanced area relative to the standard CPT cone, amounts to a 0.5-1.5 kPa higher resistance than Emden harbor water (Fig. 2). The pore pressure response during the disk deployments show coherent values near hydrostatic in the water column, followed by a subtle increase to in the fluid mud, and a strong rise to generally >10 kPa in the consolidating mud underneath (see Discussion below).

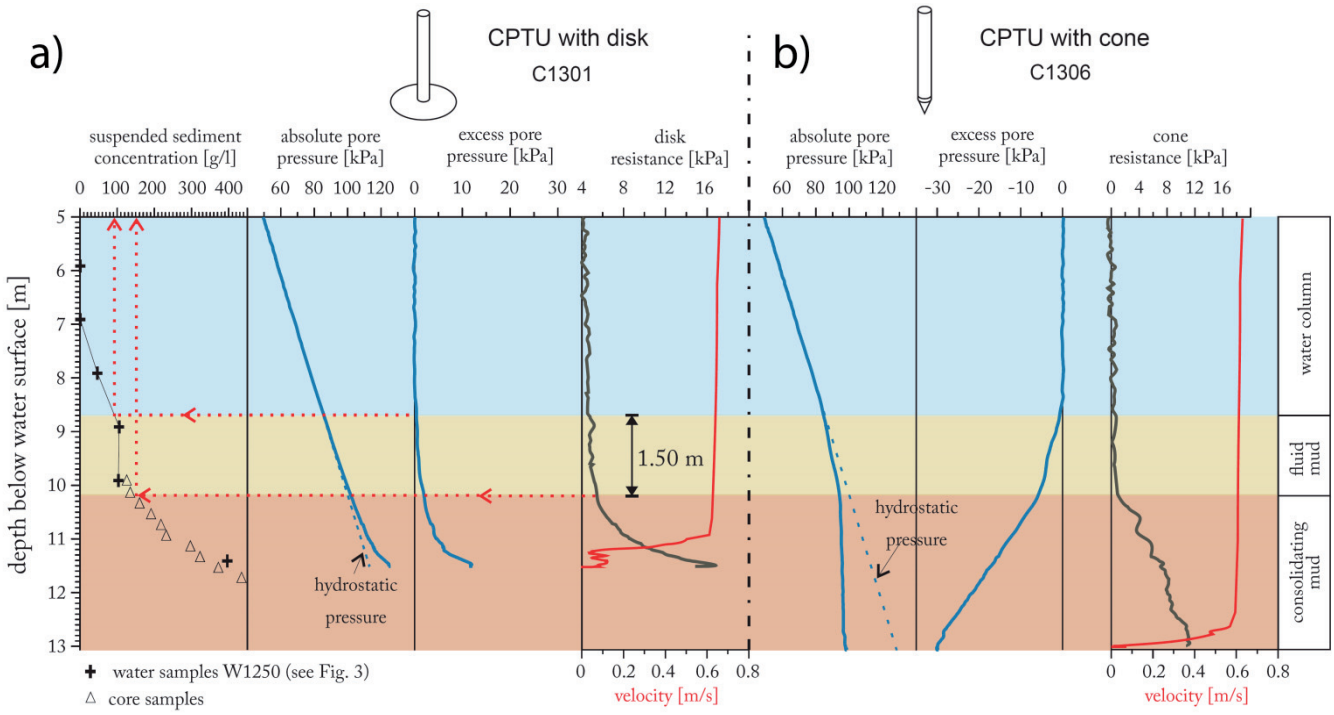

Fig. 2: Typical CPTU profiles (disk and cone configuration) of fluid mud and underlying consolidated sediment and corresponding SSC profiles. a) CPTU disk configuration with disk resistance profile. b) CPTU cone configuration with qc profile. Velocity from integrating deceleration is shown as red graphs.

Discussion

CPTU-devices, commonly used for *in situ* geotechnical sediment characterization (e.g. Lunne et al. 1997), are here shown to be a feasible technique to detect fluid mud at the transition from fluid with suspended matter to solid mud. A near-linear excess pore pressure evolution in a 150-cm-layer of fluid mud was detected by the CPTU-probe with both disk and cone configurations (Figs. 1, 2). Our observations, supported by ParCa (particle camera) monitoring, suggest that within Emden harbor properties change from a non-structural, fluid-supported suspension above this layer to a structured, framework-supported fluid mud with ~100 g/l SSC. It is known that the occurrence of fluid mud can attenuate waves due to viscous dissipation of wave energy in this layer (e.g. de Wit and Kranenburg 1997), with part of this energy being reduced by increasing pore pressures (Nairn and Willis 2002). When the CPTU-probe hits the FM layer, the stress applied to the fragile network of aggregates causes elevated excess pore pressure since the fluid cannot easily dissipate through the dense structural network. This elevated pore pressure is otherwise aiding resuspension of the FM layer once ebb currents pick up.

Depending on stress state and tip configuration during the deployment, positive excess pore pressures were recorded with the disk entering FM, while sub-hydrostatic pressures were found with the cone (Fig. 2). The different signatures are related to position of the filter element and pressure port (e.g. Song and Voyiadjis 2005, Fig. 1). The pressure resulting from the displacement generated by the disk when driving of the probe through the mud in the harbor of Emden is interpreted to be predominantly normal stress-induced (i.e. material underneath the disk is compacted) and, therefore, positive in magnitude (Burns and Mayne 2002; Fig. 2A). In cone configuration the filter is located on the shaft where the sediment experiences mainly shear stress (e.g. Burns and Mayne 1998), so that measured excess pore pressures generally decrease during CPTU-profiling. One explanation offered by Mahajan and Budhu (2006) are viscous effects on penetrating shafts in clays, which depend on the size of the disturbed zone around the shaft, the shear viscosity, and the velocity profile within this zone. Viscous drag increases if the perturbed zone around the shaft is less than four times the shaft radius, which is given in fluid mud and at least likely in the stiffer mud underneath.

From our experience based on over a thousand impacts of the CPTU-instruments in marine and lacustrine sediments, we additionally postulate that the drag force developed during the passage of cohesive, clay-rich sediments induces suction at the filter and underlying borings of the pore pressure port. This net displacement of material away from the pore pressure transducer may explain negative values, which decrease linearly while the drag force increases with sediment strength and hence penetration depth (Fig. 2B). This finding in FM agrees with sub-hydrostatic excess pore pressures in very soft muds in the Baltic Sea (Seifert et al. 2008), where the 'skin effect' was explained with a non-Newtonian flow behavior (Silva and Brandes 1998). Negative pore pressure signals and dilation during CPTU-tests were also reported from high organic soft cohesive sediments (van Baars and van de Graaf, 2007; their Figs. 7 and 8) as well as from unconsolidated mud volcano fluids, where the drag force was related to methane flux through the mud (Kopf et al. 2009). Although the detailed mechanisms governing dilation are incompletely understood, viscous effects postulated by Mahajan and Budhu (2006) are in agreement with our CPTU-results and imply dilation to occur in very soft, clay mineral-rich deposits in the shallow sub-seafloor. However, it should be noted that the deployments carried out for this study merely serve to accurately detect the fluid mud layer at a given depth, whereas absolute pressure values have not been taken further (strain rate correction, etc.) in this Technical Note.

Conclusions

This technical note mainly provides a "proof-of-concept" that *in situ* measurements of disk resistance or pore pressure of the CPTU-instrument seem to be a time-efficient and accurate method to identify fluid mud. Additional deployments over entire tidal cycles during different times in the year, ideally in different regions of fluid mud, are required (i) to fully assess the viability of this method in a given geological setting, (ii) to tune the CPTU instrument with regard to density and/or viscosity criteria to monitor navigable depth, and (iii) to come to reliable quantitative results concerning the pore pressure and tip resistance stripped of viscous rate effects.

Acknowledgements

We thank the captain and crew of the vessel *Delphin* and Uwe Boekhoff (Emden port authorities) for their support during our study. We also thank the captain and crew of the vessel *Friesland* and Martin Krebs (Waterways and Shipping Board *WSA* Emden) for their cooperation. The Waterways and Shipping Directorate Aurich is acknowledged for kindly providing the water level data. M. Lange, H. Hanff and N. Stark are acknowledged for assistance throughout the campaign. Funding was granted by DFG (via MARUM Research Centre).

References

Buchanan, L. (2005). "Surveying in Fluid Mud - The effects on bathymetry of suspended sediment in the water column." *Hydro International*, 9(6), 26-29.

Burns, S. E., and Mayne, P. W. (1998). "Monotonic and dilatory pore-pressure decay during piezocone tests in clay." *Canadian Geotechnical Journal*, 35(6), 1063-1073.

Burns, S. E., and Mayne, P. W. (2002). "Analytical cavity expansion-critical state model for piezocone dissipation in fine-grained soils." *Soils and Foundations - Japanese Geotechnical Society*, 42(2), 131-137.

Coussot, P. (1997). *Mudflow Rheology and Dynamics*, A.A. Balkema, Rotterdam.

de Wit, P. J., and Kranenburg, C. (1997). "The Wave-induced Liquefaction of Cohesive Sediment Beds." *Estuarine, Coastal and Shelf Science*, 45(2), 261-271.

Greiser, N., Gamnitzer, R., and Rupp, J. (2002). "Pseudoplasticity of Cohesive Sediments: Causes and Innovative Techniques for Pre-Dredging Surveys." *Proc., CEDA Dredging Days 2002: Dredging without boundaries,* Casablanca, Morocco*,* 1-7.

Guan, W. B., Kot, S. C., and Wolanski, E. (2005). "3-D fluid-mud dynamics in the Jiaojiang Estuary, China." *Estuarine, Coastal and Shelf Science*, 65, 747-762.

Kineke, G. C., Sternberg, R. W., Trowbridge, J. H., and Geyer, W. R. (1996). "Fluid mud processes on the Amazon continental shelf." *Continental Shelf Research*, 16(5/6), 667-696.

Kopf, A., Stegmann, S., Delisle, G., Panahi, B., Aliyev, C. S., and Guliyev, I. (2009). "In situ cone penetration tests at the active Dashgil mud volcano, Azerbaijan: Evidence for excess fluid pressure, updoming, and possible future violent eruption." *Marine and Petroleum Geology*, 26(9): 1716-1723.

Lunne, T., Robertson, P. K., and Powell, J. J. M. (1997). *Cone Penetration Testing in Geotechnical Practice*, E. & F.N. Spon, London and New York.

Mahajan, S., and Budhu, M. (2006). "Viscous effects on penetrating shafts in clays." *Acta Geotechnica*, 1(3), 157-165.

McAnally, W. H., Friedrichs, C., Hamilton, D., Hayter, E., Shrestha, P., Rodriguez, H., Sheremet, A., and Teeter, A. M. (2007a). "Management of Fluid Mud in Estuaries, Bays, and Lakes. I: Present State of Understanding on Character and Behavior." *Journal of Hydraulic Engineering*, 133(1), 9-22.

McAnally, W. H., Teeter, A. M., Schoellhamer, D. H., Friedrichs, C., Hamilton, D., Hayter, E., Shrestha, P., Rodriguez, H., Sheremet, A., and Kirby, R. (2007b). "Management of Fluid Mud in

Estuaries, Bays, and Lakes. II: Measurements, Modeling, and Management." *Journal of Hydraulic Engineering*, 133(1), 23-28.

Nairn, R. B., and Willis, D. H. (2002). "Erosion, Transport, and Deposition of Cohesive Sediments." *Coastal Engineering Manual, Part III, Coastal Sediment Processes, Chapter III-5, Engineer Manual 1110-2-1100*, D. King, ed., U.S. Army Corps of Engineers, Washington, DC.

Seifert, A., Stegmann, S., Mörz, T., Lange, M., Wever, T. and Kopf, A. (2008). "In situ pore-pressure evolution during dynamic CPT measurements in soft sediments of the western Baltic Sea." *Geo-Marine Letters*, 28(4), 213-227.

Silva, A. J., and Brandes, H. G. (1998). "Geotechnical properties and behavior of high-porosity, organic-rich sediments in Eckernförde Bay, Germany." *Continental Shelf Research*, 18, 1917-1938.

Song, C. R., and Voyiadjis, G. Z. (2005). "Pore pressure response of saturated soils around a penetrating object." *Computers and Geotechnics*, 32(1), 37-46.

Stegmann, S., Strasser, M., Anselmetti, F., and Kopf, A. (2007). "Geotechnical in situ characterisation of subaquatic slopes: The role of pore pressure transients versus frictional strength in landslide initiation." *Geophysical Research Letter*, 34, L07607.

van Baars, S., and van de Graaf, H. C. (2007). "Determination of Organic Soil Permeability Using The Piezocone Dissipation Test." *Environmental and Engineering Geoscience*, XIII(13), 197-203.

Winterwerp, J. C., and van Kesteren, W. (2004). *Introduction to the physics of cohesive sediment in the marine environment*, Elsevier B.V., Amsterdam.

Wurpts, R., and Torn, P. (2005). "15 Years Experience with Fluid Mud: Definition of the Nautical Bottom with Rheological Parameters." *Terra et Aqua*, 99, 22-32.

MANUSCRIPT 3

In situ pore-pressure evolution during dynamic CPT measurements in soft sediments of the western Baltic Sea

Annedore Seifert[1], Sylvia Stegmann[1], Tobias Mörz[1], Matthias Lange[1], Thomas Wever[2], Achim Kopf[1]

[1]*MARUM - Center for Marine Environmental Sciences, University of Bremen, P.O. Box 330440, 28334 Bremen, Germany*

[2]*Forschungsanstalt der Bundeswehr für Wasserschall und Geophysik (FWG), Klausdorfer Weg 2-24, 24148 Kiel, Germany*

Geo-Marine Letters (2008), 28 (4), 213 – 227

Abstract

We present in situ strength and pore-pressure measurements from 57 dynamic cone penetration tests in sediments of Mecklenburg (n=51), Eckernförde (n=2) and Gelting (n=4) bays, western Baltic Sea, characterised by thick mud layers and partially free microbial gas resulting from the degradation of organic material. In Mecklenburg and Eckernförde bays, sediment sampling by nine gravity cores served sedimentological characterisation, analyses of geotechnical properties, and laboratory shear tests. At selected localities, high-resolution echo-sounder profiles were acquired. Our aim was to deploy a dynamic cone penetrometer (CPT) to infer sediment shear strength and cohesion of the sea bottom as a function of fluid saturation. The results show very variable changes in pore pressure and sediment strength during the CPT deployments. The majority of the CPT measurements (n=54) show initially negative pore-pressure values during penetration, and a delayed response towards positive pressures thereafter. This so-called type B pore-pressure signal was recorded in all three bays, and is typically found in soft muds with high water contents and undrained shear strengths of 1.6–6.4 kPa. The type B signal is further affected by displacement of sediment and fluid upon penetration of the lance, skin effects during dynamic profiling, enhanced consolidation and strength of individual horizons, the presence of free gas, and a dilatory response of the sediment. In Mecklenburg Bay, the remaining small number of CPT measurements (n=3) show a well-defined peak in both pore pressure and cone resistance during penetration, i.e. an initial marked increase which is followed by exponential pore-pressure decay during dissipation. This so-called type A pore-pressure signal is associated with normally consolidated mud, with indurated clay layers showing significantly higher undrained shear strength (up to 19 kPa). In Eckernförde and Gelting bays pore-pressure response type B is exclusively found, while in Mecklenburg Bay types A and B were detected. Despite the striking similarities in incremental density increase and shear strength behaviour with depth, gas occurrence and subtle variations in the coarse-grained fraction cause distinct porepressure curves. Gaseous muds interbedded with silty and sandy layers are most common in the three bays, and the potential effect of free gas (i.e. undersaturated pore space) on in situ strength has to be explored further.

Introduction

Ever increasing anthropogenic use of coastal areas and shallow seas—e.g. for the installation of wind power stations and gas pipelines, or the dredging of sediment to maintain navigable depth—requires in-depth knowledge of various processes operating in these regions, as well as the detailed characterisation of bottom sediments. The Baltic Sea is the biggest brackish sub-basin of the global ocean, and is intensively used for sea traffic, fishing, and the mining of resources such as Fe and Mn deposits, sand and gravel, or amber and industrial minerals (Harff et al. 2004). The sedimentary environment poses a particular challenge for such activities, because sediment physicochemical properties show marked variations in both space and time, reflecting a complex postglacial development and the influence of multiple transgressions and regressions during the evolution of the Baltic Basin (Duphorn et al. 1995; Jensen et al. 1999). Sandy sediments are found mainly along the coastal fringes, whereas fine-grained mud dominates the deeper basins of the Baltic Sea (Lemke 1998). These soft muds commonly have high water contents (up to 500% relative water content at the seabed in Eckernförde Bay; Silva and Brandes 1998) and high organic matter contents (up to 10% in Mecklenburg Bay; Bobertz 2000), and reach thicknesses of 7 m in Mecklenburg Bay (Niedermeyer 1987) and even 8 m in Eckernförde Bay (Orsi et al. 1996). Remarkable for the western Baltic Sea is the occurrence of free gas in the shallow subsurface, where organic material undergoes degradation under anoxic conditions, thereby forming mainly methane (e.g. Duphorn et al. 1995; Wilkens and Richardson 1998; Albert et al. 1998; Wever et al. 1998, 2006).

Investigations of sediment properties in the western Baltic Sea have hitherto been carried out mainly by field sampling and subsequent laboratory analysis (e.g. Kolp 1966; Silva and Brandes 1998; Bohling 2003). For sediments containing free gas bubbles, such as occur in coastal seas including the Baltic Sea, North Sea and Black Sea, the recovery, storage and handling of sediment samples can cause disturbances due to degassing which, in turn, may affect measurements of physical properties. In order to overcome this problem in the case of the Baltic Sea, pressurised coring methods have been successfully used for a study of the microfabric of gassy sediments in Eckernförde Bay by Lavoie et al. (1996). If time and effort are to be reduced, however, in situ measurements of sediment physical properties are required.

Cone penetrometers (CPTs) are efficient instruments widely used for in situ determination of geotechnical properties of marine sediments (e.g. Lunne et al. 1997). For the Baltic Sea, Bennett et al. (1996) presented in situ pore-pressure response measurements in the course of six piezometer insertions into the fine-grained sediments of Eckernförde Bay. These tests were limited to the upper 100 cm, and further in situ investigations would therefore be necessary to determine sediment properties at greater depths in this region. In contrast to constant-rate CPT tests, which can result in considerable sediment disturbance because of the heavy rig, dynamic cone penetration tests show a response decelerating as the instrument impacts into the sediment, until it comes to a complete rest at a particular depth within a few seconds. During that period, very fast changes of pressure and deformation due to physical displacement of sediment and fluid are common (e.g. Schultheiss 1990a; Fang et al. 1993; Lee and Elsworth 2004; Stegmann et al. 2006a). Depending on properties such as the strength, density and permeability of the sediment, the induced pore pressure dissipates with time to reach its ambient equilibrium value.

Within this context, we present data from two research cruises carried out in 2006 to three muddy sub-basins of the western Baltic Sea, namely Mecklenburg Bay, Eckernförde Bay and Gelting Bay. The main aim of this paper is to relate differences in penetration resistance and pore-pressure evolution during and after CPT deployment to effects such as variability in the state of consolidation and degree of undersaturation (i.e. free gas in the mud). In addition to velocity-controlled, dynamic CPT measurements, we took gravity cores to determine various physicochemical sediment properties. Across some of the CPT and gravity core locations, we acquired high-resolution echo-sounder profiles to investigate the sub-bottom geological structures for data interpretation.

Materials and methods

Cruises to Mecklenburg, Eckernförde and Gelting bays (Fig. 1) were carried out aboard the R/V Kronsort in January 2006, and the R/V Planet in March 2006. Both cruises aimed at the characterisation of the shallow (< 10 m below seafloor) sub-bottom sediment, and its stability and potential for remobilisation.

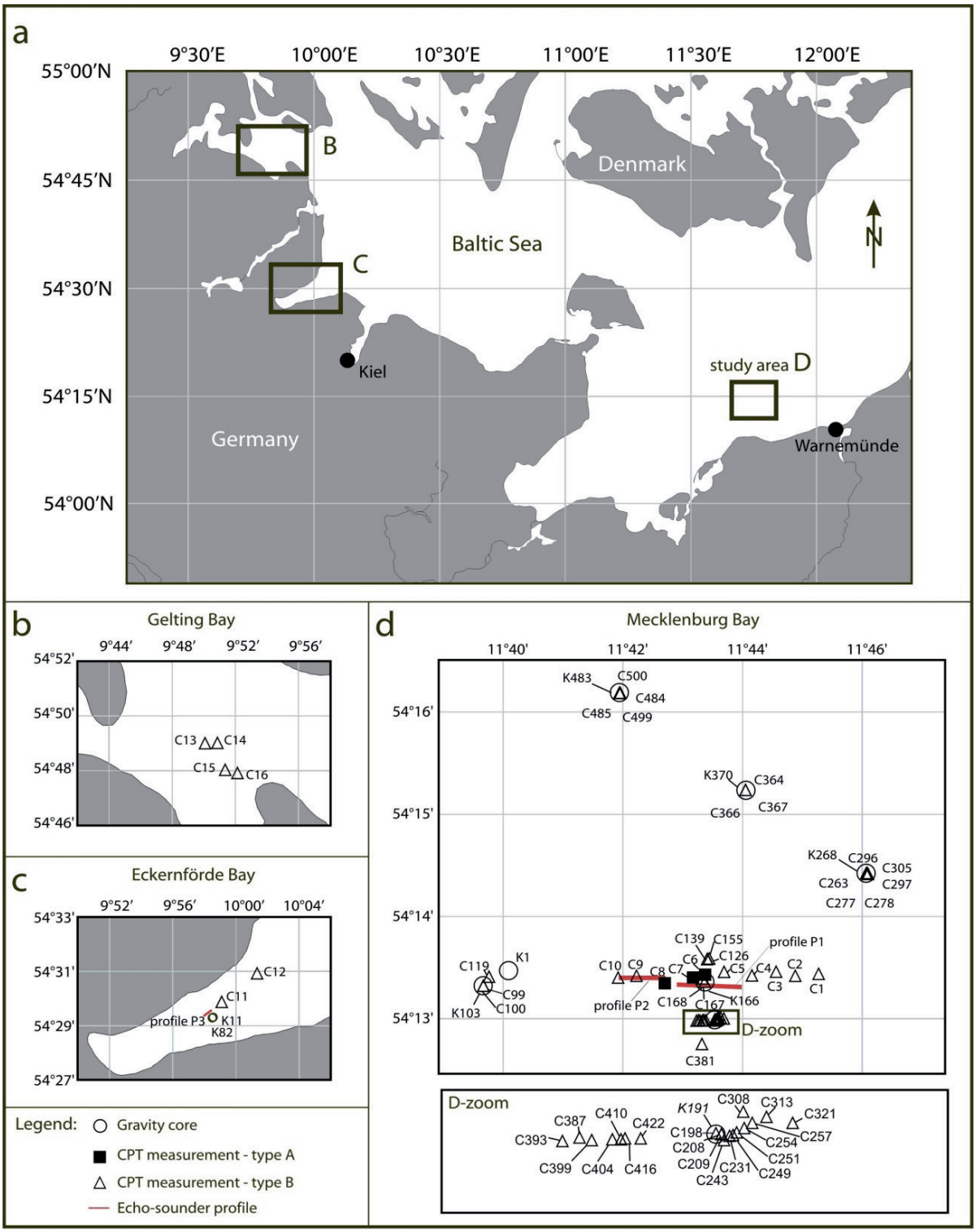

Fig. 1 **a** Map of the southwestern Baltic Sea, with the locations of the study areas Gelting Bay, Eckernförde Bay and Mecklenburg Bay. **b** Map of the Gelting Bay study area, with the CPT locations C13–C16. **c** Map of the Eckernförde Bay study area, with the locations of CPT tests C11–C12, cores K11 and K82, and echo-sounder profile P3. **d** Locations of CPT tests C99–C500, cores K1, K103, K166, K191, K268, K370 and K483, and echosounder profiles P1 and P2 in Mecklenburg Bay (see Tables 1 and 2 for details)

In all, 57 dynamic cone penetration tests were conducted in Mecklenburg (n=51, Kronsort and Planet cruises), Eckernförde (n=2, Kronsort cruise) and Gelting (n=4, Kronsort cruise) bays (Fig. 1), using a modular dynamic CPT lance designed at RCOM (Research Centre Ocean Margins), University of Bremen. It consists of a standard 15-cm^2 CPT probe to measure cone resistance (q_t), sleeve friction (f_s), and the tilt of the lance. Directly behind the cone, an absolute pore-pressure sensor (u_2) measures the pressure response during and after penetration. The pressure signal comprises the hydrostatic pressure, the ambient pore pressure, and a pore-pressure spike induced by the impact. For each CPT record, the excess pore pressure was determined as the difference between the measured absolute pressure and the hydrostatic pressure at a given depth during profiling. Any impact-induced pressure signal is given time to dissipate, so that measured pressure values are expected to approach ambient background values. A deceleration sensor, installed in the head, enables calculation of the penetration depth of the CPT via twofold integration of the deceleration. In the present case, the deceleration sensor sometimes reached the limit of its range, so that the penetration depth had to be estimated by correlating the length of the probe to which sediment had stuck with core and echo-sounding data (Table 1). The CPT raw data were further processed using MATLAB and LABVIEW routines. For further details regarding the device, the reader is referred to Stegmann et al. (2006b).

High-velocity dynamic CPT tests, in which the CPT is lowered at rates of 0.3 m/s up to free drop, differ significantly from standard cone penetrometer tests in which the lance is pushed into the sediment at a constant rate of 2 cm/s. The enhanced impact velocity affects both the initial peak of cone resistance, as well as the porepressure excursion. The former can be accounted for by introducing stress–strain factors for different materials (e.g. Dayal and Allen 1975; Roy et al. 1982), while the latter requires time for the pore-pressure value to equilibrate to its ambient value. The advantage of the time-efficient dynamic procedure is that no hydraulic platform is needed on the seabed, which otherwise could disturb the sediments being investigated.

In Gelting and Eckernförde bays, the CPT lance was operated with 3-m-long extension rods and 60 kg extra weight, and lowered at a winch speed of around 1 m/s (0.6–1.2 m/s; Table 1), depending on winch configuration and handling. In Mecklenburg Bay, ten CPT deployments (C1–C10) were carried out using 3-m rods and 60 kg extra weight

at a winch speed of around 1 m/s (0.7–1.2 m/s; Table 1). The other 41 deployments (C99–C500) had 2-m rods, 30 kg extra weight, and a winch speed of around 2 m/s (1.5–2.6 m/s; Table 1).

Table 1 CPT code number, water depth, testing mode (velocity, duration of measurement), and penetration depth for excess pore-pressure types A and B

CPT	Location	Water depth [m]	Winch velocity [m/s]	Duration of measurement [min]	Penetration depth [m]
Type A, Mecklenburg Bay					
C6	011°43.380' E / 054°13.431' N	25.5	1.1	4.5	1.77[a]
C7	011°43.178' E / 054°13.404' N	25.5	1.1	2.8	2.27[a]
C8	011°42.708' E / 054°13.348' N	25.7	0.7	9.5	2.30[a]
Type B, Mecklenburg Bay					
C1	011°45.277' E / 054°13.439' N	25.3	1.1	2	2.00[a]
C2	011°44.887' E / 054°13.420' N	25.2	1.2	2	3.40[a]
C3	011°44.567' E / 054°13.460' N	25.3	1.1	2	2.00[a]
C4	011°44.163' E / 054°13.424' N	25.3	1.1	1	2.00[a]
C5	011°43.698' E / 054°13.459' N	25.4	0.9	2.5	*
C9	011°42.234' E / 054°13.420' N	25.8	1.1	8.5	0.81[b]
C10	011°41.927' E / 054°13.403' N	25.8	1.1	9	1.33[b]
C99	011°39.674' E / 054°13.322' N	27.3	1.5	53	2.86[b]
C100	011°39.676' E / 054°13.324' N	27.3	2.1	1	2.57[b]
C119	011°39.770' E / 054°13.412' N	27.1	2.2	48.5	1.93[a]
C126	011°43.448' E / 054°13.589' N	25.6	2.3	0.6	2.27[b]
C139	011°43.414' E / 054°13.582' N	25.7	2.1	51.5	1.88[b]
C155	011°43.418' E / 054°13.586' N	25.6	2.1	1.5	1.80[b]
C167	011°43.375' E / 054°13.362' N	25.3	2.1	5	2.13[b]
C168	011°43.333' E / 054°13.393' N	25.0	2.2	54	2.40[a]
C198	011°43.541' E / 054°12.991' N	25.6	1.8	8.5	2.57[b]
C208	011°43.552' E / 054°12.990' N	25.9	2.0	1.5	2.67[b]
C209	011°43.552' E / 054°12.990' N	26.2	2.2	52	3.07[b]
C231	011°43.568' E / 054°12.988' N	25.7	2.0	53.5	3.13[b]
C243	011°43.557' E / 054°12.983' N	26.0	2.0	52	2.85[b]
C249	011°43.575' E / 054°12.989' N	25.5	1.5	0.5	2.50[a]
C251	011°43.582' E / 054°12.992' N	25.0	1.5	1	2.80[b]
C254	011°43.597' E / 054°12.997' N	25.3	1.2	0.6	2.05[b]
C257	011°43.613' E / 054°13.003' N	25.8	1.7	0.5	2.52[b]
C263	011°46.071' E / 054°14.422' N	26.0	2.1	14.5	2.00[b]
C277	011°46.080' E / 054°14.425' N	25.7	1.9	49	2.50[a]
C278	011°46.081' E / 054°14.424' N	25.6	2.3	1	1.33[b]
C296	011°46.102' E / 054°14.417' N	25.8	1.9	40	1.61[b]
C297	011°46.102' E / 054°14.418' N	25.6	2.3	1	2.13[b]
C305	011°46.100' E / 054°14.421' N	25.7	2.1	97	1.71[b]
C308	011°43.595' E / 054°13.016' N	25.1	2.4	1	2.31[b]
C313	011°43.641' E / 054°13.010' N	25.3	2.4	3	2.54[b]
C321	011°43.693' E / 054°13.003' N	25.0	1.6	2.5	1.04[b]
C364	011°44.058' E / 054°15.237' N	26.4	2.2	1.5	1.15[b]
C366	011°44.056' E / 054°15.237' N	25.0	1.8	1	0.97[b]
C367	011°44.057' E / 054°15.237' N	26.1	2.1	99	2.50[a]
C381	011°43.327' E / 054°12.754' N	24.9	2.6	10	2.13[b]
C387	011°43.271' E / 054°12.986' N	25.0	2.3	9.5	1.98[b]
C393	011°43.237' E / 054°12.982' N	25.1	2.3	10	1.55[b]
C399	011°43.295' E / 054°12.983' N	25.1	2.2	59	2.38[b]
C404	011°43.336' E / 054°12.984' N	25.1	2.4	10.5	1.72[b]
C410	011°43.353' E / 054°12.984' N	25.1	2.5	10	1.97[b]
C416	011°43.361' E / 054°12.985' N	25.4	2.5	10	1.86[b]
C422	011°43.392' E / 054°12.985' N	25.6	2.4	9.5	2.70[b]
C484	011°41.950' E / 054°16.187' N	26.4	2.3	6	2.50[a]
C485	011°41.950' E / 054°16.187' N	26.2	2.4	60	2.20[a]
C499	011°41.962' E / 054°16.185' N	26.0	2.2	9.5	2.85[b]
C500	011°41.962' E / 054°16.185' N	26.0	2.4	25	3.22[b]

Table 1 (continued)

CPT	Location	Water depth [m]	Winch velocity [m/s]	Duration of measurement [min]	Penetration depth [m]
Type B, Eckernförde Bay					
C11	009°59.100' E / 054°29.876' N	29.1	1.1	6.5	3.28[b]
C12	010°01.340' E / 054°30.927' N	29.6	0.6	2	*
Type B, Gelting Bay					
C13	009°50.080' E / 054°49.006' N	25.7	0.7	11	3.66[b]
C14	009°50.866' E / 054°49.016' N	24.4	1.1	7	3.00[b]
C15	009°51.354' E / 054°48.033' N	23.1	1.1	10	1.98[b]
C16	009°52.133' E / 054°47.919' N	21.5	1.0	3	2.39[b]

C1–C16: *Kronsort* cruise of January 2006; other CPT tests: *Planet* cruise of March 2006 (for details, see text and Fig. 1; *asterisk* poor data quality because of heave)
[a] Penetration depth measured onboard
[b] Penetration depth calculated from deceleration data

Apart from the primary CPT parameters mentioned above, a number of secondary parameters can also be derived. Most importantly, the undrained sediment shear strength (s_u) may be calculated by means of empirical equations proposed by Lunne et al. (1997), using the cone resistance $s_u = (q_t - \sigma_{v0}) / N_{kt}$, where q_t is the cone resistance corrected for pore pressure, σ_{v0} the total overburden pressure, and N_{kt} a cone factor generally varying between 10 and 20 for normally consolidated clays. Such in situ strength measurements can be compared to those measured in the laboratory using a vane shear device for sediment cores (see below).

For ground-truthing purposes, several gravity cores were taken at selected CPT locations, i.e. seven in Mecklenburg Bay and two cores in Eckernförde Bay (Fig. 1 and Table 2). No cores could be taken in Gelting Bay due to rough weather conditions. Cores K103 and K166, both further analysed by T. Garlan and P. Guyomard (SHOM Institute, France), and K191 from Mecklenburg Bay were opened immediately after recovery in the shipboard laboratory to measure undrained shear strength. For this purpose, a motorized miniature vane shear apparatus (Wykeham Farrance Engineering Ltd., Tring, UK) with a constant rotation rate of 10°/min was used, following the ASTM D 4648-87 procedure (ASTM 1987).

At RCOM, the remaining gravity cores were analysed prior to splitting, using a non-destructive GEOTEK multisensory core logger (MSCL; Gunn and Best 1998) to determine wet bulk density and magnetic susceptibility. After core splitting, cores were described sedimentologically using the Munsell colour chart. Samples were then taken for measurement of water content and grain-size distribution. The former was done by

freeze-drying, the latter by means of a Beckman Coulter Laser Particle Sizer LS200. Before measuring grain size, sodium pyrophosphate was added to the samples to prevent the formation of aggregates during analysis. Organic matter content was determined on selected samples by loss on ignition (LOI) at about 550°C, following the DIN 18128 procedure (DIN 1990). Undrained shear strength was measured using a four-blade vane viscometer (RotoVisco RV20 device, Haake, Germany) at a rotational rate of 30°/min until the peak shear strength was well exceeded.

Table 2 Gravity core code numbers, locations, lengths, and water depths (for details, see text and Fig. 1)

Core	RCOM identification	Date	Location	Water depth [m]	Core length [m]
Mecklenburg Bay					
K1	GeoB10501	23.01.2006	011°40.097' E / 054°13.471' N	26.8	0.88
K103[a]		05.03.2006	011°39.672' E / 054°13.324' N	26.8	3.36
K166[a]		08.03.2006	011°43.376' E / 054°13.361' N	25.6	1.95
K191[a]		11.03.2006	011°43.541' E / 054°12.990' N	25.8	2.40
K268	GeoB10502	12.03.2006	011°46.071' E / 054°14.423' N	25.9	1.91
K370	GeoB10503	13.03.2006	011°44.063' E / 054°15.234' N	25.5	2.06
K483	GeoB10504	16.03.2006	011°41.948' E / 054°16.189' N	26.2	4.03
Eckernförde Bay					
K11	GeoB10505	28.02.2006	009°58.559' E / 054°29.309' N	27.1	1.00
K82	GeoB10507	04.03.2006	009°58.498' E / 054°29.287' N	27.8	0.95

[a] Cores were opened and analysed in the shipboard laboratory

Selected areas within Eckernförde and Mecklenburg bays were surveyed in March 2006 using a Parametric Sediment Echo Sounder SES-2000 (Innomar Technology GmbH, Rostock, Germany), in order to acquire high-resolution subbottom profiles. The system operates with a variable central frequency (4–15 kHz) for the detection of internal sediment layers, and also emits pulses at higher frequencies (100–500 kHz) for more precise detection of the sediment surface. The penetration depth can reach 50 m, depending on sediment type, water depth, and the frequency selected.

Results

In this section, we first present the overall geological background. This includes seismic reflection profiles typical for the study area, and results from representative gravity cores nearby. For clarity, this subsection is subdivided into the three areas of interest,

i.e. Mecklenburg, Eckernförde and Gelting bays. In a second subsection, we present the main in situ results, and relate these to sedimentary conditions and the presence of microbial gas within the strata.

Sediment geotechnical properties and echo-soundings

Mecklenburg Bay

A total of seven gravity cores were taken for groundtruthing purposes. The longest core, K483 in the northern part of the study area (Fig. 1d), has a length of 4 m and provided us with the most comprehensive record. Regardless of small-scale regional differences in composition or thickness of particular horizons, three lithological units can be distinguished. We present data from three gravity cores of different length and at different locations within Mecklenburg Bay to illustrate the overall lithostratigraphy (Fig. 2).

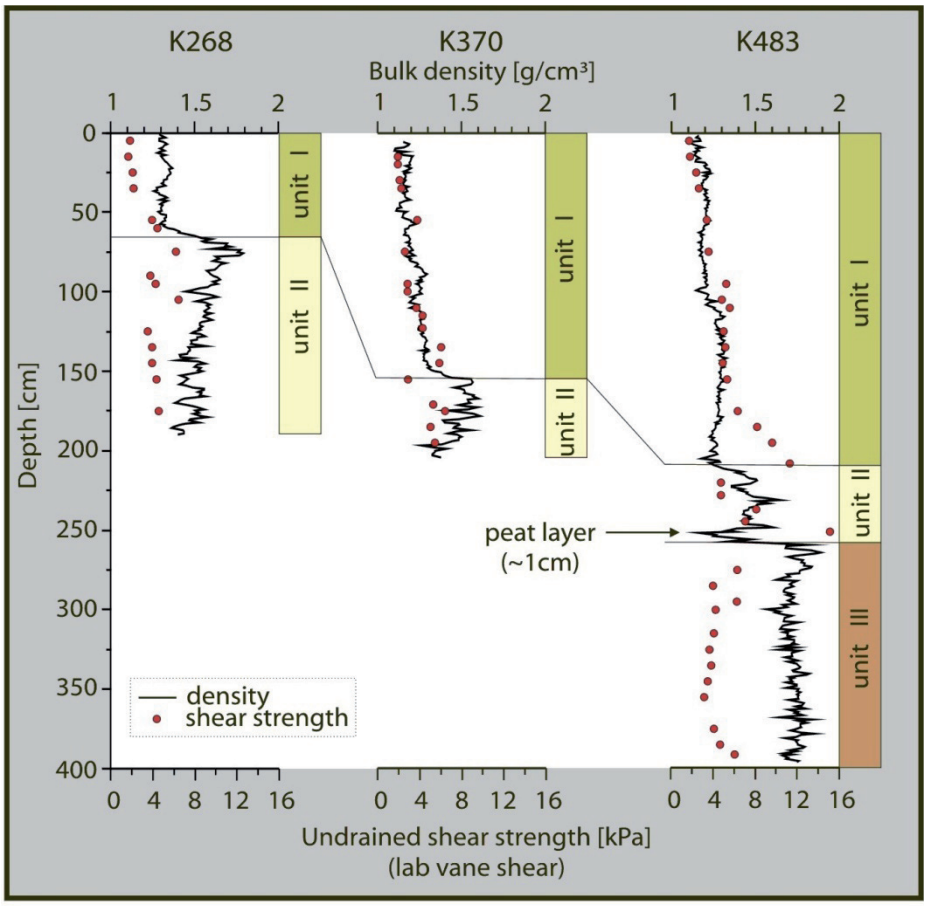

Fig. 2 Lithologs showing bulk density and undrained shear strength of cores K268, K370 and K483 in Mecklenburg Bay

The uppermost unit I is greenish black to olive grey mud or clayey silt. Fine sand is found occasionally, and often coincides with areas of slightly elevated shear strength (Fig. 2). The average wet bulk density of this unit ranges from 1.21 to 1.31 g/cm^3 (Fig. 2 and Table 3). Contents in organic material (LOI) vary moderately between 5.8 and 10.5 wt%, underlining the organic richness of the fine-grained sediments. The boundary to the underlying unit II is characterised by a stepwise increase in both wet bulk density and magnetic susceptibility. The silt is of grey to olive grey colour, containing layers of fine sand, plant debris or peat, the latter indicating a terrestrial influence. Such horizons are considerably stronger than the rest of the unit (see, e.g. the outlier of unit II at core K483; Fig. 2). The average wet bulk density in this unit ranges from 1.38 to 1.46 g/cm^3 (Fig. 2 and Table 3).

At the boundary between units II and III, a sharp increase in wet bulk density and decrease in water content are found, while grain-size distribution and colour remain very similar (Table 3). Bulk densities scatter around 1.73 g/cm^3; however, one has to acknowledge that unit III was recovered only in two gravity cores (e.g. core K483; Fig. 2). Within unit III, magnetic susceptibility increases again from values around 15–40×10^{-5} SI (unit II) to values between 50 and 95×10^{-5} SI (the horizons with high claysize contents marking the higher end of the spectrum; Table 3).

Table 3 Summary of the sediment properties from gravity cores (for details, see text)

Sediment properties		Unit I		Unit II	Unit III	Comments
		Mecklenburg Bay	Eckernförde Bay			
Clay	(%, <2 µm)	5.8 - 12.2	5.4 - 7.3	5.1 - 12.5	11.5 - 15.1	occasionally sandy beds in unit I and II: ~3 %
Silt	(%)	73.0 - 83.2	76.5 - 85.8	68.2 - 80.2	74.6 - 81.6	occasionally sandy beds in unit I and II: 54 - 57%
Sand	(%)	4.6 - 21.2	6.9 - 16.4	8.5 - 26.7	3.3 - 13.8	occasionally sandy beds in unit I and II: ~40 %
Water content	(%)	112.2 - 176.9	186.3 - 250.6	37.4 - 72.7	34.1 - 49.5	K483 peat layer (unit II) 225.6%
Wet bulk density	(g/cm³)	1.21 - 1.31	1.05 - 1.20	1.38 - 1.46	1.57 - 1.89	
Organic matter	(%)	5.8 - 10.5	10.6 - 15.5	-	-	
Magnetic susceptibility	(*10^{-5} SI)	1 - 10	1 - 4	15 - 40	50 - 95	
Undrained shear strength	(kPa)	1.7 - 6.4	1.6 - 3.1	2.9 - 8.2	3.2 - 6.3	occasionally in unit I in sandy beds up to 11.3 kPa (K483) and in clayey beds up to 19 kPa (K166) K483 peat layer (unit II) 15.2 kPa

hyphen not analysed

Within the succession of the three units, the shear strength roughly mirrors the incremental increase in bulk density (Fig. 2). In unit I, strength is about 2 kPa in the very soupy bottom layer, and then increases gradually to about 5–6 kPa (e.g. cores K268, K370 in Fig. 2) or even 11 kPa (K483 in Fig. 2). Unit II is marked by a slight drop in shear strength in each of the cores, and shows an average value of 5–6 kPa (see summary in Table 3). Surprisingly, the sharp increase in density when looking at unit III is not reflected in the vane shear data. In fact, average strength in unit III is only about 5 kPa, which represents a slight decrease.

If we regard echo-sounder profiles in the areas where long cores were taken, the discontinuities in density and other parameters at the unit I/II as well as unit II/III boundary seem to coincide with a high-amplitude reflector (e.g. Fig. 3a). Typical seismic records from Mecklenburg Bay show seafloor-parallel reflectors indicating sedimentary layering. In places, coarser-grained sub-bottom units show bodies with inclined reflectors and cross-bedding (see left portion of Fig. 3a). Lithological unit I is characterised by seafloor-parallel reflectors (i.e. bedding) and a typical downward increase in undrained shear strength (see core K166 data, Figs. 2 and 3a). At a depth of about 2 mbsf (meters below seafloor), a prominent orange reflector is most likely related to contrasts in strength or density. This depth coincides with the location of the unit I/II boundary in many of the shorter cores (e.g. K370; Fig. 2). Unit II is characterised by a somewhat chaotic signature with inclined reflectors. Changes in amplitude may stand in line with variable sand contents observed in the gravity cores. Further below, another strong green-to-orange reflector indicates the top of unit III, which shows characteristic bodies of cross-bedding and an overall increase in density below approximately 2.5–3 m (for example, see core K483, Fig. 2).

While geophysical images across Mecklenburg Bay generally show undisturbed sections of seafloor-parallel bedding throughout, there are a few discrete zones which show unusual blanking behaviour (Fig. 3b). These are vertical features of only a few meters to tens of meters in diameter, with no internal reflectors visible. This observation is typical for the presence of free gas, which adsorbs much of the seismic energy at shallow levels. The fact that gas hinders saturation of the pore volume has repercussions for the in situ CPT measurements (see next section).

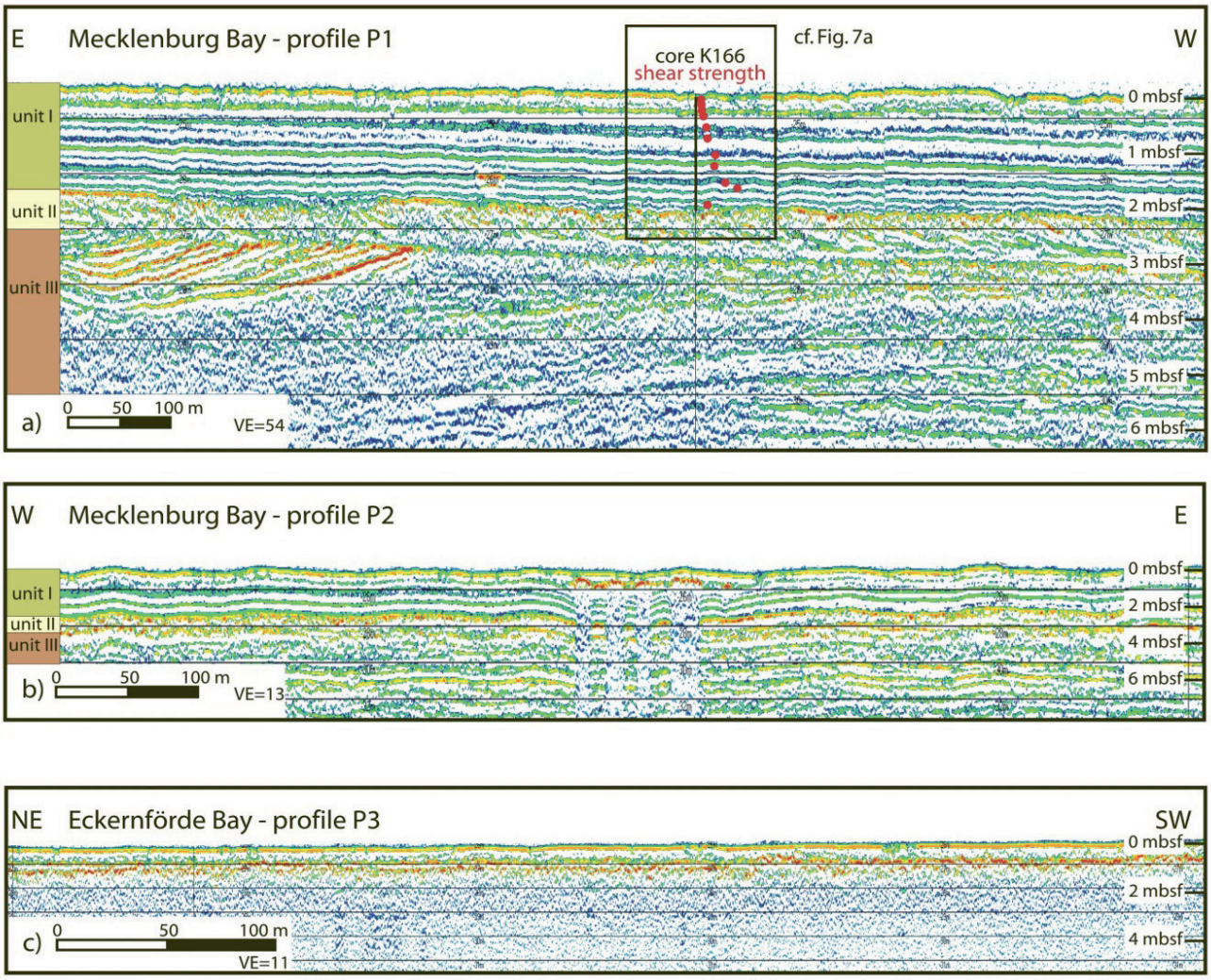

Fig. 3 Echo-sounder profiles of Mecklenburg (P1 and P2) and Eckernförde (P3) bays with lithostratigraphic units. **a** E–W profile P1 [length 1.1 km, vertical exaggeration (VE)=54], adjacent to core K166, with corresponding undrained shear strength measurements. **b** W–E profile P2 (length 846 m, VE= 13). **c** NE–SW profile P3 (length 550 m, VE=11). Note different scale in P1–P3 (see Fig. 1 for locations and text)

Eckernförde Bay

In Eckernförde Bay, only two gravity cores were taken, each yielding only about 1 m of sediment recovery (cores K11 and K82, Fig. 1, Table 2). The dominant lithology is greenish black to olive grey mud throughout, which stratigraphically represents unit I. In comparison to that of Mecklenburg Bay, however, it is much softer, with a fluffy texture, a pungent smell of H_2S, higher LOI values (10.6–15.5 %), and higher relative water contents (186–250 %; Table 3). Bulk density is only about 1.1 g/cm^3. Grain-size distribution shows little down-core variation, being dominated by silt (about 82 %), and

lesser amounts of sand (about 11%) and clay (7 %). The undrained shear strength in the upper 50 cm in Eckernförde Bay is 1.6–2.4 kPa, and increases up to 3.1 kPa at 50–100 cm depth. These values agree well with those measured in unit I of the Mecklenburg cores (e.g. Fig. 2 and Table 3).

Echo-soundings at the locations of cores K11 and K82 exhibit widespread sub-bottom zones of acoustic turbidity, i.e. evidence of gas bubbles at sediment depths as shallow as 65–100 cm (Fig. 3c). In fact, no coherent reflectors can be seen below approximately 1 mbsf beneath the lower yellowish red reflection. This observation is similar in seismic signature to the rather narrow zones seen in some areas in Mecklenburg Bay (Fig. 3b). The Eckernförde area, however, is seismically opaque and must hence be regarded as much more gaseous than is the case for the Mecklenburg area.

Gelting Bay

Owing to rough weather, no gravity cores were collected in Gelting Bay. However, the sediment recovered on board after retrieval of the CPT lance consisted of a very soft, olive black mud with a strong smell of H_2S. Similarly to Eckernförde Bay, this suggests the occurrence of free microbial gas.

Excess pore-pressure profiles

For all three bays combined, two very different signals of excess pore pressure were identified for the dissipation period after penetration, from the wealth of short-term (<15 min) CPT deployments (Fig. 4). After an initial spike, type A shows an exponential decay (Fig. 4a) of induced positive excess pore pressures, commonly reaching negligible values within a few minutes. By contrast, type B shows sub-hydrostatic values upon insertion and then increases slowly with time until a constant value is reached (Fig. 4b). In places, longer deployments (30–100 min) served to shed light on the ambient pore-pressure values. It was found that the background pore pressure was somewhat lower than the initial excursion (see test C305 in Fig. 5, Table 1).

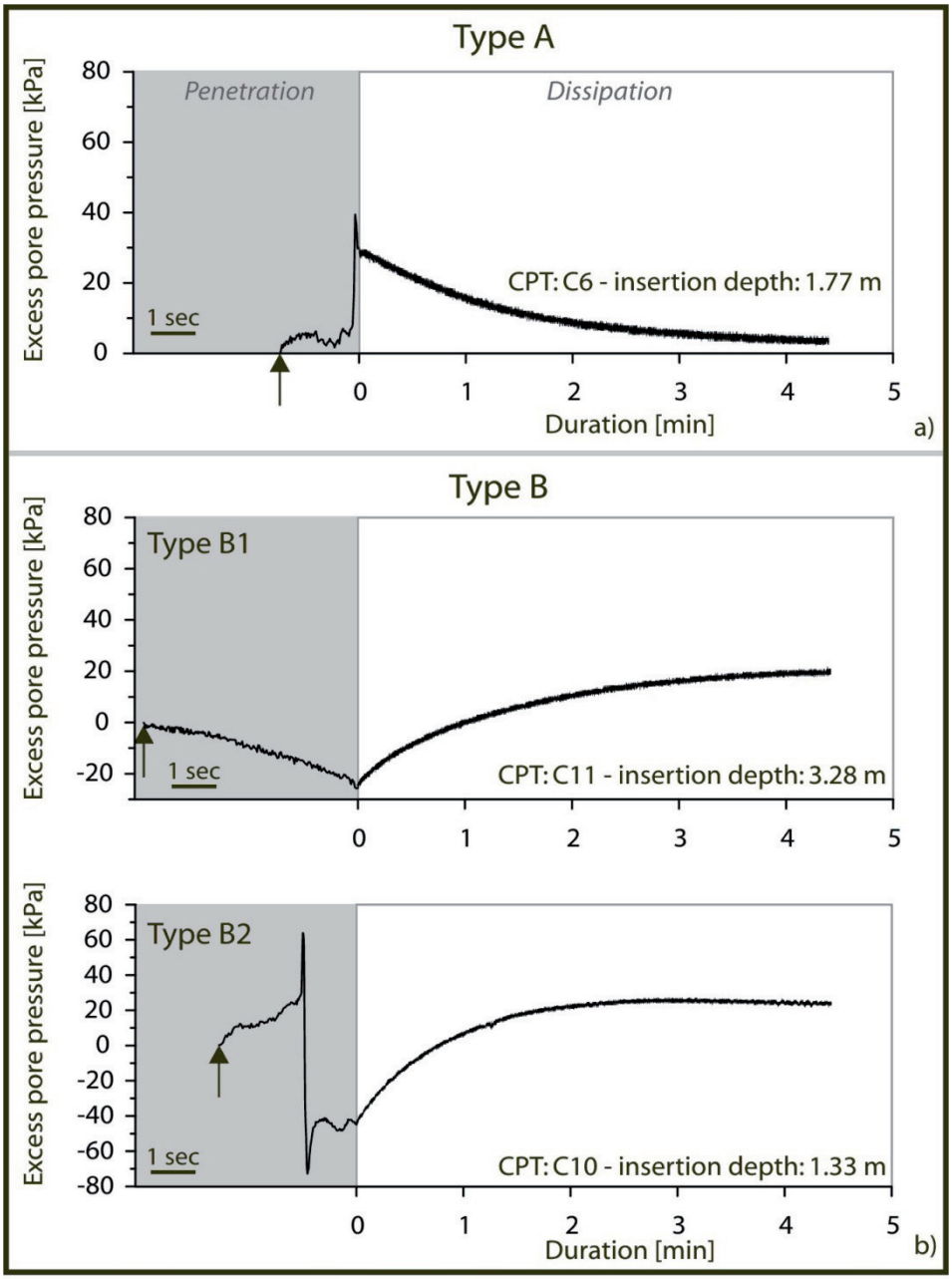

Fig. 4 Classification of excess pore-pressure evolution during and after penetration of the CPT lance in the three study areas. **a** Type A. **b** Type B1 and B2. As examples, C6, C10 and C11 are shown, all veered with winch speed of around 1.1 m/s. Arrows mark the first contact with the seafloor. Note the different timescale for the penetration and dissipation periods (for details, see text and Table 1)

In terms of penetration period, the two different pore-pressure signals (types A and B) can be further divided into subgroups. In order to illustrate the consistent trends but local variations, three examples are provided for each group (Fig. 6). Type A always shows an induced increase in excess pore pressure (Figs. 4a, 6a). For type B, pore pressure in some cases decreases to sub-hydrostatic values upon penetration of the CPT, this trend being classified as type B1 (Figs. 4b, 6b). In other cases, there is a sharp increase in excess pore pressure upon penetration, which is followed by a dramatic decrease to sub-hydrostatic pressures, this trend being classified as type B2 (Figs. 4b, 6c).

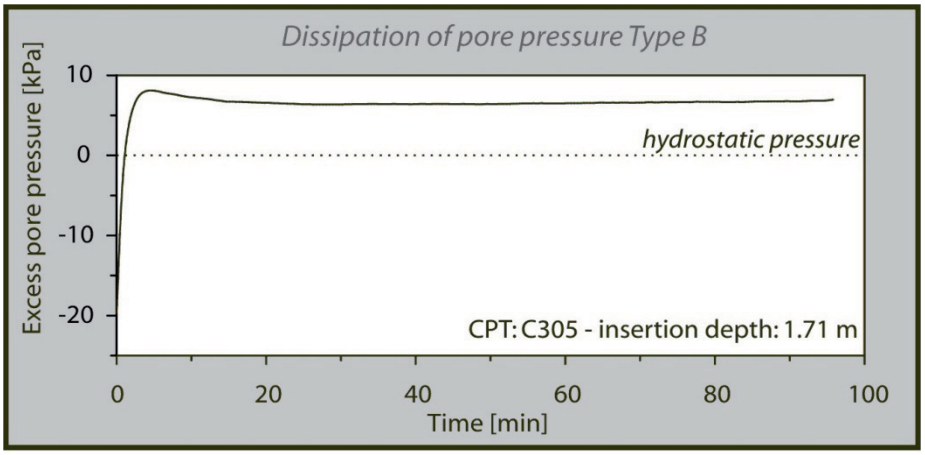

Fig. 5 Dissipation of excess pore pressure of type B (CPT test C305) after penetration of the lance

Taking all results together, type B pore-pressure curves are by far the most abundant. All CPT deployments in Gelting (n=4) and Eckernförde bays (n=2), as well as 48 of 51 deployments in Mecklenburg Bay show type B response (Fig. 1 and Table 1). Only three experiments showed type A responses (C6–C8, Table 1). In order to place these observations into a geological context, we next compare the in situ pore-pressure results with data obtained on the sediment cores in the laboratory.

Pore-pressure signal type A

If we regard the pore-pressure response of CPT tests C6, C7 and C8 (Fig. 6a), striking similarities can be seen. At depths between 1.5 and 2.1 mbsf, a sharp increase in excess

pore pressure is observed. This increase coincides with a density increase at the unit I/II boundary, which is also characterised by a change in shear strength (Fig. 2).

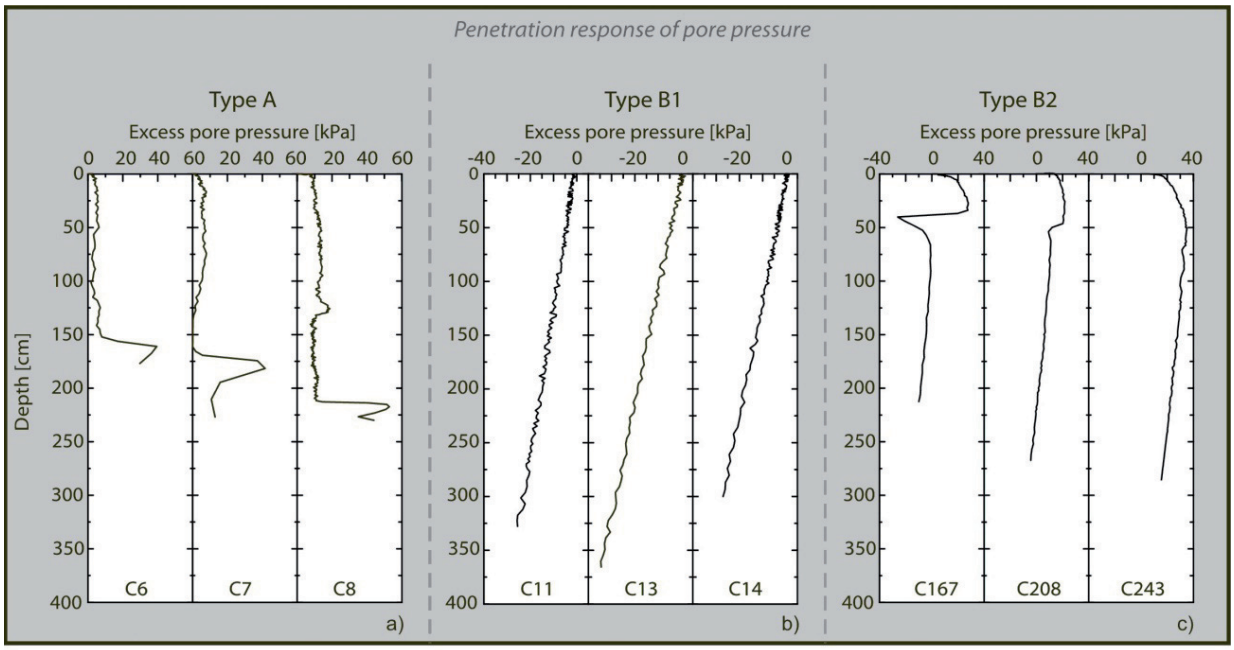

Fig. 6 Different excess porepressure response during the penetration periods of various CPT tests. **a** Type A: C6, C7, C8. **b** Type B1: C11, C13, C14. **c** Type B2: C167, C208, C243. For details, see Fig. 1 and Table 1

Below, the pore-pressure spike dissipates again. The degree of pore-pressure drop is variable (15–35 kPa), and is likely a function of the lithology of unit II. When further comparing data from CPT deployment C6 (type A) with sediments of the adjacent core K166 (Figs. 3a and 7), cone resistance and pore pressure explicitly increase at 160 cm depth where a greenish clay layer reveals s_u values of up to 19 kPa.

Both shear strength and the distinct pore-pressure maximum of 39 kPa and higher are significantly different from those for other measurements nearby (notably type B2 curves; compare Figs. 2, 6c, 7 and Table 3). Also, shear strength derived from the CPT deployment (Fig. 7a, diamonds) overestimates that from vane shear testing of the core (Fig. 7a, circles), most likely being a result of the dynamic penetration of the former.

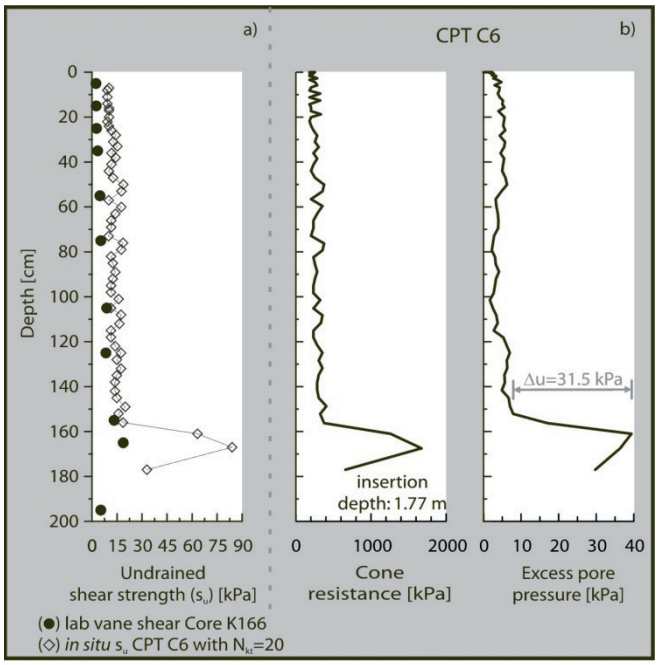

Fig. 7 Comparison of sediment properties and CPT measurements, type A, versus depth. **a** Undrained shear strength (core K166 and in situ CPT test C6 calculated from corrected cone resistance) **b** C6 parameters during penetration: cone resistance (uncorrected) and excess pore-pressure evolution (type A); C6 veered with winch speed of 1.1 m/s (see Fig. 1 for locations and text)

Pore-pressure signal type B

A similar agreement between core data and CPT results can be made between data from core K268 and CPT C263, again in Mecklenburg Bay (Figs. 1 and 8). Pore pressure shows a type B2 evolution, while cone resistance increases at 40–60 cm depth (Fig. 8b). This is related to an increase in undrained shear strength (6.2 kPa; Fig. 8a), most likely reflecting an increase in sand content. At the same depth, the pore pressure drops rapidly (Δu ~66 kPa; Fig. 8b).

The excess pore-pressure evolution of type B2 during penetration, especially the absolute difference between the penetration peak and the pressure minimum from 15 kPa (C305) to 136 kPa (C10), is highly variable within the wealth of CPT deployments during this study. Each of the pressure drops is mirrored by a sharp increase in cone resistance (e.g. 180 kPa for C305, and 701 kPa for C10). Compared to the B2 pore-pressure response (see Figs. 6c and 8b), type B1 curves show a steady decrease to sub-hydrostatic values (Fig. 6b). This observation is unexpected, given total penetration depths of > 3 mbsf (e.g. C11, C13; Fig. 6b).

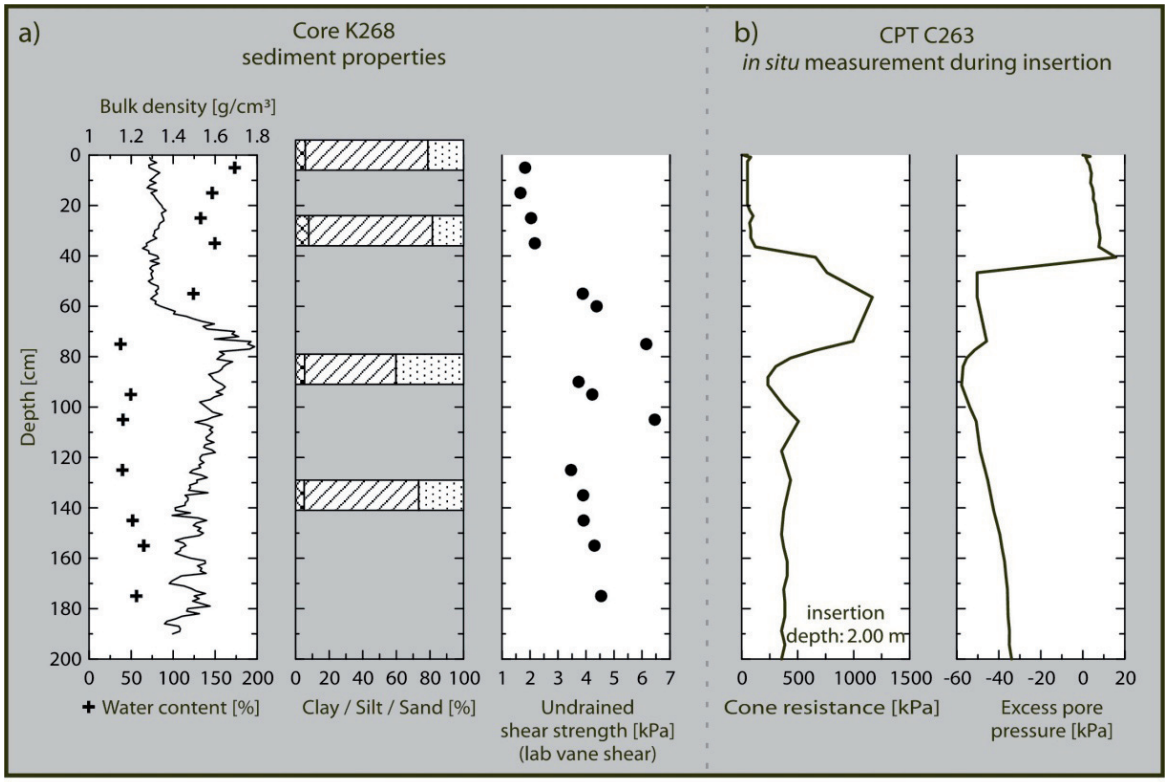

Fig. 8 Comparison of sediment properties and CPT measurements, type B2. a Bulk density, grain-size distribution, and undrained shear strength, core K268. b C263 cone resistance (uncorrected) and excess porepressure evolution (type B2) with penetration depth; C263 veered with winch speed of 2.1 m/s (see Fig. 1 for locations)

At such depths, the CPT probe already passed the unit I/II boundary (and thus the density increase) without any noticeable deviation in pore-pressure trend. On the other hand, the unit boundary may be blurred, given the poor resolution in some of the seismic lines, especially in Eckernförde Bay (see Fig. 3c). Some uncertainty remains at this point, because the observed increase in density at the two unit boundaries is not reflected by shear strength (core data) and cone resistance (CPT data).

Discussion and conclusions

The discussion is split into two subsections. First, we interpret the in situ CPT results by utilising the information from echo-sounder profiles and ground-truthing (especially data on discrete core samples). Here, we focus on the pore-pressure evolution and follow the distinction into three types of responses, i.e. A, B1 and B2. In the second part of the discussion, we then use the wealth of CPT data to carry out a sediment

classification. Given the relatively small number of cores (n=9) relative to the CPT deployments (n=57), this type of sediment characterisation without sampling may prove a versatile approach in future surveys.

Pore-pressure evolution

In general, the penetration process of a dynamic CPT device is more complex than that of standard, quasi-static CPT deployments at constant rates of 2 cm/s. Penetration at high rates causes significant disturbance of the sediment in the vicinity of the lance and, as a result, changes of the stress regime of the soil and the pore fluid. Theoretical considerations describe the excess pore pressure in two different zones surrounding the cone penetrometer during penetration (e.g. Teh 1987; Burns and Mayne 2002): (1) a plastically deformed region around the cone, influenced by normal stress-induced pore pressure, and (2) a zone along the penetrometer–soil interface, in which intense shear stresses are generated (shear-induced pore pressure). In addition, factors related to sediment physical properties (coefficient of consolidation, etc.), the interaction of sediment with the lance, the configuration of the lance (e.g. the position of the pressure sensor), the mode of deployment (e.g. penetration velocity) and, last but not least, the presence of free gas and already elevated in situ pore pressure may cause severe difficulty in interpreting the measured data. We take all those factors into account when discussing the three types of pressure responses seen in the Baltic Sea.

Pore-pressure signal type A

The consistent type A response is an induced spike in excess pore pressure upon penetration of the CPT, followed by a progressive decline during the dissipation period (Figs. 4a, 6a, 7b). Pore-pressure records similar to type A have been measured using dynamic pressure instruments in marine sediments (Schultheiss 1990b; Fang et al. 1993). The initial positive pressure rise is particularly difficult to interpret, because a likely artefact from the impact of the probe may overprint positive pressures occurring in situ due to clay compaction, layers of high sedimentation rates, or absence of gas in the pore volume (e.g. Wichman 2000). In Mecklenburg Bay, we are in favour of the first possibility because, at the depth of the 39-kPa pore-pressure spike, cone resistance

of the CPT as well as shear strength in the corresponding core rise to unusually high values (1,675 and 19 kPa respectively). In the deeper part of the CPT profiles and core (Fig. 7), the shear strength is lower and the pore pressure can dissipate, so excess pore pressure decreases rapidly (cf. Bennett et al. 1989).

Pore-pressure signal type B1

All measurements of type B1 exhibit a delayed pore-pressure increase after penetration, which is typical for Eckernförde and Gelting bays (Figs. 1, 4b, 6b). There is a number of potential explanations for such a pore-pressure response, involving either lightly consolidated sediment or undersaturated pore space (i.e. free gas attenuating the pressure signal by the profiling lance).

Initial sub-hydrostatic pressures followed by a delayed increase to ambient values occur in overconsolidated or fissured sediments due to dilatory sediment behaviour and local redistribution around the cone tip (see similar examples in Lunne et al. 1997; Burns and Mayne 1998, 2002). In isotropic sediments where the vertical coefficient of consolidation (c_v) is equal to its horizontal counterpart (c_h), pore-pressure gradients between the cone and shaft might induce vertical fluid flow, whereas a reduction of the vertical coefficient of consolidation could impede it (Teh 1987). Since the soft muds of type B1 are homogeneous, highly compressible, and have a high plasticity index (Eckernförde mud: average plasticity index of 163 %; Silva and Brandes 1998), the difference between c_v and c_h, is small, and vertical flow feasible. The two different pore-pressure zones around the CPT (see above) are interacting to achieve equilibrium and, thus, effectively delay the dissipation. Additionally, the pore pressure from the far-surrounding field flows to the zone near the penetrometer and, therefore, pore-pressure responses might be further delayed before approaching ambient pressure (Song and Voyiadjis 2005; Elsworth et al. 2006).

Although normally consolidated surficial sediments throughout the sub-basins in the Baltic Sea would be expected based on the geological history, light overconsolidation was detected in the upper 2.5 m in Eckernförde Bay by Brandes et al. (1996). The surface sediments exhibit high average organic contents of 12 % dry weight (Silva et al. 1996), with overconsolidation ratios between 1.2 and 12.7 (Brandes et al. 1996) related

to this. In deeper sections of their cores, the material approaches normally consolidated conditions. This phenomenon is referred to as apparent overconsolidation, and is considered to be due to inter-particle physicochemical bonding or cementation (Silva and Brandes 1998; Anandarajah and Lavoie 2002). This has been observed also at other locations, e.g. in the organic-rich sediments on the continental slope off Peru (Keller 1982), or in Sagueny Fjord sediments (Urgeles et al. 2002). Apparent overconsolidation could have an influence on the type B1 pore-pressure dissipation, but it is unlikely to be the main reason for this signal.

In Eckernförde and Gelting bays, type B1 trends dominate with an obvious similarity in sub-hydrostatic response during penetration, while cone resistance does not show a pronounced increase upon penetration. This has been explained by low bulk densities of 1.1 g/cm^3, high water contents of 250 %, low shear strength of 3 kPa (for details, see "Results" above), and the high permeability (Bennett et al. 1996) and high compressibility of the mud (Silva and Brandes 1998). The initially loose, open microfabric with large channels and voids (Lavoie et al. 1996) collapses during the high loading impulse upon CPT impact. The mud will be displaced, and any initially induced pore pressure will dissipate very rapidly. A net pore water flow away from the pressure sensor, nearly unrestrained throughout the highly permeable sedimentary network, causes negative pressures.

Another important aspect in understanding the negative response is the occurrence of free gas. There are three potential scenarios: (1) gas in the filter of the CPT causing artefacts, (2) microbial gas causing overpressures and variations in shear strength, and (3) 'skin effects' related to rapid CPT penetration.

1. It is known that an unsaturated filter of the pressure sensor can also cause delayed pore-pressure response (e.g. May 1987; Burns and Mayne 1998; Strout and Tjelta 2005). However, we detected very fast pore-pressure changes during penetration (e.g. type B2 response), so we are confident that partially saturated sediment due to free gas, rather than an unsaturated filter, caused a delayed response. Also, we tried to saturate the filter on deck when preparing the

instrument, and additionally allowed it to equilibrate in the water column for 5 min prior to each deployment.

2. Free gas in the sediment pore volume may be held responsible for the type B1 pore-pressure response in Mecklenburg, Eckernförde and Gelting bays. As shown above (Fig. 3b, c), opaque acoustic signatures in the echo-soundings hint to the presence of free gas. This observation reconfirms earlier work in Eckernförde and Gelting bays, where free gas was related to the degradation of organic material under anoxic conditions (Abegg and Anderson 1997; Richardson and Davis 1998; Wilkens and Richardson 1998; Albert et al. 1998; Wever et al. 1998, 2006). Free gas in the pore space influences sediment properties such as shear strength (Wheeler 1988; Wilkens and Fu 1994; Briggs and Richardson 1996; Fu et al. 1996; Grozic et al. 2005), mainly because voids partially filled with gas, rather than seawater, have a different compressibility than fully saturated pores. Therefore, free gas dramatically influences sediment deformation, although it appears ambiguous whether shear strength is increasing or decreasing with increasing gas content (e.g. Wheeler 1988; Brandes 1999). Wichman (2000) tested the consolidation of soft gassy mud in a settling tube and could show that gas significantly retards the consolidation process. Compressible gas bubbles in the fluids of the pores can attenuate pore-pressure propagation (Köhler and Schwab 2005), and also cause a decrease in permeability (Wichman 2000). After a rapid external pressure change, such as after penetration of the CPT lance, the pore pressure will need a longer time to adapt to the change and might cause the observed delayed response in our type B sediments (e.g. C10 and C11 in Fig. 4, C305 in Fig. 5).
3. Skin effects during measurement have to be taken into account. In general, gas may cause elevated pore pressure and, therefore, the formation of cracks can be induced (van Kesteren and van Kessel 2002), rendering the sediment unstable. Given the buoyancy of the gas, bubbles of variable size naturally escape upwards (see in situ tests in Eckernförde Bay by Anderson et al. 1998). A further disruption, such as the penetration of the CPT probe, could release free gas along the shaft of the lance, or could generate cavities into which fluid escapes. Equally, a thin adhesive layer of pore water and sediment suspension

may be formed along the interface between the probe and the sediment body, like a skin. During penetration, this layer moves opposite to the lance penetration, thereby causing suction at the filter covering the pore-pressure port, and thus negative pressure excursions are measured. These so-called skin effects appear related to the rate with which the CPT hits the sediment. In an earlier study, Bennett et al. (1996) measured ambient and dynamic pore pressure in Eckernförde Bay with a piezoprobe. Their measurements in the uppermost meter bsf suggest a pore-pressure behaviour of type A, whereas our data show type B1. The different pore-pressure response might be caused by the different design of the lances (their probe is almost half the diameter of ours), the different penetration depth and, most importantly, the different penetration rate. The piezoprobe of Bennett et al. (1996) was lowered slowly into the sediment, while our probe was lowered at around 1 m/s. The fragile microstructure of the aggregates and large pores in the mud of Eckernförde Bay is very sensitive to disturbance (Bennett et al. 1996; Lavoie et al. 1996), and this may have been destroyed instantaneously with the RCOM CPT. The penetration rate may thus have affected all our deployments (see penetration rates in Table 1), e.g. causing an increase in cone resistance and a higher induced initial penetration pressure with an increasing rate of penetration in clayey sediments (Lunne et al. 1997; Finke et al. 2001). Stoll and Sun (2005) and Stoll et al. (2007) compared results of quasistatic and dynamic penetrometers, and concluded that the latter accentuates excursions in the data profile. However, the results of Roy et al. (1982) indicate insignificant differences in pore-pressure profiles for variable rates of penetration (3–240 cm/min). Unfortunately, no comparative data for high penetration rates are available to further evaluate our results.

Pore-pressure signal type B2

Pore-pressure type B2 somehow presents a mixture of type A and type B1, and its evolution can be variable (Fig. 6c). We suggest that the response of type B2 is associated with indurated or even overconsolidated layers of silt containing a considerable amount of sand, which are interbedded in softer mud (Milkert 1994). Silts may show a partially drained behaviour during penetration (Lunne et al. 1997), and a

rapid drop in pore pressure, even to negative values. Robertson (1990) as well as Song and Voyiadjis (2005) found silty sediments with negative excess pore pressures during penetration. Schneider et al. (2001) made similar observations in residual soils of Singapore, and Finke et al. (2001) reported the same for residual silts and fine sands of the US Atlantic Piedmont geologic province. Similar observations were reported by Baltzer et al. (1994) when using a cone penetrometer to characterise sediments from the Nova Scotian Slope on the eastern Canadian continental margin. The authors concluded that the presence of stronger sandy layers caused a peak in cone resistance associated with a drop in pressure when penetrating these sediments. Recently, two different types of pore-pressure evolution, similar to the ones of types A and B2, were observed with the RCOM-CPT probe in lacustrine clays and silts in Lake Lucerne, Switzerland (Stegmann et al. 2007). Type A was found to be related to normally consolidated sediments with indurated interbeds (see “Discussion and conclusions” above), whereas type B2 was measured in overconsolidated, glacially overprinted sediments. Here, the pore-pressure evolution mirrors B2, with an initial drop to sub-hydrostatic values (Δu=about 35 kPa) being followed by a recovery to ambient values. In the Baltic Sea, pressure drops reached Δu values of up to 136 kPa (test C10).

With regard to the penetration process of the CPT into these sediments, the lance at first penetrates a soft mud layer followed by a sandy, more indurated layer where the lance strongly decelerates. Similar to the type A trends (compare Fig. 6a and c), an increase in pore pressure is observed. However, in contrast to type A, the penetration process does not come to a halt but proceeds into the underlying, softer sediments. The associated development of a strong negative pore-pressure signal of up to −80 kPa is as yet not totally understood, since it would involve much higher sediment permeability (and fluid displacement) than that found in Baltic Sea silts to fine sands. It is conceivable that an increase in sand content, by ~20–30 %, might enhance the drainage behaviour of the sediment, causing the induced positive pore pressure to rapidly dissipate.

Sediment classification from in situ CPT data

Often, soil classification charts are used for the identification and the classification of soil types from standard profiling CPT data (Robertson 1990; Lunne et al. 1997).

Vermeulen and Rust (1995) presented a modified classification chart where the excess pore pressure (Δu) is plotted against the net cone resistance (q_n, measured total cone resistance corrected for pore pressure and reduced by total overburden stress). This chart identifies not only the soil type but also the consistencies. The major advantage of the soil classification method is that it does not require cores to be recovered. Hence, the study is less time-consuming and laborious.

In order to test the classification method by Vermeulen and Rust (1995), we have taken cores for ground-truthing purposes (see "Results" section above). In general, our measured sediment properties in Mecklenburg Bay agree very well with previous studies in this area. The bulk density measured by Harff (2003) in the muddy area of Mecklenburg Bay corresponds exactly to the bulk density in core K268 (1.3 g/cm^3; Fig. 8a). Furthermore, Lemke (1998) investigated the sediments in the western Baltic Sea by coring and seismic exploration, and found lithological units very similar to those of this study. Silva and Brandes (1998) observed relative water contents of 200–300% for the upper 100 cm in Eckernförde Bay, which match those obtained on our cores (see Fig. 8a and Table 3). Furthermore, Briggs and Richardson (1996) report low shear strength values (2.2 kPa) recorded by means of a diveroperated vane device in the shallow sub-bottom, which mirror our results in the upper portion of unit I (see Figs. 2, 8a and Table 3). Similar agreement is reported for grain-size distribution (Silva and Brandes 1998) and organic matter (Brandes et al. 1996; Bobertz 2000). We therefore feel confident in using our core data to verify the CPT soil classification.

In Fig. 9, we have plotted the penetration data from CPT C6 for pore-pressure type A, C13 for pore-pressure type B1, and C167 for pore-pressure type B2 in the chart of Vermeulen and Rust (1995) to test their classification scheme. The data support the three defined pore-pressure types and their interpretations. Data from C13 (type B1) identify very soft clay, while C167 data (type B2; Fig. 6c) identify very soft clay and silt (Fig. 9). In the interval where the CPT shows peaks in cone resistance and pore pressure, the data points in the classification chart show a trend towards the edge of the 'very soft' field, close to the 'soft to firm' field (Fig. 9). This supports our conclusion of slightly indurated silt layers with significant amounts of sand in the mud (see above). For C6 data (type A), the soil classification chart identifies a soft to firm silt and silty sand sediment layer where the C6 data show a high peak in cone resistance and excess

pore pressure (Fig. 7b). Compared with the type B data (Fig. 9), this sediment shows the highest consistency, which is in agreement with the elevated undrained shear strength in core K166 at 160–180 cm (Fig. 7a).

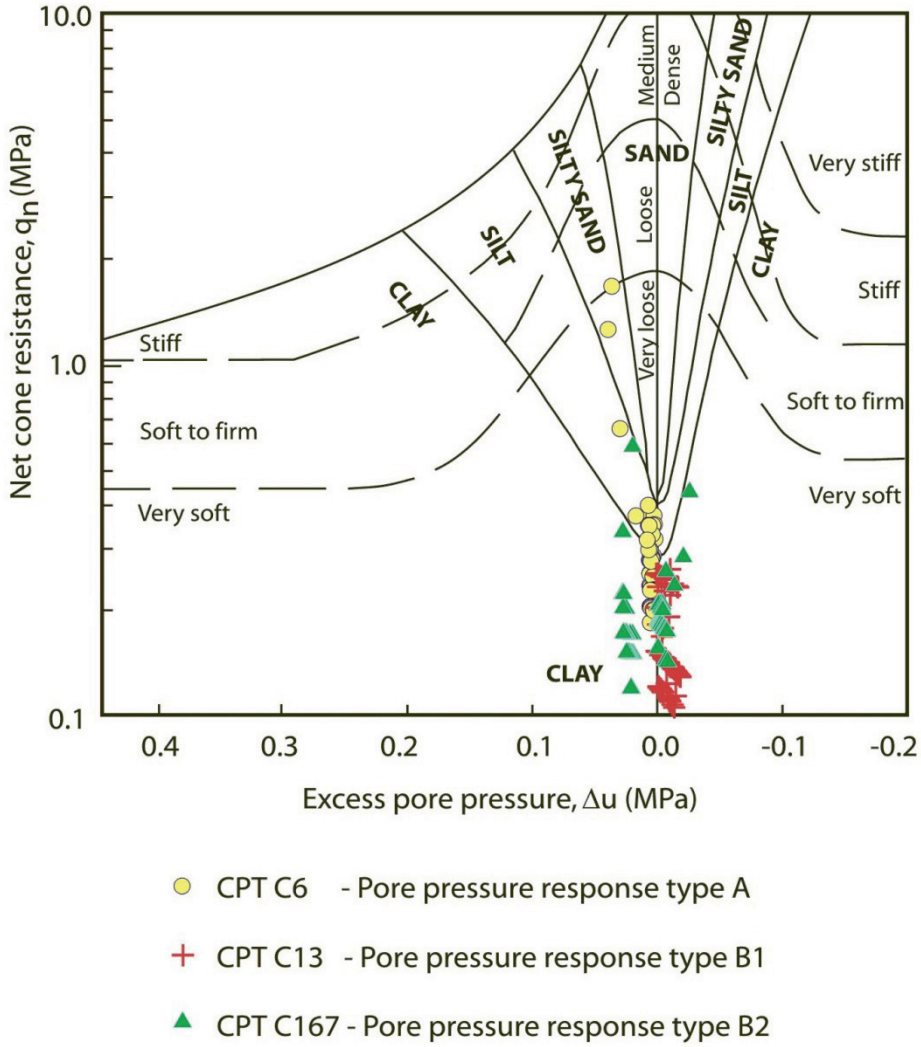

Fig. 9 Soil classification chart (following Vermeulen and Rust 1995), with profiling data from CPT tests C6, C13 and C167 (6–200 cm depth). Note that net cone resistance is on a logarithmic scale

Since higher penetration rates may increase cone resistance and induced initial pore pressure and, thus, accentuate lithological variations, our dynamic CPT measurements showing higher penetration velocity than for the standard CPT (2 cm/s) may overestimate the soil stiffness (for example, the identified classification of silty sand in the C6 data could be pure silt). However, given the overall good agreement between the soil classification data and ground-truthing evidence we gathered from the gravity

cores, we propose that the time- and cost-efficient dynamic CPT device represents a versatile approach in muddy sediments. This is particularly true in gas-rich muds on which, for stability reasons, standard CPT rigs cannot be deployed.

Acknowledgements We thank the captains and crews of the German Navy vessels Kronsort and Planet for their support during our study. Innomar Technology GmbH, in particular J. Lowag, is acknowledged for providing the sediment echo-sounding data from SES-2000. We also thank T. Garlan and P. Guyomard (SHOM, France) for kindly providing shear strength data of cores K166 and K103. S. Kreiter, R. Lühder, B. Schlue and J.B. Stuut are acknowledged for interesting discussions, and shipboard and lab support. The paper benefited from suggestions by two anonymous referees as well as the superb editorial handling by M. Delafontaine and B. Flemming. Funding was granted by DFG (via RCOM). This is RCOM publication no. 0545.

References

Abegg F, Anderson AL (1997) The acoustic turbid layer in muddy sediments of Eckernfoerde Bay, Western Baltic: methane concentration, saturation and bubble characteristics. Mar Geol 137:137–147

Albert DB, Martens CS, Alperin MJ (1998) Biogeochemical processes controlling methane in gassy coastal sediments. Part 2. Groundwater flow control of acoustic turbidity in Eckernförde Bay sediments. Cont Shelf Res 18:1771–1793

Anandarajah A, Lavoie D (2002) Numerical simulation of the microstructure and compression behavior of Eckernförde Bay sediments. Mar Geol 182:3–27

Anderson AL, Abegg F, Hawkins JA, Duncan ME, Lyons AP (1998) Bubble populations and acoustic interaction with the gassy floor of Eckernförde Bay. Cont Shelf Res 18:1807–1838

ASTM (1987) Standard test method for laboratory miniature vane shear test for saturated fine-grained clayey soil. ASTM D 4648–87. ASTM International, West Conshohocken, PA, Annual Book ASTM Standards 04.08:868–873

Baltzer A, Cochonat P, Piper DJW (1994) In situ geotechnical characterization of sediments on the Nova Scotian Slope, eastern Canadian continental margin. Mar Geol 120:291–308

Bennett RH, Li H, Burns JT, Percival CM, Lipkin J (1989) Application of piezometer probes to determine engineering properties and geological processes in marine sediments. Appl Clay Sci 4:337–355

Bennett RH, Hulbert MH, Meyer MM, Lavoie DM, Briggs KB, Lavoie DL, Baerwald RJ, Chiou WA (1996) Fundamental response of pore-water pressure to microfabric and permeability characteristics: Eckernförde Bay. Geo-Mar Lett 16:182–188

Bobertz B (2000) Regionalisierung der sedimentären Fazies der südwestlichen Ostsee. PhD Thesis, Ernst-Moritz-Arndt-Universität, Greifswald

Bohling B (2003) Untersuchungen zur Mobilität natürlicher und anthropogener Sedimente in der Mecklenburger Bucht. PhD Thesis, Ernst-Moritz-Arndt-Universität, Greifswald

Brandes HG (1999) Predicted and measured geotechnical properties of gas-charged sediments. International Journal of Offshore and Polar Engineering 9(3):219–225

Brandes HG, Silva AJ, Ag A, Veyera GE (1996) Consolidation and permeability characteristics of high-porosity surficial sediments in Eckernförde Bay. Geo-Mar Lett 16:175–181

Briggs KB, Richardson MD (1996) Variability in in situ shear strength of gassy muds. Geo-Mar Lett 16:189–195

Burns SE, Mayne PW (1998) Monotonic and dilatory pore-pressure decay during piezocone tests in clay. Can Geotech J 35:1063–1073

Burns SE, Mayne PW (2002) Analytical cavity expansion-critical state model for piezocone dissipation in fine-grained soils. Soils and Foundations Japanese Geotechnical Society 42:131–137

Dayal U, Allen JH (1975) The effect of penetration rate on the strength of remolded clay and sand samples. Can Geotech J 12:336–348

DIN (1990) Baugrund, Versuche und Versuchsgeräte—Bestimmung des Glühverlustes. DIN 18128 (November 1990). Deutsches Institut für Normung, Berlin

Duphorn K, Kliewe H, Niedermeyer RO, Janke W, Werner F (eds) (1995) Die deutsche Ostseeküste. Gebrüder Borntraeger, Berlin, Sammlung geologischer Führer 88

Elsworth D, Lee DS, Hryciw R, Shin S (2006) Pore pressure response following undrained uCPT sounding in a dilating soil. ASCE, J Geotech Geoenviron Eng 132:1485–1495

Fang WW, Langseth MG, Schultheiss PJ (1993) Analysis and application of in situ pore pressure measurements in marine sediments. J Geophys Res 98:7921–7938

Finke KA, Mayne PW, Klopp RA (2001) Piezocone penetration testing in Atlantic piedmont residuum. ASCE, J Geotech Geoenviron Eng 127:48–54

Fu SS, Wilkens RH, Frazer LN (1996) In situ velocity profiles in gassy sediments: Kiel Bay. Geo-Mar Lett 16:249–253

Grozic JLH, Nadim F, Kvalstad TJ (2005) On the undrained shear strength of gassy clays. Comput Geotech 32:483–490

Gunn DE, Best AI (1998) A new automated nondestructive system for high resolution multi-sensor core logging of open sediment cores. Geo-Mar Lett 18:70–77

Harff J (ed) (2003) Projekt DYNAS—Dynamik natürlicher und anthropogener Sedimentation; Vorhaben: Sedimentationsprozesse in der Mecklenburger Bucht; Laufzeit/Berichtszeitraum: 01.06.2000–31.05.2003. Forschungsvorhaben des Bundesministeriums für Bildung und Forschung, Institut für Ostseeforschung Warnemünde, Abschlußbericht (Meilenstein 6). http://www.io-warnemuende.de/projects/dynas/dynas2/db/data/pub/dynas_I_abschlussbericht_2seitig.pdf, accessed 11 Apr 2007

Harff J, Emelyanov EM, Schmidt-Thome M, Spiridonov M (eds) (2004) Mineral resources of the Baltic Sea. Exploration, exploitation and sustainable development, Special Issue 2:1–227

Jensen JB, Bennike O, Witkowski A, Lemke W, Kuijpers A (1999) Early Holocene history of the southwestern Baltic Sea: the Ancylus Lake stage. Boreas 28:437–453

Keller GH (1982) Organic matter and the geotechnical properties of submarine sediments. Geo-Mar Lett 2:191–198

Köhler H-J, Schwab R (2005) Fluidisierungsphänomene unter Wellenbelastung. HANSA Int Maritime J 142:49–59

Kolp O (1966) Die Sedimente der westlichen und südlichen Ostsee und ihre Darstellung. Akademie, Berlin, Beiträge zur Meereskunde 17/18:9–60

Lavoie DM, Lavoie DL, Pittenger HA, Bennett RH (1996) Bulk sediment properties interpreted in light of qualitative and quantitative microfabric analysis. Geo-Mar Lett 16:226–231

Lee DS, Elsworth D (2004) Indentation of a free-falling sharp penetrometer into a poroelastic seabed. J Eng Mech 130:170–179

Lemke W (1998) Sedimentation und paläogeographische Entwicklung im westlichen Ostseeraum (Mecklenburger Bucht bis Arkonabecken) vom Ende derWeichelvereisung bis zur Litorinatransgression. Institut für Ostseeforschung, Warnemünde, Meereswissen Ber Mar Sci Rep 31

Lunne T, Robertson PK, Powell JJM (1997) Cone penetration testing in geotechnical practice. Spon Press, London

May RE (1987) A study of the piezocone penetrometer in normally consolidated clay. DPhil Thesis, University of Oxford, Oxford

Milkert D (1994) Auswirkungen von Stürmen auf die Schlicksedimente der westlichen Ostsee (Influences of storms on muddy sediments in the western Baltic Sea). Universität Kiel, Kiel, Ber/Rep Geol-Paläontologisches Institut no 66

Niedermeyer RO (1987) Beiträge zur komplexen Untersuchung von rezenten Sedimentationsprozessen in Schlickgebieten der westlichen und mittleren Ostsee. PhD Thesis, Ernst-Moritz-Arndt-Universität, Greifswald

Orsi TH, Werner F, Milkert D, Anderson AL, Bryant WR (1996) Environmental overview of Eckernförde Bay, northern Germany. Geo-Mar Lett 16:140–147

Richardson MD, Davis AM (1998) Modelling methane-rich sediments of Eckernförde Bay. Cont Shelf Res 18:1671–1688

Robertson PK (1990) Soil classification using the cone penetration test. Can Geotech J 27:151–158

Roy M, Tremblay M, Tavenas F, La Rochelle P (1982) Development of pore pressures in quasi-static penetration tests in sensitive clay. Can Geotech J 19:124–138

Schneider JA, Peuchen J, Mayne PW, McGillivray AV (2001) Piezocone profiling of residual soils. Proceedings of the International Conference In Situ Measurements of Soil Properties and Case Histories, 21–24 May 2001, Bali, Indonesia, pp 593–598

Schultheiss PJ (1990a) Pore pressures in marine sediments: an overview of measurement techniques and some geological and engineering applications. Mar Geophys Res 12:153–168

Schultheiss PJ (1990b) In-situ pore-pressure measurements for a detailed geotechnical assessment of marine sediments: state of the art. In: Demars KR, Chaney RC (eds) Geotechnical engineering of ocean waste disposal, ASTM STP 1087. American Society for Testing and Materials, Philadelphia, PA, pp 190–205

Silva AJ, Brandes HG (1998) Geotechnical properties and behavior of high-porosity, organic-rich sediments in Eckernförde Bay, Germany. Cont Shelf Res 18:1917–1938

Silva AJ, Brandes HG, Veyera GE (1996) Geotechnical characterization of surficial high-porosity sediments in Eckernförde Bay. Geo-Mar Lett 16:167–174

Song CR, Voyiadjis GZ (2005) Pore pressure response of saturated soils around a penetrating object. Comput Geotech 32:37–46

Stegmann S, Mörz T, Kopf A (2006a) Initial results of a new free fallcone penetrometer (FF-CPT) for geotechnical in situ characterization of soft marine sediments. Norwegian J Geol 86:199–208

Stegmann S, Villinger H, Kopf A (2006b) Design of a modular, marine free-fall cone penetrometer. Sea Technol 47:27–33

Stegmann S, Strasser M, Anselmetti F, Kopf A (2007) Geotechnical in situ characterization of subaquatic slopes: the role of pore pressure transients versus frictional strength in landslide initiation. Geophys Res Lett 34:L07607

Stoll RD, Sun Y-F (2005) Using penetrometer to measure sea bed properties. Office of Naval Research, Arlington, VA, Science & Technology, Ocean Battlespace Sensing (32), Coastal Geosci Annu Rep FY05:1–5

Stoll RD, Sun Y-F, Bitte I (2007) Seafloor properties from penetrometers tests. IEEE J Oceanic Eng 32:57–63

Strout JM, Tjelta TI (2005) In situ pore pressures: what is their significance and how can they be reliably measured? Mar Petrol Geol 22:275–285

Teh CI (1987) An analytical study of the cone penetration test. DPhil Thesis, University of Oxford, Oxford

Urgeles R, Locat J, Lee HJ, Martin F (2002) The Saguenay Fjord, Quebec, Canada: integrating marine geotechnical and geophysical data for spatial seismic slope stability and hazard assessment. Mar Geol 185:319–340

van Kesteren W, van Kessel T (2002) Gas bubble nucleation and growth in cohesive sediments. In: Winterwerp JC, Kranenburg C (eds) Fine sediment dynamics in the marine environment. Proc Marine Science 5. Elsevier, Amsterdam, pp 329–341

Vermeulen N, Rust E (1995) CPTU profiling: a numerical method. Proceedings of the International Symposium on Cone Penetration Testing, CPT 95, 4–5 October 1995, Linköping, Sweden. Swedish Geotechnical Institute, SGI, Rep 3:95, vol 2, pp 343–350

Wever T, Abegg F, Fiedler HM, Fechner G, Stender IH (1998) Shallow gas in the muddy sediments of Eckernförde Bay, Germany. Cont Shelf Res 18:1715–1739

Wever TF, Lühder R, Voß H, Knispel U (2006) Potential environmental control of free shallow gas in the seafloor of Eckernförde Bay, Germany. Mar Geol 225:1–4

Wheeler SJ (1988) The undrained shear strength of soils containing large gas bubbles. Géotechnique 38:399–413

Wichman BGHM (2000) A finite strain theory for gassy sludge. Géotechnique 50:35–41

Wilkens RH, Fu SS (1994) Acoustic lance operations in Eckernförde Bay. In: Wever TF (ed) Proc Gassy Mud Worksh, 11–12 July 1994, Forschungsanstalt der Bundeswehr für Wasserschall und Geophysik, Kiel, FWG Rep 14:34–38

Wilkens RH, Richardson MD (1998) The influence of gas bubbles on sediment acoustic properties: in situ, laboratory, and theoretical results from Eckernförde Bay, Baltic Sea. Cont Shelf Res 18:1859–1892

8 CONCLUSIONS AND OUTLOOK

A novel *in situ* testing approach was developed and carried out in this study to detect fluid mud and to characterise marine soft cohesive sediments by dynamic CPTU measurements. Furthermore, the properties of natural fluid mud suspensions especially their rheological behaviour were examined. The focus lied on the verification of the influencing parameters such as suspended sediment concentration, grain size composition and organic content. A number of conclusions can be drawn from this study and are summarised in the following as bullet points:

- At first it can be stated from the dynamic CPTU measurements carried out so far that this method is capable of *in situ* detecting fluid mud suspensions and characterising soft cohesive sediments by responses in pore pressure and/or cone resistance. Due to the dynamic character of this device the sediment disturbance during the *in situ* measurements may be considerable smaller than that of the standard constant-rate CPTU tests which require heavy seabed rigs.
- Two different pore pressure signals could be identified in the soft cohesive sediments of the western Baltic Sea during dynamic CPTU measurements. One type shows a pore pressure signal with a well defined peak in both pore pressure and cone resistance during penetration. An initial marked increase is followed by exponential pore pressure decay during dissipation. It is concluded that this type of curve is associated with normally consolidated mud, with indurated clay layers showing significantly higher shear strength (up to 19 kPa). In contrast, the second type of pore pressure signal shows initially sub-hydrostatic pore pressure values upon penetration and a delayed response towards positive pressures thereafter. This type was typically found in soft muds with high water content und low undrained shear strengths of 1.6-6.4 kPa. Hence, the deployment of dynamic CPTU-instruments is powerful in characterising soft cohesive sediments by pore pressure and cone resistance response.
- The occurrence of sub-hydrostatic pore pressure signals seems to be associated with the displacement of sediment and fluid upon penetration of the CPTU-device, skin effects during dynamic profiling, enhanced consolidation and strength of individual horizons, the presence of free gas, and a dilatory response of the sediment. Free gas

in the soft sediments may be primarily responsible for the obtained pore pressure response.

- Applying the results from dynamic CPTU deployments in published standard soil classification charts may also be a suitable method for a first order identification and classification of soil types. Here, the comparison of the dynamic CPTU results (pore pressure vs. net cone resistance) with those by Vermeulen and Rust (1995) gave superb agreement for the soft sediments of the Baltic Sea. With this approach one is able not only to identify the soil types, but also their consistencies. Thus, it can be concluded that following those methods dynamic CPTU measurements are an appropriate means to classify soft sediments.
- For the first time a dynamic CPTU was deployed as an innovative and efficient method to detect fluid mud. The device is modular and utilises a disk configuration replacing the cone. The disk serves to enhance the sensitivity of the tip resistance when profiling weaker, more viscous mud. From the CPTU tests carried out so far it can be concluded that *in situ* measurements of both disk resistance and pore pressure seems to be an accurate qualitative method to identify fluid mud (suspended sediment concentration $\geq$ 90 g/l) and the transition from fluid mud to consolidating mud once concentrations exceed 150 g/l.
- In the context of *in situ* detection of fluid mud, laboratory experiments of fluid mud properties complemented the research for this thesis. The experiments focused on the verification of influencing parameters on the rheological behaviour of natural fluid mud suspensions. In general all suspensions tested exhibited non-Newtonian shear thinning behaviour. Yield stress and viscosity were increasing exponentially with an increase in suspended sediment concentration (SSC). Besides the relation of SSC and the rheological behaviour, the experimental results of the samples from the river Ems and the harbour of Emden led to the conclusion that mineral composition and grain size distribution are negligible when accounting for the differences in the rheological behaviour observed. Instead, variations in salinity, type of organic matter and floc strength may provide major controls on the rheological behaviour of the tested suspensions.

In summary, a new versatile approach for *in situ* testing of fluid mud suspensions and soft cohesive sediments was developed during this research. The sediment investigations by a dynamic CPTU reveal a huge potential of a time- and cost-effective method when standard (quasi-static) CPTU measurements or other *in situ* methods are not practicable. This is in particular true in gas-rich muds on which, for stability reasons, standard CPTU rigs cannot be deployed.

New aspects arose which require further research in the future:

- The potential effect of free gas on *in situ* strength and measurements has to be explored further.
- Modelling of the penetration of the dynamic CPTU device in soft sediment might serve to better understand the interaction between the sediment and the CPTU-device, and therewith a better interpretation of the parameters derived. Especially the partially occurrence of sub-hydrostatic pore pressures during the impact of soft sediments is not yet totally understood.
- The influence of rate effects, especially for rheological fluid mud during CPTU penetration, has to be investigated further.
- Deployments of the CPTU-device over entire tidal cycles during different times of the year, ideally in different regions of fluid mud, are required (1) to fully assess the viability of the CPTU-method for fluid mud suspension, (2) to tune the CPTU-device with regard to density and / or viscosity criteria to monitor navigable depth, (3) to shed light on seasonal variations, and (4) to come reliable quantitative results concerning the pore pressure and tip resistance.

ACKNOWLEDGEMENTS / DANKSAGUNG

Ich danke dem Fachbereich Geowissenschaften der Universität Bremen und dem Institut MARUM für die Vergabe der Doktorarbeit.

Meinem Betreuer Prof. Dr. Achim Kopf danke ich für die gute wissenschaftliche Betreuung der Arbeit, für seine Unterstützung, für die vielen Diskussionen als auch für die tatkräftigen CPT Messeinsätze vor Ort. Außerdem danke ich Prof. Dr. Tobias Mörz für die Begutachtung dieser Arbeit und die Diskussionen während der Messauswertungen.

Der Arbeitsgruppe danke ich für ihre stetige Unterstützung, für die konstruktiven Gespräche und das nette Beisammensein auch außerhalb der Universität. Insbesondere Sylvie Stegmann danke ich, die mir sehr in der Anfangszeit geholfen hat und die ihre Begeisterung für CPT Messungen auf mich übertragen hat. Matthias Lange und Hendrik Hanff danke ich für den super technischen Support und Matthias insbesonders für seinen selbstlosen Einsatz mit mir auf der eisigen Ostsee bei minus 15 Grad und Schneesturm, die CPT am laufen zu halten. Andre Hüpers und Annika Förster danke ich für die netten Gepräche. Andre möchte ich auch noch hier für seine Hilfe bei CPT Messeinsätzen danken, zu denen er mitkam, obwohl mein Thema gar nichts mit seiner Forschung zu tun hatte. Nina Stark danke ich für die Hilfe bei den Messungen im Hafen von Emden. Ich denke gerne an die Mittagsgespräche und die Grillzeiten mit der AG Mörz und danke allen für ihr offenes Ohr und die Diskussionen.

Ich danke allen, die mich bei meinen Labormessungen im MARUM und Fachbereich Geowissenschaften unterstützt haben, insbesondere Jan-Berend Stuut, Brit Kockisch, Vera Lukies und Christoph Vogt. Außerdem danke ich dem Institut für Umweltwissenschaften (IUW, Bremen), dass ich in ihren Laboren die rheologischen Messungen durchführen konnte, insbesondere Daniel Kück für seine Hilfe.

Der deutschen Marine (Thomas Wever) danke ich für die Schiffszeiten und großartige Unterstützung und Kooperation bei den zahlreichen CPT Messungen. Ohne diese Ausfahrten wäre meine Arbeit nicht möglich gewesen. Besonderer Dank auch an die Kapitäne und Crew der Schiffe Kronsort und Planet.

Dank auch an das WSA Emden (Martin Krebs) und der Emden Port Authority (Uwe Boekhoff), die mir Schiffsfahrten auf der Ems und im Hafen von Emden ermöglichten. In diesem Zusammenhang auch Dank an die Kapitäne und Crew der Schiffe Friesland und Delphin. Ich danke den Niederländern Prof. Victor de Jonge, Prof. Hub de Swart und Dr. Stefan Talke, dass sie mich am Anfang meiner Forschung mit auf ihre Ems-Schiffsfahrten genommen haben, mir somit die Möglichkeit zum Testen der CPT gaben, sowie interessante Gespräche zum Thema Ems und Schlick führten.

Dem Senckenberg Institut (auch Kapitän und Crew der Senckenberg) danke ich für die Schiffsfahrten auf der Ems, insbesondere Dr. Alex Bartholomä und Dr. Kerstin Schrottke (MARUM). Marius Becker vom MARUM danke ich für die großartigen Diskussionen über ‚mudbugs'.

Dank auch an Dr. Sabine Kasten vom AWI für die Schiffszeit und an Kaptiän und Crew der Heincke, die auch bei stürmischsten Nordseewetter versucht haben, die CPT ins Wasser zu kriegen und das Schiff auf Position zu halten.

Zum Schluss möchte ich Dr. Christian Winter für die Mitnahme auf dem Forschungsschiff Senckenberg danken, auch wenn leider zu dem Zeitpunkt kaum Fluid Mud in der Ems war und keine CPT Messungen möglich waren. Dr. Andreas Wurpts und Anna Zorndt vom Franzius-Institut Hannover danke ich für die Gespräche und den Datenaustausch während dieser Zeit.

Zum Schluss möchte ich noch meiner Familie und Daniela danken, die mich immer unterstützt und motiviert haben, insbesondere Omi und Opi, die leider die Fertigstellung dieser Arbeit nicht mehr miterleben.

ERKLÄRUNG

Hiermit versichere ich, dass ich

1. die Arbeit ohne unerlaubte fremde Hilfe angefertigt habe,

2. keine anderen als die von mir angegebenen Quellen und Hilfsmittel benutzt habe und

3. die den benutzten Werken wörtlich oder inhaltlich entnommenen Stellen als solche kenntlich gemacht habe.

Bremen, den 13.10.2010 ……..

(Unterschrift)

APPENDIX

- A1: Overview CPTU measurements of this study
- A2: Conference contributions
- A3: Cruise reports
- A4: Data of Baltic Sea sediment samples
- A5: Data of fluid mud samples from the river Ems and the harbour of Emden

APPENDIX A1 – OVERVIEW CPTU MEASUREMENTS OF THIS STUDY

Date	Location	CPTU mode	Number of tests	Deployment	Platform	Remarks
CPTU measurements for fluid mud detection						
14.02.2006	Ems	CPTU - cone	18	continous veered	vessel *Friesland* (WSA Emden)	*see also Chapter 4.2 and Manuscript 2 of this thesis* fluid mud not detected by CPTU - insufficient suspension concentration
27.02.2006	Harbour of Emden	CPTU - cone and disk	22	continous veered	vessel *Friesland* (WSA Emden)	CPTU data interpretation at that time did not show possibility of fluid mud detection; recalcultion of CPTU data: fluid mud detected (see Chapter 4.2)
16.08.2006	Ems	CPTU - cone	4	stepwise lowered	bridge	difficulties to handle CPTU from bridge; strong currents during tests
14.06.2007	Ems	CPTU - cone	2	stepwise lowered	R/V *Senckenberg* (Institute Senckenberg)	longtime steptests over slackwater (~1.5 h); fluid mud not detected by CPTU
19.06.2007	Harbour of Emden	CPTU - cone	2	stepwise lowered	vessel *Delphin* (Emden Port Authority)	longtime steptests (~2h); fluid mud not detected by CPTU
01.04.2008	Harbour of Emden	CPT - disk	25	continous veered	vessel *Delphin* (Emden Port Authority)	detection of fluid mud
23.-26.02.2009	Ems	CPTU - cone and disk	25	continous veered	R/V *Senckenberg* (Institute Senckenberg)	fluid mud not detected by CPTU; insufficient suspension concentration and technical problems
CPT measurements in soft cohesive sediments						*see also Manuscript 3 and Appendix A3 (cruise reports) of this thesis*
23.-27.01.2006 and 10.-17.03.2006	Baltic Sea	CPTU - cone	57	continous veered	R/V *Kronsort* and R/V *Planet* (FWG)	characterisation of soft cohesive sediments
data interpretation not included in this thesis - pore pressure development measured by dynamic CPTU similar to tests in Baltic Sea						
03.-04.04.2007	*North Sea*	*CPTU - cone*	*26*	*continous veered*	*R/V Planet (FWG)*	*characterisation of soft cohesive sediments*
05.-13.09.2007	*North Sea*	*CPTU - cone*	*20*	*continous veered*	*R/V Heincke (German Research Vessel)*	*characterisation of soft cohesive sediments; bad weather conditions*

APPENDIX A2 - CONFERENCE CONTRIBUTIONS

EGU General Assembly, Vienna, Austria (2007):

Pore pressure measurements with in-situ FF-CPT in the western Baltic Sea

A. Seifert, S. Stegmann, A. Kopf

Cone penetrometers are commonly used to investigate the in-situ properties of sediments such as sediment strength, pore pressure (u_2), and temperature. During two research cruises in January and March 2006 in the Baltic Sea (Mecklenburg, Eckernförde, and Geltinger Bays), 57 free-fall CPT measurements were carried out altogether. The main aim was to analyse the pore pressure evolution during and up to 15 mins. after insertion of the probe, and then compare those results to physical properties data obtained from sediment cores recovered in the same locations. As a free-fall CPT decelerates into the sediment until it rests, very rapid changes of pressure occur due to fluid displacement and sediment deformation. In the majority of the tests, pore pressure decreases to sub-hydrostatic values upon insertion into the fine-grained cohesive sediments, and then slowly increases again. In places, positive spikes in both pore pressure and cone resistance overprint this pattern where slightly indurated sandy silts are penetrated. We propose that the observed delayed pore pressure response is an indication for dilatancy of the mud as well as the presence of free (microbial) gas in the sediments, especially in Eckernförde Bay.

Geo2008, Annual conference DGG/GV, Aachen, Germany (2008)

Sediment characterisation by in-situ dynamic cone penetrometer tests in shallow Shelf Seas

A. Seifert, S. Stegmann, T. Mörz, M. Lange, T. Wever, A. Kopf

Increasing anthropogenic use of coastal areas and continental shelves, e.g. for the installation of wind power stations and gas pipelines, requires detailed characterisation of bottom sediments. For efficient in-situ determination of geotechnical properties of marine sediments cone penetrometers (CPTs) are widely used. In this context we present in-situ strength and pore-pressure measurements from dynamic cone penetration tests in sediments of Mecklenburg, Eckernförde and Gelting bays, western Baltic Sea. The study areas are characterised by thick mud layers and partially free microbial gas resulting from the degradation of organic material. The main aim is to use differences in penetration resistance and pore-pressure evolution during and after CPT deployment to relate them to effects such as variability in state of consolidation and degree of undersaturation (i.e. free gas in the sediment). Sediment sampling by gravity cores was done for reconnaissance and analyses of geotechnical properties as well as laboratory shear tests.

Despite the striking similarities in incremental density increase and shear strength behaviour with depth, gas occurrence and subtle variations in the coarse-grained fraction cause distinct pore-pressure and cone resistance curves. Focussing on the pore pressure evolution during and after penetration of the CPT two different types could be identified. In Mecklenburg Bay only a few measurements show a well-defined peak in pore pressure and cone resistance during penetration followed by exponential pore-pressure decay during dissipation (type A). This pore-pressure signal is associated with normally consolidated mud with indurated clay layers showing significantly higher undrained shear strength (up to 19 kPa). Majority of the tests exhibit so-called type B pore-pressure signals, which show initial negative pore-pressure values during penetration followed by delayed response towards positive pressures thereafter. Type B is typically found in soft muds with high water contents and undrained shear strength of

1.6-6.4 kPa in all three bays. It is further affected by displacement of sediment and fluid upon penetration of the lance, skin effects during dynamic profiling, enhanced consolidation and strength of individual horizons, and the presence of free gas.

In addition sediment type and consistency can be gained by plotting the in-situ pore pressure and cone resistance data in a soil classification chart. The overall agreement between the first-order soil classification based on CPT parameters and ground-truthing evidence supports our approach of using time- and cost-efficient dynamic penetrometer devices to characterise marine sediments.

APPENDIX A3 - CRUISE REPORTS

Research Cruise: 23.-27.01.2006 Baltic Sea (vessel Kronsort)

Physical behaviour of fine-grained, gassy sediments in the Baltic Sea using a CPT (Cone Penetration Testing) lance and geotechnical laboratory testing

Kopf, A., **Seifert, A**., Stegmann, S., Lange, M.

Research Centre Ocean Margins, University Bremen, Postfach 330440, 28344 Bremen, Germany

February, 2006 (unpublished)

Introduction and Methods

Additional to spatial high resolution tools, like multibeam and seismic surveys, Cone Penetrating Tests (CPT) are a widely used method for *in situ* sediment characterisation in onshore and offshore settings (Lunne et al., 1997). However, in marine realm such measurements become laborious since seabed rigs have to be deployed prior to the measurement. As an alternative, a new marine "free-fall" CPT has been designed at RCOM (Research Centre Ocean Margins) at Bremen University for the quick, cost-effective in situ testing in marine sediments. Parameters measured include cone resistance, sleeve friction, pore pressure upon insertion (u_1, u_2, u_3), temperature, deceleration, and tilt. Secondary parameters derived from these results include undrained shear strength and permeability. Ground truthing of the CPT data is achieved by testing discrete sediment samples in the geotechnical laboratory.

In this report, we present preliminary results from 16 CPT tests during an expedition with German vessel KRONSORT during January 23-27, 2006. The data are complemented by vane shear experiments in the *Marine Geotechnics* laboratory, RCOM Bremen.

Instrument design

The modular instrument consists of a standard 15cm^2-diameter CPT cone to measure cone resistance, the friction as well as the tilt of the lance. An absolute pore pressure sensor with a 10 MPa range, located directly behind the cone, is adapted to high pressure conditions caused by the impact during penetration. Above the friction sleeve, an electrical conductivity sensor allows for first-order characterisation of the lithologies penetrated. Owing to the rapid, non-continuous initial penetration velocities, the digital data acquisition frequency of approx. 200 Hz results in a spatial resolution of about 1 cm. Optionally, spacer rods can be added when soft materials are anticipated. Penetration depth depends primarily on the sediment properties and the weight of the lance. Variable penetration depth of the CPT is achieved by mounting weights (4 x 15 kg) to the head of the instrument. The head also hosts a microcontroller, a non-volatile RAM, a battery pack, and a deceleration sensor to calculate total penetration depth. For details regarding the device, please refer to Stegmann et al., 2006.

During the KRONSORT cruise, the CPT lance was used in a basic configuration with a 3.5 m long rod and 60 kg weight added. A picture during the deployment procedure is shown in Figure 1.

Measured and derived parameters

The RCOM “free fall” CPT instrument is equipped with a standard CPTU tip from GEOMIL, Netherlands. Pore pressure is monitored in u_2 position immediately behind the cone. In addition, temperature, deceleration, and tilt on the probe can be monitored (see Stegmann et al., 2006). A typical plot of the primary data of a CPT deployment is given in Figure 2. Apart from the primary parameters of the instrument, previous workers have proposed to calculate secondary sediment physical properties, largely using empirical equations.

Fig. 1 CPT instrument during deployment from KRONSORT.

The maximum insertion pressure produced at the probe tip can be used to estimate the undrained shear strength of the sediment (C_u). For typical deep sea sediments, Esrig et al. (1977) suggest the relation: $C_u = U_{imax}/6$, where U_{imax} is the maximum insertion pressure. The decay of excess pore pressure produced by the insertion is governed by the consolidation process around the probe and can be modeled as radial consolidation. Bennett et al. (1985) predict the coefficient of horizontal consolidation (C_h) from the time taken for 50% of U_{imax} to dissipate, and C_h can then be used to determine the permeability (k), using the expression: $k = C_h \mu m_u$, where m_u is the compressibility and μ is the viscosity of the pore water. In places where coring is too time-consuming, pogo-style will not only provide first-hand *in situ* results, but secondary parameters to estimate slope stability and hazard potential.

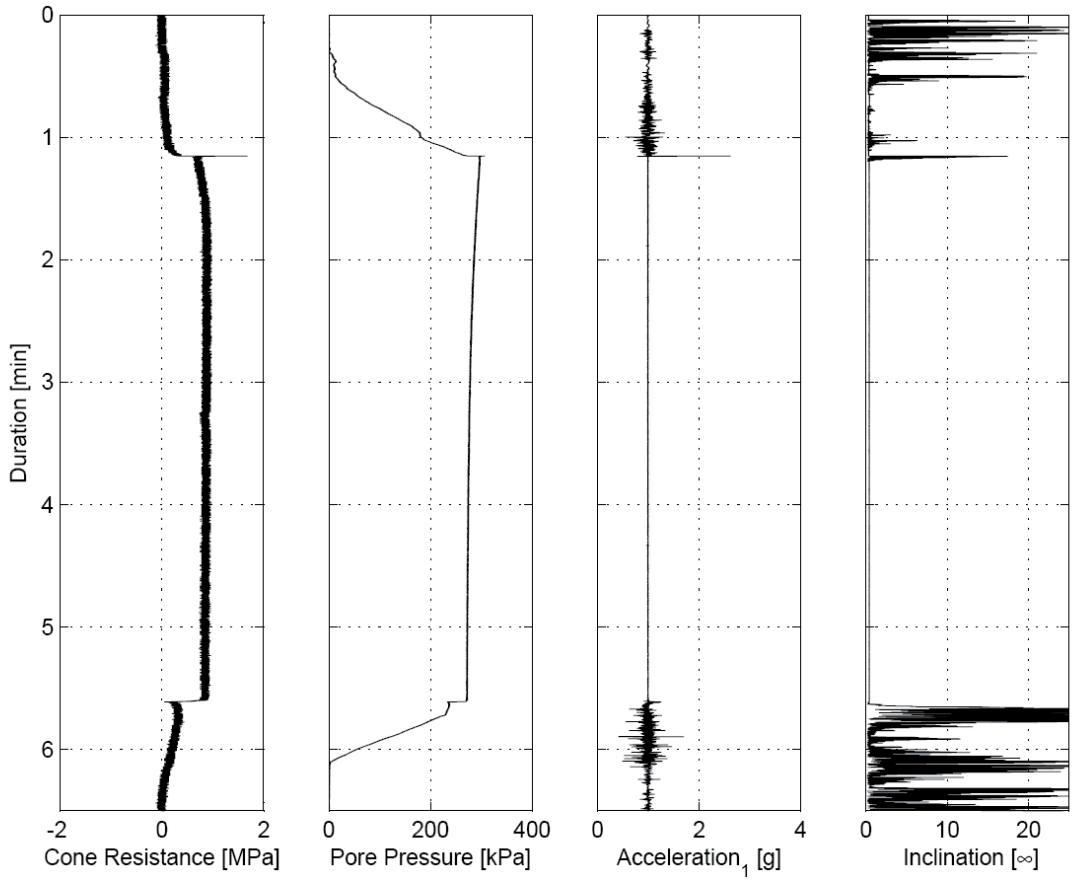

Fig. 2 Typical raw data plot showing, from left to right, cone resistance, pore pressure, acceleration, and inclination versus time. Data are from test CPT6-2, Mecklenburger Bight.

Undrained shear strength was further measured in the geotechnical laboratory using a RotoVisco RV20 device by Haake (Germany). The material available was a gravity core also taken from the KRONSORT vessel. Tests were carried with a steel blade (10 mm across, 9 mm high) at vane rotation rate of 30°/min. The blade is submerged so that its upper rim parallels the split core face of a gravity core.

Initial results and Discussion

During the KRONSORT cruise, 16 CPT sites were visited: Sites 1-10 were located in the Mecklenburg Bight, sites 11-12 in the Eckernförde Bight, and sites 13-16 in the Geltinger Bight (see Table 1 for detailed positions). A total of 49 CPT penetrations were carried out at these 16 locations in the Baltic Sea, with the number of repeat measurements at each site varying between none and twelve.

Table 1 Data from CPT tests 1 through –16, including position, winch speed, water depth (from echosounder and CPT), max. cone resisitance and pore pressure, max. effective insertion pressure and derived undrained sediment strength. See text for discussion.

Location		Deployment	Water depth [m] (hydr. pressure [kPa]) - echosounder	max. cone resistance [MPa]	max. pore pressure - CPT [kPa]	hydrostatic pressure - CPT [kPa]	max. excess pore pressure after insertion [kPa]	Shear strength [kPa]
Mecklenburg Bight								
CPT1_3	54 13,439 N; 011 45,277 E	controlled (~50cm/s)	25,3 (253)	1,51	284,2	263,0	21,2	3,5
CPT2_2	54 13,420 N; 011 44,887 E	controlled (~50cm/s)	25,2 (252)	0,76	298,0	261,4	36,6	6,1
CPT3_2	54 13,460 N; 011 44,567 E	controlled (~50cm/s)	25,3 (253)	2,27	318,0	257,4	60,6	10,1
CPT4_2	54 13,424 N; 011 44,163 E	controlled (~50cm/s)	25,3 (253)	1,38	280,6	261,0	19,6	3,3
CPT5_2	54 13,459 N; 011 43,698 E	controlled (~50cm/s)	25,4 (254)	2,13	269,0	240,7	28,3	4,7
CPT6_2	54 13,431 N; 011 43,380 E	controlled (~50cm/s)	25,5 (255)	1,68	306,3	274,0	32,3	5,4
CPT7_2	55 13,404 N; 011 43,178 E	controlled (~50cm/s)	25,5 (255)	1,86	314,5	277,4	37,2	6,2
CPT8_3	54 13,344 N; 011 42,714 E	controlled (~50cm/s)	25,7 (257)	1,22	276,5	224,0	52,5	8,8
CPT9_2	54 13,420 N; 011 42,234 E	controlled (~50cm/s)	25,8 (258)	0,70	310,2	281,0	29,2	4,9
CPT10_2	54 13,403 N; 011 41,927 E	controlled (~50cm/s)	25,8 (258)	0,70	320,9	287,1	33,8	5,6
Eckernförde Bight								
CPT11_2	54 29,876 N; 009 59,100 E	controlled (~50cm/s)	29,1 (291)	2,84	328,9*	278,5	50,5	8,4
CPT12_1	*54 30,927 N; 010 01,340 E*	*controlled (~30cm/s)*	*29,6 (296)*	*0,35*	*290,9*	*284*	*6,9*	*1,2*
Geltinger Bight								
CPT13_3	54 49,006 N; 009 50,080 E	controlled (~30cm/s)	25,7 (257)	0,48	265,7*	243,1	22,6	3,8
CPT14_2	54 49,016 N; 009 50,866 E	controlled (~50cm/s)	24,4 (244)	0,43	245,1*	225,1	20,0	3,3
CPT15_3	54 48,033 N; 009 51,354 E	controlled (~50cm/s)	23,1 (231)	0,43	236,0*	215,5	20,5	3,4
CPT16_2	54 47,919 N; 009 52,133 E	controlled (~50cm/s)	21,5 (215)	0,42	214,8*	194,1	20,7	3,5

* *max. pore pressure after 2.5 min*

CPT12_1 - poor data quality because of big ship movement

Mecklenburg Bight

An East-West transect of 10 CPT sites was visited during the cruise, with a total of 23 penetrations of the largely fine- to medium-grained seafloor sediments. Winch speed was varied between individual penetrations, with a range from 10-20, 30 and 50 cm/s (estimated from marked rope on the winch). For clarity, we here present only the fast penetration tests, i.e. the 50 cm/s tests (and 30 cm/s, where the max. winch speed was not reached). Penetration depth of the lance varied between 2 m and 3.4 m during these tests. However, as a result of the pogo-style deployment, the lance was rarely retrieved so that visual inspection (based on mud stuck to the instrument) was not an option in some cases. Penetration depth will be calculated accurately by integration of the data from the accelerometer at a later stage.

Water depths at the neighbouring sites ranged from 25.3 m to 25.8 m (echosounder information). However, a mismatch was found with the absolute pressure sensor of the CPT device, which measured the equivalent of 22.4 m to 28.7 m (see Table 1). In order to calculate the pore pressure in excess of hydrostatic, we stuck to the CPT readings for

consistency's sake. Maximum excess pore pressures hence ranged from 19.6 kPa to 60.6 kPa (see Table 1). Examples for the pore pressure behaviour, which generally showed a prominent spike upon impact of the instrument on the seafloor, followed by an exponential decay with time, are given in Figure 3a and 3b. The undrained shear strength, as calculated from the max. excess pore pressure (see above, and Esrig et al., 1977), ranges from 3.5 kPa to 10.1 kPa. These values lie within the typical shear resistance range of marine seafloor sediments, e.g. as recovered in DSDP and ODP drilling campaigns.

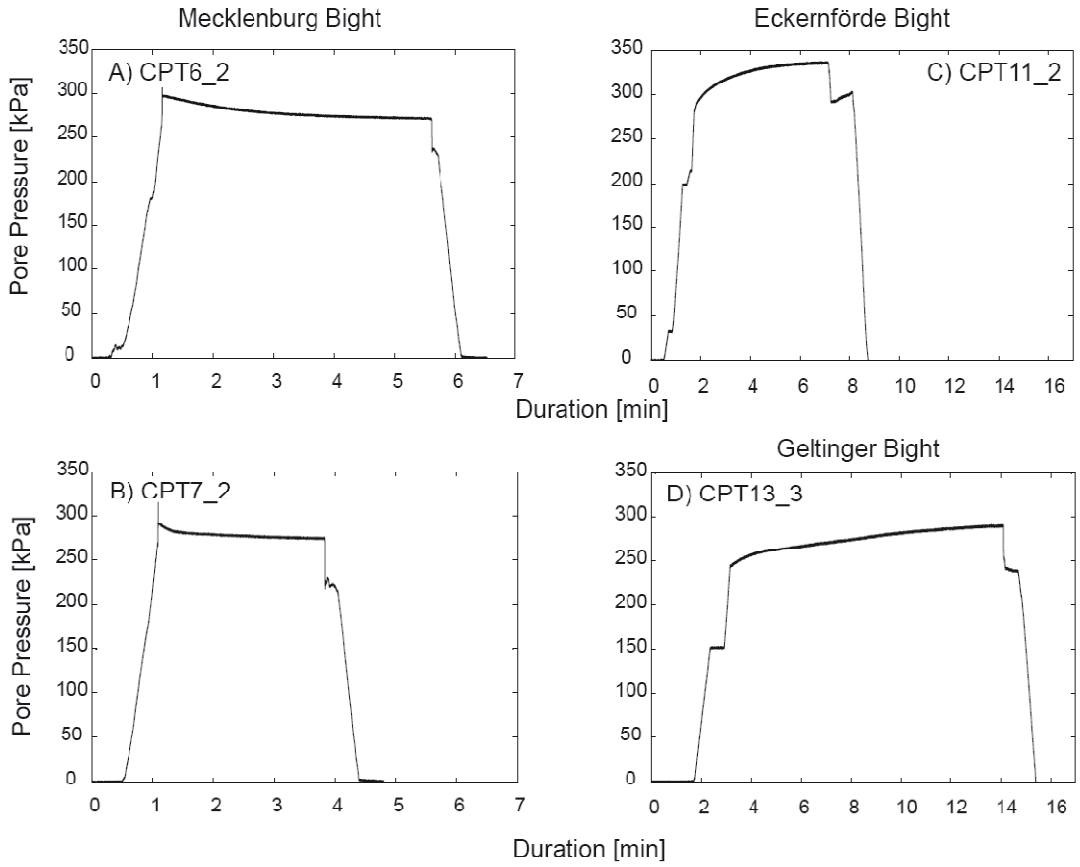

Fig. 3 Comparison of pore pressure evolution of CPT tests 6-2 (A), 7-2 (B), 11-2 (C) and 13-3 (D). Please note the different behaviour in Mecklenburger Bight (A, B) when compared tothe gassy sediments in Eckernförde (C) and Geltinger Bight (D). See text.

Eckernförde and Geltinger Bights

Compared to the Mecklenburg area, Eckenförde and Geltinger Bight are known for their more gas-rich sediments (e.g. Wever et al., 2006). A total of six sites with 26 individual penetrations was visited, with numbers of penetrations ranging from 1 to 13. At these

sites, the average water depth was similar to Mecklenburg, ranging from 29.1-29.6 m (echosounder) and 27.9-28.4 m (CPT) in Eckernförde Bight, and 21.5-25.6 m (echosounder) and 19.4-24.4 m (CPT) in Geltinger Bight (Table 1).

Maximum excess pore pressures reach up to 50.5 kPa at Eckernförde, and only 22.6 kPa in Geltinger Bight. This corresponds to undrained shear strengths of up to 8.4 and 3.8 kPa, respectively (Table 1). The fact that lower values are encountered in the gas-rich areas when compared to Mecklenburg is difficult to explain. One possible clue could be the inclination of the instrument. Weather conditions were sometimes harsh (especially in Eckernförde Bight), so that the instrument did not remain in a stable, upright position during some of the tests. As a result, overpressured gas may have escaped alongside the lance-sediment interface, this way causing the apparent low overpressure upon impact. Evidence for overpressures is provided by the shape of the pore pressure curve during the tests. As can be seen from Figures 3c (Eckernförde) and 3d (Geltinger Bight), the anticipated spike when the lance hits the sediment-water interface is absent. Instead, pore pressure rises steadily during the experiment, generally for the entire period of deployment (i.e. up to nearly 20 mins. in our longest experiment). Given that the majority of our deployments was only 3-5 mins., we assume that max. excess pressures lie well above the values presented in Table 1. Future deployments in more stable weather conditions may confirm this assumption by attempting a longer term deployment.

Accompanying laboratory experiments

In order to tie the sediment strength data derived from CPT deployments to the actual marine soils, we carried out a number of vane shear tests. Unfortunately, only one gravity core of 1 m length was available for the “ground truthing” study. This core was taken adjacent to CPT site 10, i.e. the westernmost location of the Mecklenburg Bight transect.

Vane shear tests gave shear strength values from 0.8 kPa to 4.2 kPa, showing slight variations owing to lithological changes. However, an overall downward decrease is observed (Figure 4). The maximum strength from vane experiments is similar to that derived from CPT tests (i.e. 5.6 kPa; see Table 1). Figure 4 illustrates nicely how well

the cone resistance, which naturally directly reflects the sediment strength, agrees with the laboratory data. We hence conclude that the CPT tests are a time-efficient way to collect a lot of shallow sediment physical properties data in a pogo style manner.

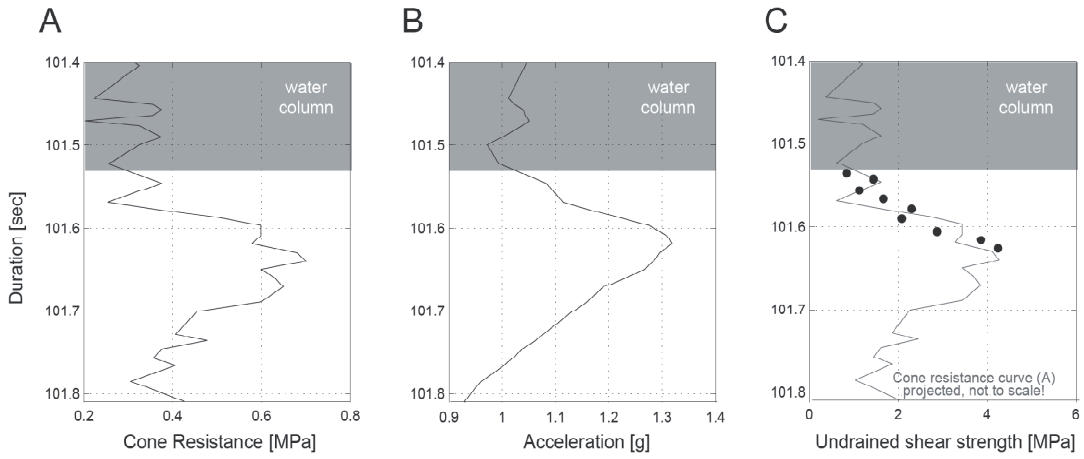

Fig. 4 Cone resistance (A), deceleration (B) from CPT test 10-2, and laboratory vane shear experiments (C) on a gravity core nearby; the latter data underlain by the graph from Fig. A), based on an assumed linear deceleration of the CPT probe upon penetration into the soft mud. See text.

Acknowledgements

The RCOM Bremen group is grateful for the outstanding support by Thomas Wever, the Forschungsanstalt der Bundeswehr für Wasserschall und Geophysik (FWG) in general, and Wehrtechnischer Dienst (WTD). Special thanks go to the master, technicians and crew of KRONSORT for their cooperation and help. The German Science Foundation (DFG) is acknowledged for funding RCOM, in particular instrument developments within Research area C.

References

Bennett, R.H., L. Huon, P.J. Valent, J. Lipkin & M.I. Esrig, 1985. In situ undrained shear strengths and permeabilities derived from piezometer measurements. In: R.C. Chaney & K.R. Demars (eds), Strength Testing of Marine Sediments: Laboratory and In Situ Measurements, American Society for Testing and Materials, 88-100.

Esrig, M.I., R.C. Kirby & R.G. Bea, 1977. Initial development of a general effective stress method for the prediction of axial capacity for driven piles in clay. Proc. 9th Offshore Technology Conference, 495-501

Lunne, T., Robertson, P.K., Powell, J.J.M. 1997. Cone Penetration Test – Geotechnical Practice, Blackie Academic & Professional London, pp. 312

Stegmann, S., Villinger, H, Kopf, A., 2006. Design of a modular, marine free-fall cone penetrometer. Sea Technology, v. 02/2006, in press (4pp.)

Wever, T.F., R. Luhder, H. Voss, U. Knispel, 2006. Potential environmental control of free shallow gas in the seafloor of Eckernfoerde Bay, Germany. Narine Geology, 225: 1-4.

Research Cruise: 10.-17.03.2006 Baltic Sea (vessel Planet)

In Situ Free-Fall Cone Penetrometer Tests In Soft Mud Of The Western Baltic Sea

Seifert, A., Stegmann, S., Kopf, A.

Research Centre Ocean Margins (RCOM), University of Bremen, Leobener Strasse / MARUM, 28359 Bremen, Germany

April, 2007 (unpublished)

Design of the RCOM Free-Fall CPT

Cone **P**enetrating **T**ests (CPT) are a widely used method for *in situ* sediment characterisation in onshore and offshore settings. However, in marine realm such measurements become time and cost intensive since seabed rigs have to be deployed prior to the measurement. As an alternative, a new marine free-fall CPT (FF-CPT) has been designed at RCOM (Research Centre Ocean Margins) at Bremen University for the quick, cost-effective *in situ* testing in marine sediments. Parameters measured include cone resistance (q_c), sleeve friction (f_s), pore pressure upon insertion (u_1, u_2, u_3), temperature, deceleration, and tilt. Secondary parameters derived from these results include undrained shear strength and permeability. Ground truthing of the CPT data is achieved by testing discrete sediment samples in the geotechnical laboratory. The modular instrument consists of a standard 15cm²-diameter CPT cone to measure cone resistance, the friction as well as the tilt of the lance. An absolute pore pressure sensor with a 10 MPa range, located directly behind the cone, is adapted to high pressure conditions caused by the impact during penetration. Owing to the rapid, non-continuous initial penetration velocities, the digital data acquisition frequency is approx. 40 Hz. Optionally, spacer rods can be added (up to 6 m) when soft materials are anticipated. The head also hosts a microcontroller, a battery pack, and a deceleration sensor to calculate total penetration depth. For details regarding the device, please refer to Stegmann et al. (2006).

CPTesting

During the KRONSORT cruise in January 2006, 16 CPT measurements were carried out with 3 m long extension rods and 60 kg weight added. The lance was lowered into the sediment with an average winch speed of around 1 m/s (0.6-1.2 m/s; Table 1), dependent on winch configuration and handling. During the PLANET cruise in March 2006, 41 CPTests were operated with the lance elongated to 2.5 m length and mounted with additionally 30 kg weights (Fig. 1). Here, the lance was lowered into sediment with a winch speed of around 2 m/s (1.6-2.6 m/s; Table 1). Penetration depth was calculated by the second integration of the deceleration data. Sometimes the deceleration sensor reached the range, so the penetration depth had to be estimated by measuring the remaining sediment stuck to the lance (Table 1). The CPT raw data were further processed using MATLAB and LABVIEW routines.

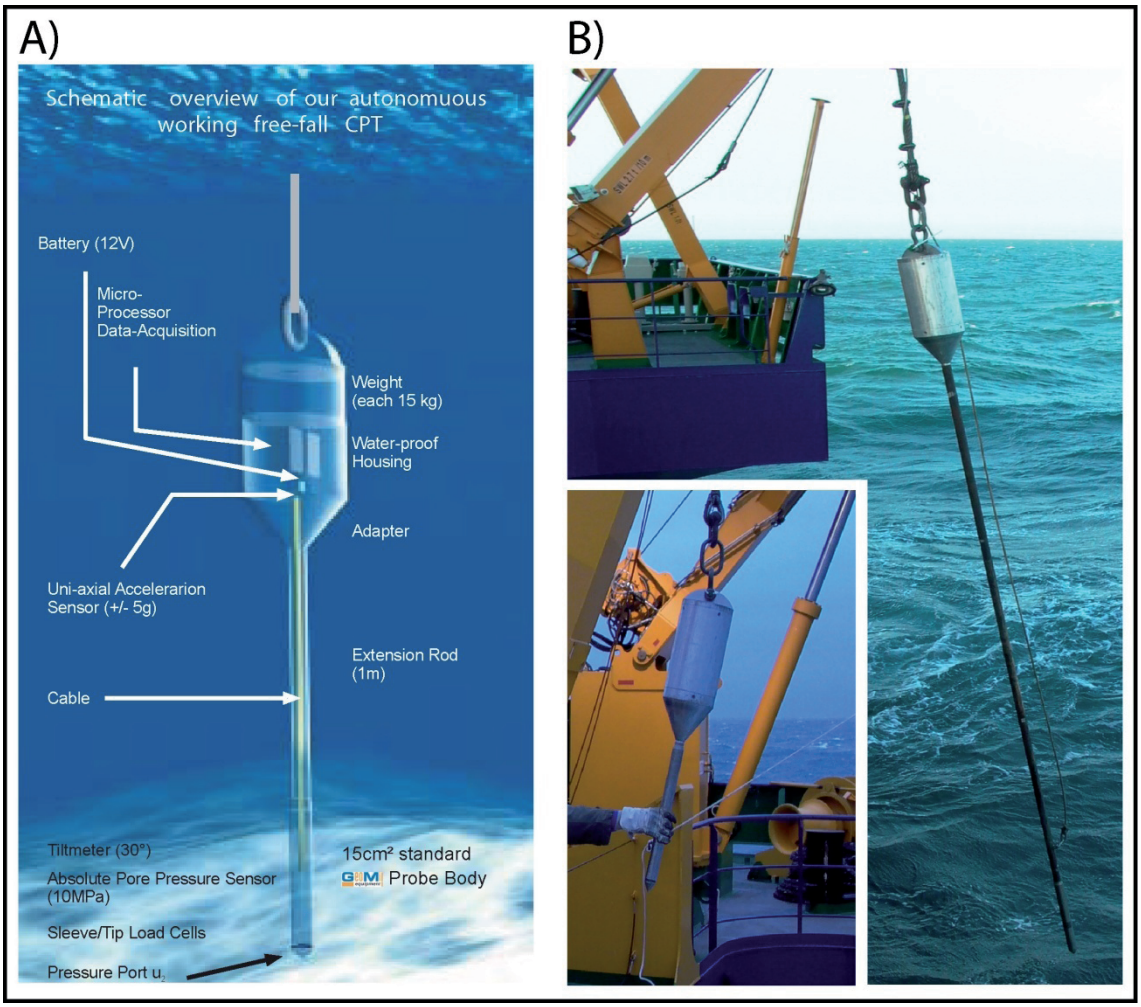

Fig. 1: Design of the RCOM FF-CPT, a) schematic overview of the CPT, b) deployment on the vessel PLANET

Table 1: CPT – Location, testing mode, derived parameters and defined excess pore pressure Types A and B

CPT	Date	Location	Water Depth [m]	Winch Velocity [m/s]	Added Weight [kg]	Rod Length [m]	Time of Measure-ment [min]	Penetration Depth [m]	Max. Cone Resistance [kPa]	Max. Absolute Pore Pressure [kPa]	Excess Pore Pressure Type
C1	24.01.2006	011:45.277 E / 054:13.439 N	25.3	1.1	60	3.5	2	2.00[a]	1513	284	Type B
C2	24.01.2006	011:44.887 E / 054:13.420 N	25.2	1.2	60	3.5	2	3.40[a]	755	298	Type B
C3	24.01.2006	011:44.567 E / 054:13.460 N	25.3	1.1	60	3.5	2	2.00[a]	2275	318	Type B
C4	24.01.2006	011:44.163 E / 054:13.424 N	25.3	1.1	60	3.5	1	2.00[a]	1381	281	Type B
C5	24.01.2006	011:43.698 E / 054:13.459 N	25.4	0.9	60	3.5	2.5	*	2132	269	Type B
C6	24.01.2006	011:43.380 E / 054:13.431 N	25.5	1.1	60	3.5	4.5	1.77[b]	1675	306	Type A
C7	24.01.2006	011:43.178 E / 054:13.404 N	25.5	1.1	60	3.5	2.8	2.27[b]	1858	315	Type A
C8	24.01.2006	011:42.708 E / 054:13.348 N	25.7	0.7	60	3.5	9.5	2.30[b]	1117	323	Type A
C9	24.01.2006	011:42.234 E / 054:13.420 N	25.8	1.1	60	3.5	8.5	0.81[b]	700	310	Type B
C10	24.01.2006	011:41.927 E / 054:13.403 N	25.8	1.1	60	3.5	9	1.33[b]	701	321	Type B
C11	25.01.2006	009:59.100 E / 054:29.876 N	29.1	1.1	60	3.5	6.5	3.28[b]	2843	337	Type B
C12	25.01.2006	010:01.340 E / 054:30.927 N	29.6	0.6	60	3.5	2	*	350	291	Type B
C13	26.01.2006	009:50.080 E / 054:49.006 N	25.7	0.7	60	3.5	11	3.66[b]	480	291	Type B
C14	26.01.2006	009:50.866 E / 054:49.016 N	24.4	1.1	60	3.5	7	3.00[b]	430	261	Type B
C15	26.01.2006	009:51.354 E / 054:48.033 N	23.1	1.1	60	3.5	10	1.98[b]	430	257	Type B
C16	26.01.2006	009:52.133 E / 054:47.919 N	21.5	1.0	60	3.5	3	2.39[b]	420	218	Type B
C99	05.03.2006	011:39.674 E / 054:13.322 N	27.3	1.5	30	2.5	53	2.86[b]	366	305	Type B
C100	05.03.2006	011:39.676 E / 054:13.324 N	27.3	2.1	30	2.5	1	2.57[b]	416	272	Type B
C119	06.03.2006	011:39.770 E / 054:13.412 N	27.1	2.2	30	2.5	48.5	1.93[a]	416	304	Type B
C126	07.03.2006	011:43.448 E / 054:13.589 N	25.6	2.3	30	2.5	0.6	2.27[b]	335	281	Type B
C139	07.03.2006	011:43.414 E / 054:13.582 N	25.7	2.1	30	2.5	51.5	1.88[b]	416	296	Type B
C155	07.03.2006	011:43.418 E / 054:13.586 N	25.6	2.1	30	2.5	1.5	1.80[b]	274	292	Type B
C167	08.03.2006	011:43.375 E / 054:13.362 N	25.3	2.1	30	2.5	5	2.13[b]	579	307	Type B
C168	08.03.2006	011:43.333 E / 054:13.393 N	25.0	2.2	30	2.5	54	2.40[a]	477	295	Type B
C198	11.03.2006	011:43.541 E / 054:12.991 N	25.6	1.8	30	2.5	8.5	2.57[b]	386	299	Type B
C208	11.03.2006	011:43.552 E / 054:12.990 N	25.9	2.0	30	2.5	1.5	2.67[b]	396	290	Type B
C209	11.03.2006	011:43.552 E / 054:12.990 N	26.2	2.2	30	2.5	52	3.07[b]	366	285	Type B
C231	11.03.2006	011:43.568 E / 054:12.988 N	25.7	2.0	30	2.5	53.5	3.13[b]	355	286	Type B
C243	11.03.2006	011:43.557 E / 054:12.983 N	26.0	2.0	30	2.5	52	2.85[b]	335	293	Type B
C249	11.03.2006	011:43.575 E / 054:12.989 N	25.5	1.5	30	2.5	0.5	2.50[a]	457	257	Type B
C251	11.03.2006	011:43.582 E / 054:12.992 N	25.0	1.5	30	2.5	1	2.80[b]	467	271	Type B
C254	11.03.2006	011:43.597 E / 054:12.997 N	25.3	1.2	30	2.5	0.6	2.05[b]	477	266	Type B
C257	11.03.2006	011:43.613 E / 054:13.003 N	25.8	1.7	30	2.5	0.5	2.52[b]	447	264	Type B
C263	12.03.2006	011:46.071 E / 054:14.422 N	26.0	2.1	30	2.5	14.5	2.00[b]	1168	284	Type B
C277	12.03.2006	011:46.080 E / 054:14.425 N	25.7	1.9	30	2.5	49	2.50[a]	1909	273	Type B
C278	12.03.2006	011:46.081 E / 054:14.424 N	25.6	2.3	30	2.5	1	1.33[b]	1411	260	Type B
C296	12.03.2006	011:46.102 E / 054:14.417 N	25.8	1.9	30	2.5	40	1.61[b]	437	272	Type B
C297	12.03.2006	011:46.102 E / 054:14.418 N	25.6	2.3	30	2.5	1	2.13[b]	426	263	Type B
C305	12.03.2006	011:46.100 E / 054:14.421 N	25.7	2.1	30	2.5	97	1.71[b]	427	278	Type B
C308	12.03.2006	011:43.595 E / 054:13.016 N	25.1	2.4	30	2.5	1	2.31[b]	498	270	Type B
C313	12.03.2006	011:43.641 E / 054:13.010 N	25.3	2.4	30	2.5	3	2.54[b]	528	279	Type B
C321	12.03.2006	011:43.693 E / 054:13.003 N	25.	1.6	30	2.5	2.5	1.04[b]	619	273	Type B
C364	13.03.2006	011:44.058 E / 054:15.237 N	26.4	2.2	30	2.5	1.5	1.15[b]	2244	317	Type B
C366	13.03.2006	011:44.056 E / 054:15.237 N	25.0	1.8	30	2.5	1	0.97[b]	1290	290	Type B
C367	13.03.2006	011:44.057 E / 054:15.237 N	26.1	2.1	30	2.5	99	2.50[a]	1696	288	Type B
C381	14.03.2006	011:43.327 E / 054:12.754 N	24.9	2.6	30	2.5	10	2.13[b]	244	279	Type B
C387	14.03.2006	011:43.271 E / 054:12.986 N	25.0	2.3	30	2.5	9.5	1.98[b]	386	280	Type B
C393	14.03.2006	011:43.237 E / 054:12.982 N	25.1	2.3	30	2.5	10	1.55[b]	396	274	Type B
C399	14.03.2006	011:43.295 E / 054:12.983 N	25.1	2.2	30	2.5	59	2.38[b]	1076	283	Type B
C404	14.03.2006	011:43.336 E / 054:12.984 N	25.1	2.4	30	2.5	10.5	1.72[b]	366	289	Type B
C410	14.03.2006	011:43.353 E / 054:12.984 N	25.1	2.5	30	2.5	10	1.97[b]	294	286	Type B
C416	14.03.2006	011:43.361 E / 054:12.985 N	25.4	2.5	30	2.5	10	1.86[b]	477	294	Type B
C422	14.03.2006	011:43.392 E / 054:12.985 N	25.6	2.4	30	2.5	9.5	2.70[b]	447	294	Type B
C484	16.03.2006	011:41.950 E / 054:16.187N	26.4	2.3	30	2.5	6	2.50[a]	223	302	Type B
C485	16.03.2006	011:41.950 E / 054:16.187 N	26.2	2.4	30	2.5	60	2.20[a]	355	293	Type B
C499	16.03.2006	011:41.962 E / 054:16.185 N	26.0	2.2	30	2.5	9.5	2.85[b]	406	306	Type B
C500	16.03.2006	011:41.962 E / 054:16.185 N	26.0	2.4	30	2.5	25	3.22[b]	406	302	Type B

*penetration depth: a - measured on board; b - calculated from deceleration data; * - poor data quality because of heave*

Measured and derived parameters in general

The RCOM FF-CPT instrument is equipped with a standard CPTU tip from GEOMIL, Netherlands. Pore pressure is monitored in u_2 position immediately behind the cone. The method of the dynamic free-fall CPT, lowered at rates of 0.5 m/s to free drop, is different from standard quasi-static cone penetrometer testing, where the CPT is pushed into the sediment with a constant rate of 2 cm/s. The enhanced impact velocity has a profound effect of initial peak resistance onto the cone as well as pore pressure excursion in cohesive soils, which has to be taken into account (Dayal and Allen 1975; Roy et al. 1982). Therefore, different deployment technique may result in a different response. Stoll and Sun (2005) compared static and dynamic penetrometers and detected a more accentuated cone resistance profile with the dynamic penetrometer PROBOS than with the static penetrometer STATPEN. The PROBOS records showed a higher cone resistance where stiffer granular layers were interbedded in the mud; in contrast, no corresponding cone resistance increase were found in the STATPEN data. Cone resistance data are affected by the strain-rate, but higher strain rates might show more information in layered sediments. However, FF-CPT requires less logistical support and is a more time and cost-efficient investigation as a standard CPT. Furthermore, there is no hydraulic platform on the seabed needed which possibly disturbs the sediments being measured.

Based on a huge number of CPTests, soil charts have been investigated to allow a first-order classification of the penetrated sediments. The classification of Robertson (1986) is based on the friction ratio (Sleeve Friction / Cone Resistance) and the Cone Resistance and divides 12 classes of sediments. Vermeulen and Rust (1995) presented a modified Jones and Rust classification chart where the excess pore pressure (Δu) is plotted against the net cone resistance (q_n) (measured total cone resistance corrected for pore pressure and reduced by total overburden stress). This chart identifies not only the soil type, but also the consistency. Apart from the primary parameters of the instrument (q_c, f_s, u_2), previous workers have proposed to calculate secondary sediment physical properties, largely using empirical equations. The maximum insertion pressure produced at the probe tip can be used to estimate the undrained shear strength of the sediment (s_u). For soft marine sea sediments, Esrig et al. (1977) suggest the relation: $s_u = U_{imax}/6$, where U_{imax} is the maximum insertion pressure. The decay of excess pore

pressure produced by the insertion is governed by the consolidation process around the probe and can be modelled as radial consolidation. Bennett et al. (1985) predict the coefficient of horizontal consolidation (C_h) from the time taken for 50% of U_{imax} to dissipate, and C_h can then be used to determine the permeability (k), using the expression: $k = C_h \mu m_u$, where m_u is the compressibility and μ is the viscosity of the pore water.

Results and Discussion

We present CPT data from three muddy sub-basins of the western Baltic Sea, namely Gelting Bay, Eckernförde Bay and Mecklenburg Bay, from two cruises with vessel KRONSORT and PLANET in winter 2006. Penetration of the CPT in the sediment will generate excess pore pressure which is typically greater than the hydrostatic water pressure. Once penetration is stopped, the excess pressure will decay with time. This report concentrates on the different pore pressure evolution regarding the two periods of CPT measurements: dynamic pore pressure response during penetration of the CPT lance into the sediment and dissipation of the induced pore pressure after insertion. Additional, CPT data were related to the physical properties of the cored sediments, which were analysed at RCOM or already in the shipboard laboratory (Table 2, Fig. 4b).

Table 2: Cores – Location, water depth, and core length

station	RCOM identification	Date	Location	Water Depth [m]	Core Length [m]
Mecklenburg Bay					
#1-3	GeoB10501	23.01.2006	011:40.097 E / 054:13.471 N	26.8	0.88
#166*		08.03.2006	011:43.376 E / 054:13.361 N	25.6	1.95
#191*		11.03.2006	011:43.541 E / 054:12.990 N	25.8	2.40
#268	GeoB10502	12.03.2006	011:46.071 E / 054:14.423 N	25.9	1.91
#370	GeoB10503	13.03.2006	011:44.063 E / 054:15.234 N	25.5	2.06
#483	GeoB10504	16.03.2006	011:41.948 E / 054:16.189 N	26.2	4.03
#102	GeoB10508	05.03.2006	011:39.673 E / 054:13.323 N	27.2	0.93
Eckernförde Bay					
#11	GeoB10505	28.02.2006	009:58.559 E / 054:29.309 N	27.1	1.00
#44, sec4,5	GeoB10506	02.03.2006	010:05.449 E / 054:30.215 N	20.8	2.03
#82	GeoB10507	04.03.2006	009:58.498 E / 054:29.287 N	27.8	0.95

**cores were opened and analysed in shipboard laboratory*

Two different signals of excess pore pressure could be classified for the dissipation period after penetration (Fig. 2). Type A shows a peak followed by an exponential decay (Fig. 2a). In contrast, Type B shows a delayed pore pressure response (Fig. 2b), by first increasing with time until a constant value is reached (e.g. C11), and then in some measurements of longer period it is exponentially decreasing with time (e.g. C305, Fig. 3). Also during penetration different pore pressure behaviour could be observed, at which Type A shows an induced increase in excess pore pressure while different trends are found in Type B (Fig. 2c).

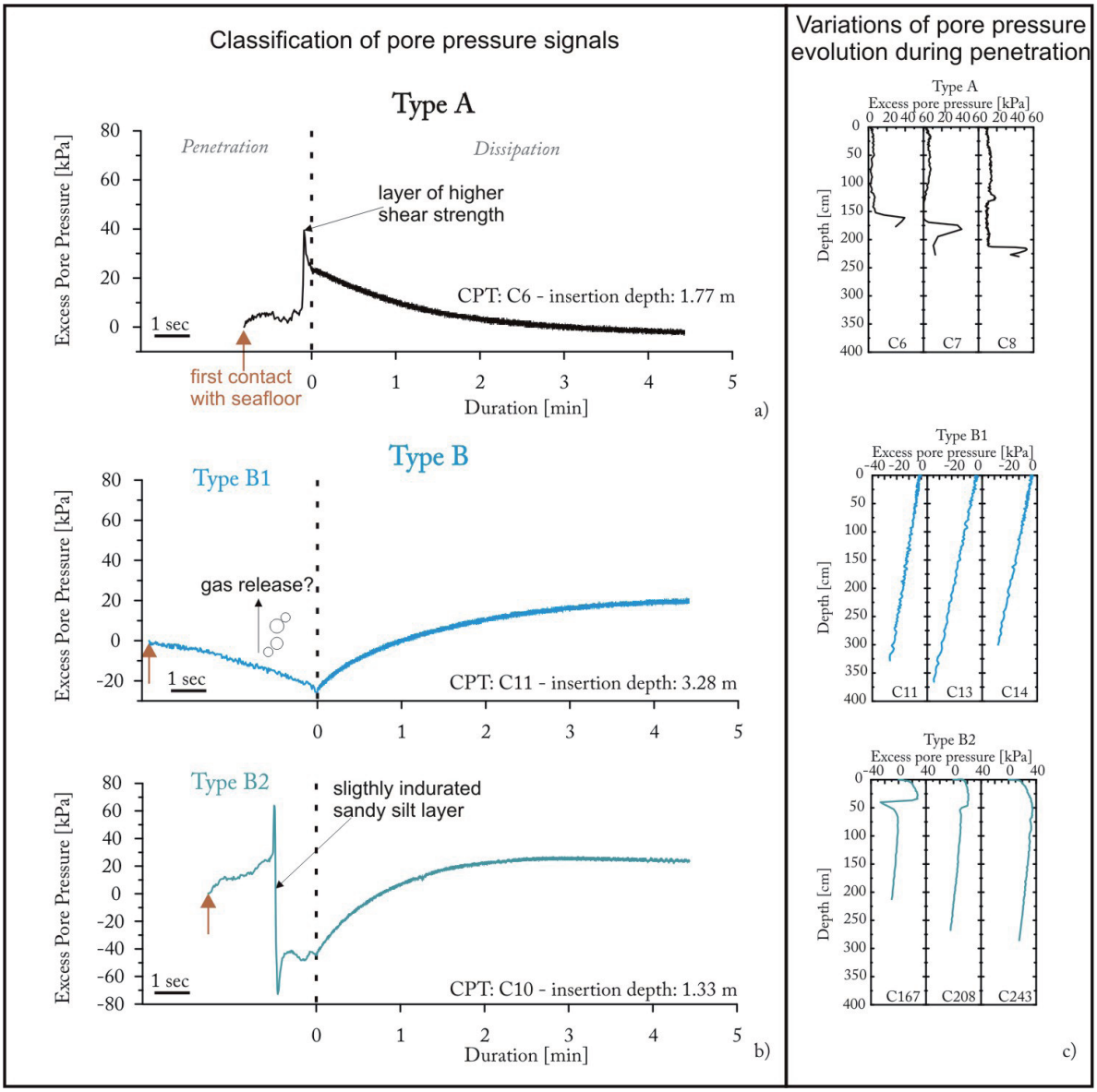

Fig. 2: Classification of excess pore pressure evolution during and after penetration of the CPT probe measured in the study areas, a) Type A, b) Type B1 and B2, and c) variations of the excess pore pressure response during penetration.

There, the excess pore pressure shows a strong pressure decrease to sub-hydrostatic values upon insertion of the CPT and is here termed Type B1 (Fig. 2b, c). Sometimes the excess pore pressure reveals a peak upon penetration similar to Type A, but furthermore during insertion of the lance, the excess pore pressure is dramatically decreasing even down to sub-hydrostatic pressures and is termed Type B2 (Fig. 2b, c).

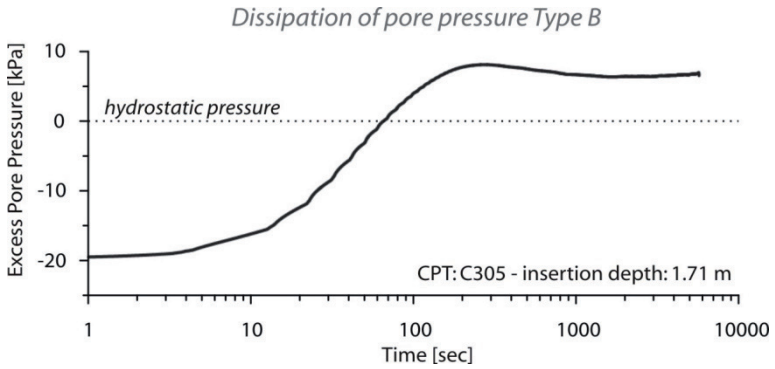

Fig. 3: Dissipation of pore pressure Type B (CPT C305) after penetration of the probe.

Penetration responses of Type A in the CPT measurements show very similar behaviour (Fig. 2c), but only occurred in one area near core K166 in Mecklenburg Bay. At a depth of around 160 cm a clay layer with maximum undrained shear strength of 19 kPa was found in core K166 sediments by T. Garlan and P. Guyomard (SHOM Institute, France) (Fig. 4c). This layer seems to coincide with the positive pore pressure excursion (CPT C6) of around 39 kPa and a peak in cone resistance of 1675 kPa at the same depth (Fig. 4c). In the deeper part of the core the shear strength is lower and the pore pressure can dissipate, so excess pore pressure is descending rapidly. This suggests that the strength of the sediments, and thereby drainage and permeability, control the insertion response (e.g. Bennett et al. 1989; Strout and Tjelta 2005).

A very different pore pressure evolution is seen in Type B, which is the only type observed in Eckernförde and Gelting Bay and dominant in Mecklenburg Bay. All measurements of Type B exhibit a delayed pore pressure response after penetration which is known to occur in overconsolidated or fissured sediments due to dilatant sediment behaviour and local redistribution around the cone tip (Lunne et al. 1997; Song and Voyiadjis 2005). Hence, the measured response Type B supports two

assumptions: (i) the mud somehow reveals dilatant behaviour during CPT insertion, and (ii) the pore pressure could be strongly affected by gas in the sediment.

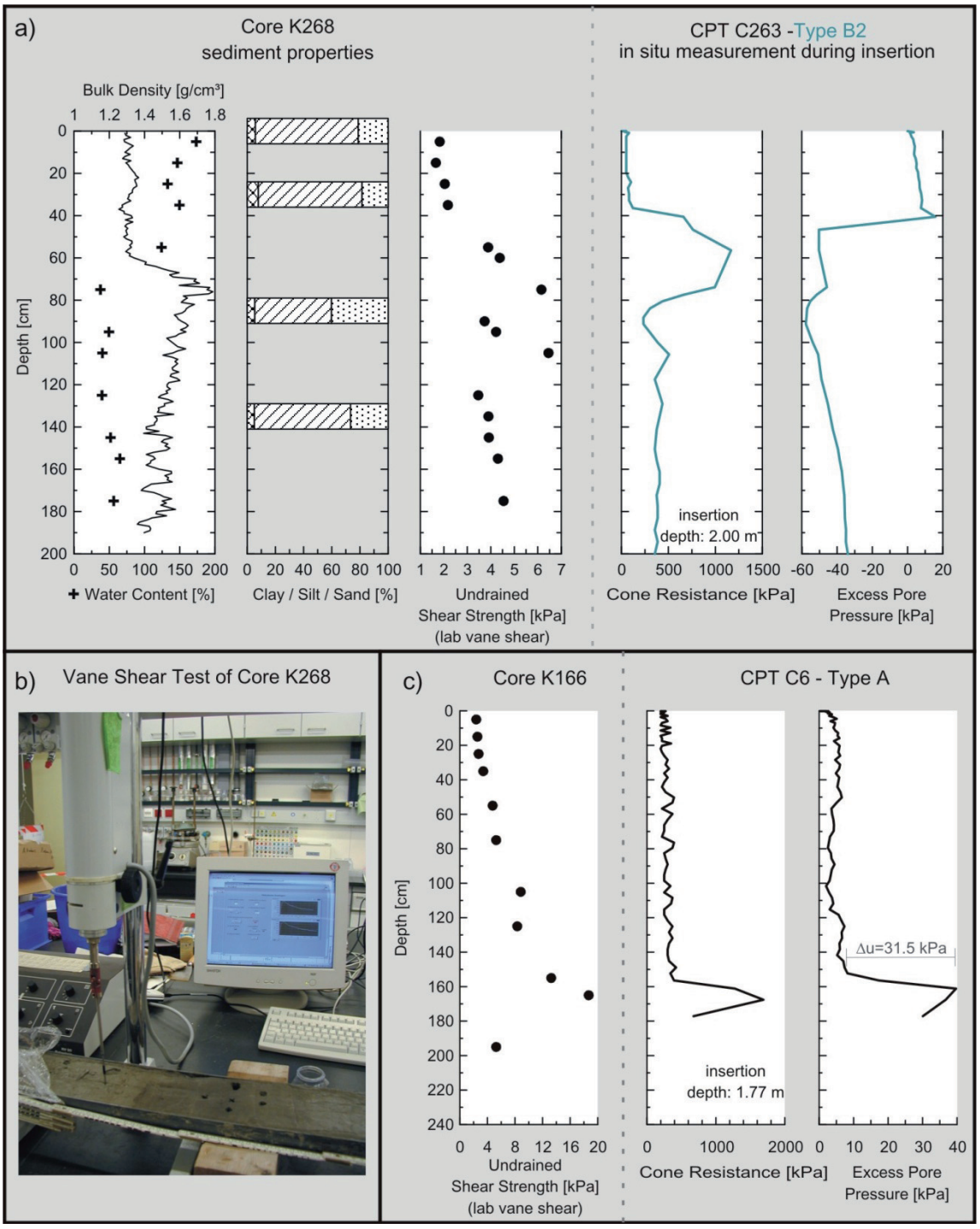

Fig. 4: Comparison of sediment properties from cores and adjacent CPT measurements, a) Bulk density, grain size distribution, undrained shear strength compared with C263 cone resistance and pore pressure evolution (Type B2) during penetration, b) Vane Shear Test of Core K268 in the laboratory of RCOM, c) Undrained shear strength of sediments of core K166 compared to cone resistance and pore pressure evolution (Type A) of C6 during penetration.

We are confident that Type B is associated with (possibly gas-charged) mud layers, because undrained shear strength and density of the mud are low and water content is high. In Eckernförde Bay we measured a bulk density of only 1.1 g/cm³ with maximum water content of 250%, and shear strength values were only up to 3 kPa for the uppermost meter below the seafloor. In Eckernförde and Gelting Bay Type B1 is dominating where the similar sub-hydrostatic response during penetration is obvious (Fig. 2b, c). CPT cone resistance of pore pressure Type B1 shows no pronounced increase upon insertion, only a slight continuous increase which emphasises the soft characteristic of the sediment. Especially in Eckernförde Bay, the sediments are very soft and highly compressible, so that the authors believe the pore pressure response Type B in Eckernförde and Gelting Bays is mainly related to free gas in the sediments. These bays are known for free gas in the sediment due to degradation of the organic material under anoxic conditions (Abegg and Anderson 1997; Wever et al. 1998, 2006). Free gas in the pore space lowers some of the properties of the sediment such as strength and pressure wave propagation (Wilkens and Fu 1994; Grozic et al. 2005). A sluggish response can be observed in Type B (e.g. C10 and C11 in Fig. 2b, C305 in Fig. 3), so we assume that local failure is responsible for negative pressures during insertion. Gas may cause higher excess pore pressure, and therefore, the formation of cracks can be induced and sediment is getting unstable. A further disruption during penetration can release free gas or cavities are generated and initial negative pressure appears.

Pore pressure Type B2 evolution somehow resembles a mixture of Type A and Type B1 behavior, and its characteristic can be variable (Fig. 2b, c and Fig. 4a). We believe that the response of Type B2 appears in slightly indurated layers of silt with considerable sand fraction which are interbedded in mud (Milkert 1994). When comparing core K268 and CPT C263 with a Type B2 pore pressure evolution, it can be seen that the cone resistance increases at 40 - 60 cm depth (Fig. 4a). This is related to an increase in the undrained shear strength and probably to an increase of the sand fraction. At the same depth, the pore pressure is dropping fast ($\Delta u \sim 66$ kPa; Fig. 4a). However, a peak in cone resistance is always associated with pressure drops in Type B2 curves (Fig. 4a). Negative pore pressure has been investigated in many other locations worldwide. Robertson (1990) and Song and Voyiadjis (2005) mentioned that silty sediments may reveal negative excess pore pressures during insertion. Baltzer et al. (1994) concluded

that the presence of sandy layers caused a peak in cone resistance associated with a drop in pressure when penetrating sediments from the Nova Scotian Slope on the eastern Canadian continental margin.

Recently, two different types of pore pressure evolution, similar to Types A and B here presented, were observed with the RCOM-probe in lacustrine clays in Lake Lucerne, Switzerland (Stegmann et al. 2007). Type A was found to be related to normally consolidated sediments, while Type B was measured in overconsolidated, glacially overprinted sediments. It can be concluded, that overpressure in sediments produce pore pressure Type B, also e.g. overpressure due to tectonic or glacial loading (Strasser et al. 2007).

Often soil classification charts are used for the identification and the classification of soil types from profiling standard CPT data. In Fig. 5 we have plotted the insertion data exemplary from CPT C6 for pore pressure Type A, C13 for pore pressure Type B1 and C167 for pore pressure Type B2 in the chart of Vermeulen and Rust (1995). To calculate the total overburden stress the density profile from core K370 was used for the insertion data of C6 and C167 which correlates with the cone resistance profile, while for C13 the density data of core K483 were taken. In this chart the profiling CPT data from 6 cm to 200 cm depth are plotted because of limited density data. Nevertheless, the data support the three pore pressure types and their interpretations. Data from C13 (Type B1) identify very soft clay and silt (Fig. 5) and confirm our results and interpretations of this pore pressure type. Furthermore, C167 data (Type B2) identify very soft clay and silt (Fig. 5). In the zone where the insertion data of C167 show peaks in cone resistance and pore pressure (Fig. 2c), the data points in the classification chart are still in the ‘very soft’ area, but closer to the field of ‘soft to firm’ consistency. This supports our former conclusion of slightly indurated silt layers with significant sand fraction in the mud (Fig. 5). For C6 data (Type A) the soil classification chart identifies a soft to firm silt and silty sand sediment layer where the C6 data show a high peak in cone resistance and excess pore pressure (Fig. 4c). Compared to the other insertion data (Fig. 5), this sediment shows the highest consistency and is in agreement with the high undrained shear strength measured in the sediments of core K166 in the depth of 160-180 cm (Fig. 4c).

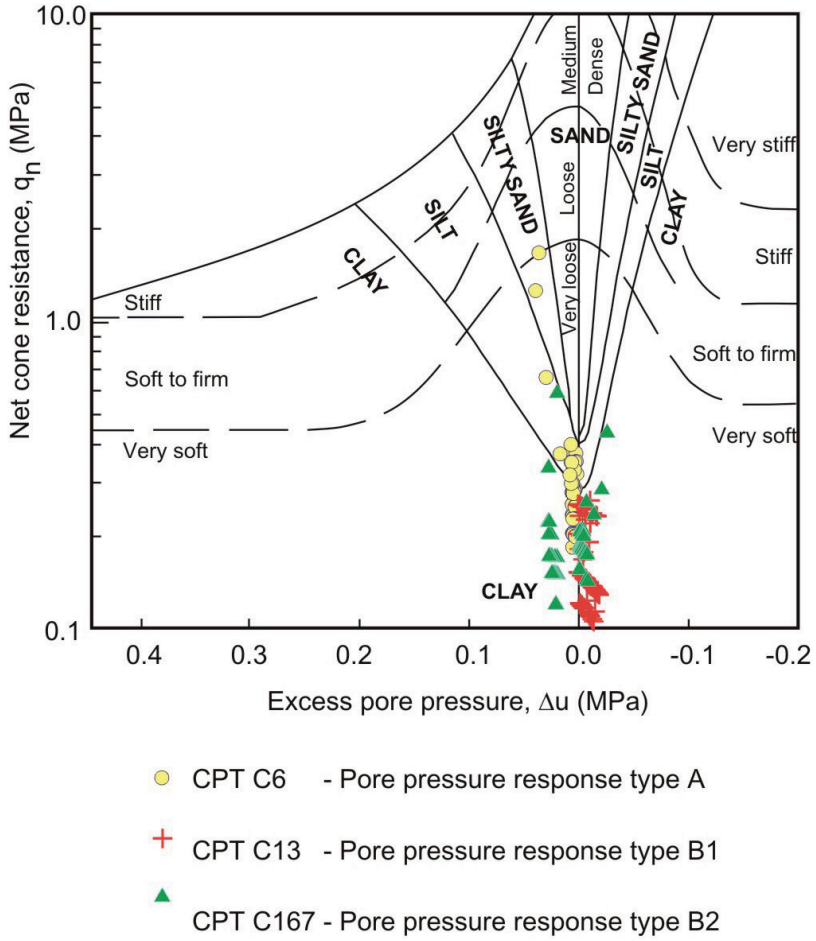

Fig. 5: Soil classification chart with profiling data from CPT C6, C13 and C167 (6 to 200 cm depth). Note net cone resistance is on log scale, modified by Vermeulen and Rust (1995).

Since higher penetration rate may cause the cone resistance and induced initial pore pressure to rise, the data points of our FF-CPT measurements with higher penetration velocity than the standard CPT might be overestimating the soil types. For example, the identified classification of silty sand in the C6 data could be only silt. Anyhow, we measured different behaviour of cone resistance and excess pore pressure during insertion and the profiling data of our FF-CPT still show that it is possible to identify different sediment types during individual profiling deployments.

Conclusions

- FF-CPT is a very efficient method to determine in situ geotechnical properties (sediment strength and pore pressure) of marine sediments
- Identification and classification of soil types from profiling FF-CPT data is possible using soil classification charts without coring efforts
- In situ CPT measurements during penetration show very good agreement with data from cores
- Overpressure in sediments leads to pore pressure Type B curves, no matter if tectonic or glacial loading or microbial gas are responsible

Acknowledgements

Special thanks go to the crew of the vessels KRONSORT and PLANET for their cooperation and help. We acknowledge the excellent support by Thomas Wever, the Forschungsanstalt der Bundeswehr für Wasserschall und Geophysik (FWG) in general, and Wehrtechnischer Dienst (WTD).

References

Abegg, F. and A. L. Anderson (1997). "The acoustic turbid layer in muddy sediments of Eckernfoerde Bay, Western Baltic: methane concentration, saturation and bubble characteristics." Marine Geology 137(1-2): 137-147.

Baltzer, A., P. Cochonat, et al. (1994). "In situ geotechnical characterization of sediments on the Nova Scotian Slope, eastern Canadian continental margin." Marine Geology 120: 291-308.

Bennett, R. H., H. Li, et al. (1989). "Application of Piezometer Probes to Determine Engineering Properties and Geological Processes in Marine Sediments." Applied Clay Sciences 4: 337-355.

Bennett, R.H., H. Li, P.J. Valent, J. Lipkin, M.I. Esrig (1985). "In-Situ Undrained Shear Strengths and Permeabilities Derived from Piezometer Measurements." In: Chaney, R.C., K.R. Demars (eds): Strength Testing of Marine Sediments: Laboratory and In-Situ Measurements, ASTM STP 883. American Society for Testing and Materials, Philadelphia: 83-100.

Dayal, U., J.H. Allen (1975). "The Effect of Penetration Rate on the Strength of Remolded Clay and Sand Samples." Can. Geotech. J. 12: 336-348.

Esrig, M.I., R.C. Kirby, R.G. Bea (1977). "Initial development of a general effective stress method for the prediction of axial capacity for driven piles in clay." Proc. 9th Offshore Technology Conference, 495-501.

Grozic, J. L. H., F. Nadim, et al. (2005). "On the undrained shear strength of gassy clays." Computers and Geotechnics 32(7): 483-490.

Lunne, T., P. K. Robertson, et al. (1997). "Cone Penetration Testing in Geotechnical Practice." London and New York, E & FN Spon.

Milkert, D. (1994). "Auswirkungen von Stürmen auf die Schlicksedimente der westlichen Ostsee (Influences of storms on muddy sediments in the western Baltic Sea)." Berichte/Reports Geol.-Paläontologisches Institut, Universität Kiel, 66.

Robertson, P. K. (1990). "Soil classification using the cone penetration test." Can. Geotech. J. **27**: 151-158.

Roy, M., M. Tremblay, F. Tavenas, P. La Rochelle (1982). "Development of pore pressures in quasi-static penetration tests in sensitive clay." Can. Geotech. J. 19: 124-138.

Song, C. R. and G. Z. Voyiadjis (2005). "Pore pressure response of saturated soils around a penetrating object." Computers and Geotechnics 32(1): 37-46.

Stegmann, S., M. Strasser, F. Anselmetti, A. Kopf (2007). "Geotechnical in situ characterization of subaquatic slopes: The role of pore pressure transients versus frictional strength in landslide initiation." Geophys. Res. Letters 34, L07607, doi:10.1029/2006GL029122.

Stegmann, S., H. Villinger, et al. (2006). "Design of a Modular, Marine Free-Fall Cone Penetrometer." Sea Technology 47(2): 27-33.

Stoll, R.D., Y.-F. Sun (2005). "Using Penetrometer to Measure Sea Bed Properties." Office of Naval Research, Science & Technology, Ocean Battlespace Sensing (32), Coastal Geosciences Annual Reports FY05: 1-5.

Strasser, M., S. Stegmann, F. Bussmann, F.S. Anselmetti, B. Rick, A. Kopf (2007). "Quantifying subaqueous slope stability during seismic shaking: Lake Lucerne as model for ocean margins." Marine Geology, doi:10.1016/j.margeo.2007.02.016.

Strout, J. M. and T. I. Tjelta (2005). "In situ pore pressures: What is their significance and how can they be reliably measured?" Marine and Petroleum Geology 22(1-2): 275-285.

Vermeulen, N. and E. Rust (1995). "CPTU profiling: A numerical method." Proceedings of the International Symposium on Cone Penetration Testing, CPT 95, Linköping, Sweden, October 4-5, Swedish Geotechnical Institute, SGI, Report 3:95, Vol. 2: 343-350.

Wever, T. F., R. Lühder, et al. (2006). "Potential environmental control of free shallow gas in the seafloor of Eckernförde Bay, Germany." Marine Geology 225: 1-4.

Wever, T., F. Abegg, et al. (1998). "Shallow gas in the muddy sediments of Eckernförde Bay, Germany." Continental Shelf Research 18: 1715-1739.

Wilkens, R.H., S.S. Fu (1994). "Acoustic Lance operations in Eckernförde Bay." In: Wever, T.F. (ed): Proc. Gassy Mud Workshop, 11-12 July 1994, FWG, Kiel, Germany. FWG Report 14: 34-38.

Research Cruise: 10.-17.03.2006 Baltic Sea (vessel Planet)

Physical Properties Of The Western Baltic Sea Mud

Seifert, A., Kopf, A.

Research Centre Ocean Margins (RCOM), University of Bremen, Leobener Strasse / MARUM, 28359 Bremen, Germany

April, 2007 (unpublished)

Sediment gravity cores were taken during two cruises with vessel KRONSORT and PLANET in winter 2006 with a gravity corer of 850 kg weight in Mecklenburg Bay and Eckernförde Bay of the Baltic Sea. Some cores were opened immediately in the shipboard laboratory and undrained shear strength was measured with a motorized miniature vane shear apparatus (Wykeham Farrance Engineering, Ltd.) with constant rotation rate of 10°/min, following the ASTM D 4648-87 procedure (ASTM 1987). At RCOM, the remaining cores were analysed: Mecklenburg Bay: GeoB10501 station #1-3, GeoB10502 station #268, GeoB10503 station #370, GeoB10504 station #483, GeoB10508 station #102; Eckernförde Bay: GeoB10505 station #11, GeoB10506 station #44, section 4 and 5, GeoB10507 station #82.

Methods at RCOM laboratories

Core Logging

At RCOM, all gravity core sections were shore-based measured prior to splitting and processing using a non-destructive GEOTEK Multi-Sensor Core Logger (MSCL http://www.geotek.co.uk; Gunn & Best, 1998). Gamma density, p-wave velocity, magnetic susceptibility, and porosity were routinely determined at 1-cm intervals after equilibration to laboratory temperature (Fig. 1). Only core GeoB10501 (core 1-3) was already opened before measuring the half-core section on the Multi-Sensor Core Logger at 2-cm intervals. The accuracy of the measured properties degrades considerably at the top and bottom of each core section in the area of the cap or in sections with gas voids or where the core does not fill the liner completely or is disturbed. Especially, the p-wave measurement is very sensitive. In case of bad acoustic coupling between the

sediment and the liner, the velocity values are generally not accurate and were removed in the data tables.

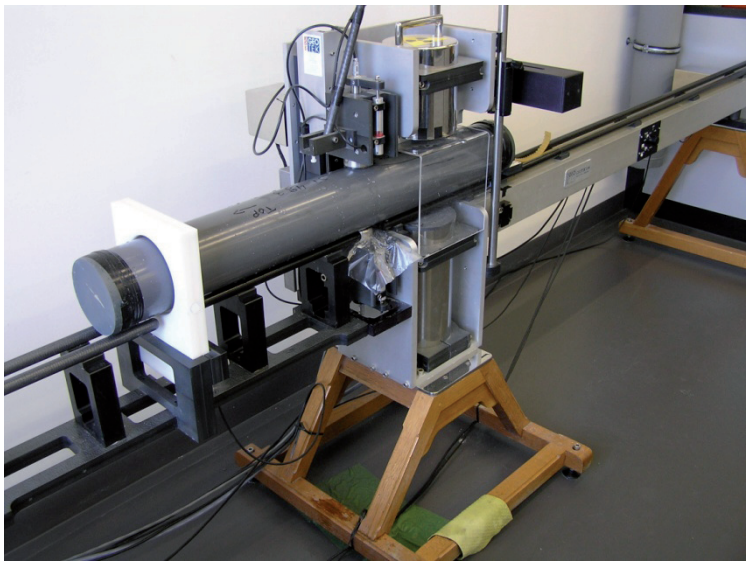

Fig. 1: GEOTEK Multi-Sensor Core Logger

Water content, grain size distribution, and organic content

The cores were split with a wire lengthwise into working and archive half. Samples were selected in conjunction with the sedimentology from the working half to determine water content, grain size distribution, and organic content. The archive half was described visually (files: SediMBES06_GeoB105xx.doc).

The water content was aquired by freeze drying. Only samples from core GeoB10501 and GeoB10508 were dried in the oven with 60°C to determine the water content. Grain size distribution was conducted using a Beckman Coulter Laser Particle Sizer LS200. Before measuring the grain size, sodium pyrophosphate was added to the samples to prevent formation of aggregates during analysis. Additional, organic matter was removed with 35 % H_2O_2 on samples from core GeoB10507 (station 82) prior to analysing to compare the influence of organic matter to the results of the laser grain size analyses. Organic content was determined on selected samples by loss on ignition (LOI) at about 550 °C following the DIN 18128 procedure (DIN 18128, 1990).

Undrained shear strength

Undrained shear strength (s_u) was measured using a four-blade vane viscometer (RotoVisco RV20 device by Haake, Germany, Fig. 2) at a rotational rate of 30°/min until the peak shear strength had been well-exceeded. The instrument measures the torque (T) at the vane and the degree of rotation and records the data on a computer. Undrained shear strength s_u can be determined by:

$$s_u = T/K$$

where K is the vane constant which is a function of the vane size and geometry (Blum, 1997).

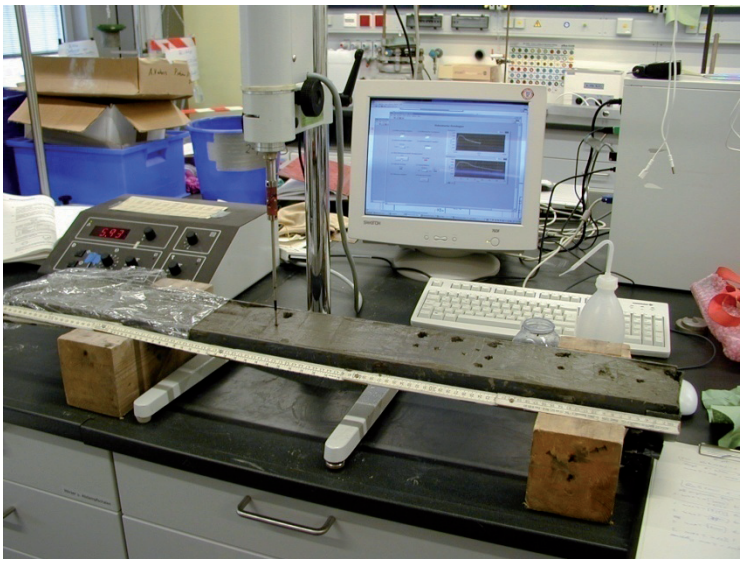

Fig. 2: Vane Shear Test

All data of the measured physical properties are summarised in tables: Files GeoB105xx.xls.

Results and Discussions

Mecklenburg Bay

Two sedimentary units for the first 2 m below seafloor could be defined in core GeoB10502 by analysing the physical properties of the sediments. The upper 65 cm are a greyish olive mud where the main component is silt with ~73 %, underlain by coarser-grained material (19-21 % sand). Sediment bulk density is around 1.3 g/cm³ (see Fig. 4a

in the chapter “Free-Fall Cone Penetrometer Tests”, this issue). However, the measured sediment properties in Mecklenburg Bay from core samples agree very well with each other, and also with previous studies in this area. The density measured by Harff et al. (2003) in the muddy area of Mecklenburg Bay corresponds exactly to our determined bulk density in core GeoB10502. Similar sediment was identified in cores GeoB10503 and GeoB10504, whereas the thickness of this mud layer is increasing from 65 cm in core GeoB10502 to 155 cm in GeoB10503 and to 180 cm in GeoB10504. Organic content (LOI) of the surficial sediments are increasing from 5.8 wt% in GeoB10502 to 8.1 wt% in GeoB10503 and to 10.5 wt% in GeoB10504 analogue to the increasing thickness of the mud layer. The second sedimentary unit from 65-190 cm depth of core GeoB10502 consists of light olive grey, fine sandy silt. Notable is dark plant debris throughout the sediment, but the organic content (LOI) with 3.4 wt% in 85 cm depth of GeoB10502 is less than in the superficial sediments. Bulk density jumps up to 1.8 g/cm³ between 65 and 80 cm depth and from 80 cm to 190 cm, it tends to lie at 1.4 g/cm³ until the terminal depth of the core. The same layer could be identified in GeoB10503, but bulk density here reaches up to 1.6 g/cm³. Grain size analysis of the sediment in 85 cm below seafloor indicates almost equal portions of silt (54.4 %) to sand (40.2 %) and a smaller fraction of clay of 5.4 % (see Fig. 4a in chapter “Free-Fall Cone Penetrometer Tests”, this issue). In 135 cm depth, the fraction of clay is almost like in 85 cm depth (5.1 %), but the sand fraction decreased to 26.7 % while the silt fraction is dominating with 68.2 %. Related to the density, the water content is high in the upper 65 cm (about 124-175 %), and lower from 65 to 190 cm (about 37-65%) in core GeoB10502. Undrained shear strength is found 1.7-4.4 kPa in the upper 50 cm of the mud layer, and increases up to 6.5 kPa in the lower part. A similar trend was observed in the upper 2 m of cores GeoB10503 and GeoB10504, with maximum shear strength of 5.6 kPa in GeoB10504 for this layer. These findings are in agreement with Lemke (1998), who investigated the sedimentation in the western Baltic Sea by coring and seismic exploration and found the same lithological units in the Mecklenburg Bay.

Eckernförde Bay

In Eckernförde Bay we detected olive grey mud in the uppermost meter. But compared to the mud in Mecklenburg Bay, it is very soft with a fluffy texture and a significant smell of H_2S. The water content of 186-250 % is higher than that of the mud in Mecklenburg Bay. Also the organic content (LOI) is higher and varying in the uppermost meter from 10.6 to 15.5 wt%. Bulk density is about 1.1 g/cm³. Grain size distribution shows only little vertical variation with dominantly silt (about 82 %), and minor sand (about 11 %) and clay (7 %). After removing of the organic content prior to grain size analysis silt is still the main fraction of about 78 %. The sand fraction is reduced to 1 % and clay is increased to 21 %. Undrained shear strength in the upper 50 cm in Eckernförde Bay is 1.6-2 kPa, and increases up to 3 kPa in 50 – 100 cm depth. Silva and Brandes (1998) classified the sediment mainly as silty clay with clay being 50% and silt being 47%. Bentley et al. (1996) investigated the development of sedimentary strata in Eckernförde Bay and observed layers of pelletal fabrics (pellets >10 %). Most fecal pellets were highly resistant to disaggregation and had to be removed prior to grain size analysis. To investigate the influence of organic matter on grain size analysis samples of core K82 were additionally analysed with the organic removed prior to measurement. However, our measurements showed that the silt fraction is still the main component (78 %) while the sand fraction decreased from 11 % to 1 % and the clay fraction increased from 7 % to 21 %. This suggests that the organic matter in the mud of Eckernförde Bay (LOI: 10.6 to 15.5 wt%) is sand sized and supports the formation of aggregates in form of fecal pellets found by Bentley et al. (1996).

References

ASTM D 4648-87 (1987), "Standard Test Method for Laboratory Miniature Vane Shear Test for Saturated Fine-Grained Clayey Soil.“ Annual Book of ASTM Standards, 04.08: 868-873.

Bentley, S. J., C. A. Nittrouer, et al. (1996). "Development of sedimentary strata in Eckernförde Bay, south western Baltic Sea." Geo-Marine Letters 16(3): 148-154.

Blum, P. (1997): "Physical properties handbook: a guide to the shipboard measurement of physical properties of deep-sea cores." ODP Tech. Note, 26 [Online]. Available from World Wide Web: <http://www.odp.tamu.edu/ publications/tnotes/tn26/INDEX.HTM>. 9. Strength: 1-10.

DIN 18128 (November 1990): Baugrund, Versuche und Versuchsgeräte - Bestimmung des Glühverlustes.

Gunn, D.E., Best, A.I. (1998): "A new automated nondestructive system for high resolution multi-sensor core logging of open sediment cores." Geo-Marine Letters 18(1):70-77.

Harff, J., R. Bahlo, et al. (2003). "Projekt DYNAS - Dynamik natürlicher und anthropogener Sedimentation; Vorhaben: Sedimentationsprozesse in der Mecklenburger Bucht - Abschlußbericht (Meilenstein 6)"; Laufzeit/Berichtszeitraum: 01.06.2000-31.05.2003. Warnemünde, Institut für Ostseeforschung Warnemünde; Fachbereich Biologie der Universtiät Rostock, Germany: p. 139.

Lemke, W. (1998). "Sedimentation und paläogeographische Entwicklung im westlichen Ostseeraum (Mecklenburger Bucht bis Arkonabecken) vom Ende der Weichelvereisung bis zur Litorinatransgression." Meereswissenschaftliche Berichte. Institut für Ostseeforschung Warnemünde, Warnemünde, Germany. 31: p. 156.

Silva, A. J. and H. G. Brandes (1998). "Geotechnical properties and behavior of high-porosity, organic-rich sediments in Eckernförde Bay, Germany." Continental Shelf Research 18: 1917-1938.

APPENDIX A4 – DATA OF BALTIC SEA SEDIMENT SAMPLES

GeoB 10501, core 1-3

Cruise: **NEST06: 23.01.-27.01.06**
Ship: MZB KRONSORT
Cruise leader: FWG, Germany, Dr. Thomas Wever
Locality: Baltic Sea, Mecklenburg Bay
Lab analyses: Annedore Seifert (RCOM)
Core: **GeoB10501, core 1-3**
(opened 01.02.2006)

legend: core logging (Geotek Multi Sensor Core Logger (MSCL)):
parameter: p-wave velocity, gamma density, magnetic susceptibility, fractional porosity
type of logging: half core
notes: fractional porosity calculated with - mineral grain density 2.65 g/cm³
and fluid phase density 1.026 g/cm³
water content: drying in oven with 60°C
vane shear strength: rotational rate 30°/min

		core logging				lab	
Depth	section number	p-wave velocity*	gamma density*	magnetic susceptibility	fractional porosity*	water content	undrained shear strength
[cm]		[m/s]	[g/cm³]	[10^{-5} SI]		[%]	[kPa]
0	1					192,78	
2	1			2			
4	1		1,4991	1	0,7256		
5	1					196,57	0,8
6	1		1,4746	1	0,7398		
8	1		1,6497	2	0,6382		
10	1		1,6365	3	0,6459	182,71	1,41
12	1		1,599	3	0,6676		
14	1		1,6298	3	0,6498		
15	1					174,21	
16	1		1,6641	3	0,6299		
18	1		1,5968	2	0,6689		
20	1		1,5397	3	0,702	174,83	1,09
22	1		1,5093	2	0,7197		
24	1		1,5217	1	0,7125		
26	1		1,5733	2	0,6825		
28	1		1,6315	2	0,6488		
29	1						1,63
30	1		1,5978	1	0,6683	195,44	
32	1		1,4833	2	0,7347		
34	1		1,4902	2	0,7307		
36	1		1,5151	2	0,7163		
38	1		1,536	1	0,7042		
40	1		1,5232	0	0,7116	207,33	2,31
42	1		1,5294	1	0,708		
44	1		1,5594	2	0,6906		
46	1		1,5624	1	0,6889		
48	1		1,5347	2	0,7049		
50	1		1,5489	2	0,6967	182,01	2,16
52	1		1,5453	2	0,6988		
54	1		1,5529	2	0,6944		
56	1		1,423	2	0,7697		
58	1		1,6188	2	0,6561		
60	1		1,5918	2	0,6718	131,62	2,92
62	1		1,6073	3	0,6628		
64	1		1,596	2	0,6693		
66	1		1,5709	2	0,6839		
68	1		1,5391	3	0,7024		
70	1		1,5575	3	0,6917	133,65	
72	1		1,6125	2	0,6598		3,76
74	1		1,5757	2	0,6812		
76	1		1,5373	1	0,7034		
78	1		1,575	1	0,6815		
80	1		1,6255	3	0,6523	147,24	
82	1		1,5739	2	0,6822		
83	1						4,23
84	1		1,4845	2	0,7341		
86	1		1,4662	2	0,7447		
88	1		1,3957	2	0,7855	164,27	

* empty fields: results are not reliable (probably, liner not completely filled with sediment; cap at the end of the liner disturbed measurement; p-wave transducer had not good contact)

Description of core : GeoB10502 – **Station 268**

Date: 12/ 03 / 2006 - 09:53

Latitude	54° 14.423′ N
Longitude	011° 46.071′ E
Water depth	25.9 m
Total core length	191 cm

	Description	Vane Shear Test
↓ core analysed perpendicular to the core axis	0-20 cm: olive gray silty mud, slightly finesandy 20-66 cm: grayish olive silty mud, coarsening down to a finesandy silt 66-101 cm: light olive gray finesandy silt with black/brown plant material 101-191 cm: light olive gray silt, slightly finesandy with black/brown plant material	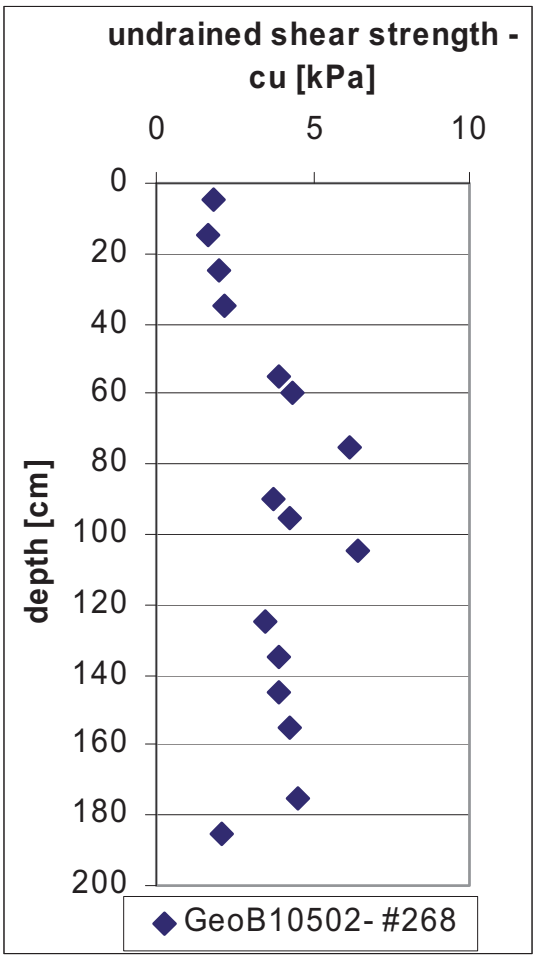

Cruise: **NEST06: 28.02.-17.03.06**
Ship: FS PLANET
Cruise leader: FWG, Germany, Dr. Thomas Wever
Locality: Baltic Sea, Mecklenburg Bay
Lab analyses: Annedore Seifert (RCOM)
Core: **GeoB10502, station #268**
(opened 17.05.2006)

legend: core logging (Geotek Multi Sensor Core Logger (MSCL)):
parameter: p-wave velocity, gamma density, magnetic susceptibility, fractional porosity
type of logging: whole core prior to splitting
notes: fractional porosity calculated with - mineral grain density 2.65 g/cm³ and fluid phase density 1.026 g/cm³
water content: freeze drying
vane shear strength: rotational rate 30°/min
grain size distribution: Beckman Coulter laser particle sizer LS200
organic content: loss on ignition (LOI) at 550°C

		core logging				lab								
Depth	section number	p-wave velocity*	gamma density*	magnetic susceptibility *	fractional porosity*	water content	undrained shear strength	grain size distribution			grain size distribution	*organic material was removed before measuring*		organic content (LOI)
[cm]		[m/s]	[g/cm³]	[10^{-5} SI]		[%]	[kPa]	Clay [%]	Silt [%]	Sand [%]	Clay [%]	Silt [%]	Sand [%]	[wt%]
0	1							5,81	73,03	21,15	13,49	63,07	23,39	5,78
1	1			2										
2	1		1,2887	2	0,8476									
3	1		1,2946	3	0,8442									
4	1		1,3208	3	0,829									
5	1		1,2842	3	0,8503	173,42	1,82							
6	1		1,2862	3	0,849									
7	1		1,3124	3	0,8339									
8	1		1,3357	3	0,8204									
9	1		1,3174	3	0,831									
10	1		1,305	3	0,8382									
11	1		1,289	4	0,8474									
12	1		1,3183	4	0,8305									
13	1		1,2889	3	0,8475									
14	1		1,2761	3	0,8549									
15	1		1,3226	3	0,828	146,55	1,66							
16	1		1,2942	4	0,8445									
17	1		1,308	3	0,8365									
18	1		1,3149	4	0,8325									
19	1		1,3246	3	0,8268									
20	1		1,3344	4	0,8211									
21	1		1,3455	5	0,8147									
22	1		1,3503	4	0,8119									
23	1		1,3665	4	0,8025									
24	1		1,3452	4	0,8149									
25	1		1,3479	4	0,8133	132,82	2,04							
26	1		1,3533	5	0,8102									
27	1		1,3562	5	0,8085									
28	1		1,3374	5	0,8194									
29	1		1,3313	6	0,8229									
30	1		1,3315	7	0,8228			7,87	73,65	18,47				7,83
31	1		1,3122	8	0,834									
32	1		1,3113	9	0,8345									
33	1		1,3037	10	0,8389									
34	1		1,3217	8	0,8285									
35	1		1,2948	8	0,8441	149,66	2,17							
36	1		1,2728	7	0,8569									
37	1		1,2754	7	0,8553									
38	1		1,2541	6	0,8677									
39	1		1,284	6	0,8503									
40	1		1,2848	5	0,8499									
41	1		1,3243	5	0,8269									
42	1		1,331	5	0,8231									
43	1		1,291	4	0,8463									
44	1		1,3335	5	0,8217									
45	1		1,3004	5	0,8408									
46	1		1,2891	5	0,8474									
47	1		1,3051	5	0,8381									
48	1		1,2943	5	0,8444									
49	1		1,2981	4	0,8422									
50	1		1,3029	5	0,8394									
51	1		1,2825	5	0,8512									
52	1		1,2976	4	0,8425									
53	1		1,3284	4	0,8246									
54	1		1,33	4	0,8237									
55	1		1,3158	5	0,8319	124,14	3,89							
56	1		1,3245	5	0,8268									
57	1		1,3073	4	0,8368									
58	1		1,2939	4	0,8446									
59	1		1,3183	4	0,8305									
60	1		1,3148	3	0,8325		4,38							
61	1		1,3405	4	0,8176									
62	1		1,3753	4	0,7974									
63	1		1,4093	3	0,7776									
64	1		1,4025	4	0,7816									
65	1		1,4636	3	0,7462									
66	1		1,4968	3	0,7269									
67	1		1,5389	3	0,7025									
68	1		1,5961	2	0,6693									
69	1		1,5429	2	0,7002									
70	1		1,5617	2	0,6893									
71	1		1,693	1	0,6131									
72	1		1,681	1	0,6201									
73	1		1,7118	1	0,6022									
74	1		1,5978	1	0,6683									
75	1		1,7707	1	0,5681	37,44	6,15							
76	1		1,7551	1	0,5771									
77	1		1,7878	0	0,5581									
78	1		1,7642	2	0,5718									
79	1		1,6208	2	0,655									
80	1		1,6435	4	0,6418									
81	1		1,6232	5	0,6536									
82	1		1,609	7	0,6618									
83	1		1,6829	7	0,619									
84	1		1,6556	8	0,6348									
85	1		1,6377	9	0,6452			5,39	54,39	40,26				3,44
86	1		1,6315	9	0,6488									
87	1		1,6146	9	0,6586									
88	1		1,5699	9	0,6845									
89	1		1,5844	9	0,6761									
90	1		1,5916	9	0,6719		3,74							

Table continued - core GeoB 10502, station 268

Depth	section number	core logging p-wave velocity*	gamma density*	magnetic susceptibility *	fractional porosity*	lab water content	undrained shear strength	grain size distribution			grain size distribution	*organic material was removed before measuring*		organic content (LOI)
[cm]		[m/s]	[g/cm³]	[10^{-5} SI]		[%]	[kPa]	Clay [%]	Silt [%]	Sand [%]	Clay [%]	Silt [%]	Sand [%]	[wt%]
91	1		1,6106	9	0,6609									
92	1		1,6333	9	0,6477									
93	1		1,6479	9	0,6392									
94	1		1,6345	9	0,647									
95	1		1,6051	8	0,6641	49,51	4,22							
96	1		1,6352	8	0,6467									
97	1		1,5954	8	0,6697									
98	1		1,5775	7	0,6801									
99	1		1,5266	7	0,7096									
100	1		1,4758	7	0,7391									
101	1		1,4417		0,7589									
102	2			9										
103	2	2788,466	1,5888	11	0,6735									
104	2	2807,002	1,6337	14	0,6475									
105	2		1,5889	17	0,6735	40,28	6,46							
106	2		1,5599	18	0,6903									
107	2	2971,743	1,5052	17	0,722									
108	2	2663,82	1,5576	16	0,6917									
109	2	2286,235	1,5887	15	0,6736									
110	2	2543,687	1,5725	16	0,683									
111	2	2504,205	1,5877	15	0,6742									
112	2	2398,51	1,5734	17	0,6825									
113	2	2289,752	1,5568	17	0,6921									
114	2	2289,56	1,5606	18	0,6899									
115	2	2305,265	1,5945	19	0,6702									
116	2	2360,087	1,5518	19	0,695									
117	2	2493,719	1,5466	18	0,698									
118	2	2486,329	1,5837	18	0,6765									
119	2	2312,366	1,6011	17	0,6664									
120	2	2336,931	1,5388	16	0,7025									
121	2	2395,092	1,5278	15	0,7089									
122	2	2434,471	1,5291	16	0,7082									
123	2	2427,232	1,5461	16	0,6983									
124	2	2383,707	1,5225	16	0,712									
125	2	2376,771	1,5316	17	0,7067	39,63	3,47							
126	2	2463,193	1,4936	17	0,7288									
127	2	2523,194	1,4792	17	0,7371									
128	2	2408,411	1,5342	18	0,7052									
129	2	2125,045	1,5622	18	0,689									
130	2		1,5125	19	0,7178									
131	2		1,5144	20	0,7167									
132	2		1,4781	21	0,7378									
133	2		1,4823	24	0,7353									
134	2		1,4735	27	0,7405									
135	2		1,566	30	0,6868		3,90	5,09	68,18	26,7				
136	2		1,457	32	0,75									
137	2		1,4712	34	0,7418									
138	2		1,4704	36	0,7422									
139	2		1,4575	38	0,7497									
140	2		1,4569	40	0,7501									
141	2		1,4093	38	0,7776									
142	2		1,4114	38	0,7765									
143	2		1,4823	35	0,7353									
144	2		1,3953	33	0,7858									
145	2		1,5181	31	0,7146	51,82	3,92							
146	2		1,5594	31	0,6906									
147	2		1,5114	29	0,7184									
148	2		1,4963	30	0,7272									
149	2		1,5317	29	0,7067									
150	2		1,5165	27	0,7155									
151	2		1,5438	28	0,6997									
152	2		1,5231	29	0,7116									
153	2		1,4504	29	0,7538									
154	2		1,4105	28	0,777									
155	2		1,4498	27	0,7542	65,00	4,30							
156	2		1,4607	27	0,7479									
157	2		1,4364	27	0,762									
158	2		1,4333	26	0,7637									
159	2		1,4094	25	0,7776									
160	2		1,4457	24	0,7566									
161	2		1,4837	24	0,7345									
162	2		1,5519	24	0,695									
163	2		1,5535	23	0,6941									
164	2		1,5159	22	0,7158									
165	2		1,5362	20	0,704									
166	2		1,5292	20	0,7081									
167	2		1,5571	19	0,6919									
168	2		1,4389	19	0,7605									
169	2		1,4177	20	0,7728									
170	2		1,3945	20	0,7863									
171	2		1,3814	20	0,7938									
172	2		1,452		0,7529									
173	2		1,4856	20	0,7334									
174	2		1,5099	19	0,7193									
175	2		1,5536	19	0,694	56,27	4,54							
176	2		1,4998	19	0,7252									
177	2		1,524	18	0,7112									
178	2		1,493	18	0,7291									
179	2		1,5343	17	0,7052									
180	2		1,5758	17	0,6811									

Table continued - core GeoB 10502, station 268

Depth	section number	core logging				lab					grain size distribution	*organic material was removed before measuring*		organic content (LOI)
		p-wave velocity*	gamma density*	magnetic susceptibility *	fractional porosity*	water content	undrained shear strength	grain size distribution						
[cm]		[m/s]	[g/cm³]	[10^{-5} SI]		[%]	[kPa]	Clay [%]	Silt [%]	Sand [%]	Clay [%]	Silt [%]	Sand [%]	[wt%]
181	2		1,47	18	0,7425									
182	2		1,4646	18	0,7456									
183	2		1,5251	18	0,7105									
184	2		1,4435	18	0,7578									
185	2		1,4134	17	0,7753		2,09							
186	2		1,3716	17	0,7996									
187	2		1,359	17	0,8069									
188	2		1,4276	16	0,767									
189	2		1,4342	16	0,7632									
190	2		1,4313	16	0,7649									
191	2		1,3973	16	0,7847									

* empty fields: results are not reliable (probably, liner not completely filled with sediment; cap at the end of the liner disturbed measurement; p-wave transducer had not good contact)

Description of core : GeoB10503 – **Station 370**

Date: 13/ 03 / 2006 - 13:54

Latitude	54° 15.234′ N
Longitude	011° 44.063′ E
Water depth	25.5 m
Total core length	206 cm

	Description	Vane Shear Test
↓ core analysed perpendicular to the core axis	0-15 cm: greenish black mud with shell fragments 15-89 cm: olive gray silty mud 89-106 cm: grayish olive silty mud, slightly clayey and finesandy 106-156 cm: grayish olive silty mud, slightly finesandy 156-188 cm: light olive gray silt, slightly finesandy with black/brown plant material 188-206 cm: greenish gray silt, slightly clayey and finesandy	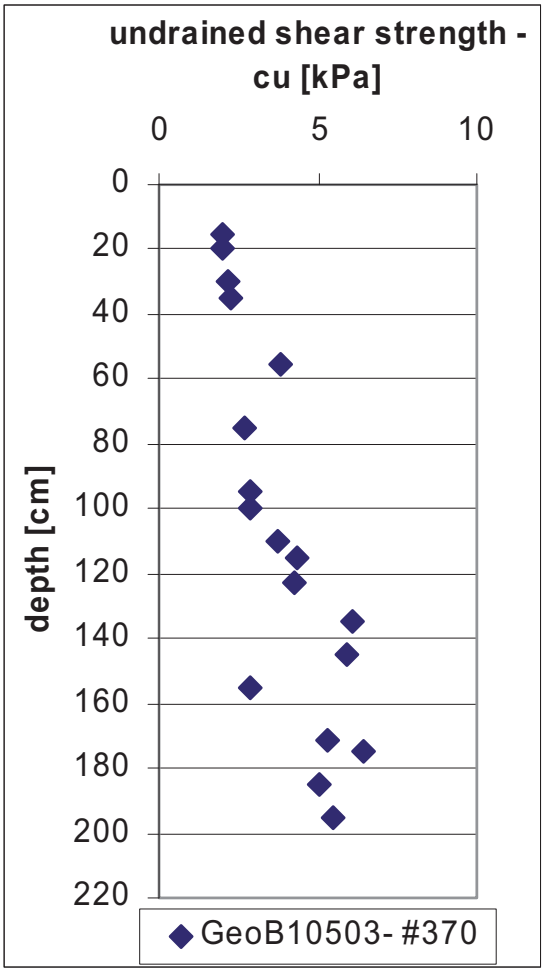

Cruise: **NEST06: 28.02.-17.03.06**
Ship: FS PLANET
Cruise leader: FWG, Germany, Dr. Thomas Wever
Locality: Baltic Sea, Mecklenburg Bay
Lab analyses: Annedore Seifert (RCOM)
Core: **GeoB10503, station #370;**
core starting at 5 cm below seafloor!
(opened 17.05.2006)

legend: core logging (Geotek Multi Sensor Core Logger (MSCL)):
parameter: p-wave velocity, gamma density, magnetic susceptibility, fractional porosity
type of logging: whole core prior to splitting
notes: fractional porosity calculated with - mineral grain density 2.65 g/cm³ and fluid phase density 1.026 g/cm³
water content: freeze drying
vane shear strength: rotational rate 30°/min
grain size distribution: Beckman Coulter laser particle sizer LS200
organic content: loss on ignition (LOI) at 550°C

		core logging				lab					
Depth	section number	p-wave velocity*	gamma density*	magnetic susceptibility *	fractional porosity*	water content	undrained shear strength	grain size distribution			organic content (LOI)
[cm]		[m/s]	[g/cm³]	[10^{-5} SI]		[%]	[kPa]	Clay [%]	Silt [%]	Sand [%]	[wt%]
5	1					135,11		6,14	82,95	10,93	8,05
6	1			2							
7	1	2767,972	1,1546	2	0,9254						
8	1		1,1926	4	0,9033						
9	1	2231,22	1,1866	3	0,9068						
10	1	2832,128	1,1608	4	0,9218						
11	1	2636,575	1,107	3	0,953						
12	1	2673,152	1,1039	3	0,9548						
13	1	2122,616	1,1675	4	0,9179						
14	1	2320,406	1,1255	3	0,9423						
15	1	2343,24	1,1536	3	0,926	150,95	1,98				
16	1	2302,649	1,2108	3	0,8928						
17	1	2410,039	1,2021	2	0,8978						
18	1	2457,491	1,1989	4	0,8997						
19	1	2386,295	1,1967	3	0,901						
20	1	2458,316	1,189	3	0,9055		1,98				
21	1	2463,813	1,1951	3	0,9019						
22	1	2289,09	1,1689	3	0,9171						
23	1	2489,971	1,2002	3	0,899						
24	1	2554,008	1,1896	3	0,9051						
25	1	2329,554	1,157	3	0,924	128,49					
26	1	2320,483	1,1838	2	0,9085						
27	1	2311,482	1,158	3	0,9234						
28	1	2490,18	1,1693	3	0,9169						
29	1	2380,543	1,1678	3	0,9177						
30	1	2373,431	1,1617	3	0,9213		2,14				
31	1	2548,76	1,1708	3	0,916						
32	1	2412,467	1,1583	3	0,9232						
33	1	2425,346	1,1535	3	0,9261						
34	1	2389,301	1,1614	3	0,9215						
35	1	2667,412	1,1867	3	0,9068	123,79	2,29				
36	1	2370,702	1,171	3	0,9159						
37	1	2492,269	1,176	3	0,913						
38	1	2492,896	1,1789	3	0,9113						
39	1	2574,202	1,1554	3	0,9249						
40	1	2566,33	1,1629	3	0,9206						
41	1	2544,873	1,1637	3	0,9201						
42	1	2484,187	1,1698	2	0,9166						
43	1	2481,189	1,1987	3	0,8998						
44	1	2512,734	1,1668	3	0,9183						
45	1	2456,285	1,1342	2	0,9372						
46	1	2484,187	1,1328	3	0,938						
47	1	2497,804	1,134	3	0,9373						
48	1	2373,484	1,1431	3	0,9321						
49	1	2329,497	1,1163	2	0,9476						
50	1	2531,171	1,1147	3	0,9485						
51	1	2546,948	1,1748	3	0,9137						
52	1	2365,602	1,1533	3	0,9262						
53	1	2443,646	1,1513	3	0,9273						
54	1	2333,66	1,1487	3	0,9288						
55	1	2286,784	1,1659	3	0,9188	135,86	3,81				
56	1	2371,724	1,2022	3	0,8978						
57	1	2319,822	1,2032	3	0,8972						
58	1	2248,073	1,2321	3	0,8805						
59	1	2232,419	1,2137	3	0,8911						
60	1	2307,945	1,1918	3	0,9038			9,58	78,22	12,19	7,44
61	1	2462,045	1,1856	3	0,9074						
62	1	2316,686	1,1629	3	0,9206						
63	1	2230,526	1,1664	2	0,9186						
64	1	2136,94	1,1684	3	0,9174						
65	1	2419,935	1,1607	3	0,9219						
66	1	2314,446	1,1856	4	0,9074						
67	1	2339,328	1,1898	4	0,905						
68	1	2253,248	1,1946	4	0,9022						
69	1	2319,628	1,189	4	0,9054						
70	1	2333,984	1,1741	3	0,9141						
71	1	2512,708	1,1971	4	0,9007						
72	1	2745,868	1,1863	4	0,907						
73	1	2374,702	1,196	4	0,9014						
74	1	2376,466	1,2069	3	0,8951						
75	1	2466,364	1,2115	4	0,8924	133,70	2,66				
76	1	2501,466	1,1804	4	0,9104						
77	1	2336,92	1,2001	4	0,899						
78	1	2304,574	1,2214	4	0,8867						
79	1	2387,323	1,176	3	0,913						
80	1	2273,472	1,2023	3	0,8977						
81	1	2420,604	1,1898	4	0,905						
82	1	2310,298	1,1963	3	0,9012						
83	1	2520,059	1,2365	4	0,8779						
84	1	2415,503	1,2426	4	0,8744						
85	1	2328,131	1,2301	4	0,8816						
86	1	2403,343	1,2542	4	0,8677						
87	1	2348,947	1,2721	4	0,8573						
88	1	2368,181	1,2689	5	0,8591						
89	1	2526,661	1,2816	4	0,8517						
90	1	2537,824	1,2963	4	0,8432						

Table continued - core GeoB 10503, station 370

Depth		core logging				lab					organic
	section number	p-wave velocity*	gamma density*	magnetic susceptibility *	fractional porosity*	water content	undrained shear strength	grain size distribution			content (LOI)
[cm]		[m/s]	[g/cm³]	[10^{-5} SI]		[%]	[kPa]	Clay [%]	Silt [%]	Sand [%]	[wt%]
91	1	2410,008	1,279	5	0,8532						
92	1	2399,518	1,2525	5	0,8686						
93	1	2428,397	1,2633	5	0,8623						
94	1	2440,81	1,2417	5	0,8749						
95	1	2448,318	1,265	5	0,8614	122,60	2,85				
96	1	2275,067	1,2327	5	0,8801						
97	1	2369,539	1,251	5	0,8695						
98	1	2390,503	1,2529	5	0,8684						
99	1	2329,623	1,2636	5	0,8622						
100	1	2382,94	1,252	5	0,8689		2,86				
101	1	2471,819	1,2487	5	0,8708						
102	1	2443,627	1,2639	4	0,862						
103	1	2489,681	1,2365	4	0,8779						
104	1	2424,82	1,2018	4	0,898						
105	1	2616,887	1,2202	4	0,8874	138,68					
106	1	2673,11	1,2112	4	0,8926						
107	2			1							
108	2	2587,573		2							
109	2	2541,078		2							
110	2	2687,487	1,2455	3	0,8727		3,74				
111	2	2604,509	1,2255	4	0,8843						
112	2	2677,896	1,1941	5	0,9025						
113	2	2319,405	1,2265	4	0,8837						
114	2	2231,447	1,2549	4	0,8672						
115	2	2331,571	1,2651	5	0,8613		4,33	7,49	76,06	16,43	
116	2	2633,267	1,2702	5	0,8584						
117	2	2320,6	1,2621	5	0,863						
118	2	2511,707	1,2581	5	0,8654						
119	2	2725,006	1,2741	6	0,8561						
120	2	2476,2	1,2554	5	0,867						
121	2	2559,063	1,2607	5	0,8638						
122	2	2291,29	1,2616	5	0,8633						
123	2	2513,605	1,2633	5	0,8624	128,99	4,28				
124	2	2477,24	1,2471	5	0,8718						
125	2	2267,504	1,2449	5	0,873						
126	2	2324,815	1,2461	5	0,8723						
127	2	2268,074	1,2719	6	0,8574						
128	2	2342,369	1,2748	6	0,8557						
129	2	2322,43	1,2594	5	0,8646						
130	2	2816,336	1,2687	6	0,8592						
131	2	2806,869	1,2872	5	0,8485						
132	2	2551,967	1,2893	5	0,8472						
133	2	3119,446	1,2966	6	0,843						
134	2	2547,162	1,2844	5	0,8501						
135	2	2865,339	1,2872	5	0,8485		6,06				
136	2	2987,487	1,2802	5	0,8525						
137	2	2364,284	1,2793	5	0,8531						
138	2	2343,995	1,3007	4	0,8407						
139	2	2336,92	1,2649	5	0,8614						
140	2	2437,054	1,3014	5	0,8403						
141	2	2339,601	1,2726	5	0,857						
142	2	2384,354	1,2797	5	0,8528						
143	2	2481,105	1,2757	5	0,8552						
144	2	2315,055	1,278	5	0,8538						
145	2	2517,488	1,2758	5	0,8551	112,39	5,88				
146	2	2483,891	1,2933	5	0,845						
147	2	2381,579	1,3012	5	0,8404						
148	2	2340,914	1,2977	6	0,8424						
149	2	2512,734	1,3166	5	0,8314						
150	2	2364,843	1,3014	5	0,8402						
151	2	2385,123	1,3207	4	0,8291						
152	2	2454,901	1,3435	4	0,8158						
153	2	2294,163	1,3778	4	0,7959						
154	2	2316,476	1,3897	4	0,7891						
155	2	2218,785	1,4026	4	0,7815	72,65	2,91				
156	2		1,4434	5	0,7579						
157	2	2272,9	1,5585	5	0,6911						
158	2		1,564	5	0,6879						
159	2		1,5674	5	0,6859						
160	2	2128,205	1,56	6	0,6903						
161	2	2550,79	1,5261	6	0,7099						
162	2	2404,747	1,4573	7	0,7498						
163	2	2392,914	1,4978	8	0,7263						
164	2	2456,638	1,5182	7	0,7145						
165	2	2378,432	1,5196	8	0,7137						
166	2		1,5184	8	0,7144						
167	2	2302,061	1,5742	8	0,682						
168	2	2382,177	1,567	8	0,6862						
169	2	2252,971	1,6021	8	0,6659						
170	2	2245,067	1,5355	8	0,7045						
171	2	2265,984	1,5422	8	0,7006		5,33				
172	2	2243,939	1,5535	9	0,694						
173	2	2347,031	1,4843	10	0,7342						
174	2	2288,344	1,5198	10	0,7136						
175	2		1,5931	11	0,6711	53,04	6,44				
176	2	2466,088	1,5373	11	0,7034						
177	2	2321,067	1,4155	11	0,7741						
178	2	2373,232	1,5265	13	0,7097						
179	2	2691,143	1,5734	13	0,6825						
180	2	2387,886	1,6131	14	0,6594						

Table continued - core GeoB 10503, station 370

Depth		core logging				lab					organic content (LOI)
	section number	p-wave velocity*	gamma density*	magnetic susceptibility *	fractional porosity*	water content	undrained shear strength	grain size distribution			
[cm]		[m/s]	[g/cm³]	[10^{-5} SI]		[%]	[kPa]	Clay [%]	Silt [%]	Sand [%]	[wt%]
181	2	2259,97	1,5623	14	0,6889						
182	2	2213,17	1,4851	15	0,7337						
183	2	2311,504	1,3894	15	0,7892						
184	2	2293,29	1,4023	16	0,7818						
185	2	2471,42	1,4847	18	0,7339		5,08	11,32	80,17	8,48	
186	2	2425,831	1,4882	20	0,7319						
187	2	2356,124	1,4606	22	0,7479						
188	2	2301,394	1,4559	22	0,7506						
189	2	2257,311	1,559	22	0,6908						
190	2	2399,717	1,4729	22	0,7408						
191	2	2550,902	1,4201	21	0,7714						
192	2	2395,279	1,4769	20	0,7385						
193	2	2381,65	1,5032	20	0,7232						
194	2	2430,886	1,4873	21	0,7324						
195	2	2429,86	1,4838	20	0,7344	69,19	5,50	12,47	77,95	9,57	
196	2	2267,573	1,4475	21	0,7555						
197	2	2408,674	1,4272	22	0,7673						
198	2	2303,839	1,3862	24	0,7911						
199	2	2497,146	1,262	25	0,8631						
200	2	2416,087	1,3428	26	0,8162						
201	2		1,4119	26	0,7762						
202	2		1,3411	28	0,8172						
203	2		1,3459	28	0,8145						
204	2		1,3286	27	0,8245						
205	2		1,3282	26	0,8247						
206	2		1,3816	24	0,7937						

* empty fields: results are not reliable (probably, liner not completely filled with sediment; cap at the end of the liner disturbed measurement; p-wave transducer had not good contact)

Description of core : GeoB10504 – **Station 483**

Date: 16/ 03 / 2006 - 11:08

Latitude	54° 16.189′ N
Longitude	011° 41.948′ E
Water depth	26.2 m
Total core length	403 cm

	Description
↓ core analysed perpendicular to the core axis	0-4 cm: greenish black mud 4-102 cm: olive gray silty mud 102-180 cm: grayish olive silty mud, slightly clayey with rare shell fragments 180-211 cm: greenish black silt, slightly clayey 211-233 cm: olive gray finesandy silt 233-241 cm: olive gray silt, slightly clayey and finesandy 241-260 cm: greenish gray silt laminated with black/brown layers, 251-252cm black layer (peat?) 260-295 cm: greenish gray silt, slightly clayey and finesandy 295-403 cm: light olive gray clayey silt laminated with grayish olive layers

Vane Shear Test

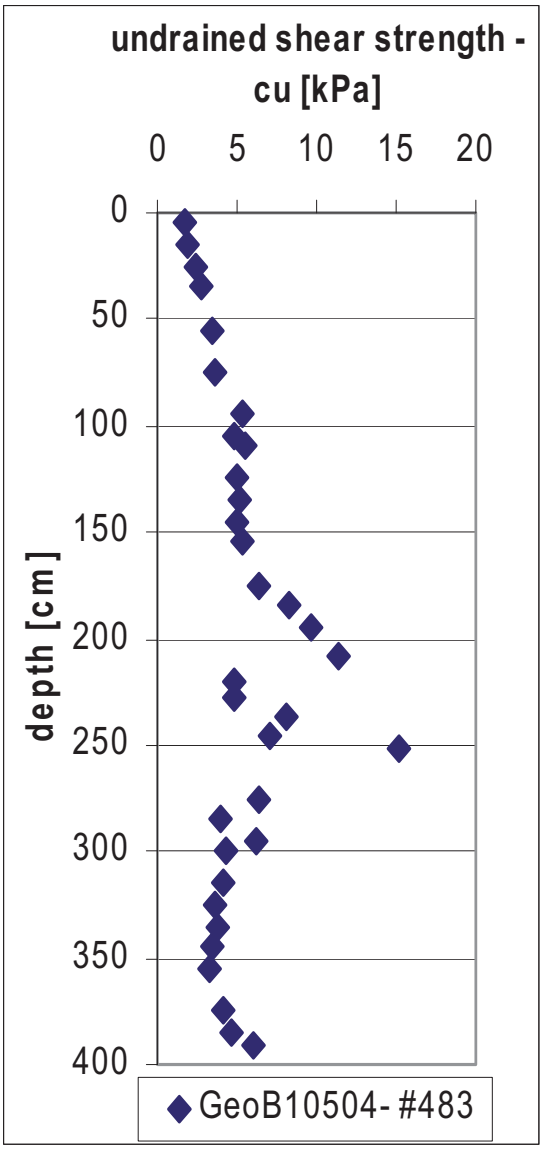

Cruise: **NEST06: 28.02.-17.03.06**
Ship: FS PLANET
Cruise leader: FWG, Germany, Dr. Thomas Wever
Locality: Baltic Sea, Mecklenburg Bay
Lab analyses: Annedore Seifert (RCOM)
Core: **GeoB10504, station #483**
(opened 17.05.2006)

legend: core logging (Geotek Multi Sensor Core Logger (MSCL)):
parameter: p-wave velocity, gamma density, magnetic susceptibility, fractional porosity
type of logging: whole core prior to splitting
notes: fractional porosity calculated with - mineral grain density 2.65 g/cm³ and fluid phase density 1.026 g/cm³
water content: freeze drying
vane shear strength: rotational rate 30°/min
grain size distribution: Beckman Coulter laser particle sizer LS200
organic content: loss on ignition (LOI) at 550°C

		core logging				lab					
Depth	section number	p-wave velocity*	gamma density*	magnetic susceptibility *	fractional porosity*	water content	undrained shear strength	grain size distribution			organic content (LOI)
[cm]		[m/s]	[g/cm³]	[10^{-5} SI]		[%]	[kPa]	Clay [%]	Silt [%]	Sand [%]	[wt%]
0	1							7,09	81,69	11,17	10,54
1	1			3							
2	1	3603,289	1,1661	4	0,9187						
3	1	2782,88	1,1497	5	0,9282						
4	1	2775,356	1,1723	5	0,9151						
5	1	2705,499	1,1803	4	0,9105	133,33	1,78				
6	1	3028,773	1,1038	4	0,9549						
7	1	2946,01	1,1295	4	0,9399						
8	1		1,1479	4	0,9293						
9	1		1,1911	3	0,9042						
10	1		1,1544	3	0,9255						
11	1	2388,911	1,1702	3	0,9164						
12	1	2541,312	1,1393	3	0,9343						
13	1	2541,312	1,1499	3	0,9282						
14	1	2784,181	1,1404	2	0,9336						
15	1	2563,144	1,1544	3	0,9255	176,87	1,87				
16	1	2398,513	1,1717	3	0,9155						
17	1	2437,704	1,1528	2	0,9264						
18	1	2447,703	1,1493	2	0,9285						
19	1	2597,041	1,2036	3	0,897						
20	1	2440,401	1,2153	3	0,8902						
21	1	2473,27	1,2014	3	0,8982						
22	1	2560,824	1,21	3	0,8933						
23	1	3242,597	1,2283	3	0,8827						
24	1	2960,804	1,2371	3	0,8776						
25	1	2666,22	1,2006	3	0,8987	141,88	2,45				
26	1	2516,979	1,2378	4	0,8771						
27	1	2698,937	1,2018	3	0,898						
28	1	2630,071	1,2213	3	0,8867						
29	1	2406,78	1,2097	3	0,8934						
30	1	2635,44	1,1933	2	0,903						
31	1	2570,351	1,1932	3	0,903						
32	1	2592,697	1,1817	3	0,9097						
33	1	2392,7	1,1873	3	0,9064						
34	1	2307,291	1,1872	3	0,9065						
35	1	3437,338	1,1862	3	0,9071	140,22	2,68				
36	1		1,2126	3	0,8918						
37	1		1,2052	3	0,896						
38	1		1,2171	3	0,8892						
39	1		1,2009	3	0,8986						
40	1		1,2108	3	0,8928						
41	1		1,2195	4	0,8878						
42	1		1,2054	3	0,896						
43	1		1,2303	3	0,8815						
44	1		1,2226	3	0,886						
45	1		1,2258	3	0,8841						
46	1		1,2161	3	0,8897						
47	1		1,2214	4	0,8867						
48	1		1,2041	3	0,8967						
49	1		1,2175	4	0,8889						
50	1		1,2117	4	0,8923			7,75	79,45	12,81	7,88
51	1		1,2092	3	0,8937						
52	1		1,2095	3	0,8936						
53	1		1,2183	3	0,8885						
54	1		1,2186	3	0,8883						
55	1		1,2374	3	0,8774	126,77	3,45				
56	1		1,221	3	0,8869						
57	1		1,2248	4	0,8847						
58	1		1,2105	4	0,893						
59	1		1,1978	3	0,9003						
60	1		1,1947	3	0,9022						
61	1		1,1968	3	0,9009						
62	1		1,1848	3	0,9079						
63	1		1,1677	3	0,9178						
64	1		1,1933	3	0,903						
65	1		1,1798	4	0,9108						
66	1		1,1866	4	0,9069						
67	1		1,1874	4	0,9064						
68	1		1,1829	4	0,909						
69	1		1,1677	4	0,9178						
70	1		1,1851	3	0,9077						
71	1		1,1771	3	0,9123						
72	1		1,1868	4	0,9067						
73	1		1,1762	4	0,9129						
74	1		1,1656	3	0,919						
75	1		1,1876	4	0,9063	155,64	3,61				
76	1		1,1857	4	0,9074						
77	1		1,1728	3	0,9148						
78	1		1,1864		0,9069						
79	1		1,1864	4	0,9069						
80	1		1,188	4	0,906						
81	1		1,1927	3	0,9033						
82	1		1,1935	4	0,9029						
83	1		1,2096	4	0,8935						
84	1		1,2013	4	0,8983						
85	1		1,2072	3	0,8949						
86	1		1,201	4	0,8985						
87	1		1,2099	4	0,8933						
88	1		1,1942	3	0,9024						
89	1		1,2129	4	0,8916						
90	1		1,2146	3	0,8906						

Table continued - core GeoB 10504, station 483

		core logging				lab					
Depth	section number	p-wave velocity*	gamma density*	magnetic susceptibility *	fractional porosity*	water content	undrained shear strength	grain size distribution			organic content (LOI)
[cm]		[m/s]	[g/cm³]	[10^{-5} SI]		[%]	[kPa]	Clay [%]	Silt [%]	Sand [%]	[wt%]
91	1		1,1996	4	0,8993						
92	1		1,2173	4	0,8891						
93	1		1,2157	4	0,89						
94	1		1,2049	4	0,8962						
95	1		1,2102	4	0,8932	137,62	5,31				
96	1		1,2186	4	0,8883						
97	1		1,2105	4	0,893						
98	1		1,1774	4	0,9122						
99	1		1,1507	4	0,9276						
100	1		1,1726	3	0,9149						
101	1		1,2169	3	0,8893						
102	1		1,2244	3	0,8849						
103	2			3							
104	2	2626,619	1,2179	3	0,8887						
105	2	2721,404	1,2118	4	0,8922	122,97	4,87				
106	2	2573,858	1,2731	5	0,8567						
107	2	2680,068	1,2332	5	0,8798						
108	2	2619,807	1,2106	5	0,8929						
109	2	2668,985	1,2254	5	0,8843						
110	2	2385,138	1,2648	5	0,8615		5,59				
111	2	2370,135	1,2546	5	0,8674						
112	2	2486,149	1,2776	5	0,854						
113	2	2326,447	1,2999	6	0,8412						
114	2	2368,379	1,2962	5	0,8433						
115	2	2443,921	1,2954	5	0,8437						
116	2	2856,494	1,3208	5	0,829						
117	2	2506,504	1,3029	6	0,8394						
118	2	2398,715	1,2696	6	0,8587						
119	2	2443,059	1,2666	6	0,8604						
120	2	2340,384	1,2637	6	0,8621						
121	2	2233,227	1,2733	6	0,8566						
122	2		1,275	6	0,8556						
123	2		1,287	6	0,8486						
124	2		1,2706	6	0,8581						
125	2		1,3004	7	0,8408	118,87	5,06				
126	2		1,3139	6	0,833						
127	2		1,2849	6	0,8498						
128	2		1,313	6	0,8335						
129	2		1,2965	6	0,8431						
130	2		1,3044	7	0,8385						
131	2		1,3223	7	0,8281						
132	2		1,3074	6	0,8368						
133	2		1,2875	7	0,8483						
134	2		1,3175	6	0,8309						
135	2		1,3078	7	0,8365		5,23				
136	2		1,3059	7	0,8377						
137	2		1,3086	7	0,8361						
138	2		1,3201	7	0,8294						
139	2		1,3151	7	0,8323						
140	2		1,2829	6	0,851						
141	2		1,3071	7	0,8369						
142	2		1,3307	6	0,8233						
143	2		1,3007	6	0,8407						
144	2		1,3208	7	0,829						
145	2		1,2947	7	0,8441	112,68	4,97				
146	2		1,3038	7	0,8389						
147	2		1,3215	7	0,8286						
148	2		1,3013	7	0,8403						
149	2		1,3006	7	0,8407						
150	2		1,2966	7	0,843			12,17	83,19	4,62	
151	2		1,2886	8	0,8477						
152	2		1,2971	8	0,8427						
153	2		1,3002	7	0,8409						
154	2		1,2961	7	0,8433						
155	2		1,3072	7	0,8369	112,18	5,38				
156	2		1,3188	8	0,8302						
157	2		1,3016	7	0,8401						
158	2		1,2925	7	0,8454						
159	2		1,2871	7	0,8485						
160	2		1,2758	7	0,8551						
161	2		1,2856	8	0,8494						
162	2		1,313	8	0,8336						
163	2		1,2837	8	0,8505						
164	2		1,2884	7	0,8478						
165	2		1,2868	7	0,8487						
166	2		1,2761	7	0,8549						
167	2		1,2944	9	0,8443						
168	2		1,2813	8	0,8519						
169	2		1,2917	8	0,8459						
170	2		1,2715	8	0,8576						
171	2		1,282	8	0,8515						
172	2		1,283	8	0,8509						
173	2		1,2848	9	0,8499						
174	2		1,2865	8	0,8489						
175	2		1,2873	8	0,8485	117,65	6,41				
176	2		1,2843	8	0,8502						
177	2		1,2829	7	0,851						
178	2		1,2785	7	0,8535						
179	2		1,3082	8	0,8363						
180	2		1,2921	8	0,8457						

Table continued - core GeoB 10504, station 483

Depth		core logging				lab					
	section number	p-wave velocity*	gamma density*	magnetic susceptibility *	fractional porosity*	water content	undrained shear strength	grain size distribution			organic content (LOI)
[cm]		[m/s]	[g/cm³]	[10^{-5} SI]		[%]	[kPa]	Clay [%]	Silt [%]	Sand [%]	[wt%]
181	2		1,2968	7	0,8429						
182	2		1,2678	7	0,8598						
183	2		1,2836	7	0,8506						
184	2		1,2677	7	0,8598						
185	2		1,268	8	0,8596		8,24				
186	2		1,27	8	0,8584						
187	2		1,2557	7	0,8668						
188	2		1,2453	8	0,8728						
189	2		1,2522	8	0,8688						
190	2		1,2489	8	0,8707						
191	2		1,2326	8	0,8802						
192	2		1,2547	8	0,8673						
193	2		1,2418	7	0,8748						
194	2		1,2577	8	0,8656						
195	2		1,2697	8	0,8587	124,74	9,62	2,68	56,97	40,39	
196	2		1,2794	7	0,853						
197	2		1,2784	7	0,8536						
198	2		1,258	7	0,8654						
199	2		1,2522	7	0,8688						
200	2		1,2369	6	0,8777						
201	2		1,2652	7	0,8613						
202	2		1,2767	6	0,8546						
203	3			3							
204	3	2538,858		4							
205	3			5							
206	3		1,2909	7	0,8464						
207	3		1,2954	7	0,8437						
208	3		1,2322	6	0,8804		11,34				
209	3		1,2559	6	0,8667						
210	3		1,2786	6	0,8535						
211	3		1,3114	6	0,8344						
212	3		1,3418	6	0,8168						
213	3		1,4234	6	0,7695						
214	3		1,3961	6	0,7853						
215	3		1,439	6	0,7604						
216	3		1,4443	5	0,7574						
217	3		1,4696	5	0,7427						
218	3		1,5086	5	0,7201						
219	3		1,5171	5	0,7152						
220	3		1,4895	5	0,7311	59,62	4,77	3,31	53,66	43	
221	3		1,4723	4	0,7411						
222	3		1,3618	5	0,8052						
223	3		1,361	6	0,8057						
224	3		1,4309	5	0,7651						
225	3		1,4077	5	0,7786						
226	3		1,459	5	0,7489						
227	3		1,4509	5	0,7536						
228	3		1,4794	5	0,737		4,79				
229	3		1,4915	5	0,73						
230	3		1,5611	6	0,6896						
231	3		1,6542	6	0,6356						
232	3		1,5084	6	0,7202						
233	3		1,5814	6	0,6779						
234	3		1,5167	8	0,7153						
235	3		1,5065	9	0,7213						
236	3		1,4692	10	0,7429						
237	3		1,4602	11	0,7481	64,91	8,16				
238	3		1,4383	12	0,7609						
239	3		1,435	13	0,7628						
240	3		1,4329	14	0,764						
241	3		1,4704	13	0,7422						
242	3		1,4623	14	0,7469						
243	3		1,4772	14	0,7383						
244	3		1,4314	14	0,7649						
245	3		1,4573	14	0,7498		7,11				
246	3		1,4473	13	0,7556						
247	3		1,5509	13	0,6955						
248	3		1,6075	13	0,6627						
249	3		1,3924	14	0,7875						
250	3		1,334	14	0,8213						
251	3		1,3812	13	0,794	225,56	15,16				
252	3		1,1675	13	0,9179						
253	3		1,2676	13	0,8599						
254	3		1,2562	13	0,8665						
255	3		1,3975	13	0,7845						
256	3		1,4789	13	0,7373						
257	3		1,3395	13	0,8181						
258	3		1,5368	14	0,7037						
259	3		1,813	15	0,5435						
260	3		1,6898	17	0,615						
261	3		1,6846	18	0,618						
262	3		1,7499	21	0,5801						
263	3		1,8383	23	0,5288						
264	3		1,8939	25	0,4966						
265	3		1,8627	28	0,5147						
266	3		1,7394	31	0,5862						
267	3		1,6979	35	0,6102						
268	3		1,7479	39	0,5813						
269	3		1,7872	40	0,5584						
270	3		1,7764	39	0,5647						

Table continued - core GeoB 10504, station 483

Depth		core logging				lab					organic
	section number	p-wave velocity*	gamma density*	magnetic susceptibility *	fractional porosity*	water content	undrained shear strength	grain size distribution			content (LOI)
[cm]		[m/s]	[g/cm³]	[10^{-5} SI]		[%]	[kPa]	Clay [%]	Silt [%]	Sand [%]	[wt%]
271	3		1,8006	38	0,5507						
272	3		1,7959	36	0,5534						
273	3		1,8419	36	0,5267						
274	3		1,8353	40	0,5305						
275	3		1,7773	45	0,5642	34,05	6,33	11,54	74,63	13,82	
276	3		1,7672	53	0,5701						
277	3		1,7683	62	0,5694						
278	3		1,6947	70	0,6121						
279	3		1,7074	79	0,6048						
280	3		1,6746	85	0,6238						
281	3		1,6333	91	0,6477						
282	3		1,7532	95	0,5782						
283	3		1,7225	96	0,596						
284	3		1,7107	91	0,6028						
285	3		1,7296	81	0,5919		4,02				
286	3		1,7112	71	0,6025						
287	3		1,6811	62	0,62						
288	3		1,6713	56	0,6257						
289	3		1,6749	51	0,6236						
290	3		1,7237	48	0,5953						
291	3		1,6944	46	0,6123						
292	3		1,7359	43	0,5882						
293	3		1,7316	41	0,5907						
294	3		1,6983	40	0,61						
295	3		1,7141	42	0,6008		6,28				
296	3		1,7473	44	0,5816						
297	3		1,6651	45	0,6293						
298	3		1,6937	46	0,6127						
299	3		1,6542	48	0,6356						
300	3		1,5705	49	0,6841	40,00	4,29				
301	3		1,6443	50	0,6414						
302	3		1,6275	52	0,6511						
303	3		1,6806	53	0,6203						
304	3		1,7224	52	0,5961						
305	3		1,6808	48	0,6202						
306	4	2719,062		31							
307	4	2726,581	1,6718	43	0,6254						
308	4	2623,115	1,7604	50	0,574						
309	4	2592,845	1,6986	55	0,6099						
310	4	3105,564	1,6659	55	0,6288						
311	4	2736,102	1,6637	56	0,6301						
312	4	2492,662	1,6508	57	0,6376						
313	4	2569,92	1,7327	58	0,5901						
314	4	2365,602	1,6749	59	0,6236						
315	4	2266,679	1,697	59	0,6108	45,75	4,08				
316	4	2453,199	1,6928	57	0,6132						
317	4	2450,884	1,7243	57	0,5949						
318	4	2286,618	1,6714	57	0,6256						
319	4	2446,268	1,7376	57	0,5872						
320	4	2340,855	1,7341	57	0,5893						
321	4		1,7247	56	0,5947						
322	4		1,7443	57	0,5833						
323	4		1,6567	57	0,6341						
324	4		1,7531	57	0,5782						
325	4		1,6469	60	0,6399		3,69				
326	4		1,766	60	0,5707						
327	4		1,7217	61	0,5965						
328	4		1,7199	61	0,5975						
329	4		1,7274	59	0,5931						
330	4		1,6841	58	0,6183						
331	4		1,7112	57	0,6026						
332	4		1,7588	56	0,575						
333	4		1,697	57	0,6108						
334	4		1,7536	57	0,578						
335	4		1,7585	58	0,5751	35,53	3,84	15,11	81,62	3,32	
336	4		1,7756	60	0,5652						
337	4		1,7669	62	0,5702						
338	4		1,725	61	0,5945						
339	4		1,7284	60	0,5926						
340	4		1,8234	59	0,5375						
341	4		1,8103	59	0,5451						
342	4		1,7085	58	0,6041						
343	4		1,7301	58	0,5916						
344	4		1,7092	58	0,6037						
345	4		1,7275	57	0,5931		3,52				
346	4		1,6869	56	0,6166						
347	4		1,7522	54	0,5787						
348	4		1,7497	53	0,5802						
349	4		1,6899	54	0,6149						
350	4		1,7642	55	0,5718						
351	4		1,7506	55	0,5797						
352	4		1,7746	56	0,5658						
353	4		1,7503	55	0,5799						
354	4		1,7633	56	0,5723						
355	4		1,7581	58	0,5753	41,65	3,20				
356	4		1,7612	58	0,5735						
357	4		1,7028	59	0,6074						
358	4		1,766	50	0,5708						
359	4		1,795	58	0,5539						
360	4		1,784	59	0,5603						

Table continued - core GeoB 10504, station 483

Depth		core logging				lab					
	section number	p-wave velocity*	gamma density*	magnetic susceptibility *	fractional porosity*	water content	undrained shear strength	grain size distribution			organic content (LOI)
[cm]		[m/s]	[g/cm³]	[10^{-5} SI]		[%]	[kPa]	Clay [%]	Silt [%]	Sand [%]	[wt%]
361	4		1,7453	61	0,5828						
362	4		1,8021	61	0,5498						
363	4		1,7057	64	0,6058						
364	4		1,7549	66	0,5772						
365	4		1,7414	71	0,585						
366	4		1,7893	77	0,5572						
367	4		1,7179	84	0,5986						
368	4		1,6511	91	0,6374						
369	4		1,8413	95	0,5271						
370	4		1,7555	95	0,5768						
371	4		1,8119	93	0,5441						
372	4		1,7744	88	0,5659						
373	4		1,7714	82	0,5676						
374	4		1,7781	75	0,5638						
375	4		1,7403	67	0,5857	43,30	4,10				
376	4		1,7173	61	0,599						
377	4		1,7799	57	0,5627						
378	4		1,8517	55	0,521						
379	4		1,7781	55	0,5638						
380	4		1,7452	52	0,5828						
381	4		1,6828	51	0,619						
382	4		1,756	50	0,5765						
383	4		1,7458	51	0,5825						
384	4		1,7543	52	0,5775						
385	4		1,7572	54	0,5759		4,73				
386	4		1,7974	55	0,5525						
387	4		1,7898	54	0,5569						
388	4		1,7172	53	0,5991						
389	4		1,7498	52	0,5802						
390	4		1,6746	50	0,6238						
391	4		1,7233	50	0,5956		6,08				
392	4		1,6687	50	0,6272						
393	4		1,6981	50	0,6101						
394	4		1,6901	51	0,6148						
395	4		1,7622	51	0,573	49,49					
396	4		1,7524	51	0,5786						
397	4		1,6525	49	0,6366						
398	4										
399	4										
400	4										
401	4										
402	4										
403	4										

* empty fields: results are not reliable (probably, liner not completely filled with sediment; cap at the end of the liner disturbed measurement; p-wave transducer had not good conta

Description of core : GeoB10505 – **Station 11**

Date: 28/ 02 / 2006 - 14:54	
Latitude	54° 29.309′ N
Longitude	09° 58.559′ E
Water depth	27.1 m
Total core length	100 cm

	Description
↓ core analysed perpendicular to the core axis	core not completely filled with sediment and a lot of areas are disturbed: 0-45 cm: greenish black silty mud, very soft, slightly smell of H_2S when opening the core, some shell fragments 45-100 cm: olive gray silty mud, very soft

Vane Shear Test

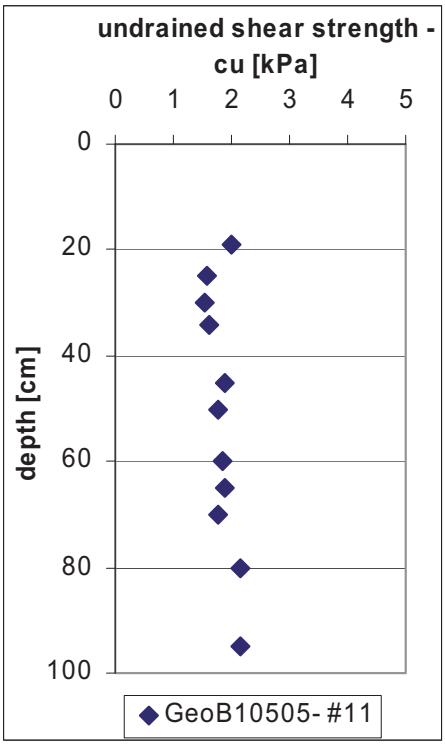

Cruise: **NEST06: 28.02.-17.03.06**
Ship: FS PLANET
Cruise leader: FWG, Germany, Dr. Thomas Wever
Locality: Baltic Sea, Eckernförde Bay
Lab analyses: Annedore Seifert (RCOM)
Core: **GeoB10505, station #11**
(opened 23.06.2006)

legend: core logging (Geotek Multi Sensor Core Logger (MSCL)):
parameter: p-wave velocity, gamma density, magnetic susceptibility, fractional porosity
type of logging: whole core prior splitting
notes: fractional porosity calculated with - mineral grain density 2.65 g/cm³ and fluid phase density 1.026 g/cm³
water content: freeze drying
vane shear strength: rotational rate 30°/min
grain size distribution: Beckman Coulter laser particle sizer LS200

Depth	core logging					lab				
	section number	p-wave velocity	gamma density	magnetic susceptibility	fractional porosity	water content	undrained shear strength	grain size distribution		
[cm]		[m/s]	[g/cm³]	[10^{-5} SI]		[%]	[kPa]	Clay [%]	Silt [%]	Sand [%]
	Liner was not completely filled with sediment (results of p-wave, density and porosity not reliable)									
1	1			2						
2	1			1						
3	1			2						
4	1			3						
5	1			2		210,98				
6	1			2						
7	1			1						
8	1			2						
9	1			2						
10	1			3						
11	1			3						
12	1			4						
13	1			4						
14	1			4						
15	1			4		196,49				
16	1			3						
17	1			3						
18	1			3						
19	1			2			1,99			
20	1			3						
21	1			3						
22	1			2						
23	1			2						
24	1			2						
25	1			1		186,33	1,57			
26	1			2						
27	1			2						
28	1			2						
29	1			2						
30	1			2			1,55			
31	1			2						
32	1			2						
33	1			1						
34	1			2			1,61			
35	1			1		220,79				
36	1			1						
37	1			1						
38	1			1						
39	1			0						
40	1			1						
41	1			0						
42	1			0						
43	1			1						
44	1			0						
45	1			1			1,89			
46	1			1						
47	1			0						
48	1			1						
49	1			1						
50	1			1		219,02	1,78	6,59	82,57	10,81
51	1			0						
52	1			1						
53	1			0						
54	1			0						
55	1			0						
56	1			0						
57	1			0						
58	1			0						
59	1			1						
60	1			1			1,84			
61	1			0						
62	1			1						
63	1			1						
64	1			0						
65	1			0		235,41	1,89			
66	1			0						
67	1			1						
68	1			0						
69	1			0						
70	1			0			1,76			
71	1			1						
72	1			1						
73	1			1						
74	1			1						
75	1			1						
76	1			1						
77	1			1						
78	1			1						
79	1			0						
80	1			1			2,14			
81	1			0						
82	1			1						
83	1			1		226,42				
84	1			1						
85	1			0						
86	1			1						
87	1			1						
88	1			1						
89	1			0						
90	1			1						
91	1			1						
92	1			1						
93	1			1						
94	1			1						
95	1			1		249,19	2,15			
96	1			1						
97	1			1						
98	1			1						
99	1			1						
100	1									

Description of core : GeoB10506 – **Station 44**

Date: 02/ 03 / 2006 - 10:39

Latitude	54° 30.215′ N
Longitude	010° 05.449′ E
Water depth	20.8 m
Total core length	Section 4 and 5: 203 cm

	Description	Vane Shear Test
↓ core analysed perpendicular to the core axis	311-413 cm: olive gray silt, slightly clayey 413-514 cm: olive gray silt, slightly clayey and laminated with olive green layers Layers with a lot of shell fragments in depth of 350-360 cm and 430-440 cm	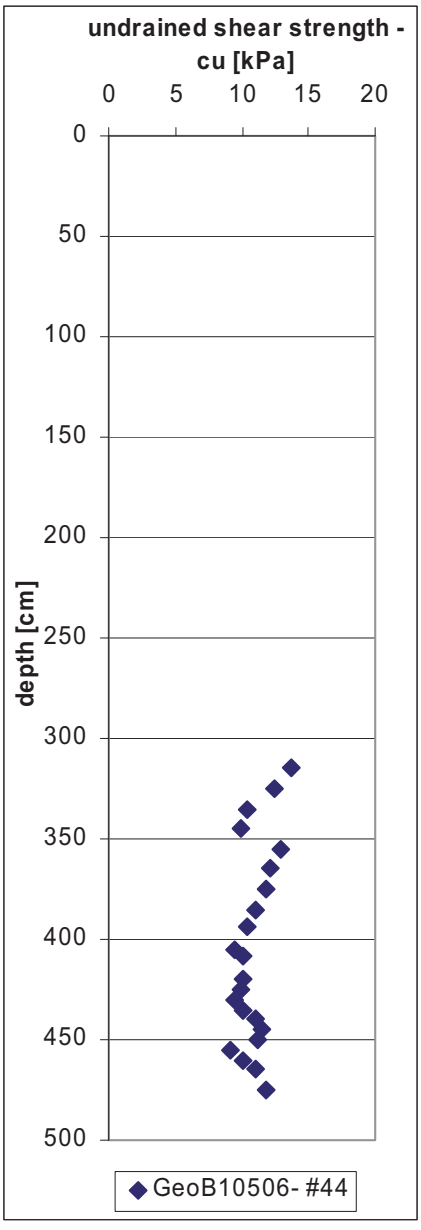

Cruise: **NEST06: 28.02.-17.03.06**
Ship: FS PLANET
Cruise leader FWG, Germany, Dr. Thomas Wever
Locality: Baltic Sea, Eckernförde Bay
Lab analyses: Annedore Seifert (RCOM)
Core: **GeoB10506, station #44 section 4 and 5**
(opened 23.06.2006)

legend: core logging (Geotek Multi Sensor Core Logger (MSCL)):
parameter: p-wave velocity, gamma density, magnetic susceptibility, fractional porosity
type of logging: whole core prior splitting
notes: fractional porosity calculated with - mineral grain density 2.65 g/cm³
and fluid phase density 1.026 g/cm³
water content: freeze drying
vane shear strength: rotational rate 30°/min

		core logging				lab	
Depth	section number	p-wave velocity*	gamma density*	magnetic susceptibility *	fractional porosity*	water content	undrained shear strength
[cm]		[m/s]	[g/cm³]	[10^{-5} SI]		[%]	[kPa]
313	4	2764,132		1			
314	4	2768,496	1,1282	2	0,9407		
315	4	2792,19	1,1519	3	0,927	161,46	13,73
316	4	3027,554	1,1117	2	0,9503		
317	4	2705,42	1,1072	2	0,9529		
318	4	2909,352	1,1192	3	0,946		
319	4	2624,586	1,1827	3	0,9091		
320	4	2758,061	1,2043	3	0,8966		
321	4	2653,202	1,2155	2	0,8901		
322	4	2819,972	1,2016	3	0,8981		
323	4	2820,446	1,1943	2	0,9024		
324	4	2656,836	1,1612	2	0,9216		
325	4	2633,525	1,0548	2	0,9833	173,85	12,42
326	4	2711,582	1,2123	2	0,8919		
327	4	2651,36	1,2234	2	0,8855		
328	4	2681,47	1,2082	3	0,8943		
329	4	2672,658	1,172	2	0,9153		
330	4	2685,173	1,2002	2	0,899		
331	4	2600,306	1,1488	2	0,9288		
332	4	2496,853	1,1524	2	0,9267		
333	4	2242,744	1,1824	2	0,9093		
334	4		1,1928	3	0,9032		
335	4	2259,78	1,1956	2	0,9017	177,08	10,36
336	4		1,1884	3	0,9058		
337	4	2266,426	1,178	3	0,9118		
338	4	2537,412	1,1735	2	0,9144		
339	4	2469,405	1,1744	2	0,9139		
340	4	2490,483	1,1661	2	0,9187		
341	4	2490,483	1,1753	2	0,9134		
342	4	2395,896	1,169	2	0,917		
343	4	2109,812	1,1829	2	0,909		
344	4	2409,624	1,1763	2	0,9128		
345	4	2367,951	1,1746	2	0,9138		9,98
346	4		1,1706	2	0,9161		
347	4		1,1752	2	0,9134		
348	4		1,1632	2	0,9204		
349	4		1,158	2	0,9234		
350	4		1,1651	2	0,9193		
351	4		1,1743	2	0,914		
352	4		1,1463	2	0,9302		
353	4		1,1706	2	0,9161		
354	4		1,173	2	0,9147		
355	4		1,165	1	0,9194	192,62	12,95
356	4		1,1648	2	0,9195		
357	4		1,1803	1	0,9105		
358	4		1,188	2	0,906		
359	4		1,187	2	0,9066		
360	4		1,1849	2	0,9079		
361	4		1,1623	2	0,9209		
362	4		1,1803	3	0,9105		
363	4		1,1916	1	0,904		
364	4		1,1763	3	0,9128		
365	4		1,1579	1	0,9235		12,11
366	4		1,173	3	0,9147		
367	4		1,1683	2	0,9174		
368	4		1,1706	2	0,9161		
369	4		1,1659	2	0,9189		
370	4		1,1835	2	0,9086		
371	4	3151,475	1,173	2	0,9147		
372	4	2684,021	1,1738	2	0,9143		
373	4	3097,125	1,1745	2	0,9138		
374	4	2686,363	1,1768	2	0,9125		
375	4	2615,401	1,1743	3	0,914	184,94	11,80
376	4	2752,822	1,1598	2	0,9224		
377	4	2854,754	1,1667	2	0,9184		
378	4	2609,256	1,175	2	0,9135		
379	4	2862,069	1,1719	3	0,9154		
380	4	2643,663	1,1805	2	0,9104		
381	4	2673,451	1,1853	2	0,9076		
382	4	2612,325	1,1749	2	0,9136		
383	4	2650,188	1,1846	2	0,908		
384	4	2624,012	1,1895	3	0,9052		
385	4	2812,279	1,1884	2	0,9058		11,04
386	4	2575,954	1,1824	1	0,9093		
387	4	2612,762	1,1818	2	0,9096		
388	4	2559,623	1,185	2	0,9077		
389	4	2477	1,1446	3	0,9312		
390	4	2715,974	1,1837	3	0,9085		
391	4	2667,039	1,1888	3	0,9056		
392	4	2714,61	1,1838	3	0,9085		
393	4	2650,688	1,1808	2	0,9102		
394	4	2947,174	1,1916	3	0,9039		10,43
395	4	2942,061	1,1906	3	0,9045	173,09	
396	4	2609,276	1,1819	2	0,9095		
397	4	2746,372	1,2038	2	0,8969		
398	4	2626,102	1,2037	3	0,8969		
399	4	2960,458	1,2241	2	0,8851		
400	4	2546,778	1,2294	2	0,882		

Table continued - core GeoB 10506, station 44, section 4 and 5

		core logging				lab	
Depth	section number	p-wave velocity*	gamma density*	magnetic susceptibility *	fractional porosity*	water content	undrained shear strength
[cm]		[m/s]	[g/cm³]	[10^{-5} SI]		[%]	[kPa]
401	4	2584,003	1,2455	2	0,8727		
402	4	2449,598	1,249	2	0,8706		
403	4	2399,111	1,2571	3	0,866		
404	4	3112,684	1,2635	3	0,8623		
405	4	2324,203	1,2669	3	0,8603		9,53
406	4	2567,661	1,2676	3	0,8599		
407	4	2711,025	1,2531	2	0,8683		
408	4	2539,164	1,2294	3	0,882	164,92	10,08
409	4		1,1951	2	0,9019		
410	4		1,1866	3	0,9068		
411	4		1,2301	2	0,8816		
412	4		1,2302	2	0,8816		
413	4		1,2059	2	0,8956		
415	5			1			
416	5	2945,189		1			
417	5	2750,824	1,1688	1	0,9172		
418	5	2888,915	1,1444	2	0,9313		
419	5	2634,648	1,1429	2	0,9322		
420	5	2607,973	1,1742	2	0,914	159,25	10,06
421	5	2491,625	1,2027	2	0,8975		
422	5	2552,242	1,1976	3	0,9005		
423	5	2535,707	1,1802	3	0,9105		
424	5	2498,215	1,1744	2	0,9139		
425	5	3195,915	1,1784	2	0,9116		9,98
426	5	2540,269	1,2081	2	0,8944		
427	5	2502,841	1,1981	3	0,9002		
428	5	2500,21	1,2136	3	0,8912		
429	5	2479,358	1,2097	2	0,8934		
430	5	2677,775	1,2085	3	0,8941		9,47
431	5	2689,889	1,2096	3	0,8935		
432	5	2484,747	1,2225	3	0,886		
433	5	2579,267	1,2134	3	0,8913		
434	5	2487,973	1,1928	3	0,9033		
435	5	2599,65	1,2048	3	0,8963	164,73	10,11
436	5	2560,482	1,2165	2	0,8895		
437	5	2530,313	1,1884	3	0,9058		
438	5	2585,742	1,2014	3	0,8983		
439	5	2447,439	1,1975	2	0,9005		
440	5	2558,159	1,2281	2	0,8828		11,04
441	5	2515,324	1,2234	3	0,8855		
442	5	2466,017	1,2443	3	0,8734		
443	5	2450,989	1,2265	3	0,8837		
444	5	2463,672	1,2586	2	0,8651		
445	5	2504,946	1,2471	3	0,8717		11,51
446	5	2510,23	1,2471	3	0,8717		
447	5	2713,635	1,2339	2	0,8794		
448	5	2840,372	1,1859	2	0,9073		
449	5	2621,669	1,1885	2	0,9058		
450	5	2570,935	1,1933	2	0,903		11,25
451	5	2630,137	1,2417	2	0,8749		
452	5	2482,068	1,252	3	0,8689		
453	5	2800,047	1,2389	2	0,8765		
454	5	2559,45	1,2354	3	0,8785		
455	5	2686,301	1,2158	3	0,8899	167,30	9,15
456	5	2630,579	1,1802	3	0,9105		
457	5	2633,267	1,1782	2	0,9117		
458	5	2563,711	1,1961	2	0,9013		
459	5	2588,376	1,202	2	0,8979		
460	5	2645,603	1,2113	2	0,8925		10,10
461	5	2552,121	1,2154	2	0,8901		
462	5	2614,276	1,2061	3	0,8955		
463	5	2345,084	1,1991	2	0,8996		
464	5	2239,469	1,2043	3	0,8966		
465	5	2278,99	1,2251		0,8845		11,03
466	5		1,2733	2	0,8565		
467	5		1,2409	2	0,8753		
468	5		1,2391	2	0,8764		
469	5	2670,556	1,2341	3	0,8793		
470	5		1,2491	3	0,8706		
471	5	2918,793	1,2169	3	0,8893		
472	5	2522,477	1,217	3	0,8892		
473	5	2274,135	1,2076	2	0,8947		
474	5	2954,545	1,201	2	0,8985		
475	5		1,2199	3	0,8875	165,17	11,88
476	5	2412,29	1,2403	2	0,8757		
477	5		1,2066	2	0,8952		
478	5		1,1805	1	0,9104		
479	5		1,1958	1	0,9015		
480	5	2387,874	1,1967	2	0,901		
481	5	2382,889	1,2258	2	0,8841		
482	5	2474,199	1,2476	2	0,8714		
483	5	2260,217	1,2396	2	0,8761		
484	5	2283,903	1,234	2	0,8793		
485	5	2411,478	1,2488	2	0,8708		
486	5	2277,533	1,2164	2	0,8895		
487	5	2556,439	1,19	2	0,9049		
488	5	2899,049	1,1625	2	0,9208		
489	5	2580,764	1,1675	2	0,9179		
490	5	2437,654	1,1942	2	0,9024		

Table continued - core GeoB 10506, station 44, section 4 and 5

		core logging				lab	
Depth	section number	p-wave velocity*	gamma density*	magnetic susceptibility *	fractional porosity*	water content	undrained shear strength
[cm]		[m/s]	[g/cm³]	[10^{-5} SI]		[%]	[kPa]
491	5	2785,982	1,202	2	0,8979		
492	5	3232,862	1,2021	2	0,8978		
493	5	2625,718	1,1999		0,8991		
494	5	2611,294	1,2104	2	0,893		
495	5	2402,548	1,1918	2	0,9038	165,32	
496	5	2549,024	1,2052	1	0,8961		
497	5	2438,924	1,1855	2	0,9075		
498	5	3137,348	1,189	2	0,9055		
499	5	2676,736	1,2249	2	0,8846		
500	5	2652,368	1,2028	1	0,8975		
501	5	2520,059	1,2359	1	0,8783		
502	5	2460,008	1,2399	2	0,8759		
503	5	2277,874	1,2344	3	0,8791		
504	5	2765,789	1,2301	2	0,8816		
505	5	2426,089	1,2274	2	0,8832	135,22	
506	5	2641,728	1,2259	2	0,884		
507	5	2307,528	1,2506		0,8697		
508	5	2276,531	1,2408	2	0,8754		
509	5	2457,936		2			
510	5	2238,185		1			
511	5	2581,109		2			
512	5	2460,48		2			
513	5	2596,758		1			
514	5	2822,891		1			

* empty fields: results are not reliable (probably, liner not completely filled with sediment; cap at the end of the liner disturbed measurement; p-wave transducer had not good contact)

Description of core : GeoB10507 – **Station 82**

Date: 04/ 03 / 2006 - 14:13

Latitude	54° 29.287′ N
Longitude	09° 58.498′ E
Water depth	27.8 m
Total core length	95 cm

	Description
↓ core analysed perpendicular to the core axis	0-95 cm: olive gray silty mud, very soft, some areas have black inclusions, small wholes in the sediment structure perhaps formed by gas 81 cm: grayish olive green layer (slightly smell of H_2S when opening the core, some areas are disturbed)

Vane Shear Test

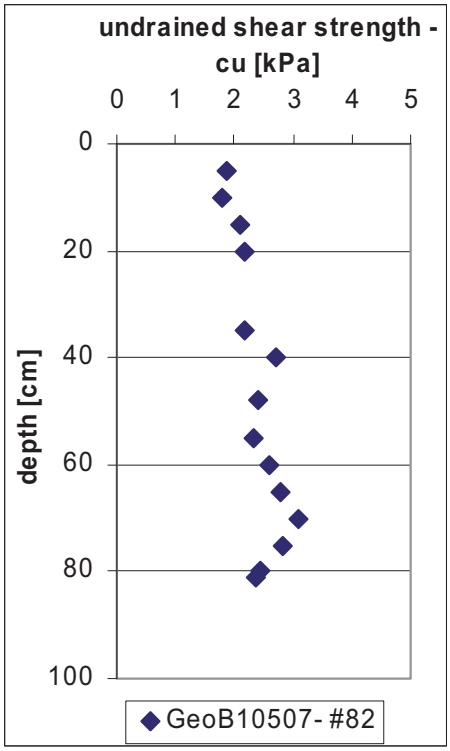

Cruise: **NEST06: 28.02.-17.03.06**
Ship: FS PLANET
Cruise leader: FWG, Germany, Dr. Thomas Wever
Locality: Baltic Sea, Eckernförde Bay
Lab analyses: Annedore Seifert (RCOM)
Core: **GeoB10507, station #82**
(opened 23.06.2006)

legend: core logging (Geotek Multi Sensor Core Logger (MSCL)):
parameter: p-wave velocity, gamma density, magnetic susceptibility, fractional porosity
type of logging: whole core prior to splitting
notes: fractional porosity calculated with - mineral grain density 2.65 g/cm³ and fluid phase density 1.026 g/cm³
water content: freeze drying
vane shear strength: rotational rate 30°/min
grain size distribution: Beckman Coulter laser particle sizer LS200
organic content: loss on ignition (LOI) at 550°C

		core logging				lab								
Depth	section number	p-wave velocity*	gamma density*	magnetic susceptibility*	fractional porosity*	water content	undrained shear strength	grain size distribution			grain size distribution	*organic material was removed before measuring*		organic content (LOI)
[cm]		[m/s]	[g/cm³]	[10^{-5} SI]		[%]	[kPa]	Clay [%]	Silt [%]	Sand [%]	Clay [%]	Silt [%]	Sand [%]	[wt%]
1	1			5										
2	1	2767,087		8										
3	1	2758,552	1,1696	9	0,9167									
4	1	2878,229	1,1516	0	0,9272									
5	1	2988,958	1,1389	8	0,9345	205,81	1,89	7,33	85,76	6,92	22,07	77,59	0,35	10,58
6	1		1,0785	6	0,9696									
7	1		1,0982	5	0,9581									
8	1		1,1325	4	0,9382									
9	1		1,1033	3	0,9552									
10	1		1,1397	4	0,934		1,79							
11	1		1,1262	3	0,9419									
12	1		1,1416	3	0,9329									
13	1		1,0892	3	0,9633									
14	1		1,1037	3	0,9549									
15	1		1,0775	2	0,9701	246,02	2,08							
16	1		1,0784	2	0,9696									
17	1		1,0816	2	0,9677									
18	1		1,0978	2	0,9584									
19	1		1,1005	2	0,9568									
20	1		1,0828	2	0,9671		2,17							
21	1		1,0894	2	0,9632									
22	1		1,1101	2	0,9512									
23	1		1,0799	2	0,9687									
24	1		1,1014	2	0,9562									
25	1		1,1358	2	0,9363	233,31								
26	1		1,0919	2	0,9618									
27	1		1,0959	2	0,9595									
28	1		1,0858	1	0,9653									
29	1		1,1182	2	0,9465									
30	1		1,0945	2	0,9603									
31	1	2320,868	1,091	2	0,9623									
32	1	2626,398	1,0975	2	0,9585									
33	1		1,097	2	0,9588									
34	1		1,0785	2	0,9695									
35	1		1,1083	2	0,9523	246,82	2,18							
36	1		1,0814	2	0,9678									
37	1		1,0794	2	0,9691									
38	1	2357,213	1,0851	2	0,9657									
39	1		1,0893	2	0,9633									
40	1		1,0989	2	0,9577		2,70							
41	1		1,0933	2	0,9609									
42	1	3015,613	1,0938	2	0,9607									
43	1	2660,298	1,1015	3	0,9562									
44	1	2748,852	1,0959	2	0,9594									
45	1	2730,506	1,0912	2	0,9622									
46	1	2968,533	1,0973	2	0,9586									
47	1	2709,218	1,0904	2	0,9627									
48	1	2306,185	1,0692	2	0,975		2,39							
49	1	2410,159	1,1017	2	0,9561									
50	1		1,0912	2	0,9622	250,58		5,38	83,03	11,6	20,91	77,34	1,8	14,57
51	1	2752,296	1,0931	2	0,9611									
52	1	2413,626	1,0864	1	0,965									
53	1		1,109	2	0,9518									
54	1		1,1031	2	0,9553									
55	1	2620,018	1,1096	3	0,9515		2,32							
56	1		1,0653	2	0,9772									
57	1		1,0968	3	0,9589									
58	1		1,0941	2	0,9605									
59	1		1,0822	2	0,9674									
60	1		1,0749	3	0,9717		2,58							
61	1		1,1014	3	0,9562									
62	1		1,0805	2	0,9684									
63	1		1,0647	2	0,9775									
64	1	2242,356	1,0973	3	0,9587									
65	1		1,0622	2	0,979	245,79	2,78							
66	1	2180,259	1,1032	2	0,9552									
67	1		1,0928	3	0,9613									
68	1	2285,878	1,095	2	0,96									
69	1		1,1082	2	0,9523									
70	1	2601,394	1,0968	2	0,959		3,09	7,05	76,54	16,38	19,49	78,85	1,7	15,54
71	1		1,069	2	0,9751									
72	1	3435,27	1,0539	3	0,9838									
73	1	3243,684	1,088	2	0,964									
74	1	3216,653	1,1197	3	0,9456									
75	1	3404,449	1,1035	3	0,9551	216,43	2,84							
76	1	2430,055	1,0991	3	0,9576									
77	1	3508,38	1,1079	4	0,9525									
78	1	2686,332	1,0959	3	0,9594									
79	1	2603,798	1,1134	3	0,9493									
80	1	2828,51	1,1281	4	0,9408		2,43							
81	1	2507,149	1,1127	4	0,9497		2,35							
82	1		1,1412	3	0,9332									
83	1		1,0614	4	0,9795									
84	1	2596,602	1,065	3	0,9774									
85	1		1,0688	3	0,9752									
86	1		1,0829	2	0,967									
87	1		1,1246	2	0,9428									
88	1			2										
89	1			2										
90	1			2										
91	1			2										
92	1			2										
93	1			4										
94	1			4										
95	1			3										

* empty fields: results are not reliable (probably, liner not completely filled with sediment; cap at the end of the liner disturbed measurement; p-wave transducer had not good contact)

Description of core : GeoB10508 – **Station 102**

Date: 05/ 03 / 2006 - 11:57

Latitude	54° 13.323′ N
Longitude	011° 39.673′ E
Water depth	27.2 m
Total core length	93 cm

	Description
↓ core analysed perpendicular to the core axis	0-18 cm: greenish black silty mud, slightly laminated 8-9 cm: 1 cm thick black silty mud layer 18-93 cm: olive gray silty mud with shell fragments at 29-33 cm and at 46-49 cm

Cruise: **NEST06: 28.02.-17.03.06**
Ship: FS PLANET
Cruise leader: FWG, Germany, Dr. Thomas Wever
Locality: Baltic Sea, Mecklenburg Bay
Lab analyses: Annedore Seifert (RCOM)
Core: **GeoB10508, station #102**
(opened 30.04.2007)

legend: core logging (Geotek Multi Sensor Core Logger (MSCL)):
parameter: p-wave velocity, gamma density, magnetic susceptibility, fractional porosity
type of logging: whole core prior to splitting
notes: fractional porosity calculated with - mineral grain density 2.65 g/cm³
and fluid phase density 1.026 g/cm³
water content: drying in oven with 60°C

Depth		core logging				lab
	section number	p-wave velocity*	gamma density*	magnetic susceptibility *	fractional porosity*	water content
[cm]		[m/s]	[g/cm³]	[10^{-5} SI]		[%]
0	1					
1	1			4		
2	1			6		
3	1			8		
4	1			8		
5	1		1,0747	8	0,9718	194,30
6	1		1,0414	9	0,991	
7	1		1,0431	8	0,9901	
8	1		1,0506	8	0,9857	
9	1		1,0701	8	0,9744	
10	1		1,0431	8	0,9901	
11	1	2860,393	1,0479	7	0,9873	
12	1	2615,874	1,0646	7	0,9776	
13	1		1,0702	6	0,9743	
14	1		1,0734	6	0,9725	
15	1		1,0722	6	0,9732	164,28
16	1		1,0653	5	0,9772	
17	1		1,0455	5	0,9887	
18	1		1,0668	5	0,9764	
19	1		1,057	4	0,982	
20	1		1,0862	4	0,9651	
21	1		1,0528	4	0,9844	
22	1		1,079	3	0,9692	
23	1		1,0618	3	0,9793	
24	1		1,0544	3	0,9835	
25	1		1,0397	3	0,9921	189,98
26	1		1,0302	3	0,9975	
27	1		1,0723	2	0,9731	
28	1		1,0537	2	0,9839	
29	1		1,0656	3	0,977	
30	1		1,0584	3	0,9812	
31	1		1,0629	2	0,9786	
32	1		1,0846	3	0,966	
33	1		1,0862	2	0,9651	
34	1		1,0817	2	0,9677	
35	1		1,0605	2	0,98	195,96
36	1		1,0787	2	0,9694	
37	1		1,0709	3	0,974	
38	1		1,1009	2	0,9566	
39	1		1,1259	2	0,9421	
40	1		1,1078	3	0,9525	
41	1		1,1404	2	0,9337	
42	1		1,1417	2	0,9329	
43	1		1,1279	3	0,9409	
44	1		1,1432	3	0,932	
45	1		1,1528	3	0,9265	189,76
46	1		1,1595	3	0,9226	
47	1		1,1628	3	0,9206	
48	1		1,1648	3	0,9195	
49	1		1,1651	3	0,9193	
50	1		1,0713	2	0,9737	
51	1		1,0325	2	0,9962	
52	1		1,0603	2	0,9801	
53	1		1,0661	2	0,9767	
54	1		1,1478	3	0,9293	
55	1		1,1327	2	0,9381	138,43
56	1		1,1297	3	0,9398	
57	1		1,1245	3	0,9429	
58	1		1,1558	3	0,9247	
59	1		1,1805	3	0,9104	
60	1		1,2013	3	0,8983	
61	1		1,1769	3	0,9125	
62	1		1,1716	3	0,9155	
63	1		1,1715	3	0,9156	
64	1		1,173	3	0,9147	
65	1		1,1756	3	0,9132	129,03
66	1		1,1871	3	0,9065	
67	1		1,1933	2	0,9029	
68	1		1,1991	3	0,8996	
69	1		1,1825	3	0,9092	
70	1		1,2029	4	0,8974	
71	1		1,192	3	0,9037	
72	1		1,2163	3	0,8896	
73	1		1,2038	3	0,8969	
74	1		1,1828	4	0,909	
75	1		1,1916	3	0,9039	146,71
76	1		1,2073	4	0,8948	
77	1		1,1949	4	0,902	
78	1		1,1726	4	0,9149	
79	1		1,1677	4	0,9178	
80	1		1,1899	4	0,9049	
81	1		1,1802	4	0,9106	
82	1		1,1653	3	0,9192	
83	1		1,1638	4	0,9201	
84	1		1,1723	3	0,9151	
85	1		1,1766	4	0,9127	158,02
86	1		1,1887	3	0,9056	
87	1		1,1752	4	0,9135	
88	1		1,1752	3	0,9135	
89	1		1,1736	3	0,9144	
90	1		1,1757	3	0,9132	
91	1		1,1724	3	0,9151	165,99
92	1		1,143	3	0,9321	
93	1			3		

* empty fields: results are not reliable (probably, liner not completely filled with sediment; cap at the end of the liner disturbed measurement; p-wave transducer had not good contact)

Description of core : **KS12 – Station 191**

Date: 11/ 03 / 2006 - 08 :36

Latitude	54° 12.990′ N
Longitude	011° 43.541′ E
Water depth	25.8 m
Total core length	240 cm

	Description
Core cut in 10 cm sections for the study of Shear strength	0-10 cm: green-brown mud with slight smell of H2S, mussel and shells 10-20 cm: olive green mud with very slight smell of H2S 20-30 cm: olive green mud with very slight smell of H2S 30-40 cm: olive green mud with very slight smell of H2S 50-60 cm: olive greenish, light grey with very slight smell of H2S 70-80 cm: olive greenish, light grey mud with very slight smell of H2S 100-110 cm: olive greenish grey mud with very slight smell of H2S 150-160 cm: olive greenish, dark grey mud with very slight smell of H2S 190-200 cm: greenish, light grey silt/mud with plant material and slight smell of H2S 230-240 cm: greenish, light grey silt/mud with plant material

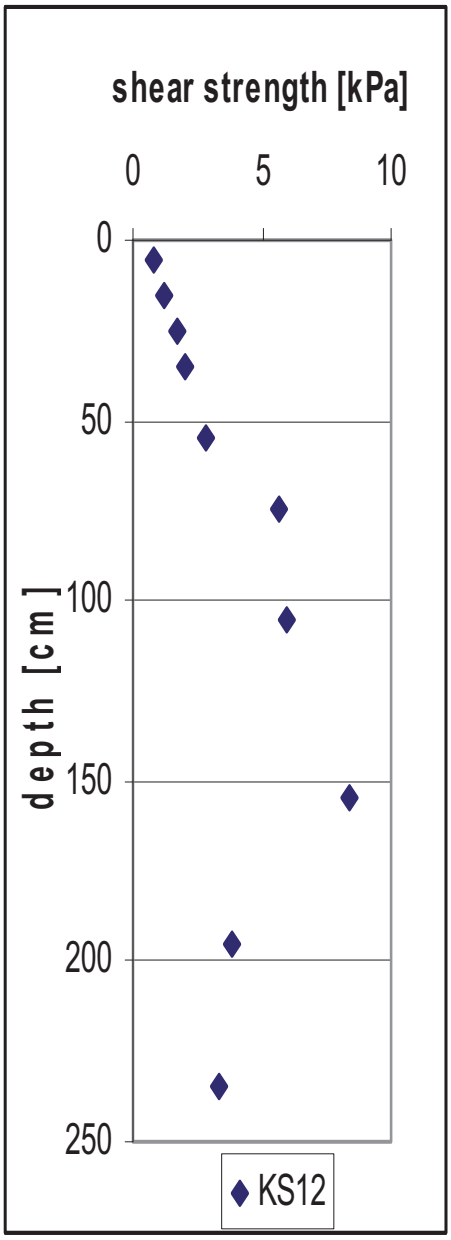

Data of Core **KS12 – Station 191**

Field Vane Shear Test

Depth (cm)	Measured Orientation	Undrained Shear strength Cu (kPa)	
5	↓ ‖	0,841	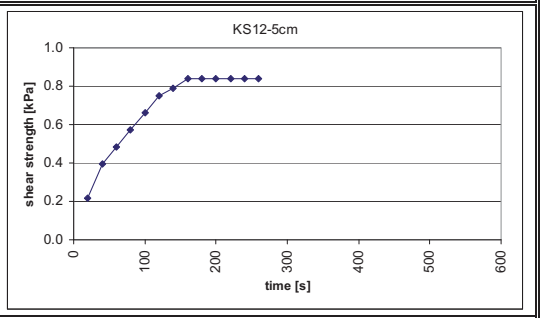
15	↓ ‖	1,249	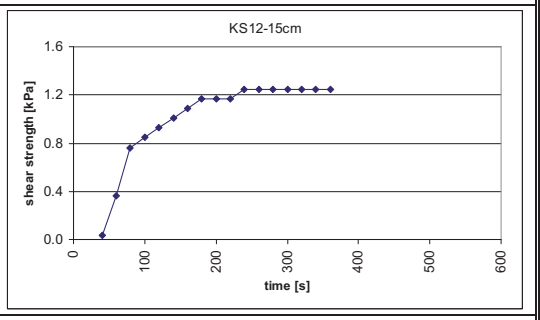
25	↓ ‖	1,735	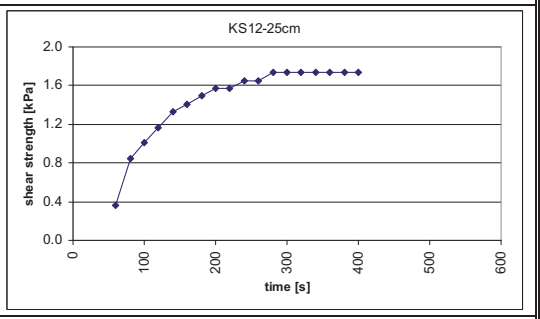
35	↓ ‖	1,977	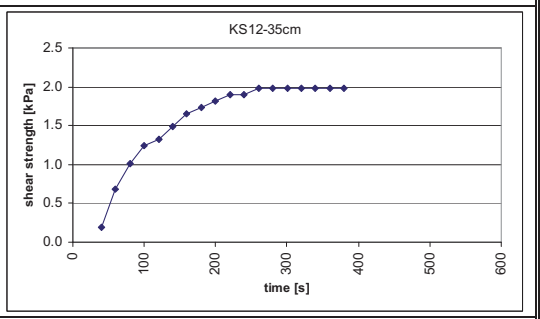
55	↓ ‖	2,786	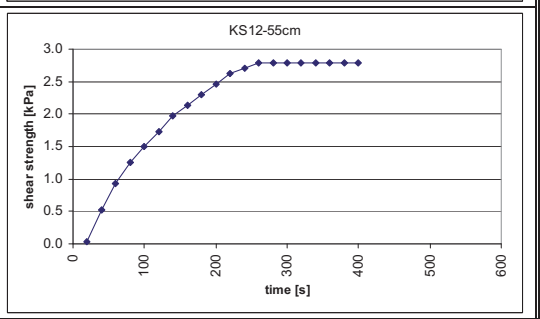

75	↓	5,698	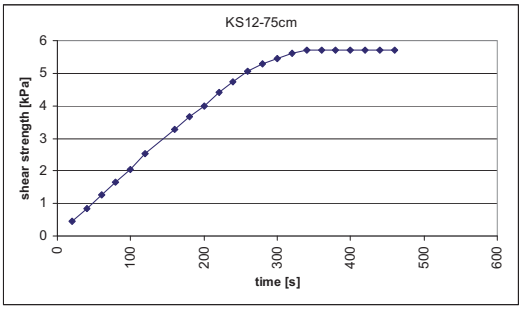
105	↓	5,941	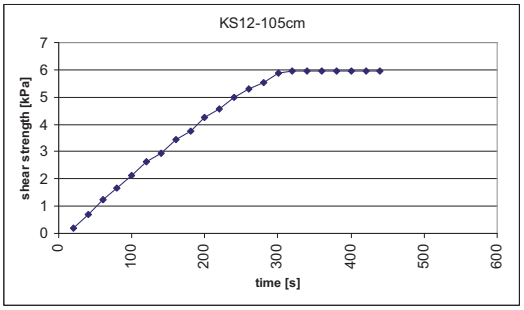
155	↓	8,367	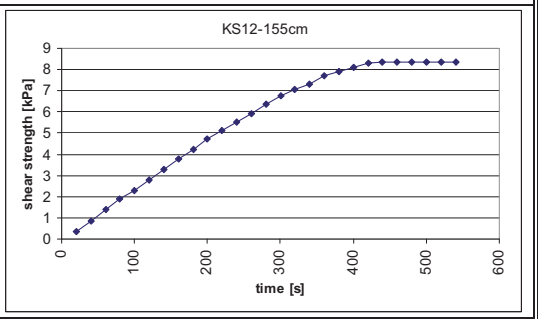
195	↓	3,838	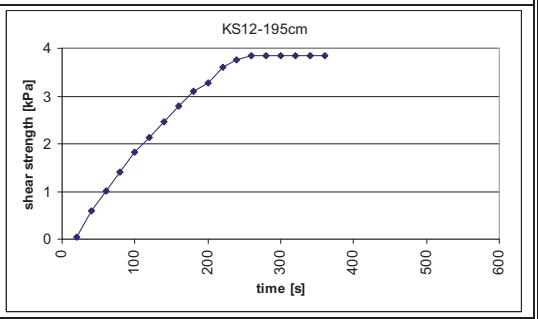
235	↓	3,352	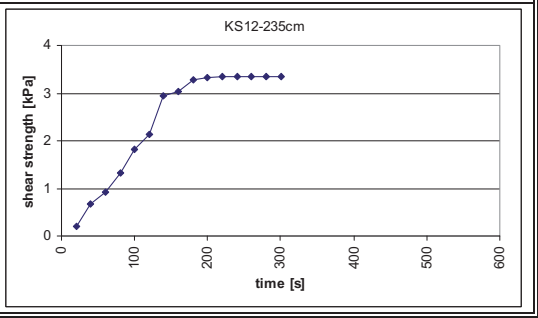

Grain size distribution
(Beckman Coulter laser particle sizer LS200):

depth (cm)	clay (%)	silt (%)	sand (%)
5	6.11	72.61	21.29
25	6.1	70.02	23.88
105	11.5	76.7	11.82
200	13.91	76.52	9.59

APPENDIX A5 – DATA OF FLUID MUD SAMPLES FROM THE RIVER EMS AND THE HARBOUR OF EMDEN

(see also Manuscript 1)

location and sample no.	date	time CEST	Yield stress [Pa]	Viscosity at yield point [Pas]	SSC [g/l]	Organic content TOC %	conductivity [mS/cm]	Salinity	Oxygen content [mg/l]	grain size distribution [%] Clay	Silt	Sand
river Ems - km 18												
E1	14.06.2007	02:15 pm			55		2,0	1	3,5			
E2	core E				59		1,9	1	3,29			
E3					61		1,9	1	2,7			
E4					60		2,0	1	3,64			
E5					70		2,0	1	2,62			
E6			0,5	72	113	3,8	2,1	1,1	1,82	18,0	78,0	4,1
E7			3,4	4250	182	3,8	2,1	1	0,06	17,8	77,4	4,9
E8					341		1,6	0,8	0,08			
E9					642							
E10					711							
inner harbour of Emden												
b1	19.06.2007	01:35 pm			0,2		23,9	14,5	7,3			
b2	core b				0,2		24,0	14,6	7,18			
b3					0,2		24,1	14,6	7,32			
b4					42	3,7	23,3	14,2	3,85	21,9	76,1	2,0
b5					256		16,0	9,4	0,06			
b6					330							
b7					358							
b8					374							
b9					452							
b10					450							
tide affected outer harbour of Emden												
a 1	19.06.2007	10:45 am	0,5	74	117	3,6	22,5	13,5	0,10	21,7	75,3	3,0
a 2	core a		0,8	294	144	3,6	22,8	13,7	0,08	22,7	75,5	1,8
a 3			2,1	1405	182	3,5	21,5	12,8	0,06	21,5	76,5	2,0
a 4			3,7	4579	200	3,6	19,8	11,8	0,06	23,4	74,6	2,0
a 5					201							
a 6					256							
a 7					294							
a 8					350							
a 9					385							
a 10					417							
a1-1	01.04.2008	08:45 am	0,6	122	127	4,1	10,6	5,8	0,50	21,9	77,5	0,6
a1-2	core a1		0,7	175	136	4,2	9,4	5,2	0,55	19,9	77,8	2,4
a1-3			1,6	670	161	4,2	13,0	7,3	0,36	19,8	77,9	2,3
a1-4			3,8	5142	192	4,5	15,5	8,8	0,04	21,0	78,3	0,7
a1-5					219		13,3	7,5	0,05			
a1-6					233		11,6	6,4	0,03			
a1-7					298		12,4	6,9	0,03			
a1-8					324							
a1-9					373							
a1-10					436							
a2-1	01.04.2008	11:40 am			84		11,1	6,1	1,79			
a2-2	core a2				116		11,1	6,1	0,24			
a2-3					136		12,0	6,7	0,15			
a2-4					168		14,3	8	0,05			
a2-5					201		14,0	7,9	0,05			
a2-6					218		13,3	7,4	0,04			
a2-7					248		11,7	6,4	0,05			
a2-8					267		10,2	5,6	0,04			
a2-9					322							
a3-1	01.04.2008	02:10 pm			82		9,6	5,3	2,62			
a3-2	core a3				120		10,7	5,9	1,29			
a3-3					135		11,2	6,2	0,58			
a3-4					167		12,8	7,1	0,09			
a3-5					181		12,7	7,1	0,04			
a3-6					224		13,4	7,5	0,02			

legend:

sampling by 2 m-long Rumohr-type gravity core: sub-sampling of mud suspension every 20 cm (no. 1=top, no.10=bottom of the core)
yield stress and viscosity at yield point: Bohlin CS 10 rheometer
SSC: weighing dry mass per unit sample volume
organic content (TOC): LECO CS 200 analyser
conductivity, salinity, oxygen content: multi-parameter instrument (WTW Multi 350i) - measured immediately after sampling on bord
grain size distribution: Beckman Coulter Laser Particle Sizer LS200; organic removed prior testing

Water levels at core sampling

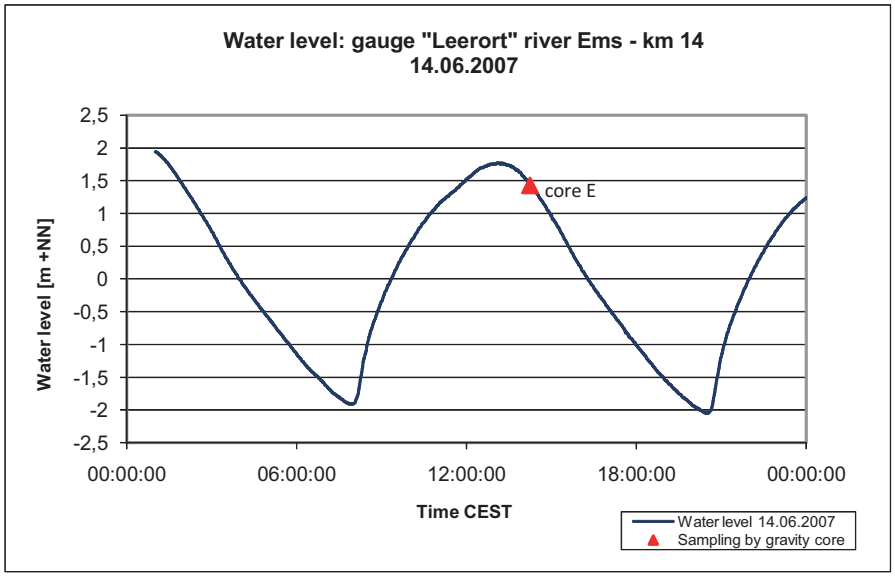

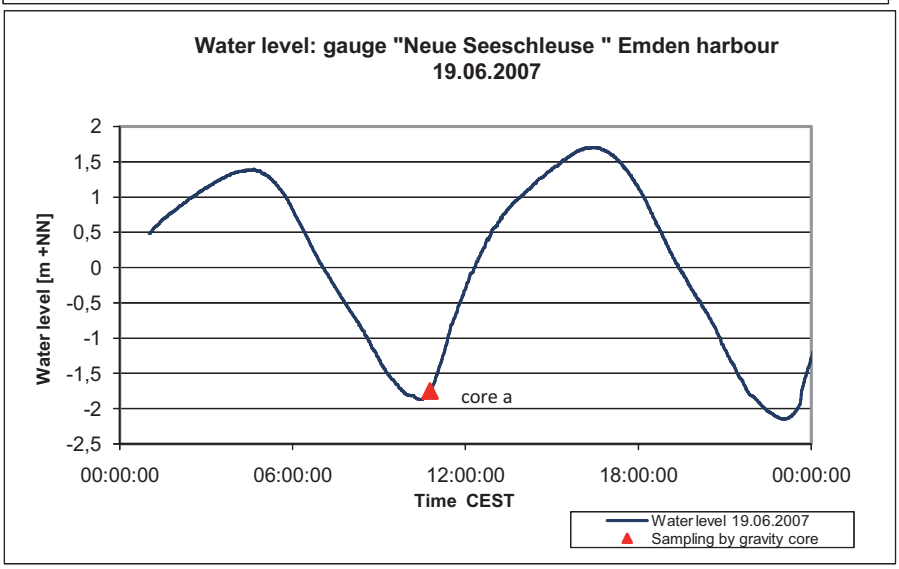

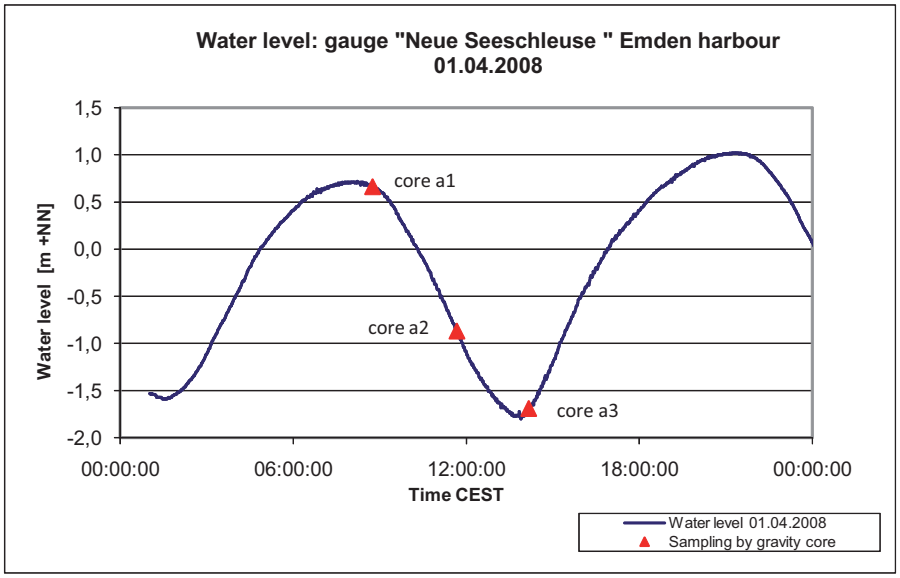

credit Water level: WSD Nordwest, Aurich